CRANFIELD UNIVERSITY

MUHAMMAD HANAFI AZAMI

Towards Optimisation for Novel Brayton Cycles & Biofuels for Reducing Engine Emission

SCHOOL OF AEROSPACE, TRANSPORT AND MANUFACTURING
Full-Time PhD Candidate

PhD
Academic Year: 2014- 2017

Supervisor: Prof. Mark A. Savill
Co-Supervisor: Dr. Timoleon Kipouros
July 2017

CRANFIELD UNIVERSITY

SCHOOL OF AEROSPACE, TRANSPORT AND MANUFACTURING
Full-Time PhD Candidate

PhD

Academic Year 2014 - 2017

MUHAMMAD HANAFI AZAMI

Towards Optimisation for Novel Brayton Cycles & Biofuels for Reducing Engine Emission

Supervisor: Prof. Mark A. Savill
Co-Supervisor: Dr. Timoleon Kipouros

July 2017

ABSTRACT

Aviation industries potentially contribute to the vulnerable energy crisis and simultaneously pose environmental concerns. With the stringent policies and targeted plans, it has been found that drop-in biofuels could potentially offer solutions but that alternative combustor technologies may also be required to meet new 2050 target. The purpose of this research was thus to evaluate the feasibility of the biofuels in both conventional and pressure-rise gas turbine engine to obtain the best trade-off between performance and emission. The investigated contents encompass the evaluation of biofuels (spray analysis, engine performance analysis, and zero-dimensional detonation analysis) and emission analysis. Spray analysis modelled the atomization and spray penetration of the droplets and comparisons have been made at different injection conditions. It was found that biofuels have shorter penetration length and could potentially encourage soot formation. Subsequently, engine performance analysis utilizes an in-house software, PYTHIA, for modelling a three-shaft high-bypass-ratio engine, similar to RB211 variant at various off-design conditions using biofuels was studied. Results showed that Jatropha and Camelina biofuels potentially increase the engine performance. Further analysis is conducted utilizing Zel'dovich–von Neumann–Doering modelling of shock waves in detonative combustion. Results prominently exhibit high thermodynamic efficiency in isochoric heat addition. Focusing on NOx formation, an emission analysis was carried out for both combustors separately using an in-house HEPHAESTUS emission model prediction. Biofuels have shown NOx reductions for both combustors. Finally, the research brings together all the analyses and a trade-off assessment is conducted. Small reductions were found in the key objectives considered over the design space investigated. In the spray analysis, the contribution lies on the modelling of evaporation and penetration of third generation biofuel droplets. In gas engine performance, this research has contributed to a wider off-design engine flight cycles utilizing these third generations of biofuels. Moreover, detonative combustion in a simplified model by utilizing one-step chemistry over various initial conditions are also added the benefaction of this research.

ACKNOWLEDGEMENTS

In the Name of Allah, the Most Gracious, the Most Merciful.

All the praises are due to Allah, the Lord of the Mankind. May peace and blessing be upon the last Prophet Muhammad. I thank Allah for His Mercy and blessings in giving me knowledge, strength and determination throughout the process of completing this research. All the beneficial and correct results in this thesis are due to the mercy and guidance of Allah, and all the errors in this thesis are due to my own limitations and ignorance. I must record my deepest appreciation to my supervisor Prof Mark A. Savill for his guidance, suggestions, encouragement, supports and willingness to guide me throughout this research work. I would like to extent my gratitude to my co-supervisor Dr Timoleon Kipouros for advising me in several occasions. Special thanks also dedicated to the International Islamic University Malaysia and Ministry of Higher Education Malaysia for the financial and funding support throughout this course.

I am grateful for the fact that I have received plenty of supports and assistances from various individuals throughout the period. I am highly indebted to my beloved mother, Martinelli Hashim and my father Dr Azami Zaharim, my beloved in laws Wan Rameli and Zainab Hussin and not to forget my beloved wife, Wan Norhajaratul Nurin Wan Rameli and my children ‘Aqif Naufal and Ammar Naquib for all their support, sacrifices, encouragement, patience and prayers that made me what I am today. Not to forget, my grandmother, Fatimah, who always prays for me every night and my siblings especially Syakirah Azami.

My motivation to complete this research is also helped by a circle of friends who always share their passion and encouragement. This includes my neighbours, Hazim Zainuddin, Nur Aisyah Khalid, Dr Yunus, and Dr Azlina. The supports from members of Cranfield Malaysian Society and the Cranfield Islamic Society are appreciated.

TABLE OF CONTENTS

ABSTRACT i
ACKNOWLEDGEMENTS iii
LIST OF FIGURES vii
LIST OF TABLES xi
LIST OF EQUATIONS xiii
LIST OF ABBREVIATIONS xvi
LIST OF SYMBOLS xviii
1 INTRODUCTION TO THE RESEARCH TOPIC 1
1.1 Introduction 1
1.2 Significance of Research and Problem of Statement 1
1.3 Research Gap 3
1.4 Aim and Objectives 4
1.5 Research Contents 5
1.6 Contribution to Knowledge 5
1.7 Methodology 6
1.8 Scope of Research 8
1.9 Thesis Structure 9
1.10 Concluding Remarks 13
2 RESEARCH BACKGROUND 14
2.1 Introduction 14
2.2 Worldly Issues 15
2.2.1 Environment & Energy Crisis 15
2.3 Technological Advancement in Aviation 17
2.3.1 Technological Program/Plan 17
2.3.2 Technologies in Aviation 19
2.3.3 Advanced Engine Technologies 25
2.4 Why Biofuels? 27
2.4.1 Definition of Biofuels 27
2.4.2 Available Feed stocks (generations, oil yield, standard requirements and properties & qualities of biofuels) 29
2.4.3 Potential of 3rd Generation of Biofuels 33
2.5 Pulse Detonation Engine 36
2.5.1 Introduction to PDE 36
2.5.2 History of PDE 37
2.5.3 Literature surveys on PDE 38
2.6 Concluding Remarks 45
3 EVALUATION OF BIOFUEL – SPRAY ANALYSIS 47
3.1 Introduction 47
3.2 Literature Review 48
3.3 Methods 50

3.4 Results & Discussion 56
3.4.1 Atomization and penetration of alternative fuels comparison 56
3.4.2 The influence of initial conditions on atomization and penetration ... 60
3.5 Concluding Remarks 66
4 EVALUATION OF BIOFUEL – ENGINE PERFORMANCE ANALYSIS (PYTHIA) 68
4.1 Introduction 68
4.2 Literature Review 69
4.3 Methods 72
4.3.1 Varying Flight Conditions 78
4.3.2 Varying Mixing Ratio Percentages 79
4.4 Results and Discussions 79
4.4.1 Engine performance comparison 79
4.4.2 Influence of blended fuel on LHV 80
4.4.3 Influence of 50% blended fuel on aircraft engine performance under different flight conditions 82
4.4.4 Influence of various mixing ratio blended fuel on aircraft engine performance at cruising condition 89
4.5 Concluding Remarks 94
5 EVALUATION OF BIOFUEL - DETONATIVE COMBUSTION ANALYSIS 96
5.1 Introduction 96
5.2 Literature Review 97
5.3 Theoretical Formulation and Numerical Frameworks 100
5.4 Results & Discussions 105
5.4.1 Model Comparison 105
5.4.2 Conditions for Detonation 107
5.4.3 Comparative detonation analysis of alternative biofuels using ZND model 110
5.4.4 Influence of various initial conditions 113
5.5 Concluding Remarks 128
6 EMISSION ANALYSIS 130
6.1 Introduction 130
6.2 Literature Review 131
6.2.1 Formation of NOx 134
6.2.2 Efforts of reducing NOx 137
6.2.3 Emission Models Prediction 142
6.3 Methods 145
6.3.1 Conventional combustor 145
6.3.2 Pressure rise combustor 148
6.4 Main Results and Discussion 152
6.4.1 Conventional combustor 152
6.4.2 Pressure-rise combustor 167

6.5 Concluding Remarks 182
7 TRADE-OFF ASSESSMENT 185
7.1 Introduction 185
7.2 Literature Review 186
7.3 Methods 189
7.3.1 Conventional combustor 189
7.3.2 Pressure-rise combustor 191
7.4 Main Results and Discussion 194
7.4.1 Conventional combustor 194
7.4.2 Pressure-rise combustor 204
7.5 Concluding Remarks 213
8 GENERAL CONCLUSION AND RECOMMENDATIONS 216
8.1 Conclusion 216
8.2 Recommendations and future works 220
REFERENCES 224
APPENDICES 239
Appendix A (Literature Surveys) 239
Appendix B (Spray Analysis) 253
Appendix C (Detonation Analysis) 256
Appendix D (Emission Analysis) 269
Appendix E (Trade-Off Assessment) 272
Appendix F (Research Outputs and Trainings) 283

LIST OF FIGURES

Figure 1-1 Flowchart 7

Figure 1-2 Thesis structure road map 9

Figure 2-1 Flow of the literature survey 14

Figure 2-2 Timeframe ERA Technological Plan (Hughes, 2011) 18

Figure 2-3 Carbon dioxide emission reduction plan (Payan *et al.*, 2014) 19

Figure 2-4 Advanced Engine contribution (Hughes, 2011) 25

Figure 2-5 Direction of turbofan technology (Hughes, 2011) 26

Figure 2-6 Percentage oil content and oil yield (Atabani *et al.*, 2012) 31

Figure 2-7 Parameter correlations (Hoekman *et al.*, 2012) 32

Figure 2-8 Standard requirements (Hoekman *et al.*, 2012) 32

Figure 2-9 PDE Operation Process (Blanco, 2014) 39

Figure 3-1 Transient condition of evaporation process for each fuel 58

Figure 3-2 Transient condition of penetration process for each fuel 58

Figure 3-3 Transient condition of temperature variation for each fuel 59

Figure 3-4 Transient condition of density variation for each fuel 60

Figure 3-5 Transient condition of evaporation process for KE under different temperatures 61

Figure 3-6 Transient condition of penetration process for KE under different temperatures 62

Figure 3-7 Transient condition of evaporation process for KE under different initial velocity 62

Figure 3-8 Transient condition of penetration process for KE under different initial velocity 63

Figure 3-9 Comparison of evaporation process for alternative fuels at higher initial temperature (Tp=500K) 64

Figure 3-10 Comparison of penetration process for alternative fuels at higher initial temperature (Tp=500K) 65

Figure 3-11 Comparison of evaporation process for alternative fuels at higher initial velocity (Vp=300m/s) 65

Figure 3-12 Comparison of penetration process for alternative fuels at higher initial velocity (Vp=300m/s) 66

Figure 4-1 PYTHIA engine model schematic diagram. 74

Figure 4-2 PYTHIA data process flowchart. 75

Figure 4-3 Performance comparison of blended KE+BJ 80

Figure 4-4 LHV variation at different mixing ratio percentage 81

Figure 4-5 LHV percentage difference with respect to pure kerosene at different mixing ratio 82

Figure 4-6 Variation of gross thrust at different Mach number 83

Figure 4-7 Variation of fuel flow at different Mach number 84

Figure 4-8 Variation of SFC at different Mach number 84

Figure 4-9 Variation of gross and net thrust at different altitude 87

Figure 4-10 Gross and net thrust percentage difference with respect to pure kerosene at a different altitude 88

Figure 4-11 Variation of fuel flow at a different altitude 88

Figure 4-12 Variation of SFC at a different altitude 89

Figure 4-13 Variation of gross thrust at different percentage of mixing ratio 90

Figure 4-14 Variation of fuel flow at different percentage of mixing ratio 91

Figure 4-15 Variation of SFC at different percentage of mixing ratio 91

Figure 4-16 Performance comparison of pure alternative fuel at the ground condition 93

Figure 4-17 Performance comparison of pure alternative fuel at cruise condition 93

Figure 5-1 Illustrations of different states adapted from Blanco (2014) 101

Figure 5-2 Pressure ratio at different state 111

Figure 5-3 Temperature ratio at different state 112

Figure 5-4 Density ratio at different state 112

Figure 5-5 Variation of (a) pressure and temperature ratios, and (b) specific volume and Mach number ratios for ACN fuel at different mass flux (P=1atm T=300K) 114

Figure 5-6 Comparison of (a) pressure ratios; (b) temperature ratios; (c) specific volume ratios; (d) and Mach number ratios at different initial mass flux under influence of strong detonation (P = 1 atm, T = 2000 K) 116

Figure 5-7 Comparison of (a) pressure ratios; (b) temperature ratios; (c) specific volume ratios; (d) and Mach number ratios at different initial mass flux under influence of weak detonation (P = 1 atm, T = 2000 K) 117

Figure 5-8 Influence of initial temperature to (a) pressure ratio, (b) temperature ratio, and (c) density ratio of ACN fuel in each state 118

Figure 5-9 Variation of (a) pressure and temperature ratios, and (b) specific volume and Mach number ratios for ACN fuel at different initial temperatures (P=1atm G=2612kg/s.m²) 119

Figure 5-10 Comparison of (a) pressure ratios; (b) temperature ratios; (c) specific volume ratios; (d) and Mach number ratios at different initial temperature under influence of strong detonation (P=1 atm, G=6000 kg/s.m²) 121

Figure 5-11 Comparison of (a) pressure ratios; (b) temperature ratios; (c) specific volume ratios; (d) and Mach number ratios at different initial temperature under influence of weak detonation (P=1 atm, G=6000 kg/s.m²) 122

Figure 5-12 Influence of initial pressure and mass flux on the Mach number for AG fuel (T = 2000 K) 123

Figure 5-13 Comparison of (a) pressure ratios; (b) temperature ratios; (c) specific volume ratios; (d) Mach number ratios; and (e) Mach number at different initial pressure under influence of strong detonation (T = 2000 K, G = 6000 kg/s·m^2) 126

Figure 5-14 Comparison of (a) pressure ratios; (b) temperature ratios; (c) specific volume ratios; (d) Mach number ratios; and (e) Mach number at different initial pressure under influence of strong detonation (T = 2000 K, G = 6000 kg/s·m^2) 127

Figure 6-1 GHG Emission savings with 100% pure alternatives fuel and blended fuels (Payan *et al.*, 2014) 133

Figure 6-2 Low emission window (Levy, Sherbaum and Arfi, 2004) 138

Figure 6-3 Range of permissible combustors temperature (Khandelwal, 2012) 138

Figure 6-4 Classification of NOx emission prediction techniques (Chandrasekaran and Guha, 2012). 143

Figure 6-5 Configuration of divided zone in the reactor of the combustor (Mazlan, 2012) 145

Figure 6-6 Comparison of the model using HEPHAESTUS with ICAO bank data 152

Figure 6-7 EINOx emission at different (a) combustor inlet temperature, (b) combustor inlet pressure, (c) mass flow, and (d) fuel flow for 25% Power setting 156

Figure 6-8 EINOx emission at different (a) combustor inlet temperature, (b) combustor inlet pressure, (c) mass flow, and (d) fuel flow for 85% Power setting 157

Figure 6-9 EINOx emission at different (a) combustor inlet temperature, (b) combustor inlet pressure, (c) mass flow, and (d) fuel flow for 100% Power setting 158

Figure 6-10 Molar mass fraction variations at different combustion types 163

Figure 6-11 (a) Flame temperature variation of different fuels and (b) comparison with respect to KE Fuel. 164

Figure 6-12 Effects of P3 and T3 variations on EINOx using correlation-based models 166

Figure 6-13 NOx emission at different zones; variations of introducing air mass flow fraction (left) and variations of combustion zone length (right) 176

Figure 6-14 Influence of KE fuel flow on NOx emission 177

Figure 6-15 Flame temperature variations at different combustion mixtures .. 178

Figure 6-16 Influence of chamber pressure on NOx 179

Figure 7-1 Optimization techniques 188

Figure 7-2 Flow process of conventional combustor trade-off assessment 189

Figure 7-3 Flow process of pressure-rise combustor trade-off assessments . 191

Figure 7-4 Trade-off plots for Case 1 197

Figure 7-5 Trade-off plots for (a) Cruise and (b) Ground 200

Figure 7-6 Trade-off plots for Case 3 203

Figure 7-7 Relation of thermal efficiencies and NOx emission for KE fuel 205

Figure 7-8 Effects of initial temperatures for Case 1 (AG fuel) 207

Figure 7-9 Trade-off plots for Case 1 – Individual Fuel 210

Figure 7-10 Trade-off plots for Case 2 213

LIST OF TABLES

Table 2-1 ERA work plan on airframe technologies 20

Table 2-2 ERA work plan on engine technologies 21

Table 2-3 Mitigation using technological concept for challenges area 23

Table 2-4 Source of feed stocks (Atabani *et al.*, 2012) 29

Table 2-5 PDE Operations Process 40

Table 2-6 List of challenges and difficulties of PDE 42

Table 2-7 Advantages of PDE 44

Table 2-8 Disadvantages of PDE 45

Table 3-1 Initial Conditions and Constant Parameters 51

Table 3-2 Thermochemical Properties 51

Table 3-3 Antoine Coefficients 54

Table 4-1 GHG Emission reduction with different feed stocks in relative to jet fuel (Payan *et al.*, 2014) 71

Table 4-2 Biofuel properties. 76

Table 4-3 Engine parameters and performance for baseline fuel. 77

Table 5-1 Model comparison with analytical and experimental studies 106

Table 5-2 Chemical equation used for stoichiometric condition 108

Table 5-3 Minimum initial temperature & mass flux for detonation 109

Table 5-4 Thermochemical properties during the reaction 110

Table 5-5 Effects of initial conditions to burned states 125

Table 6-1 Aircraft turbine engine emissions formation based on operating conditions (Levy, Sherbaum and Arfi, 2004) 132

Table 6-2 Input parameters 146

Table 6-3 List of correlation-based model (Chandrasekaran and Guha, 2012) 148

Table 6-4 Constant parameters 150

Table 6-5 Baseline for emission index analysis 153

Table 6-6 Baseline NOx emission analysis 154

Table 6-7 Stoichiometry combustion 160

Table 6-8 Lean combustion (30%) 161
Table 6-9 Rich combustion (30%) 162
Table 6-10 Constant parameters for correlation-based model 165
Table 6-11 Comparison of flame temperature of KE 168
Table 6-12 EINOx emission in detonation combustion 169
Table 6-13 Constants used for propulsive performance evaluation 170
Table 6-14 Conditions for detonation and propulsive performance 171
Table 6-15 NOx exhausted in a pressure-rise combustor 172
Table 6-16 Thermodynamic efficiency of a pressure-rise combustor 173
Table 6-17 Estimated range of EINOx obtained by Yungster and Breisacher (2005) 181
Table 7-1 Case study of conventional combustor 190
Table 7-2 Case study of pressure-rise combustor 193
Table 7-3 Main and combined effects of TSFC and NOx for Case 1 195
Table 7-4 Contour plots for the interactions of responses and the factors for Case 1 196
Table 7-5 Trade-off solutions for Case 1 197
Table 7-6 Main effects of TSFC and EINOx for Case 2 198
Table 7-7 Interaction plot of TSFC and EINOx for Case 2 199
Table 7-8 Trade-off solutions for Case 2 200
Table 7-9 Main effects plots for Case 3 201
Table 7-10 Trade-off solutions for Case 3 203
Table 7-11 Main effects plot for Case 1 under influences of strong and weak waves (AG Fuel) 206
Table 7-12 Interaction plots for Case 1 under influences of strong and weak waves 208
Table 7-13 Trade-off solutions for Case 1 – Individual Fuel 209
Table 7-14 Main effects and the interaction of the factors for Case 2 211
Table 7-15 Trade-off solutions for Case 2 212

LIST OF EQUATIONS

(3-1)..... 52
(3-2)..... 53
(3-3)..... 53
(3-4)..... 53
(3-5)..... 53
(3-6)..... 53
(3-7)..... 53
(3-8)..... 53
(3-9)..... 53
(3-10)..... 54
(3-11)..... 54
(3-12)..... 54
(3-13)..... 54
(3-14)..... 54
(3-15)..... 55
(3-16)..... 55
(3-17)..... 55
(3-18)..... 55
(3-19)..... 55
(3-20)..... 55
(3-21)..... 55
(3-22)..... 55
(3-23)..... 56
(4-1)..... 75
(4-2)..... 75
(4-3)..... 85
(5-1)..... 101
(5-2)..... 101

(5-3)..... 101
(5-4)..... 101
(5-5)..... 101
(5-6)..... 102
(5-7)..... 102
(5-8)..... 102
(5-9)..... 102
(5-10)..... 102
(5-11)..... 102
(5-12)..... 103
(5-13)..... 103
(5-14)..... 103
(5-15)..... 103
(5-16)..... 103
(5-17)..... 103
(5-18)..... 103
(5-19)..... 104
(5-20)..... 104
(5-21)..... 104
(5-22)..... 104
(5-23)..... 104
(5-24)..... 104
(5-25)..... 104
(5-26)..... 104
(5-27)..... 105
(6-1)..... 144
(6-2)..... 144
(6-3)..... 144
(6-4)..... 144

(6-5)..... 147
(6-6)..... 147
(6-7)..... 147
(6-8)..... 151
(6-9)..... 151
(6-10)..... 151
(6-11)..... 151
(6-12)..... 151
(6-13)..... 154
(6-14)..... 169
(6-15)..... 169
(6-16)..... 170
(6-17)..... 170
(6-18)..... 173
(6-19)..... 173

LIST OF ABBREVIATIONS

ACARE	Advisory Council for Aeronautics Research in Europe
ACN	Acetylene
AG	Algae Biofuel
ASTM	American Society for Testing and Materials
BC	Camelina Biofuel
BJ	Jatropha Biofuel
BPR	Bypass Ratios
CAEP	Committee on Aviation Environmental Protection
CEA	Chemical Equilibrium Application
CFD	Computational Fluid Dynamic
CJ	Chapman-Jouget
CO	Carbon Monoxide
DoE	Design of Experiment
DZ	Dilution Zone
DZL	Dilution Zone Length
EICO	Carbon Monoxide Emission Index
EINOx	Nitrous Oxide Emission Index
ERA	Environmentally Responsible Aviation
ETA	Engine Efficiency
ETH	Ethanol Fuel
FAME	Fatty Acid Methyl Ester
FAR	Fuel-to-air Ratio
FF	Flame Front
FFL	Flame Front Length
FPR	Fan Pressure Ratio
FRAIRD	Dilution Air Mass Flow Rate Fraction
FRAIRFF	Flame Front Air Mass Flow Rate Fraction
FRAIRI	Intermediate Air Mass Flow Rate Fraction
FRAIRP	Primary Air Mass Flow Rate Fraction
GHG	Green House Gas
ICAO	International Civil Aviation Organization
IEA	International Energy Agency

IPCC	Intergovernmental Panel on Climate Change
IZ	Intermediate Zone
IZL	Intermediate Zone Length
JTI	Joint Technology Initiative
KE	Kerosene Fuel
LHV	Lower Heating Value
LTO	Landing and Take-off
MA	Microalgae Biofuel
MDO	Multi-Disciplinary Optimization
MMD	Mass Median Diameter
MTH	Methanol
NOx	Nitrous Oxide
OD	Off-Design
OPR	Overall Pressure Ratio
PDE	Pulse Detonation Engine
PM	Particulate Matter
PR	Pressure Ratio
PZ	Primary Zone
PZL	Primary Zone Length
RDE	Rotational Detonation Engine
SFC	Specific Fuel Consumption
SMD	Sauter Mean Diameter
SPK	Synthetic Paraffinic Kerosene
TIT	Turbine Inlet Temperature
TF	Fuel Temperature
TRL	Technology Readiness Level
TSFC	Thrust Specific Fuel Consumption
WA	Total Air Mass Flow Rate
WF	Fuel Mass Flow Rate
Z	Surge Margin Parameter
ZND	Zel’dovich-von Neumann-Doering

LIST OF SYMBOLS

SYMBOL	DEFINITION	UNIT
A	Area	m^2
c	Speed of Sound	m/s^2
c_d	Drag Coefficient	
$c_{i,s}$	Vapour Concentration at Droplet Surface	$mol/s.m^2$
c_p	Constant Pressure Specific Heat	$J/kg.K$
$D_{i,m}$	Diffusion Coefficient of Vapour Pressure in a Bulk	
D_o	Nozzle Diameter	m
d	Diameter	m
F_{sp}	Specific Thrust	$N.s/kg$
f	Fuel-to-Air Ratio	
G	Mass Flux	$kg/m.s$
g	Gravitational Acceleration	m/s^2
h	Convective Heat Transfer Coefficient	W/m^2K
hi	Enthalpy	J
h_{fg}	Latent Heat	J/kg
I_{sp}	Specific Impulse	$1/s$
k	Mass Transfer Coefficient	
M	Mach Number	
MW	Molecular Weight	kg/mol
m	Mass	kg
$\dot{m}$	Mass Flow Rate	kg/s
$\dot{m}''$	Mass Flux	$kg/m.s$
N	Number of Moles	
N_i	Molar Flux of Vapour	mol/m^2s
Nu	Nusselt Number	
P	Pressure	Pa
Pr	Prandtl Number	
q	Heat Addition	J/kg

R	Specific Gas Constant	$J/kg.K$
R_u	Universal Gas Constant	$J/kg.K$
Re	Reynolds Number	
r	Radius	m
Sc	Schmidt Number	
s	Penetration Distance	m
T	Temperature	K
TIM	Time in Mode	s
T_{ad}	Adiabatic Temperature	K
T_{fl}	Flame Temperature	K
T_g	Temperature of Continuous Phase	K
t	Time	s
V	Velocity	m/s
V_D	Detonation Velocity	m/s
v	Specific Volume	m^3/kg
W	Work	J
W_f	Fuel Flow Rate	kg/s
WAR	Water-to-Air Ratio	
Y	Molar Mass Fraction	

GREEK SYMBOLS

α	Volume Fraction of Droplet Spray	
γ	Specific Heat Ratio	
θ	Half Angle of Spray Cone	°
ρ	Density	kg/m^3
μ	Molecular Viscosity	$kg/m.s$
η_B	Brayton Cycle Efficiency	
η_H	Humphrey Cycle Efficiency	
η_P	Propulsive Efficiency	
η_T	Thermal Efficiency	
∀	Volume	m^3
χ	Number of Mole Fraction	

π_C	Combustor Efficiency

SUBSCRIPT

1	State 1 (unburned condition)
2	State 2 (at the wave)
2'	State 2' (at the wave –arbitrary)
3	State 3 (burned condition)
4	State 4 (downstream)
A	Total
a	Ambient
c	Chamber
d	Droplet Spray
e	Exit
f	Fuel
g	Gas
i	Species
n	Nth Stage (Component)
°	Initial
p	Droplet Particle
res	Resident Time
sat	Saturation
x	Axial Direction
∞	Free Stream

1 INTRODUCTION TO THE RESEARCH TOPIC

1.1 Introduction

This chapter specifies an introduction to the topic of this research. It comprises the motivation of the research, problem statement, research gap, aim and objectives, the contributions of this research to knowledge, research methodology, scope of research, and thesis structure.

1.2 Significance of Research and Problem of Statement

In a modern world, people prefer airplanes to travel safely and frequently. These demands urge aerospace industries to grow expansively. However, this growth embraces myriad of problems, economically, and environmentally. There are two main concerns needing to be tackled: energy crisis and environmental crisis. For instance, hike in oil demand not only increases fuel prices but increases uncontrollably pollutant emissions into the atmosphere. The primary motivations are (1) concerns on greenhouse gas (GHG) emissions and global climate change, (2) a desire for renewable/sustainable energy sources, and (3) an interest in developing domestic and more secure fuel supplies (Hoekman *et al.*, 2012). The concerns are more severe when looking at the statistical numbers. Currently, one-fifth of the global carbon dioxide emissions is from transportation sector. This sector does not look promising to the climate as the number of light vehicles on the roads is estimated to increase to over 2 billion vehicles by 2050 (Rawat *et al.*, 2013). It is expected that about 4.1 billion metric tons of carbon dioxide will be released into the atmosphere from 2007 to 2020 and an additional 8.6 billion metric tons of carbon dioxide will be released into the atmosphere from 2020 to 2035 (Atabani *et al.*, 2012). These unfriendly gasses from the combustion of fossil fuels will inevitably accentuate climate change.

The energy crisis is the second issue that needs to be addressed. The International Energy Agency (IEA) reported that the world will need 50% more energy in 2030 than today (Ashraful *et al.*, 2014), with transportation sector becoming the second largest energy consuming sector after the industrial. Nearly all fuel energy consumption in the transportation sector comes from fossil fuels (more than 90%), with a small amount from natural gas and renewable energy sources (Atabani *et al.*, 2012; Maity *et al.*, 2014). However, as energy demand increases, the conventional oil reserves and natural gas that can be commercially exploited is expected to diminish after approximately 41.8 and 60.3 years, respectively (Ashraful *et al.*, 2014). The Kyoto Protocol of 1997 pointed out for a 5.2% reduction in GHG emissions worldwide from the 1990 values. With this rapid increase in transportation fuel demand trends, environmental concerns and depletion of fossil fuels, it has become increasingly important to adopt policies to minimize impacts of global warming (Brennan and Owende, 2010), and for scientists and researchers to develop alternatives fuels that approximate the properties and performance of petroleum-based fuel (Tüccar and Aydın, 2013). An alternative and renewable energy sources need to be more feasible and are, indeed, urgently needed.

The awareness of these crises has prompted tremendous research, for example, Clean Sky JTI Projects by the European countries, The Environmentally Responsible Aviation Project (ERA) by NASA and several more. However, studies have shown that the current development of more efficient technologies in aircraft engines that can reduce GHG emission up to 18% is still far below the goal of reducing 50% CO_2 emissions by 2050 (Payan *et al.*, 2014). Due to these circumstances, the aviation industries have shifted their strategy to utilize alternative fuels based on biofuels. The use of drop-in fuels and blended fuels in aircraft engines have particularly attracted the attention and interest of engineers and researchers throughout the world. Drop-in fuels need minor or no modifications at all in the aircraft engine in service. They offer a future ‘greener’ aircraft with less dependency on crude oil.

Following the successful flights of many commercial aircraft running with different biofuels, this makes biofuel a reliable option to sustain the environment as well as energy. However, there are shortcomings associated with the use of biofuels alone in aircraft engines such as in terms of thermodynamic efficiency and performance. Because of higher thermodynamic efficiency inherent in detonation combustion based engine, there is now a growing interest to the development of wave rotor, pulse detonation engine and rotating detonation engine configurations as alternative technologies for the next generation of the aerospace propulsion systems. Running an engine using biofuels with pressure-rise combustors certainly forms as a viable strategy to satisfy greener technology with better performance. It is also believed that these alternative combustor technologies fuelled by alternative fuels could meet 2050 emissions targets plan for aviation.

1.3 Research Gap

Interest in the biofuels that are based on microalgae, algae, Jatropha, and Camelina to achieve the targeted performance enhancement and emission reduction provides a clear drive for research to be developed. Corresponding to the fuel requirements set by the standards in American Society for Testing Materials (ASTM) and European Committee for Standardization (EN14214), it is crucial to explore the influence of biofuels properties. In the present context, it is worth highlighting that there have been three successful biofuel flights of commercial aircraft, which are Air New Zealand's Boeing 747-400 in 2008, Continental Airlines Boeing 737-800 and Japan Airline Boeing 747-300 in 2009. These flights used bio-SPK blends of up to 50% with conventional fuel and found no abnormal impacts for different engine operations (Rahmes *et al.*, 2009) and minimum level emission in the gas turbine engine. However, no research works have been done until this moment—neither through experiment nor numerical—that examines the liquid biofuel in pressure rise combustors, especially in Pulse Detonation Engine. This motivates the research work for predicting the feasibility of these biofuels for detonation within certain objectives

and constraints. Moreover, it is worth to explore the spray behaviour of these biofuels to increase the thermal efficiency of the combustion process and reduce the emission at the same time (Ejim, Fleck and Amirfazli, 2007). Additionally, there is a great opportunity to use and extend the capability of the developed in-house engine performance and emissions computer tools in Cranfield University, namely PYTHIA and HEPHAESTUS, and integrate with the variety of different biofuels and different mode of combustion. Finally, the best trade-off assessments are conducted to combine all numerical analyses mentioned above in coherent best solutions for every prescribed biofuel.

1.4 Aim and Objectives

This research aims to evaluate the feasibility of the previously mentioned biofuels in conventional and pressure-rise gas turbines engine to obtain the trade-off between performance and emissions. To achieve this aim, the following specific objectives are highlighted:

- To identify the technological advancement in aviation, main characteristics of biofuels and pressure-rise combustors.
- To study the chemical and physical properties of the selected biofuels and evaluate them in spray analysis.
- To conduct engine performance analysis using in-house computer tools (PYTHIA and TURBOMATCH) for different wide-range of operations using different biofuels.
- To study the feasibility of these biofuels in detonation combustion.
- To conduct the emissions analysis using in-house computer tools (HEPHAESTUS) in different modes of combustion.
- To implement trade-off assessment solutions for the best performance and minimum emissions configurations.

1.5 Research Contents

This research comprises of the following:

- Evaluation of spray characteristics of these biofuels under prescribed conditions.
- Accommodation of biofuels into wide-range of engine operations in terms of the performance and emission using the in-house computer tools.
- Evaluation of the feasibility of these potential biofuels in detonation combustion.
- Exploration of the capabilities of in-house emission computer tools predictions over the wide range of combustion conditions.
- Identification of trade-off solutions on engine performance and emissions using biofuels at different configurations.

1.6 Contribution to Knowledge

Contributions of this work to knowledge or existing knowledge comprise of the followings:

- Improvising the model of spray analysis (evaporation and penetration) work done by Mazlan (2012) by adopting third generation of biofuels.
- Evaluation of the engine performance in off-design conditions by utilizing third generation of biofuels in a new version of PYTHIA.
- Evaluation of biofuels under detonative combustion in a simplified model by utilizing one-step chemistry.
- Pareto optimally criteria is applied to assess the best trade-off configurations between performance and emission for different types of combustors.

1.7 Methodology

This section outlines the methodology of this research. Further details are provided in subsequent chapter. Figure 1-1 presents the flowchart of this research and comprises several stages. The first stage covers the literature survey, which includes worldly issues, technological advancement in aviation, identification of the wide range of biofuels, and finally identification of novel Brayton cycle-pressure rise combustors. World issues of importance to the environment and energy crisis are highlighted. This is followed by technological advancement in aviation section, which identified several technological programs and technologies in aviation. The biofuels section discusses and identifies the selection of biofuels used in this work for comparison, and important fuel properties are collected from the open literature. The selection of pressure rise combustors is proves crucial so that the scope of this research is well focused. A pulse detonation engine is chosen for simplicity but effective to enhance the performance.

The second stage focuses on atomization and sprays analysis. This analysis involved the atomization and spray penetration. Equations were adopted from the FLUENT 6.3 User Guide Manual and were calculated and plotted using Excel spreadsheet. Next, the in-house computational tools—namely PYTHIA and TURBOMATCH—are utilized to evaluate and compare the engine performance using different biofuels, whilst HEPHAESTUS is used to assess pollution of the fuels selected. These computational tools need appropriate modifications in order to evaluate these biofuels. The research is moving further to model a zero-dimensional detonation analysis for these biofuels. An analytical model accounting for Rankine-Hugoniot Equation, Rayleigh Line Equation, and Zel'dovich–von Neumann–Doering model and taking into account single step chemistry and thermophysical properties for a stoichiometric mixture. The zero-dimensional detonation analysis predicts the detonability of the biofuels and the performance parameter at each state. Finally, all analyses are brought together in a trade-off assessment. This assessment was carried out to evaluate the best solution on the performance and emissions trade-off

configurations. Conclusively, all the results are combined, analysed and discussed.

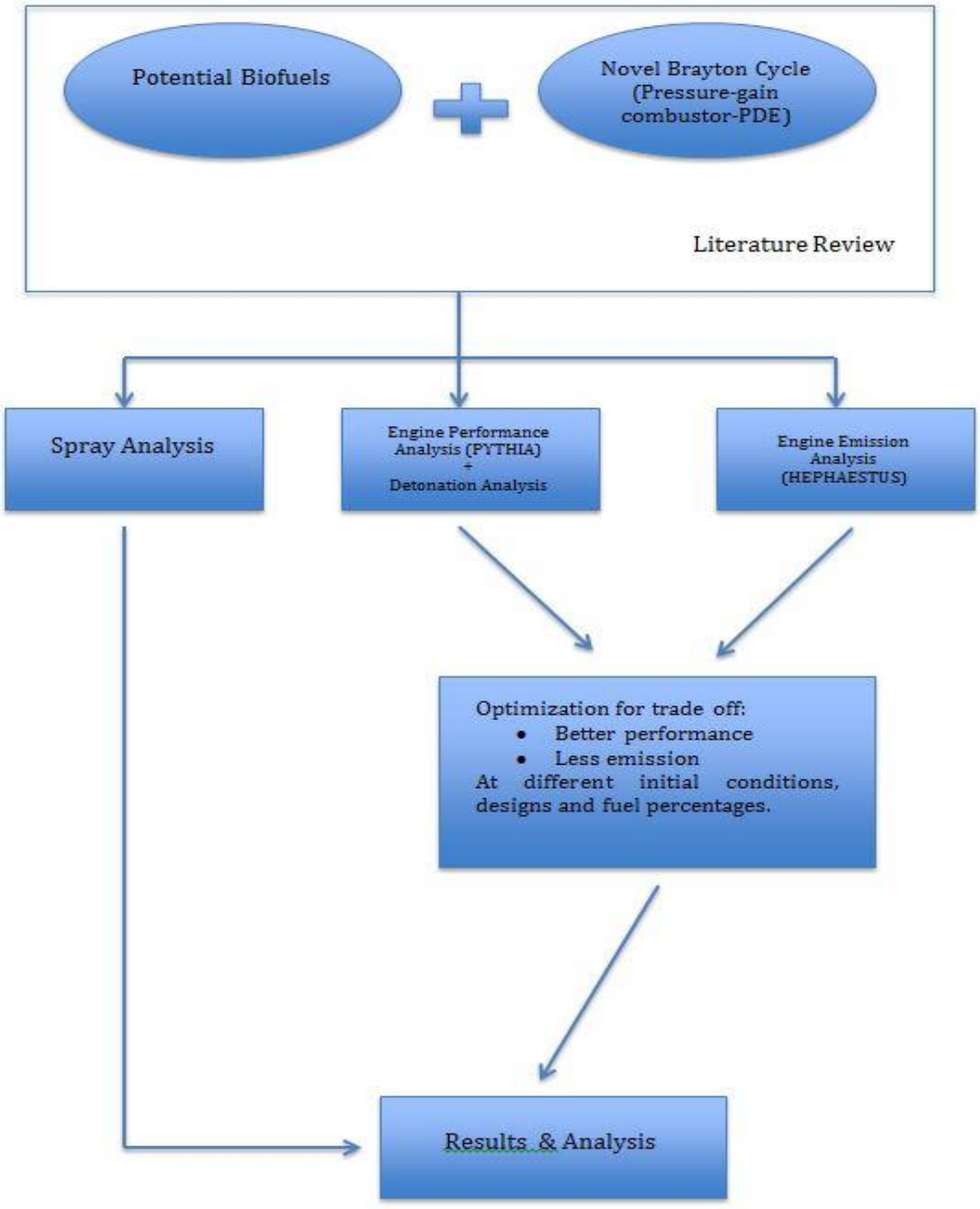

Figure 1-1 Flowchart

1.8 Scope of Research

Biofuels are targeted to be used in the near future, so it is certainly worth exploring the wider capability of these fuels as well. Present research evaluates biofuels in terms of performance and emission by understanding its spray behaviour, combustion in conventional combustor and detonation. In the later part, the trade-off solution is considered to find the best configurations between the best performances with lesser emissions. However, the research is confined by several limitations. Since the focus is primarily to evaluate and obtain the trade-off solutions for biofuels performance and emission, the research only focuses on the analytical works. Whilst present research can also be categorized as a first examination of the applicability and feasibility of the selected alternative fuels for varieties of conditions; spray behaviour, detonation combustion, and emission analysis. Therefore, it is necessary to evaluate and understand the performance and emission formed in combustion first before the trade-off solution is determined. Notably, the thermochemical and physical properties used for the analysis are based on the published literature and the data in software's library. The considerations of the variability about a particular type of fuel and its characteristics are not being taken into account. Processes of these fuels were also neglected. Specifically, the in-house software used for engine performance analysis (PYTHIA) and emission analysis (HEPHAESTUS) accommodate a specific type of engine only within specific assumptions which are elaborated in each chapter. The detonation analysis uses one-step chemistry reactions for a start in order to make a straight comparison for different fuels and to assess whether these might be sufficiently accurate to be useful. Thus, remaining differences with experiment are most probably due to not using full multi-step chemistry and leave open this extension for further investigations and improvements. In the emission analysis, a chemical kinetic model is also not being considered. Lastly, a full CFD analysis is not included in the research because of time limitation and overlaps with other studies.

1.9 Thesis Structure

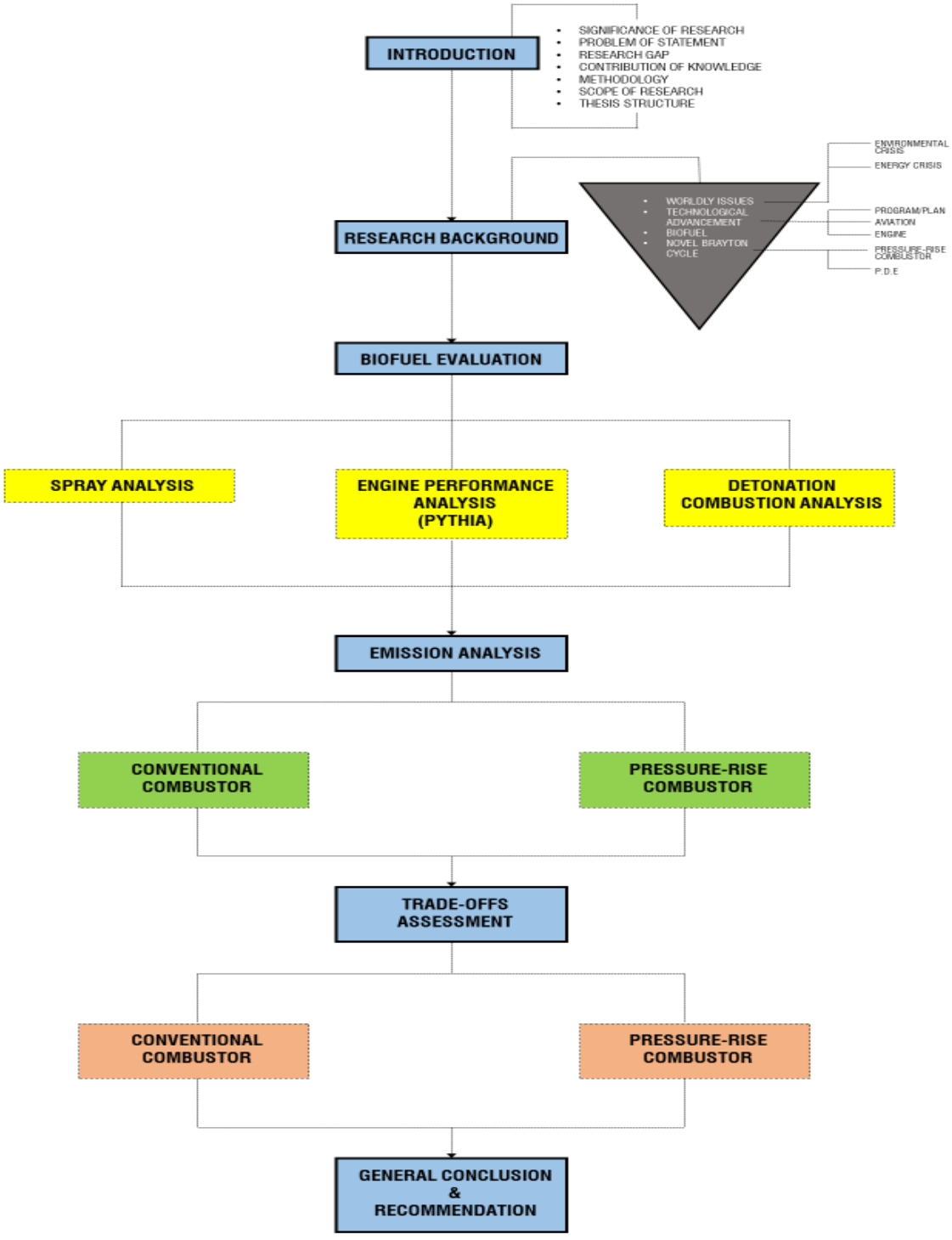

Figure 1-2 Thesis structure road map

The structure of this Ph.D. thesis is based on the objectives mentioned in the previous section and the road map is illustrated in Figure 1-2. Each of the later chapter is already the part of the published journal paper, which identified and addressed the research objectives.

Chapter 1. Introduction

This chapter covers the motivation of the research, problem statement, research gap, aim and objectives, the contribution of this research to the knowledge, research methodology, the scope of the research, and the organization of the thesis.

Chapter 2. Research Background

Literature review takes most part of this chapter ranging from global issues, technological advancement plans for mitigation, and the applications of biofuels and pressure-rise combustors.

Chapter 3. Evaluation of Biofuel - Spray Analysis

This chapter focuses on the modelling of atomization and spray penetration for alternative fuels. The results are shown in a time variant condition. Comparisons have been made to visualize the transient behaviour of these fuels. The influences of initial conditions such as temperature and droplet velocity are also explored numerically.

Output: This work has been published in Fuel Journal, Azami, M. H. and Savill, M. (2016) ‘Modelling of spray evaporation and penetration for alternative fuels’, *FUEL*. Elsevier Ltd, 180, pp. 514–520. doi: 10.1016/j.fuel.2016.04.050.

Chapter 4. Evaluation of Biofuel - Engine Performance Analysis (PYTHIA)

This chapter addresses the analysis of aircraft engine performance in terms of thrust, fuel flow and specific fuel consumption (SFC) at different mixing ratio percentages of biofuel blends at different flight conditions. In-house computer software codes, PYTHIA & TURBOMATCH were used for the analysis and modelling of a three-shaft high-bypass-ratio engine which is similar to RB211 variant. This study is a crucial step in understanding the influence of different blended biofuels on the performance of aircraft engines.

Output: This work has been published in Azami, M. H. and Savill, M. (2016) 'Comparative Study of Alternative Biofuels on Aircraft Engine Performance', PROCEEDING OF THE IMECHE, PART G: JOURNAL OF AEROSPACE ENGINEERING. SAGE Publishing and Azami, M. H. and Savill, M. (2016) 'Comparison of Aircraft Engine Performance Using Alternative Fuels'. In: Proceeding of the International Symposium on Sustainable Aviation (ISSA 2016). Istanbul, Turkey; 2016.

Chapter 5. Evaluation of Biofuel – Detonation Combustion Analysis

This chapter presents an assessment for biofuels under detonation combustion conditions. For simplicity, the analysis is modelled using an open tube geometry. The analysis employs the Rankine-Hugoniot Equation, Rayleigh Line Equation, and Zel'dovich–von Neumann–Doering model and takes into account species mole, mass fraction, and enthalpies-of-formation of the reactants. Initially, minimum conditions for the detonation of each fuel are determined. Pressure, temperature, and density ratios at each state of the combustion tube for different types of fuel are then explored systematically. Finally, the influence of different initial conditions is numerically examined and compared.

Output: This work has been presented at the 52nd AIAA/SAE/ASEE Joint Propulsion Conference, AIAA Propulsion and Energy Forum and Exposition 2016, Salt Lake City, Utah and also has been published in Azami, M.H. and Savill, M. (2017) 'Pulse Detonation Assessment for Alternative Fuels', ENERGIES. MDPI AG. Moreover, this chapter was submitted as a technical paper for Whittle Reactionaries Prize nomination and received a reviewer recommendation.

Chapter 6. Emission Analysis (HEPHAESTUS)

This chapter evaluates emission formed (NOx) from these biofuels. The chapter is divided into two sections; emission analysis from the conventional combustor and pressure-rise combustor. For conventional combustor, the emission analysis was conducted at various flight conditions and different power settings. Moreover, further off-design conditions are explored to visualize different combustor inlet conditions such as different inlet pressure and temperature, total mass flow and fuel flow. While, for the pressure-rise combustor, zero-dimensional performance analysis from the previous chapter is needed and incorporate for modelling the geometry tube design and to establish the initial conditions for detonation. The variations of emission at different tube (combustor) conditions such as introducing air mass flow fraction at different zones, fuel flow, combustion zone lengths and chamber pressure were also discussed thoroughly.

Output: Partly of this work has been accepted for publication as Azami, M.H, Savill, M., and Li, Yi-Guang (2017) 'Comparison of Aircraft Engine Performance and Emission Analysis using Alternative Fuels', INTERNATIONAL JOURNAL OF SUSTAINABLE AVIATION. Inderscience Publishers.

Chapter 7. Trade-off Assessment

This chapter puts together all the analyses in the trade-off assessment. This assessment finds the best solutions configurations between performance and emission. The work is divided into two separate studies and different approaches; with the conventional combustor and with pressure gain combustor. The procedures and detailed explanation of the selected case study are thoroughly discussed and presented.

Chapter 8. Conclusions and Recommendations

Finally, this chapter puts together important findings while providing discussion for future works and effective implementations.

1.10 Concluding Remarks

This chapter gives an introduction to the research topic. Firstly, the significance of the research and the problem statement are highlighted to address the necessity of this research. Secondly, what is the opportunities for further studies are discussed in the research gap. From these, aim and objectives are listed to give direction and contributions of the research. A reasonable flow of the research is well planned in the methodology. As boundaries, the scope of research is addressed to highlight some general constraints of the research based on the timeline given for the research. The specific assumptions and constraints are well elaborated in each chapter. The thesis structure is included at the end of this chapter to give an overview of the research and brief summary of each chapter.

2 RESEARCH BACKGROUND

2.1 Introduction

This chapter presents a comprehensive literature review to provide general background of the research. Firstly, it is vital to look at global issues relating to the environment and energy demand. Necessary plans or programs are then identified to handle these issues with the emergence of technological advancement in the aviation industry. At the moment, the future use of alternative fuels look promising to fulfil the target. This overview includes other edible and non-edible feed stocks in terms of their properties & qualities and standard requirements. The 3rd generation microalgae-based biofuels is discussed in the following section, including the brief outline of their conversion process, properties and quality standards as a drop-in fuel in the industry. Pulse detonation engine (PDE) section is also reviewed in the later section. PDE is used to enhance performance of the gas turbine engine by improving its thermal efficiencies. PDE operates in a novel Brayton cycle named Humphrey cycle where the detonation combustion takes place. The flow of the research background is described in Figure 2-1.

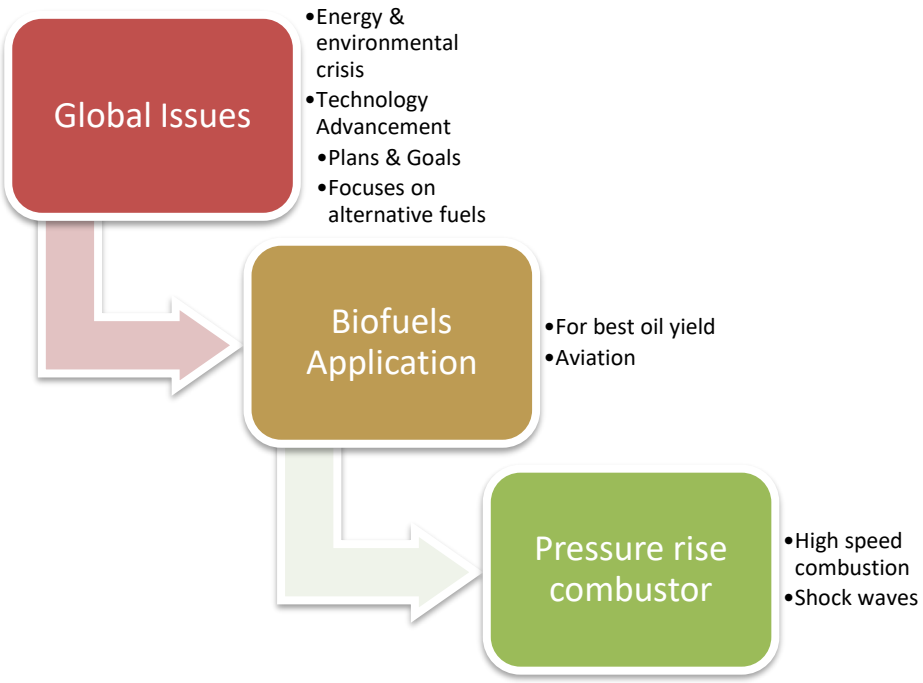

Figure 2-1 Flow of the literature survey

2.2 Worldly Issues

According to evolution, a life began from Cyanobacterium and algae billions of years ago, which was filled with carbon dioxide. These photosynthetic organisms use carbon dioxide and releasing oxygen to evolve into new life on Earth, but these organisms' survivability are now threatened due to global warming (Demirbas, 2010). Global warming has to increase Earth's average temperature by 0.6°C in the twentieth century and will continue to increase anywhere from 1.5°C to 4.5°C by the year 2100 as reported by The Intergovernmental Panel on Climate Change (IPCC). The main driving force is due to anthropogenic carbon dioxide emission, which accounts for 80% of all greenhouse gasses produced into the atmosphere (Padmanabhan MR and Stanley, 2012) and other emissions such as nitrogen oxide, sulphur oxides, unburned hydrocarbons and the list goes on. The impact will be devastatingly horrifying to the climate such as flooding, storms, hurricanes, sea water level rises, drought and other natural disasters caused by no other than human hands.

2.2.1 Environment & Energy Crisis

There are two vital issues need to be noted, which are environmental crisis, due to global warming caused by fossil fuels, and energy crisis, that leads to increasing global petroleum crude oil prices which impacts on the domestic energy situations as well as on local society life (Amin, 2009). The primary motivations of research are (1) concerns on greenhouse gas (GHG) emissions and global climate change, (2) a desire for renewable/sustainable energy sources, and (3) an interest in developing domestic and more secure fuel supplies (Hoekman *et al.*, 2012). The concerns are, in reality, more worrying according to statistical numbers.

Presently, one-fifth of the global carbon dioxide emissions come from the transportation. This sector does not look reassuring to the environment as the

number of light vehicles on the roads is estimated to increase to over 2 billion vehicles by 2050 (Rawat *et al.*, 2013). It is expected that about 4.1 billion metric tons of carbon dioxide will be released into the atmosphere from 2007 to 2020 and an additional of 8.6 billion metric tons carbon dioxide will be released into the atmosphere from 2020 to 2035 (Atabani *et al.*, 2012). These unfriendly gasses from the combustion of fossil fuels have a direct impact in accelerating climate change.

The energy crisis is the second vital issue needs to be addressed. International Energy Agency (IEA) has reported that the world will need 50% more energy in 2030 (Ashraful *et al.*, 2014), with the transportation sector becoming the second largest energy consuming sector after the industrial. More than 90% of fossil fuel energy consumption in the transportation sector is sourced from fossil fuels, with only small remaining from natural gas and renewable energy sources (Atabani *et al.*, 2012; Maity *et al.*, 2014). However, as energy demand increases, conventional oil reserves and natural gas, that can be commercially exploited, will no longer be able to keep up after approximately 41.8 and 60.3 years, respectively (Ashraful *et al.*, 2014).

The Kyoto Protocol of 1997 targeted a 5.2% reduction in GHG emissions worldwide from 1990 values due to the fact that there is ongoing rapid increase in transportation fuel demand trends, environmental concerns while fossil fuels is depleting. This has made the world aware of the significance to adopt such policies to minimize impacts of global warming (Brennan and Owende, 2010) as well as to force scientists and researchers into developing alternatives fuels that can sustain properties and performance of petroleum-based fuel (Tüccar and Aydın, 2013). This resulted in the urgency of producing more feasible alternative resources and renewable energy.

2.3 Technological Advancement in Aviation

2.3.1 Technological Program/Plan

There is €1.6 billion worth of budget allocated for a Clean Sky JTI project that is equally shared between European Commission and industry, over the period from 2008 to 2013. This public-private partnership is expected to speed up technological breakthrough developments and also shorten the time for new tested solutions sets by ACARE -Advisory Council for Aeronautics Research in Europe - the European Technology Platform for Aeronautics & Air Transport and to be reached in 2020. The main goals are (Jiminez, Pfaender and Mavris, 2012):

1. 50% reduction of CO_2 emissions through reduction of fuel consumption
2. 80% reduction of NOx (nitrogen oxide) emissions
3. 50% reduction of external noise
4. A green product life cycle: design, manufacturing, maintenance and disposal/recycling
5. Estimating that 20–25% will be realized through airframe improvements
6. 15–20% through engine improvements
7. 5–10% through air-traffic-management operational improvements

In 2009, NASA has developed The Environmentally Responsible Aviation Project (ERA) that is responsible to explore and document the feasibility, benefits, technical risks of vehicle concepts and identified technologies to mitigate the impact of aviation towards the environment (Hughes, 2011; Suder, 2012). Specifically, ERA focuses on subsonic transport technologies that could achieve a TRL of 6 by 2020 (N+2) time frame that are capable of being integrated into an advanced vehicle concept that simultaneously meets the project metrics for noise margin, LTO NOx emissions reduction and fuel burn reduction (Schutte, Jimenez and Mavris, 2011; Jiminez, Pfaender and Mavris,

2012). There is indeed a timeframe given for this project that is shown in the Figure 2-2. The project mainly emphasizes on the environmental issues such as noise, emission and fuel energy consumption.

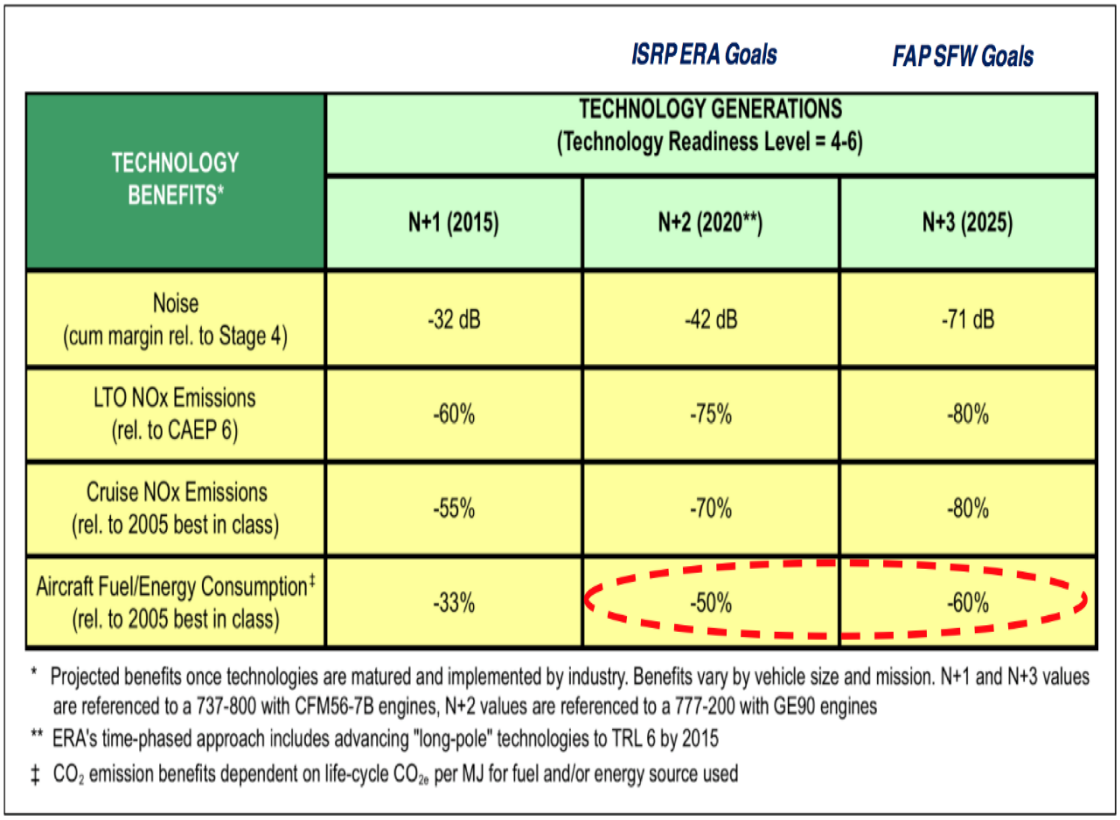

	ISRP ERA Goals		FAP SFW Goals
TECHNOLOGY BENEFITS*	TECHNOLOGY GENERATIONS (Technology Readiness Level = 4-6)		
	N+1 (2015)	N+2 (2020**)	N+3 (2025)
Noise (cum margin rel. to Stage 4)	-32 dB	-42 dB	-71 dB
LTO NOx Emissions (rel. to CAEP 6)	-60%	-75%	-80%
Cruise NOx Emissions (rel. to 2005 best in class)	-55%	-70%	-80%
Aircraft Fuel/Energy Consumption‡ (rel. to 2005 best in class)	-33%	-50%	-60%

* Projected benefits once technologies are matured and implemented by industry. Benefits vary by vehicle size and mission. N+1 and N+3 values are referenced to a 737-800 with CFM56-7B engines, N+2 values are referenced to a 777-200 with GE90 engines

** ERA's time-phased approach includes advancing "long-pole" technologies to TRL 6 by 2015

‡ CO_2 emission benefits dependent on life-cycle CO_2, per MJ for fuel and/or energy source used

Figure 2-2 Timeframe ERA Technological Plan (Hughes, 2011)

One of the solution options to achieve 50% net reduction in CO_2 emissions by 2050 is by changing the source of jet fuel from fossil-based to biomass-based known as bio-fuels as illustrated in Figure 2-3. The International Air Transport Association has aspired to use 6% biofuel blends in aircraft by 2020 by performing several test flights on blends of conventional jet fuel and bio-jet fuel from algae, Camelina, Jatropha and other plant-based feed stocks on commercial airlines and military aircraft (Fortier *et al.*, 2014). However, sustainability is the main concern for these biofuels to become the main source of the jet fuel, which is depending on their ability to conserve ecological balance between productivity, biodiversity and natural sources. It is also worth to

mention that the usage of biofuels should not compete with food production, even though they need to have high oil yield in fast-growing crops.

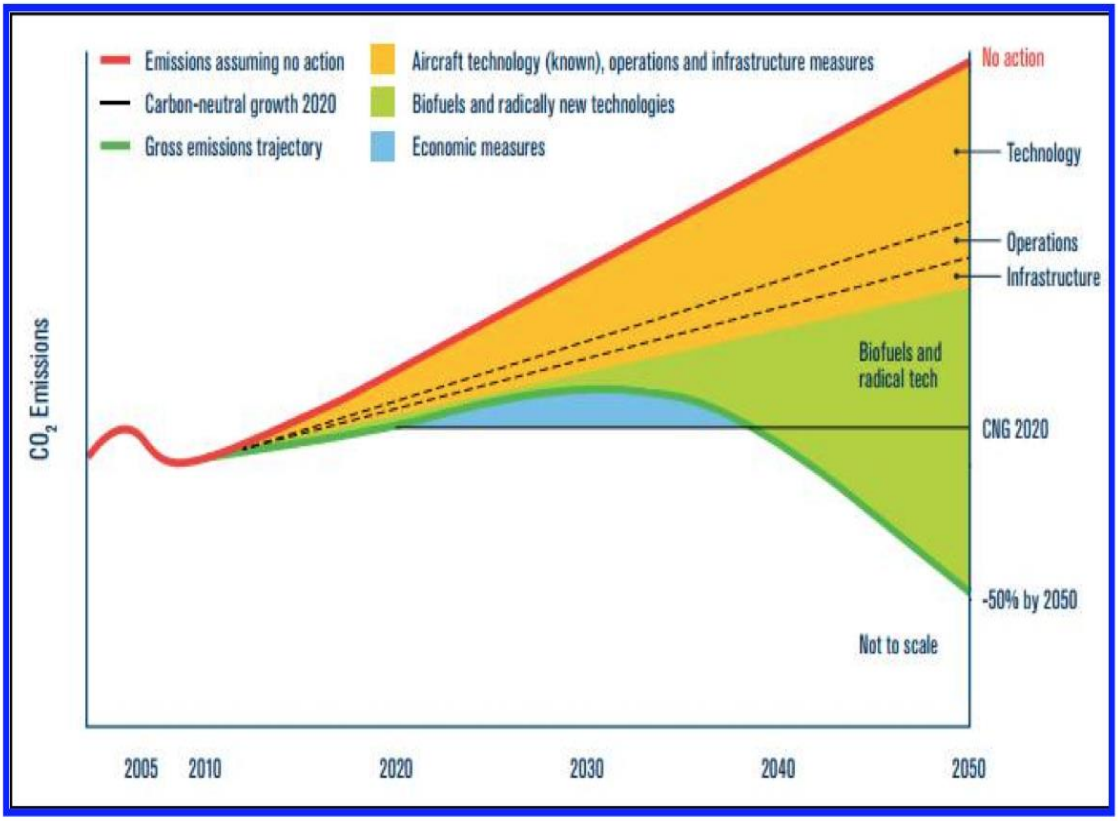

Figure 2-3 Carbon dioxide emission reduction plan (Payan *et al.*, 2014)

2.3.2 Technologies in Aviation

There are tremendous improvements in aviation technologies have been made worldwide. Numerous of researches have been conducted in universities and industries to achieve the targeted goals as mentioned in the previous section. Firstly, ERA work plan technologies are divided into two main themes, which are Airframe Technologies and Engine Technologies. Airframe technologies are categorized into three divisions; airframe lightweight structures, airframe aerodynamic and airframe noise, while Engine Technologies has four divisions; engine core, engine material, engine noise and combustors. The list of these ERA work technological plans is described in Table 2-1 and Table 2-2.

Table 2-1 ERA work plan on airframe technologies

<table>
<tr><th colspan="3">ERA WORK PLAN AIRFRAME TECHNOLOGIES</th></tr>
<tr><th>Airframe Lightweight Structures</th><th>Airframe Aerodynamic</th><th>Airframe Noise</th></tr>
<tr><td>Stitched Composites/PRSEUS</td><td>Hybrid Laminar Flow Control</td><td>Landing Gear Fairings</td></tr>
<tr><td>MEA Electro-Mechanical Actuator</td><td>Natural Laminar Flow Control</td><td>Continuous Moldline Link for Flaps</td></tr>
<tr><td rowspan="5"></td><td>Rudder Active Flow Control</td><td>Blowing on Gears</td></tr>
<tr><td>Adaptive Wing Trailing Edge Camber</td><td>Slat Cove Filler</td></tr>
<tr><td>Riblets</td><td>Slat Inner Acoustic Liner</td></tr>
<tr><td rowspan="2">Discrete Roughness Elements</td><td>Flaplets/Flap Fences</td></tr>
<tr><td>Porous Flap Edge Treatment</td></tr>
</table>

Table 2-2 ERA work plan on engine technologies

ERA WORK PLAN ENGINE TECHNOLOGIES				
Engine Core	**Engine Material**	**Engine Noise**		**Combustor**
Active Compressor Flow Control	Ceramic Matrix Composites	Over the Rotor Foam Liner		Lightweight CMC Liner
Highly Loaded Compressor	High Temp CMC Erosion Coat	Soft Vanes	HQ Tubes	Active Combustion Control
Active Turbine Flow Control	MMC's	Acoustic Splitter	Beveled Nozzle	RQL Combustor
Highly Loaded Turbine	PMC's	Active Blade Tone Control		Lean Burn Combustor
Active Film Cooling	PM Disk	Aft Cowl Liner	Nose/Lip Liner	LDI Combustor
Active Compressor Clearance Control	Advanced TBC Coatings	Rotor Sweep	Active Stator	
Active Turbine Clearance Control	Nickel Based Turbine Alloys	Variable Geometry Chevrons		
Chilled Cooling Air	PMC Fan Metal Edge	Scarfed Inlet	Combustor Liner	
	High Temp PMC Erosion Coat	Long-Cowl Common Nozzle		
		Stator Sweep & Lean		

Suder (2012) has also listed the following technologies that are being developed and/or demonstrated:

1. Drag reduction by extending the laminar flow regions using natural and hybrid laminar flow technologies
2. Weight reduction through advanced composite structures
3. Reduction of specific fuel consumption by improving both propulsive and thermal efficiency of the gas turbine engines
4. Reduction of airframe noise by reducing the noise attributed to high lift systems and landing gear
5. Reduction of propulsion noise by addressing fan, core and jet noise
6. Optimization of propulsion airframe integration to minimize the propulsion airframe aeroacoustics
7. Advancement of low-noise open rotor systems
8. Integration of Ultra High By-pass (UHB) fan, low weight nacelle systems, with advanced noise reduction technologies such as OTR (Over-The-Rotor) liners & soft vane technology
9. Integration of efficient, stable, embedded high bypass engine systems into vehicles

However, there are three challenges area include (1) reducing vehicle weight, (2) increasing the ratio of lift over drag and (3) reducing thrust specific fuel consumption. These challenges area has several technological concepts to mitigate, which are described in Table 2-3.

Table 2-3 Mitigation using technological concept for challenges area

Challenges Area	Technology Concepts	Descriptions & Advantages
Reducing weight	Stitched composites	No mechanical fasteners Reduce de-lamination Improve damage tolerance Encourage non-circular pressure vessels
	Multifunctional skins	Acoustic treatment Thermal insulation Lightning strike protection Impact deflection & indication Ice protection
	Metal structures	Curvilinear stiffeners New alloys Novel manufacturing techniques (additive & fogging)
	Active structural control	Gust load alleviation Load limiting control allocation Nodal suppression Distributed control
Increase L/D by reducing drag	Reducing viscous drag	Reduce wetted area (hybrid wing body, active flow control on control surfaces) Maintaining laminar flow (discrete roughness elements)
	Reducing induced drag	Improved span wise lift distribution (large wingspan, high AR wing, active aero elastic wing shaping control, variable camber trailing edge flaps)
	Reducing wave drag	Circulation control around aft wing
Reduce TSFC (with minimal impact on weight, drag,	Improving thermal efficiency	Turbomachinery operation with HPHT – (ceramic matrix component, environmental barrier, coating system, turbine vanes) Lean partial mixed combustors

noise & emission)		Lean direct multi-injection
	Improving propulsive efficiency	Advanced ultra-high bypass ratio propulsors (open rotor, counter rotating) Embedded engines (integrated inlet/fan embedded system)
	Hybrid electric engine	Superconducting materials, superconducting motors, cryo-inverters, cryo-coolers)

There are many technical issues when it comes to core technologies associated with high power density and highly efficient cores. This is because having higher combustor inlet pressures and temperatures inevitably cause NOx formation. Having a higher engine exhaust temperatures and jet velocities also increases noise. Suder (2012) has listed down 3 approaches to overcome these challenges:

1. To increase thermal efficiency (fuel burn), minimize core diameter and increase power density
2. To maximize engine Overall Pressure Ratio (OPR) and turbine inlet temperature and reduce cooling flow and weight

Furthermore, emission reduction is also one of the main goals in ERA plans. In order to improve specific fuel consumption and simultaneously reduce NOx formation, an advanced combustor technology is required. Below are the following approaches that may be taken to achieve the goals (Suder, 2012):

1. To use multiple concepts including Lean Partial-Mixed Combustor and Lean Direct Multi- Injection
2. To select the most promising candidates for sector rig and annular combustor development and testing

3. To develop an integrated Ceramic Matrix Composite (CMC) and Environmental Barrier Coating (EBC) liner system to provide more air for fuel/air mixing

4. To develop/demonstrate combustion control capabilities to provide stability for lean burn systems

2.3.3 Advanced Engine Technologies

Prior to the plan, more advanced engine contributes to more to the reduction of energy consumption and emission. This is illustrated in Figure 2-4. The advanced engine's propulsion system mainly focuses on three main themes; (i) cleaner, compact higher bypass ratio propulsion, (ii) unconventional propulsion-airframe integration, and (iii) hybrid gas-electric propulsion (Hathaway, DelRosario and Madavan, 2013).

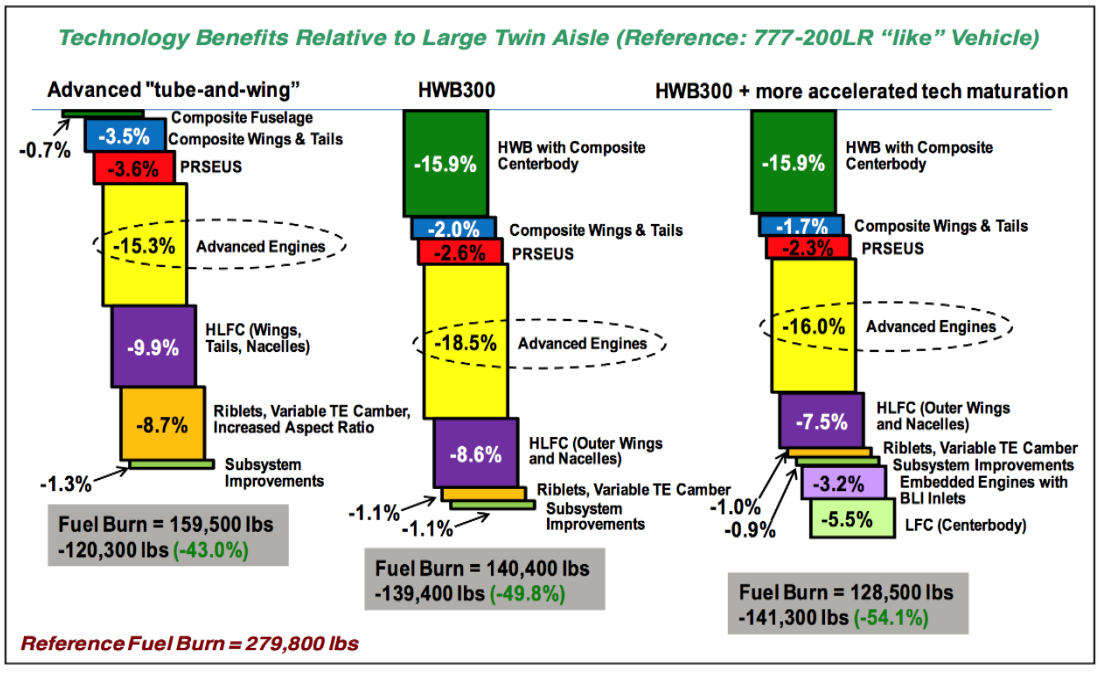

Figure 2-4 Advanced Engine contribution (Hughes, 2011)

Turbofan technology has been moving toward higher engine bypass ratios (BPR) and lower fan pressure ratios (FPR) as it is more efficient to make a smaller change in a large volume of air than a larger change in velocity (Hughes, 2011). This is shown in Figure 2-5. As the BPR increases and the corresponding FPR decreases, the amount of fuel burned decreases. However, as FPR decreases and BPR rises, the fan diameter becomes larger to produce the same thrust. Fan speed also must be kept as low as possible to reduce its noise. Thus, lower fan speeds mean lower compressor and turbine speeds in the engine core as well, since it drives a common drive shaft.

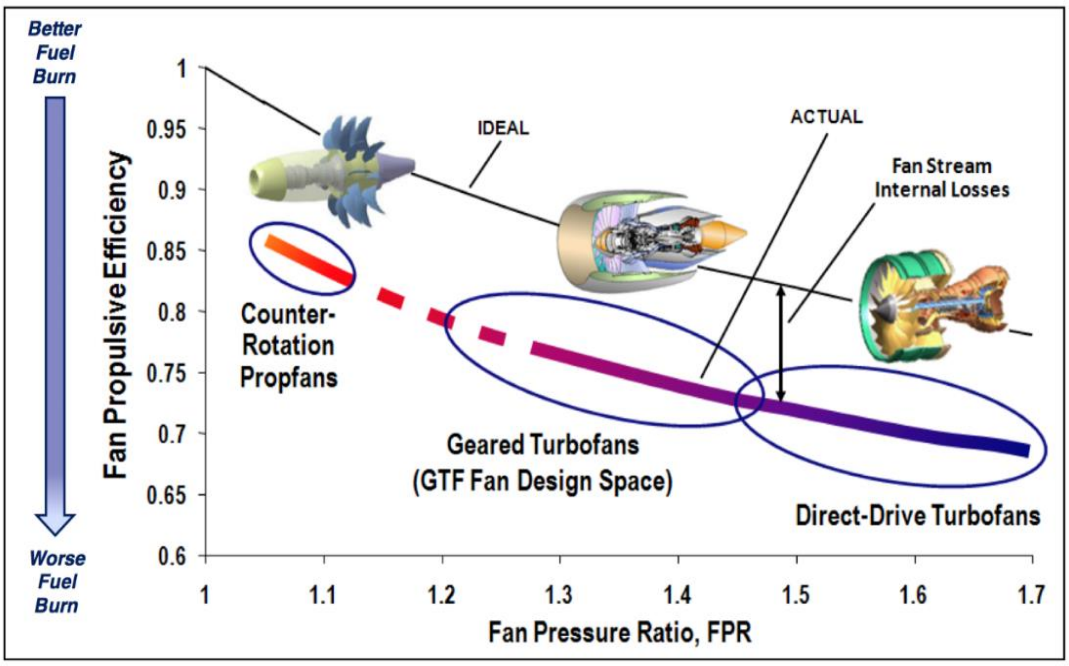

Figure 2-5 Direction of turbofan technology (Hughes, 2011)

Another viable approach is to improve thermal and propulsive efficiency. This approach requires higher cycle pressures and temperatures, improved component efficiency and reduced cooling from secondary air. Other than that, improving thermodynamic efficiency requires an increase in overall cycle pressure ratio (OPR), turbine rotor inlet temperature (TIT) and component efficiency while focusing on reducing compressor bleed air to be used for

turbine cooling. Propulsive efficiency also requires low fan pressure ratio designs (Epstein, 2013).

A hybrid gas-electric propulsion concept has been appropriately planned to achieve the main goal. The concept includes non-superconducting (e.g., Boeing Sugar Volt) or superconducting (e.g., the NASA Turbo-Electric Distributed Propulsion concept, TeDP), in which involve both gas turbine and electric motor (powered by batteries or other energy sources) on the same shaft driving the fan/propulsors, or vice versa. Safety issues and energy storage are the main concerns in the electric grid which is distributed in the propulsion system (Hathaway, DelRosario and Madavan, 2013).

Yet, so far, there are some achievements reported by Ballal and Zelina (2004) such as an increase in thrust up to 100 fold for civil aircraft and 20 fold for military aircraft based on 1930's, approaching 7 thrust-to-weight ratio, having 10000 flight hours for civil & 800 hours for military aircraft, 30% increase in a single stage compressor pressure ratio, number of stages & blade count reduced, TIT capability withstand up to 3200 degree Fahrenheit and thrust specific fuel consumption (TSFC) is reduced to 0.34. Although there is numerous potential of advanced technologies in aviation technology, some are not feasible to be implemented in the targeted year. It may need more time to be ready for use and this can be measured based on the technological readiness level (TRL).

2.4 Why Biofuels?

2.4.1 Definition of Biofuels

Biofuel is defined as a fuel comprised of mono- alkyl esters of long-chain fatty acids derived from renewable resources that can be produced by a simple chemical process known as transesterification, by which the triglycerides are

reacted with alcohols, in the presence of a catalyst (Giakoumis *et al.*, 2012) using edible, non-edible, waste vegetable oils and animal fats produced by organism (Hoekman *et al.*, 2012; Padmanabhan MR and Stanley, 2012; Ashraful *et al.*, 2014). Biodiesel (methyl or ethyl ester) is commonly used for biofuels, which is considered as a very promising fuel in transportation. It possesses similar properties with diesel fuel and has the miscible capability at any proportion of the fuel mixture (Giakoumis *et al.*, 2012) without changes in the existing distribution infrastructure of the fuel (Giakoumis, 2013). The main benefits of biofuel are its environmentally friendliness and non-toxicity as it emits lesser harmful pollutants. Whereas the main problems associated are higher production cost (largely owing to the high cost of the feedstock), susceptibility to oxidation difficulties and poor low-temperature properties (Giakoumis, 2013).

Biofuel is compatible in diesel engines in either pure form or by blending it with petroleum diesel with a certain ratio (Singh and Gu, 2010) to improve ignition quality, fuel flow properties in cold temperature, and fuel stability (oxidation). This is because biofuel quality and properties are highly dependent on the presence of fatty acid (FA) composition, the size distribution of FA and the degree of unsaturation within these FA chains in the fuel blend (Hoekman *et al.*, 2012; Ashraful *et al.*, 2014). Biofuel should have low concentrations of long-chain saturated FAME for a good low-temperature performance, and for good oxidative stability (Hoekman *et al.*, 2012). Researchers recently discovered that biofuel cetane number, cloud point and stability all increase with the presence of saturated fatty acid alkyl ester in the fuel blend (Ashraful *et al.*, 2014).

2.4.2 Available Feed stocks (generations, oil yield, standard requirements and properties & qualities of biofuels)

Biofuel feed stocks are divided into four sources; edible oils, non-edible oils, animal fats and others. The lists of available feed stocks are shown in Table 2-4.

Table 2-4 Source of feed stocks (Atabani *et al.*, 2012)

Edible oils	Non-edible oils		Animal fats	Other sources
Soybeans	Salmon oil	Coffee ground	Pork lard	Bacteria
Rapeseed	Mahua	Karanja	Beef tallow	Algae
Safflower	Pongamia	Camelina	Poultry fat	Microalgae
Rice bran oil	Cumaru	Neem	Fish oil	Tarpenes
Barley	Tall	Nagchampa	Chicken fat	Poplar
Sesame	Jojoba	Moringa		Switchgrass
Groundnut	Cottonseed	Rubber seed		Miscanthus
Sorghum	Tobacco seed	Passion seed		Latexes
Wheat	*Abutilon muticum*			Fungi
Corn	*Jatropha curcas*			Waste cooking oil
Coconut	*Croton megalocarpus*			
Canola	*Aleurites moluccana*			
Peanut	*Pachira glabra*			
Palm & palm kernel	*Terminalia belerica*			
Sunflower	*Cynara cardunculus*			

Terminologies of various biofuels generations are normally used but have no legal or regulatory meaning. Generally, the term ‘1st Generation’ refers to biofuels produced from commonly available and edible feed stocks that use well-established conversion technologies, which is derived from terrestrial crops such as sugarcane, sugar beet, maize, rapeseed, corn, and others. It, however, put enormous strain on world food markets, contributing to water shortages and destruction of the world’s forests. They also pose a threat on food security and potential crop cost increase as biofuels production are more expensive (Rawat *et al.*, 2013).

‘2nd Generation’ biofuels derived from all forms of cellulosic biomass which are produced from either advanced, non-food feed stocks or produced via advanced processing technology (or both) to address some of ‘1st Generation’ problems which have no effects on food security especially. However, there is a concern over competing land usage and sustainability which is not favourable (Brennan and Owende, 2010; Hoekman *et al.*, 2012). Biofuels, derived from second generation feed stocks, raise many issues such as poor cold flow properties, production difficulties and potential biosafety hazard due to their solid nature at room temperature (Rawat *et al.*, 2013).

The ‘3rd and 4th Generation’ of biofuel derived from ‘‘algae-to-biofuels’’ and microalgae biofuel technologies are based on algae biomass processing for biofuel production and metabolic engineering from oxygenic photosynthetic microorganisms (Lü, Sheahan and Fu, 2011). It is considered to be a technically viable alternative energy resources to major drawbacks associated with first and second generation biofuels (Brennan and Owende, 2010). The main advantage of algae and microalgae-based biofuels is that they have highest oil yield compares to other types of feed stocks because of its unique fast growing capabilities as shown in Figure 2-6.

Feedstocks	Oil content (%)	Oil yield (L/ha/year)
Castor	53	1413
Jatropha	Seed: 35–40, kernel: 50–60	1892
Linseed	40–44	–
Neem	20–30	–
Pongamia pinnata (karanja)	27–39	225–2250[a]
Soybean	15–20	446
Sunflower	25–35	952
Calophyllum inophyllum L.	65	4680
Moringa oleifera	40	–
Euphorbia lathyris L.	48	1500–2500[a]
Sapium sebiferum L.	Kernel 12–29	–
Rapeseed	38–46	1190
Tung	16–18	940
Pachira glabra	40–50	–
Palm oil	30–60	5950
Peanut oil	45–55	1059
Olive oil	45–70	1212
Corn (Germ)	48	172
Coconut	63–65	2689
Cottonseed	18–25	325
Rice bran	15–23	828
Sesame	–	696
Jojoba	45–50	1818
Rubber seed	40–50	80–120[a]
Sea mango	54	–
Microalgae (low oil content)	30	58,700
Microalgae (medium oil content)	50	97,800
Microalgae (high oil content)	70	136,900

[a] (kg oil/ha).

Figure 2-6 Percentage oil content and oil yield (Atabani *et al.*, 2012)

Biofuels properties were registered during the data collection process, namely kinematic viscosity; density; cetane number; heating values; iodine value; flash point; cold filter plugging point; weight percentage of carbon, hydrogen, oxygen and nitrogen atoms; acid value; oxidation stability; and weight content of sulphur. These properties are listed in Appendix A.1 for comparison. Hoekman et al., (2012) and Giakoumis (2013) have listed and disclosed crucial findings of the correlation of Fatty Acid Methyl Ester (FAME) composition towards the properties of the fuel. The correlation table is shown in Figure 2-7. The European and the United States have underlined several methods used, standards, and requirement for biodiesel. These standards are shown in Figure 2-8. To provide a wider picture in biofuel work, a mind map is included in Appendix A.2.

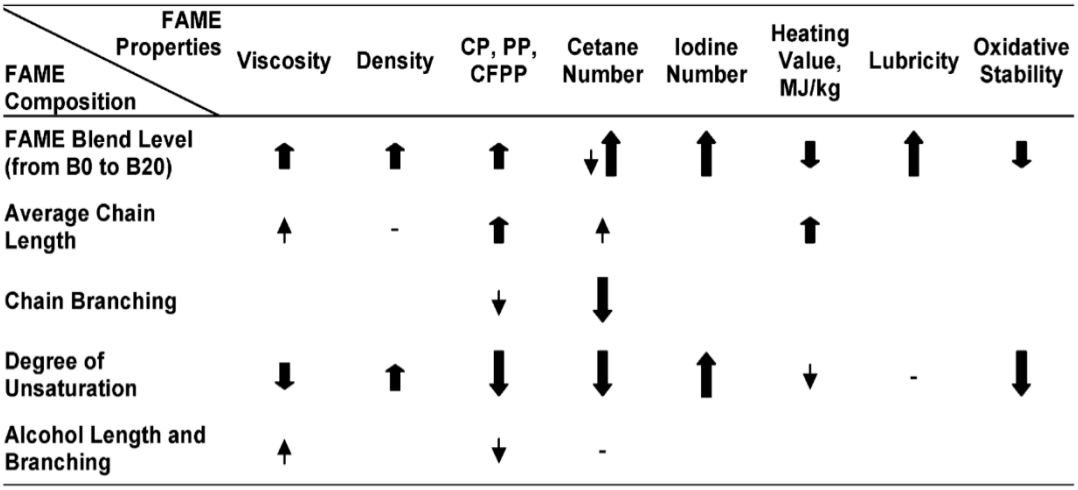

[a] *Notes*: Length of arrow indicates relative magnitude of effect.
Thickness of arrow indicates certainty/consistency of effect.
Symbol "–" indicates highly uncertain, or conflicting information.
Blank box indicates that no relevant information was found.
Impact of FAME blend level on Cetane Number depends upon the base fuel's CN.

Figure 2-7 Parameter correlations (Hoekman *et al.*, 2012)

U.S. and European specifications for biodiesel (B100) and biodiesel blends.

Property	Biodiesel blendstock (B100)				B6–B20 Blends	
	U.S. (ASTM D6751-08)		Europe (EN 14214)		U.S. (ASTM D7467-08)	
	Limits	Method	Limits	Method	Limits	Method
Water and sediment (vol.%, max)	0.05	D 2709	0.05	EN 12937[g]	0.05	D 2709
Total contamination (mg/kg, max.)			24	EN 12662		
Kinematic viscosity @ 40 °C (mm^2/s)	1.9–6.0	D 445	3.5–5.0	EN 3104/3105	1.9–4.1	D 445
Flash point, closed cup (°C, min)	93	D 93	101	EN 3679	52	D 93
Methanol (wt.%, max.)	0.20[a]	EN 14110	0.20	EN 14110		
Cetane no. (min)	47	D 613	51	EN 5165	40	D 613
Cloud point (°C)	Report[d]	D 2500	Country Specific[d]		Report[d]	D 2500
Sulfated ash (wt.%, max.)	0.020	D 874	0.020	EN 3987		
Total ash (wt.%, max.)					0.01	D 482
Gp I metals Na + K (mg/kg, max.)	5.0	EN 14538	5.0	EN 14108/14109		
Gp II Metals Ca + Mg (mg/kg, max.)	5.0	EN 14538	5.0	EN 14538		
Total Sulfur (ppm, max.)	15[b]	D 5453	10	EN 20846	15	D 5453
Phosphorous (ppm, max.)	10	D 4951	4	EN 14107		
Acid no. (mg KOH/g, max.)	0.50	D 664	0.50	EN 14104	0.3	D 664
Carbon residue (wt.%, max)	0.05	D 4530	0.30[e]	EN 10370	0.35[e]	D 524
Free glycerin (wt.%, max.)	0.02	D 6584	0.02	EN 14105/14106		
Total glycerin (wt.%, max.)	0.24	D 6584	0.25	EN 14105		
Mono glyceride (wt.%, max)			0.80	EN 14105		
Diglyceride (wt.%, max)			0.20	EN 14105		
Triglyceride (wt.%, max)			0.20	EN 14105		
Distillation (T_{90} °C, max.)	36[c]	D 1160			343	D 86
Copper strip corrosion (3-h at 50° C, max.)	No. 3	D 130	No. 1	EN 2160	No. 3	D 130
Oxidation Stability (h @ 110 °C, min)	3.0	EN 14112	6.0	EN 14112	6	EN 14112
Linolenic acid methyl ester (wt.%, max)			12.0	EN 14103		
Polyunsaturated acid methyl esters (wt.%, max)			1.0	prEN 15799		
Ester Content (wt.%, min)			96.5	EN 14103	6–20 vol.%	D 7371
Iodine Value (g I_2/100 g, max.)			120	EN 14111		
Density (kg/m^3)			860–900	EN 3675		
Lubricity @ 60 °C, WSD, microns (max.)					520	D 6079
Cold Soak Filterability (seconds, max.)	360[f]	D 7501				

[a] Alternatively, flash point must be >130 °C.
[b] For blending with ULSD. For other fuels, higher sulfur levels are allowed.
[c] Atmospheric equivalent T-90 point.
[d] Low temperature properties are not strictly specified, but should be agreed upon by the fuel supplier or purchaser.
[e] This limit is based on the bottom 10% fraction of the fuel, not the entire fuel.
[f] 200 s max. for use in diesel blends at low temperature (<−12 °C).
[g] Method EN 12937 measures total water (in units of μg/g), but not sediment.

Figure 2-8 Standard requirements (Hoekman *et al.*, 2012)

2.4.3 Potential of 3rd Generation of Biofuels

In attempt to resolve energy crisis, studies on microalgae-based liquid fuel had begun in the mid-1980s during the World War II by the German scientists to extract lipids from diatom and soon later in the US by a group of scientists at the Carnegie Institution of Washington (Huang *et al.*, 2010). Microalgae have been suggested as potential candidates for fuel production as they are capable of meeting globally sustainable demand for transport fuels (Atabani *et al.*, 2012) . This is mostly contributed by a number of advantages including higher energy yields per hectare, higher photosynthetic efficiency, higher biomass production, higher growth rate and non-requirement of agricultural land compared to other energy crops (Huang *et al.*, 2010; Mata, Martins and Caetano, 2010). Some microalgae were also reported as good producers of hydrogen which produce high energy and almost no pollution (Suali and Sarbatly, 2012). As a matter of fact, microalgae biofuel has properties similar to those of petro diesel in terms of density, viscosity, flash point, cold flow and heating value. No other potential sources of biodiesel are realistically at the same par as microalgae to replace petrol diesel sustainability. (Rawat *et al.*, 2013).

Microphytes or microalgae are unicellular or multicellular photosynthetic microorganisms that can be categorized as prokaryotic (*Cyanophyceae*) or eukaryotic (*Chlorophyta*) organisms that photosynthesize light and are among the oldest living microorganisms on Earth (Brennan and Owende, 2010; Demirbas, 2010; Mata, Martins and Caetano, 2010; Maity *et al.*, 2014; Zhu *et al.*, 2014). Microalgae is a simple photosynthetic organisms living in aquatic environments (saline or freshwater) with lacks of roots, stem, leaves and have chlorophyll ‘a’ (Brennan and Owende, 2010; Demirbas, 2010; Tüccar and Aydın, 2013; Zhu *et al.*, 2014).

Microalgae transforms the solar energy into the carbon storage products, leading to large amount of lipids and fatty acids accumulation quantity inside

their entire cells (A, Padmanaban and Subramaniam, 2013; Tüccar and Aydın, 2013), including TAG (triacylglycerol), which can be transformed into biodiesel, bioethanol and bio-methanol (Hoekman *et al.*, 2012; Lam and Lee, 2012; Maity *et al.*, 2014). TAG is a glycerol esterified with three fatty acids, and in the presence of alcohol, it reacts to form biodiesel with glycerol as a by-product (Suali and Sarbatly, 2012). Depending on species, microalgae produce many different kinds of hydrocarbons, other complex oils (Chisti, 2007), lipids and fatty acids in membrane components (Amin, 2009). Fatty acids come in two types, which are saturated (animal products) and unsaturated (most vegetable oils). Microalgae lipids are mostly neutral lipids with a lower degree of unsaturation (Singh and Gu, 2010). There are 50,000 microalgae species, but only about 40,000 species of them have been studied and analysed until now with many more remain unidentified. Algae are often classified into the following major groupings (Hoekman *et al.*, 2012; Zhu *et al.*, 2014):

- Cyanobacteria (*Cyanophyceae*)
- Green algae (*Chlorophyceae*)
- Yellow-green algae (*Xanthophyceae*)
- Golden algae (*Chrysophyceae*)
- Red algae (*Rhodophyceae*)
- Brown algae (*Phaeophyceae*)
- Diatoms (*Bacilleriophyceae*)
- Pico-plankton (*Eustigmatophyceae*)

There is no one strain or species of algae that can be safely claimed to produce the highest oil yield for biodiesel. However, diatoms and green algae (*Chlorophyceae*) are the most promising species for biodiesel although several other types have also been reported (Demirbas and Fatih Demirbas, 2011; Hoekman *et al.*, 2012). Green microalgae has much higher lipid production rate

(mg/L/day) than other types of microalgae. The lipid content (% dry weight biomass) is in such decreasing order: Lipid Algae green > Algae Yellow-green > Algae red > Algae blood-red > Algae blue- green and lipid productivity (mg/L/day) was observed Algae green > Algae red (Maity *et al.*, 2014).

Chlorella is a single-celled, largest strain green alga that is capable of producing more than 63% lipid content on a dry biomass basis and of adapting at extreme culture conditions. The biodiesel produced from this species were acid methyl ester, linoleic acid methyl ester and oleic acid methyl ester (Suali and Sarbatly, 2012). *Chlorella sp.* and *Chlorococcum sp*. are deemed to be the best for biofuel production to be used in biodiesel, bio-ethanol and hydrogen production (Mata, Martins and Caetano, 2010; Maity *et al.*, 2014). Biodiesel produced from *Chlorella* complies with ASTM 6751, the US Standard for biodiesel with the heating value reported of being 41 MJ/kg (Suali and Sarbatly, 2012). The making of biodiesel and jet fuel from microalgae involves several processes that are systematically shown in Appendix A.3. However, technology for conversion of biomass, are preliminary for: (1) direct use, (2) blending with petro diesel, (3) microemulsions with solvents or alcohols, (4) pyrolysis, and (5) transesterification (Rawat *et al.*, 2013). Brennan and Owende (2010) have listed the ideal algal strain characteristics for biofuel production such as:

(1) High lipid productivity

(2) Robust and able to survive the in photo bioreactors and open pond

(3) Have high CO_2 sinking capacity

(4) Have limited nutrient requirements

(5) Tolerant to a wide range of temperatures

(6) Provide valuable co-products

(7) Fast productivity cycle

(8) Display self- flocculation feature

Benefits of biofuels over traditional fuels include greater energy security and foreign exchange savings and reduced environmental impact and socioeconomic issues (Demirbas, 2010). According to biodiesel standard published by the ASTM, biodiesel from microalgae oil is similar in terms of properties to the standard biodiesel and is also more stable when looking at their flash point values. These advantages and disadvantages are grouped in each theme and are elaborated in Appendix A.3.1 and A.3.2. Sustainability and environmental friendliness issues are commonly emphasized in the literature reviews. In terms of cost effectiveness, it depends on the processing stage. The main drawbacks mentioned in some reviews are mostly related to biofuel properties and also lack of information. Additionally, it should be noted that these biofuels are relatively new to engine performance applications and more efforts are needed for them to be fully developed.

2.5 Pulse Detonation Engine

2.5.1 Introduction to PDE

Pulse detonation engines (PDE) are unsteady high pressure propulsion systems that is dependent on the repetitive mode of detonative combustion to develop thrust (Ebrahimi and Merkle, 2002; Kaemming, 2003; Qiu *et al.*, 2012). It differs from conventional propulsion systems in two ways: unstable operation and detonation combustion (Ma, Choi and Yang, 2004; Li *et al.*, 2009). This promising new engine uses a detonation wave which is extremely fast and thermodynamically efficient process for converting chemical energy in a combustible mixture to mechanical energy and tremendous kinetic energy (Li and Kailasanath, 2001; Wu, Ma and Yang, 2002; Li *et al.*, 2013; Frolov, 2014) compared to deflagration wave in the combustion process (Hutchins and Metghalchi, 2003).

In principle, pulse detonation engines are very simple devices that consist of primarily a tube in which a fuel/oxidizer mixture is initiated repeatedly at either

the closed or the open end of a detonation chamber (Kailasanath, 2000) resulting in the ejection of combustion gasses from the engine at very high velocities followed blowdown process and refill cycle (Hitch, 2002). A cycle has three main components: detonation and blow down of burned gasses, purging of the expanded burned products and refilling of the tube with fresh reactants in a constant volume combustion chamber (Harris *et al.*, 2002; Wintenberger and Shepherd, 2003). Most PDE studies employ unsteady gas dynamic calculations to determine the instantaneous pressures and forces acting on the surfaces of the device and integrate them into a cycle to determine thrust performance (Heiser and Pratt, 2002)**.**

2.5.2 History of PDE

During early development of jet-propulsion engines, it was known from thermodynamic analysis cycle that an engine is dependent on a constant-volume combustion process in order to achieve higher thermodynamic efficiency than a constant pressure engine. The earliest non-piston-engine-type prime mover known to employ constant volume combustion with a deflagration, not a detonative reaction, was the Holzwarth gas turbine manufactured by Brown-Boveri (now ABB) in Switzerland during the early part of the last century. Its success was, however, limited (Kentfield, 2002a).

Eidelman, Grossmann, Lottati (1991), Ma, Choi and Yang (2005) have summarized the first report on intermittent detonation attributed to Hoffman in 1940 using acetylene and benzene as fuels with oxygen. After the work was terminated during World War II, Nicholls and co-workers reinitiated the effort in the 1950s by experimenting a series of single- and multiple- cycle detonation experiments with different mixtures of hydrogen, oxygen, acetylene and air in a six-foot tube. In a similar setup, Krzycki performed an experimental investigation using propane/air mixtures, but, he concluded that the intermittent detonation device was not deemed to be promising for propulsion application and had to be

suspended in the late 1960s. The JPL work was directed to some very specific applications such as propulsion efficiency. Helman et al. in Naval Postgraduate School (NPS) re-examined the PDE concept in the late 1980s and successfully demonstrated a self-aspirating feature of air breathing PDE using ethylene/oxygen and ethylene/air mixtures. Since then, there has been a growing interest in PDEs as a propulsion technology for both air-breathing and rocket systems. While Camblier and Adelman carried out the first quasi-zero-dimensional numerical simulations using a modern CFD method of a non-steady pulsed detonation, engine cycle is incorporated into finite-rate chemistry. More detailed historical background have also been presented in Eidelman, Grossmann and Lottati (1991).

2.5.3 Literature surveys on PDE

Researchers throughout the world have done an extensive work on PDE. In addition to Ma, Choi and Yang (2006) have also summarized the findings of both numerical and experimental work on air breathing PDE using hydrogen fuel in a review article. Meanwhile, Roy *et al.* (2004), and Kailasanath (2000, 2003, 2006) have presented detailed review discussions of PDE work. A review of PDE is presented in a mind map (Appendix A.4) which summarizes the entire topic covered across their identified themes based on keywords and illustrates the wide breadth of PDE research. Appendix A.4.1 describes the works in PDE that have been studied. It should be noted, however, that two previous numerical studies have been conducted to investigate detonation characteristics of biofuel and the feasibility of biogas; by Shimada *et. al.* (2011) and Dairobi *et. al* (2013) using bio-ethanol and biogas respectively. Shimada at al. utilized STANJAN for 2D bio-ethanol chemical reaction to study two-phase detonation of bio-ethanol/air, which showed that the biofuel resulted in a smaller cell size. Biogas studies also suggested that this requires supplementary additives for higher detonation pressure.

In general, the Humphrey cycle consists of four processes. The first is an isentropic compression that occurs ahead of the detonation wave in PDEs. Compression is then followed by constant volume combustion. Another isentropic process transforms into combustion products back to atmospheric pressure. In PDE, the rarefaction waves cause this expansion process to a final stage involving an isobaric process that brings the cycle back to the beginning. Figure 2-9 illustrates the PDE processes and Table 2-5 describes the detail of the process in order.

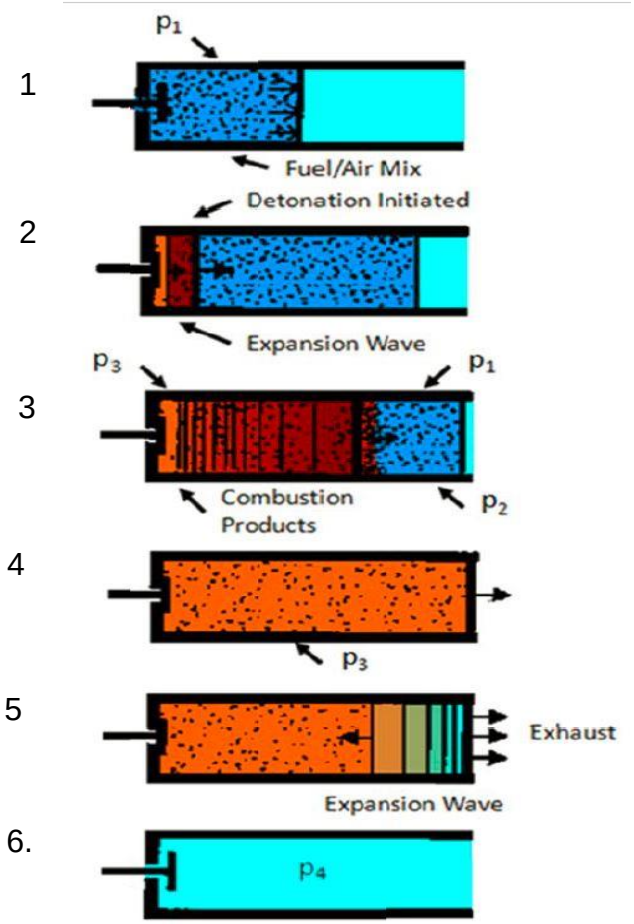

Figure 2-9 PDE Operation Process (Blanco, 2014)

Table 2-5 PDE Operations Process

No.	Process
1.	Mixtures Filling Fully/Partially Fuel and oxidizer are admitted into the combustion chamber by a combination of unsteady and steady expansions (Wintenberger and Shepherd, 2003) through the inlet valves and closed at the beginning of each cycle.
2.	Initiation/Ignition The detonation is initiated either directly or indirectly through deflagration to detonation transition (Hutchins and Metghalchi, 2003) near the head end.
3.	Wave Propagation The deflagration wave propagates downstream towards the unburned mixture which rapidly transitions into detonation generating a series of compression waves or shock waves ahead of the flame increasing pressure, density and temperature, thus producing substantial head pressure at the closed end, which in turn yields the thrust (Brophy, Sinibaldi and Damphousse, 2002; Hutchins and Metghalchi, 2003; Li *et al.*, 2013) while rarefaction waves follow the detonation wave (Hutchins and Metghalchi, 2003) to reduce the velocity to zero at the closed end of the tube (Kailasanath, 2000).
4.	Wave Exit The detonation wave then ejects a slug of burned gas from the exit of the combustion chamber at high velocity, yielding thrust pulse (Hitch, 2002).
5.	Reflecting Wave When the detonation wave leaves the tube, a strong set of expansion waves propagates towards the closed end of tube (Kailasanath, 2000),

	reducing the pressure to a constant 'plateau pressure' value (Kailasanath, Patnaik and Li, 2002) and velocity (Ebrahimi and Merkle, 2002) and simultaneously removes hot products from thrust tube (Brophy, Sinibaldi and Damphousse, 2002) at lower rate. Thus, thrust reduces gradually (Li and Kailasanath, 2001). The upstream-traveling expansion waves passing through the downstream-traveling Taylor wave interact and travel back towards the open end causing a further decrease in the pressure and acceleration of the fluid towards the open end (Wintenberger and Shepherd, 2003) leading to a more complicated shock wave structure (Ma, Choi and Yang, 2004).
6.	<u>At the nozzle</u> The primary shock wave further proceeds through nozzle and reflects from the convergent wall. The situation resembles shock diffraction over a convex curved wall. In inner region near the edge of the nozzle exit, the flow accelerates from subsonic to sonic due to the expansion waves emanating from the edge, and finally, a Prandtl-Meyer expansion fan is formed (Ma, Choi and Yang, 2004).
7.	<u>Blowdown and purging.</u> Purging is done when combustion products are expelled from the tube. There are two distinct cycles in PDE operations; single or multicycle. For multicycle, the tube is filled with combustible mixtures that pass through valves. The delay of filling time for the next cycle would undeniably affect performance.

Several issues from design and analysis of PDE phenomena also arise, including 1) initiation of a sustainable detonation wave, 2) transition of a deflagration wave to a detonation shock, 3) appropriateness of propellant procedures, 4) heat transfer to the chamber walls and the resultant propellant heating before detonation, and 5) generation of acoustic wave levels (Ebrahimi and Merkle, 2002). Table 2-6 listed several challenges and difficulties in PDE.

Table 2-6 List of challenges and difficulties of PDE

Challenges/Difficulties	References
Creating a droplet-free or extremely fine (droplets diameters <10 μm) fuel and air mixture quickly enough and initiating or transitioning detonations at a high frequency to create practical thrust levels with liquid HC fuel	(Brophy, Sinibaldi and Damphousse, 2002; Li and Kailasanath, 2003; Panicker *et al.*, 2007; Tucker, King and Schauer, 2008; Carter and Lu, 2011; Lu, Carter and Wilson, 2011) (Lu, Carter and Wilson, 2011; Li *et al.*, 2013)
Coupling the inlet flow with unsteady flow in the tubes that degrades performance, and the lack of common understanding about the influence of nozzles on static PDE performance modelling	(Heiser and Pratt, 2002; Wintenberger and Shepherd, 2003) (Ma, Choi and Yang, 2004)
Attaining repetitive and consistent detonations at highly unsteady pressure and thermal loading that requires cooling or heat exchanger	(Kailasanath, 2000; T. H. New *et al.*, 2006)
Auto-ignition or premature ignition from the interaction between shock waves generated by impulsive jets and their reflections from the confining walls in the mixture resulted in irregular firing, loss of thrust and unbalanced stresses and vibrations ensuing material damage in harsh and high temperature	(Kailasanath, 2003; T. H. New *et al.*, 2006)
High frequency with minimum ignition energy, injection of the fuel-oxidizer mixture and difficulty in achieving detonations in the shortest distances	(Hutchins and Metghalchi, 2003; T. H. New *et al.*, 2006; T. New

possible after ignition even in multiple chambers and harsh environment	*et al.*, 2006; Rakitin and Starikovskii, 2010; Lu, Carter and Wilson, 2011)
Noise during operations	(Panicker, Wilson and Lu, 2006)
Air intake, mixing chamber design and nozzle designs that perform well over the full range of Mach numbers in unsteady operations	(Hutchins and Metghalchi, 2003; Kailasanath, 2003)
Influence of rotational speed of the turbine on fluid dynamic processes	(Qiu *et al.*, 2012)
Lack of understanding in DDT process involving complex chemistry, multiphase mixtures, turbulence and unsteady pressure waves	(Li *et al.*, 2009) (Kailasanath, 2000)
Lower thrust density due to cyclic nature and pressure ratio recovery at the inlet	(Kaemming, 2003)

Since PDE technologies have received considerable attentions as means to achieve revolutionary advancements, myriads of novel innovation techniques are brought under the spotlight to address drawbacks and challenges of PDE-related issues as mentioned above. These innovations are explored and developed to account for the deflagration-detonation transition, initiation techniques, fuel mixing, valve timing, NOx emission and noise. In Appendix A.4.2, these enhancement techniques proposed and its' side effects are further discussed and elaborated. Also, Table 2-7 and Table 2-8 summarize PDE advantages and disadvantages of PDE accordingly.

Table 2-7 Advantages of PDE

Advantages	References
High energy heat release rate and propulsive thrust	(Panicker, Wilson and Lu, 2006; Nikitin *et al.*, 2009) (T. New *et al.*, 2006)
High specific impulse compared with ramjet under similar operating condition	(Nikitin *et al.*, 2009)
Simple manufacturing and operation, less moving parts, low cost, high range flight Mach numbers, low weight and more compact	(Harris *et al.*, 2002; Kailasanath, Patnaik and Li, 2002; Panicker, Wilson and Lu, 2006; Caldwell and Gutmark, 2007; Tucker, King and Schauer, 2008; Singleton *et al.*, 2009; Vutthivithayarak, Braun and Lu, 2011) (Lu, Carter and Wilson, 2011)
High thermodynamic cycle efficiency, operation stability and reliability	(Wu, Ma and Yang, 2002; Ma, Choi and Yang, 2004; Panicker, Wilson and Lu, 2006; Caldwell and Gutmark, 2007; Vutthivithayarak, Braun and Lu, 2011)
Improved fuel efficiencies in high speed and long ranges	(Kaemming, 2003; Panicker, Wilson and Lu, 2006) (Hinkey *et al.*, 1997)
Flexible to be used with other developing technologies	(Kaemming, 2003; Panicker, Wilson and Lu, 2006; Lu, Carter and Wilson, 2011)

Table 2-8 Disadvantages of PDE

Disadvantages	References
Noise	(Panicker, Wilson and Lu, 2006)
Bulkier liquid fuelled PDEs	(Panicker *et al.*, 2007)
Noticeable total pressure loss during both the filling (valve) and detonation portion of the cycle	(Brophy, 2009) (Kaemming, 2003)
Additional loss mechanism which required cooling for increased longevity	(Brophy, 2009)
Lower thrust density or thrust-per-unit cross-sectional area than turbo-ramjet engine	(Kaemming, 2003)
Very low thrust and SFC, at low speeds	(Kaemming, 2003)
Requiring a long runway for take-off	(Kaemming, 2003)
Requiring an additional mixture on-board oxygen generator	(Li and Kailasanath, 2003)

2.6 Concluding Remarks

A wide literature review has been presented chronologically in the chapter to highlight global issues, potential technological advancement in aviation and opportunities of biofuels in the present context. It is very crucial to understand the issues before identifying potential solutions. Potential mitigation measures relating to the energy and environmental crisis can be resolved by using

alternative energy sources, in this context, is the use of biofuels. Furthermore, it is also shown that advanced engine provides an effective solution. Following successful flights of many commercial aircraft running with different biofuels, it proves that they are, indeed, a viable option to sustain the environment as well as the energy. Notably, a comprehensive review on a pressure-rise combustor is also included to recognize potential of biofuels in a novel type of combustor. This review in PDE compasses the history behind PDE technology, works on PDE, its operations, advantages, challenges and enhancement techniques in PDE. To summarize the literature surveys on biofuels and PDE, three mind maps are included in Appendix A for a clear overview on the topics. By referring to the mind maps, this work covers a few topics highlighted in red to ensure that direction of the research can be tailored to the breadth work of the field.

3 EVALUATION OF BIOFUEL – SPRAY ANALYSIS

3.1 Introduction

The chapter focuses on the modelling of evaporation and spray penetration for alternative fuels. Based on many numerical analysis and experimental works done by researchers to characterize micro and macroscopic droplet atomization and penetration process, studies on the different type of alternative fuels are still rarely done. It is equally important to underline issue of environmental sustainability and at the same time, to understand the behaviour of these alternative fuels. It also believed that spray behaviour determines the combustion performance. The difference between the present study and Mazlan et al. (2011) is on how the modelling is conducted. As an extension of their work, different alternative fuels are used for the analysis. To the best of author's knowledge, this study is the first to analyse atomization and spray penetration of Microalgae biofuel. The analytical comparisons are essential as this '3rd generation' of biofuels has been commercialized and used for aviation purposes. This chapter begins with a focused literature on works have been done on sprays analysis and their outcomes. It is then discussed on the approach being used adopting methods conducted by Mazlan et al. (2011) and equations in FLUENT manual book. Given the thermochemical properties of particular alternative fuels, the evaporation and penetration of each droplet is modelled, compared and analysed.

The extension model approach is presented and validated for alternative fuels, namely, Kerosene (KE), Ethanol (ETH), Methanol (MTH), Microalgae biofuel (MA), Jatropha biofuel (BJ) and Camelina biofuel (BC). The results for atomization and spray penetration are shown in a time variant condition. Comparisons have been made to visualize the evaporation and penetration of fuel's droplets. The vapour pressure tendencies are found to have significant effects on the transient shape of the evaporation process. In a given time frame, ethanol fuel exhibits the highest evaporation rate, followed by methanol,

kerosene and other biofuels. Methanol also propagates the farthest distance, followed by ethanol and kerosene. It is, however, found that all biofuels have a shorter penetration length in the given time. These give penalty costs to biofuels emissions formation. The influences of initial conditions such as temperature and droplet velocity are also explored numerically. High initial temperature and velocity could potentially accelerate evaporation rate. Nevertheless, high initial temperature results in low penetration length, while high initial velocity produces contrasting results.

3.2 Literature Review

Increasing thermal efficiency can optimize combustion process and simultaneously reduce emission (Ejim, Fleck and Amirfazli, 2007). One of the methods is based on spray characteristics. Spray behaviour is a critical factor in an engine performance (Chen *et al.*, 2013) and emission that mainly influenced by the atomization of the fuel, the motion, evaporation and the mixing of fuel with air (Jiang *et al.*, 2010). Jiang et al. (2010) have described that in spray combustion process, several elements are put into considerations: atomization, liquid transport, vaporisation, and the combustion. Spray atomization is a process which involves breaking-up bulk of liquid jets into small droplets using atomizer or nozzles (Ejim, Fleck and Amirfazli, 2007). On the other hand, spray penetration is defined as propagation of droplets until they are fully vaporized. Liquid sprays are formed by discharging liquid at a high velocity from a nozzle. The use of spray is extensive in agriculture, internal combustion engine and gas turbine combustors. A high velocity liquid induces break-up streams to droplets and ensures sufficient inertial forces to transfer momentum, matter and heat effectively to gas environment (Ghosh and Hunt, 1994). Spray zones can be classified into three zones; (1) at the nozzle tip where liquid discharge velocity is much larger than the stream velocity, (2) forced jet zone where the droplets' velocity decelerate and comparable to stream's velocity, and (3) falling droplet zone where the droplets' velocity is lower than the terminal velocity (Ghosh and Hunt, 1994; Sazhin, Feng and Heikal, 2001).

Chen et al. (2013) have classified fuel spray behaviours into two categories: (1) macroscopic conditions and (2) microscopic conditions. They further added that macroscopic parameters include spray tip penetration and cone angle while the microscopic parameters are related to droplet velocity, size and distribution. From the point of views of macroscopic spray properties, its tip penetration is directly proportionate to injection pressure, time duration and blend of biodiesel mixing ratio. However, higher blending ratio results in a smaller cone angle, area and volume, but higher velocity of spray. These effects lead to an overall reduction of quality in spray atomization. In contrast, spray tip penetration is inversely related to ambient pressure, so, as ambient pressure increases, spray cone angle becomes larger. Spray volume is also increased as the injection pressure increases until it reaches a certain limit.

For microscopic spray properties, Sauter Mean Diameter (SMD) is increased at a higher ambient pressure, radial and axial distance from the nozzle tip and also, at higher blending mixing ratio. However, a higher blend of mixing ratio results in a more concentrated fuel distribution, larger Mass Median Diameter (MMD) and span factor due to higher viscosity and surface tension. In contrast, again, higher injection pressure reduces SMD, but increases the peak droplet's size volume frequency distribution. The reduction in droplet's diameter and the increase of surface temperature were both found to be strongly dependent on fuel properties. For faster vaporization rate of the droplets, the fuel should have a combination of high vapour pressure, low latent heat thermochemical properties (Gu, Basu and Kumar, 2012), low viscosity, low surface tension, low density (Ejim, Fleck and Amirfazli, 2007) and low boiling point. They also added that pre-heating process could improve vaporization performance of the SMD reduction.

Yule & Filipovic (1992) have predicted that the break-up length which refers to the distance of fully atomized droplet is equivalent to 35% of the penetration length. Later, Ryu et al. (2005) showed that the spray penetration length is

directly proportional to the power of ¼ of back pressure. They also discovered that spray impingements with ambient density results in a greater influence on fuel evaporation and mixture as compared to pressure and temperature intake condition. Concurrently, Chen et al. (2013) concluded that break-up length increases with diameter of the nozzle, but, reduces with injection pressure. For the time variant of spray penetration, Kostas et al. (2009) found that spray tip penetration is proportional to time power of 3/2 at early stage until it reaches maximum velocity. However, they added that spray tip velocity is found to be the square root of time at the same stage. Lee & Park (2002) have studied both experiment and numerical analysis of fuel break-up using Kelvin-Helmholtz (KH) and Rayleigh-Taylor (RT) hybrid model in high-pressure diesel injection sprays. They discovered that KH breakup occurs near the injector, while RT occurs at the secondary breakup and distributes wider. For further improvement, Roisman et al. (2007) have included shock wave propagation in the air after injection stage in their paper. The normal adiabatic shock wave has proven its impact on the tip velocity immediately after the injection stage.

3.3 Methods

In the beginning, initial conditions are defined. These include the temperature, velocity, diameter and volume of the particle. The ambient conditions are also specified such as velocity, temperature, density, pressure and viscosity of the gas. These initial conditions are compiled in Table 3-1. For comparison purposes, several thermochemical properties used are shown in Table 3-2.

Table 3-1 Initial Conditions and Constant Parameters

Properties	Value
Particle's temperature, $T_P\ (K)$	294.15
Particle's velocity, $V_p\ (m/s)$	100
Particle's diameter, $d_P\ (m)$	2E-5
Particle's volume, $\forall_P (m^3)$	4.19E-15
Particle's radius, $r_P\ (m)$	1E-5
Gas flow velocity, $V_g (m/s)$	0
Gas flow temperature, $T_g\ (K)$	1000
Gas density, $\rho_g\ (kg/m^3)$	0.353
Gas ambient pressure, $P_g\ (Pa)$	101325
Gas viscosity, $\mu_g\ (m^2/s)$	4.27E-5

Table 3-2 Thermochemical Properties

	KE	ETH	MTH	MA	BC	BJ
$\boldsymbol{MW\ (kg/mol)}$	0.182	0.046	0.032	0.169	0.156	0.157
$\boldsymbol{h_{fg}\ (kJ/kg)}$	251	846	1100	251*	251*	251*
$\boldsymbol{c_p\ (J/kg.K)}$	2010	2300	2510	2010*	2010*	2010*
$\boldsymbol{k_g\ (W/m.K)}$	0.15	0.17	0.17	0.15*	0.15*	0.15*
$\boldsymbol{\rho_p\ (kg/m^3)}$	810	789	792	755.2	753	749
$\boldsymbol{\mu_p\ (N.s/m^2)}$	0.0016	0.0011	0.0006	0.0039	0.0033	0.0037

*(Lefebvre and Ballal, 2010)

Modelling an evaporation process is necessary to ensure that fuels are completely vaporized in the mixture before they are burned. Equations in the FLUENT Manual book are used to simulate the process. In FLUENT, the droplet trajectory is obtained by integrating drag force, gravitational force and other additional force acting on the droplets. In order to assess their evaporation process, some assumptions are made to simplify the calculation. The assumptions are:

1. The droplet is a spherical single droplet where convective effect is neglected;
2. The initial droplet diameter is defined for simplicity;
3. No radiation heat transfer is included during the evaporation process;
4. Gas is stagnant and the droplet is evaluated in a stationary condition;
5. The bulk mole fraction of those fuels is assumed as zero, as we are considering that the fuel is evaporating into pure air.

From the above assumptions, it is worth-noting that droplets produced by a pressure swirl atomizer are initially a well-defined spherical droplet. With the exception of radiation heat transfer, only convection heat transfer is considered. However, practically, radiation heat transfer are considered when the system at high pressure and temperature. Considering that the fuel is evaporating into pure air, the molar flux of droplet's vapour in equation (3-14) is reduced and term $c_{i,\infty}$ is equal to zero.

Reynolds number is defined as:

$$Re_p = \frac{\rho d_p \left(v_p - v_{\bowtie}\right)}{\mu_p} \quad \textbf{(3-1)}$$

Meanwhile, the drag coefficient is reduced through (Morsi and Alexander, 1972) particle trajectory of two-phase flow system:

$$c_d = \frac{24}{Re_p}\left(1 + \frac{Re_p^{\frac{2}{3}}}{6}\right) \quad \textbf{(3-2)}$$

By neglecting gravitational and additional forces, the motion of the particle is described as:

$$\frac{dv_p}{dt} = (\frac{18\mu}{\rho_p d_p^2})(\frac{c_d Re_p}{24})(v_\infty - v_p) \quad \textbf{(3-3)}$$

Since Reynolds number and Prandtl number are known, a Nusselt number is calculated by the Ranz-Marshall correlation (Gu, Basu and Kumar, 2012):

$$Nu = 2.0 + 0.6Re_p^{\frac{1}{2}}Pr^{\frac{1}{3}} \quad \textbf{(3-4)}$$

Convective heat transfer relation is then calculated as a function of mass transfer coefficient:

$$h = \frac{Nu.k_\infty}{d_p} \quad \textbf{(3-5)}$$

The area and the mass particle are simply calculated as:

$$A_p = 4\pi r_p^2 \quad \textbf{(3-6)}$$

$$m_p = \rho_p \forall_p \quad \textbf{(3-7)}$$

By rearranging the Nusselt number with the function of Reynolds number, Schmidt number is obtained as:

$$Sc = \left(\frac{Nu - 2.0}{0.6Re_p^{\frac{1}{2}}}\right)^3 \quad \textbf{(3-8)}$$

By obtaining Schmidt number and Nusselt number, the diffusion coefficient of vapour pressure in the bulk and mass transfer coefficient are then calculated:

$$D_{i,m} = \frac{\mu_p}{\rho_p Sc} \quad \textbf{(3-9)}$$

$$k_c = \frac{Nu.D_{i,m}}{d_p} \quad \textbf{(3-10)}$$

Numerically, Kerosene saturation vapour pressure is obtained from this correlation (Mazlan, Savill and Kipouros, 2011):

$$P_{sat} = 1886058.95e\left(\frac{-4576.45}{T_p}\right) \quad \textbf{(3-11)}$$

For Ethanol and Methanol, Antoine equations are used where A, B and C coefficients are sorted in Table 3-3.

Table 3-3 Antoine Coefficients

	A	B	C
ETH	8.04494	1554.3	222.65
MTH	7.97328	1515.14	232.85

$$\log_{10} P_{sat}(mmHg) = A - \frac{B}{T(℃) + C} \quad \textbf{(3-12)}$$

The concentration of vapour at droplet surface is calculated by assuming that partial pressure of vapour at interface is equal to saturated vapour pressure at temperature of particle droplet.

$$c_{i,s} = \frac{P_{sat}}{\mathcal{R}T_p} \quad \textbf{(3-13)}$$

Then, molar flux of droplet's vapour is calculated by using this relation as an equation (3-14). The flux of droplet's vapour corresponds to difference in the concentration of vapour between droplet surface and bulk gas (Mazlan, Savill and Kipouros, 2011).

$$Ni = k_c c_{i,s} \quad \textbf{(3-14)}$$

Because of condition of fuel's droplet temperature is less than the boiling temperature, change of mass is calculated by using this relation:

$$\frac{dm_p}{dt} = -NiA_pMW_p \quad \textbf{(3-15)}$$

Change of temperature in fuel's droplet is calculated from the heat balance. By assuming that no radiation heat transfer occurs, the equation from FLUENT can be rearranged as follows:

$$\frac{dT_p}{dt} = \frac{hA_p(T_g - T_p) + \frac{dm_p}{dt}h_{fg}}{m_p c_p} \quad \textbf{(3-16)}$$

Next, these relations are used:

$$v_{p_2} = v_{p_1} + \frac{dv_{p_1}}{dt}dt \quad \textbf{(3-17)}$$

$$m_{p_2} = m_{p_1} + \frac{dm_{p_1}}{dt}dt \quad \textbf{(3-18)}$$

$$T_{p_2} = T_{p_1} + \frac{dT_{p_1}}{dt}dt \quad \textbf{(3-19)}$$

By applying conservation of mass theory, values of new particle area, radius and diameter can be calculated by using these relations:

$$A_{p_2} = \frac{\dot{m}_2}{\rho_{p_2} v_{p_2}} \quad \textbf{(3-20)}$$

$$r_{p_2} = \left(\frac{m_{p_2}}{4/3\,\pi\rho_{p_2}}\right)^{\frac{1}{3}} \quad \textbf{(3-21)}$$

$$d_{p_2} = 2r_{p_2} \quad \textbf{(3-22)}$$

Lastly, all the equations above are repeated until mass and velocity turn to zero, which indicates that the droplet is fully vaporized. Spray penetration determines

propagation distance of a droplet in the combustor. To predict penetration length of the droplet, (Mazlan, 2012) and (Sazhin, Feng and Heikal, 2001) have recommended this relation:

$$s = \frac{\sqrt{V_i D_o t}}{(1-\alpha_d)^{1/4}\tilde{\rho}^{1/4}\sqrt{\tan\theta}}\left(1 - \frac{\sqrt{D_o}}{4\sqrt{V_i(1-\alpha_d)^{1/4}\tilde{\rho}^{1/4}\sqrt{\tan\theta}\,\sqrt{t}}}\right) \quad \textbf{(3-23)}$$

While s is a distance measured from the nozzle, $\tilde{\rho} = \frac{\rho_a}{\rho_d}$ is a dimensionless parameter. Using values of D_0= 1mm, θ= 34.89^0 and $\alpha_d = 1e^{-4}$, spray penetration of biofuels can be calculated. The whole spreadsheet of spray analysis is included in Appendix B.1.

3.4 Results & Discussion

3.4.1 Atomization and penetration of alternative fuels comparison

This section reports all the predictions of the developed spray atomization and penetration model results. It is worth mentioning that model validation is comparable to the model developed by Sazhin et al. (2001) for spray penetration and Ghassemi et al. (2006) for atomization general behaviour. Variations of vapour pressure and functions of temperature for all fuels are calculated prior to analysis. This is done because vapour pressure has a strong dependence on temperature and thermochemical properties of the fuel. All fuels show an increase in vapour pressure as the temperature increases until they reach a certain limit. As stated in previous section, modelling is conducted until mass and velocity reach zero. In comparison, MTH has the highest vapour pressure at prescribed temperature, followed by ETH, KE, BC, BJ and MA fuels.

Each fuel is given the same initial conditions for both atomization and sprays penetration process. All fuels droplets have increased its diameter slightly

before it declines as shown in Figure 3-1. All biofuels have similar evaporating trends as Kerosene because they exhibit the same saturation vapour pressure correlation as in Kerosene and other bulk physical properties such as bulk modulus, specific heat and thermal conductivity (Lefebvre and Ballal, 2010). Although MTH and ETH fuels have higher vapour pressure, droplets are shown to have slower vaporization rate. This is most likely due to high vaporization latent heat that prevents an increase in droplets temperature. It is thus consistent with the work of (Gu, Basu and Kumar, 2012) that show that ETH fuel has the largest droplet particle reduction followed by MTH and KE fuels. All three biofuels result in more than 50% diameter reduction before they stop. BJ fuel is found to have the largest remaining droplet diameter, followed by MA, and BC biofuels. Average evaporation rate is taken based on the gradient of each droplet fuel trend line. Gradient values show that ETH is the highest, and this corresponds to higher evaporation rate. These followed by MTH, BC, MA, BJ and KE. As expected, alternative fuels are proven to produce less emission because of higher evaporation rate compared to KE.

Transient variations of spray penetration process of various alternative fuels are plotted in Figure 3-2. Spray penetration is an important parameter for combustor design, size and geometry since it provides a significant effect on engine performance and emission. Numerous soot forms as a result of the short penetration due to fuel coke (Mazlan, Savill and Kipouros, 2011). All fuels exhibit the same trends as discussed in the literature where they are accelerated at the early stage and later propagate at almost a constant speed. When the particle stops, MTH propagates the farthest distance, followed by ETH and KE fuels. However, all biofuels have shorter penetration length that gives cost penalties to the biofuels as they exhibit more emissions in the existing combustors. Therefore, necessary engine design geometry needs to be study carefully to overcome soot formations.

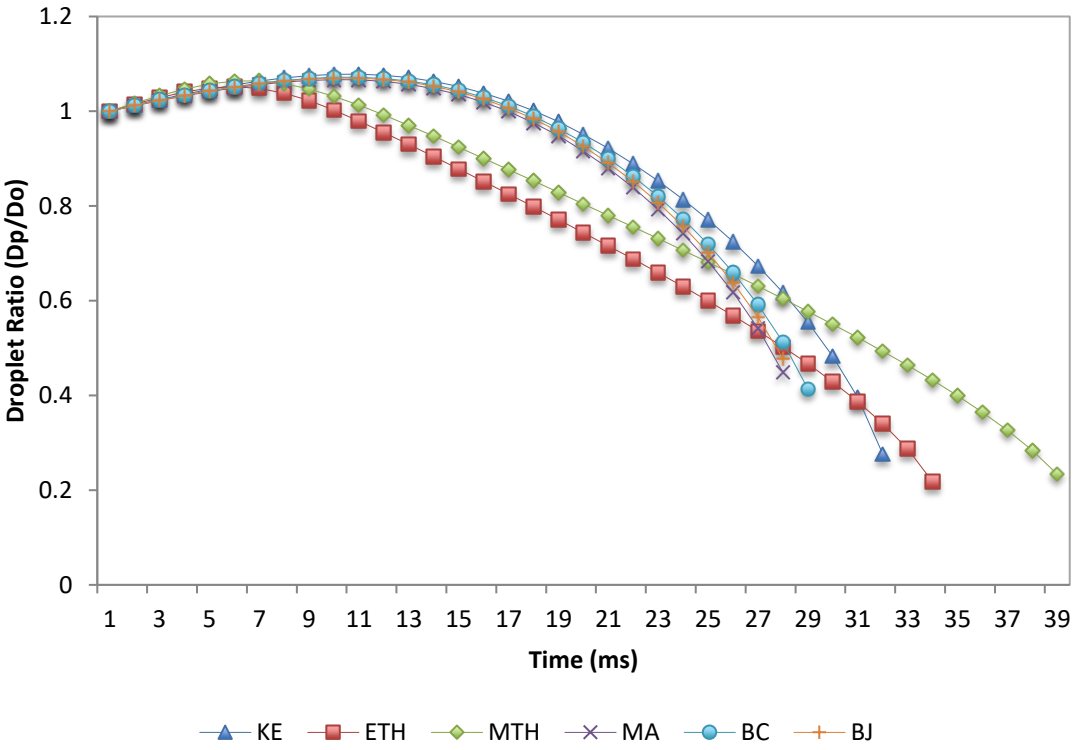

Figure 3-1 Transient condition of evaporation process for each fuel

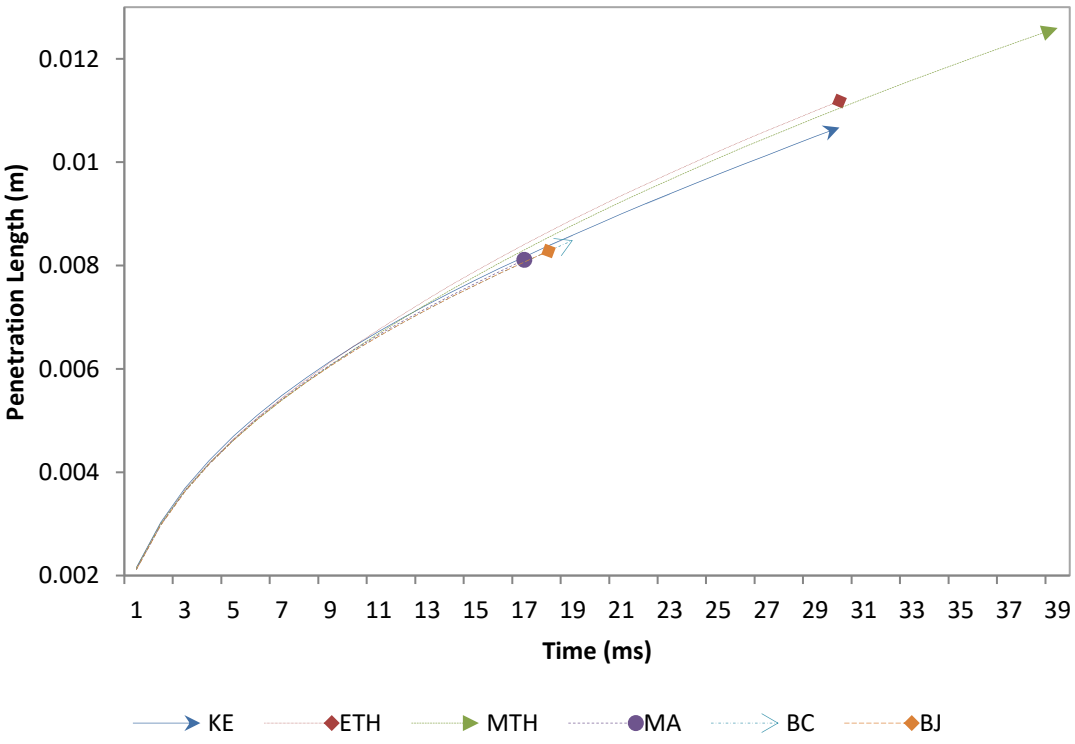

Figure 3-2 Transient condition of penetration process for each fuel

The transient condition of temperature and density for each fuel are presented in Figure 3-3 and Figure 3-4. It is observed that there is an increase in temperature for all fuels at first, but later the temperature remains constant for a period of time. Each fuel shows different constant temperatures, in which ETH has the lowest constant temperature, while KE achieved the highest. All other biofuels appear to have an almost similar constant temperature. Their density also reduces to a certain value until it reaches a certain point before remaining at a constant value. These changes in are reflected by the change of temperature and particle velocity. Notably, changes of droplet's temperatures are determined in equation (3-16) are influenced by factors such as the latent heat, viscosity, evaporation rate (changes of mass) and molecular weight of the fuels.

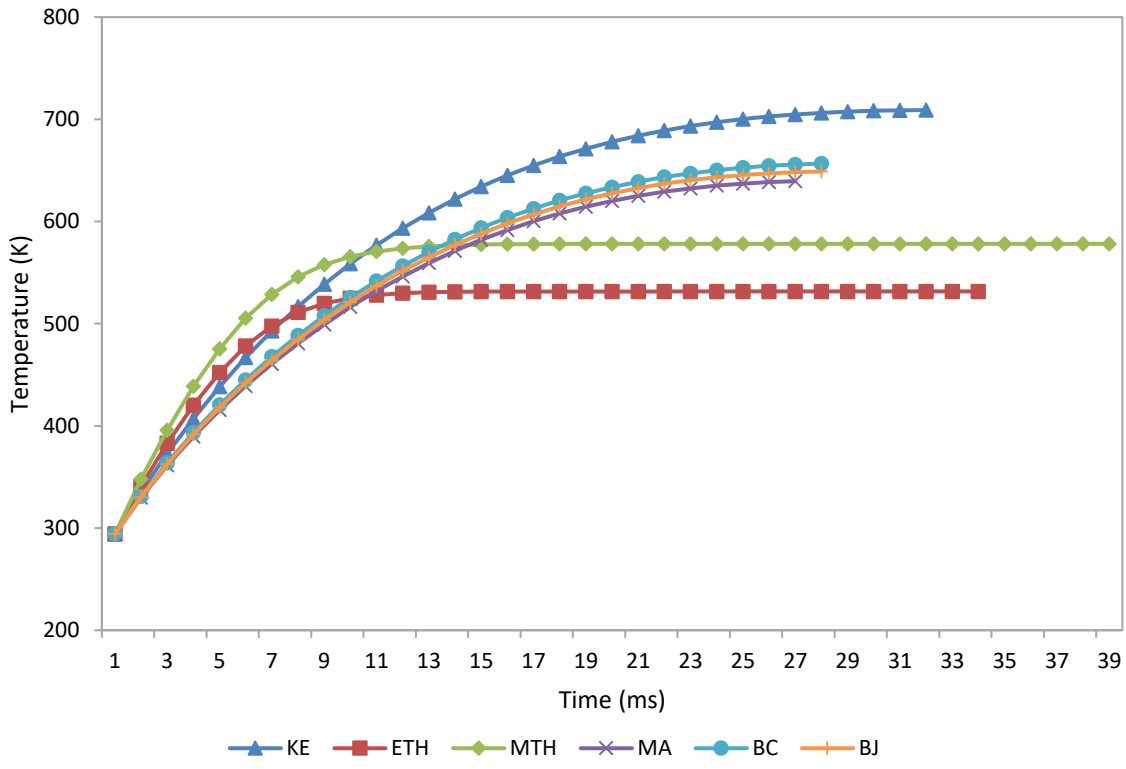

Figure 3-3 Transient condition of temperature variation for each fuel

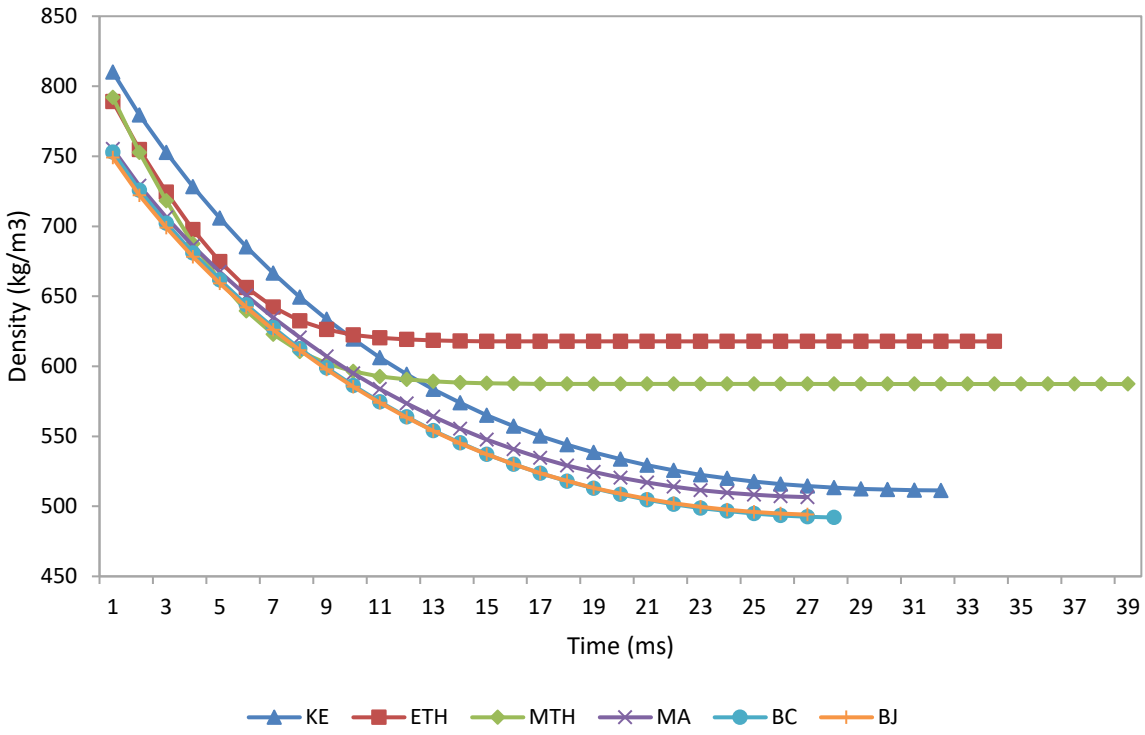

Figure 3-4 Transient condition of density variation for each fuel

3.4.2 The influence of initial conditions on atomization and penetration

This section discusses effects of various initial conditions such as different initial temperature and velocity of droplet particle that have significant effects on atomization and penetration process. However, only KE fuel is closely examined and discussed. In the later paragraphs, different alternative fuels are compared and analysed, despite having higher initial temperature and velocity. KE fuel droplet is given a prescribed time until its droplet particle stops. High initial temperature is preferable as it accelerates evaporation rate and exhibits greater changes to the droplet diameter, directly producing much smaller droplet diameter in a shorter time. These higher energy-contained droplet particles may enhance mass transfer to the surrounding. On the other hand, high initial temperature also reduces the droplet particle's velocity much faster as illustrated in Figure 3-5. It results in low penetration length as shown in

Figure 3-6 and stops much earlier. Penetration length of high energy-contained droplet is reduced as the droplet is completely vaporized.

Similarly, high initial velocity results in higher diameter gradient that indicates higher evaporation rate. This is due to the higher mass transfer rate from droplet surface to the surrounding. Although it has much higher evaporation rate, high-velocity droplet penetrates much longer before it stops. Their primary influences seem to appear in the inertial forces and the lesser amount of time for it to stop. Drag forces also play a substantial role as the velocity increases. Variations of different initial velocity are illustrated in Figure 3-7 and Figure 3-8 based on evaporation and penetration process. As a conclusion, higher droplet velocities show faster evaporation rate and longer penetration length.

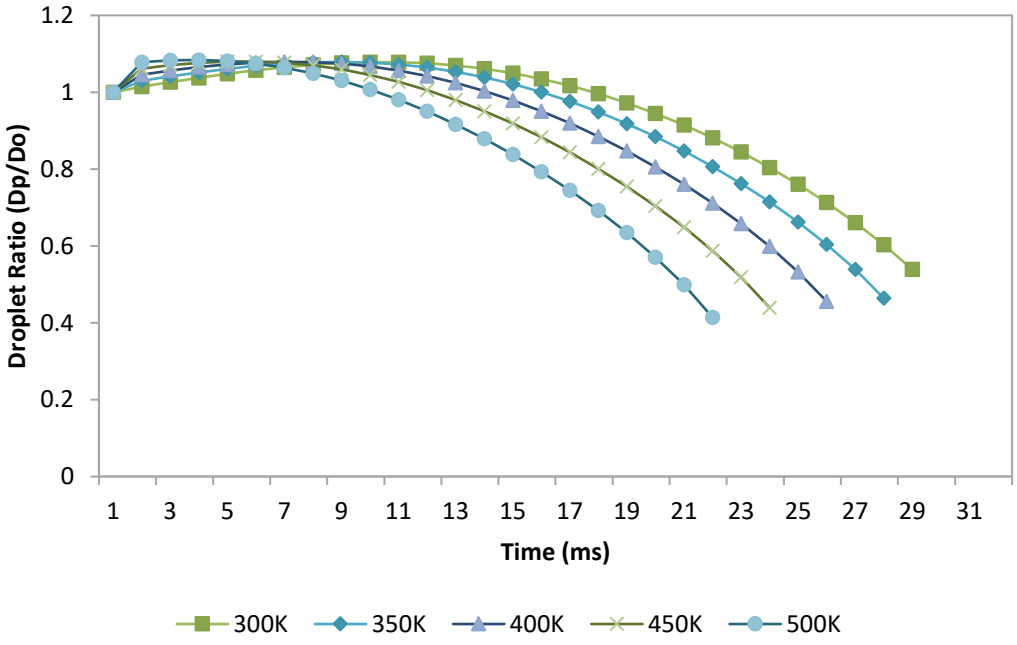

Figure 3-5 Transient condition of evaporation process for KE under different temperatures

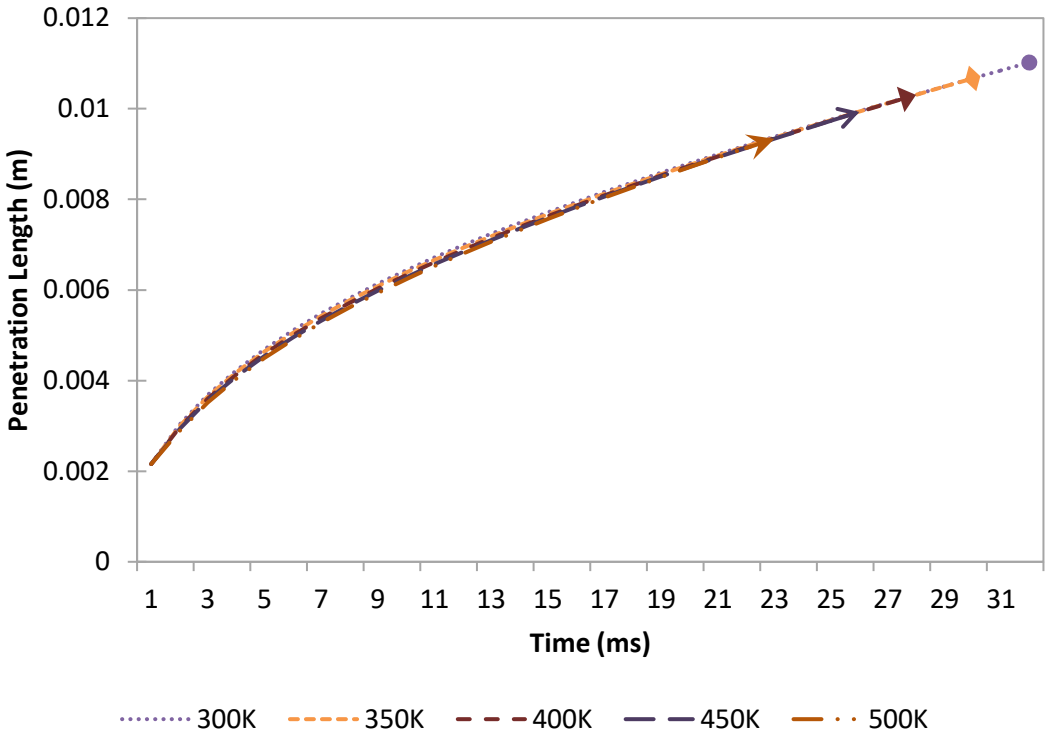

Figure 3-6 Transient condition of penetration process for KE under different temperatures

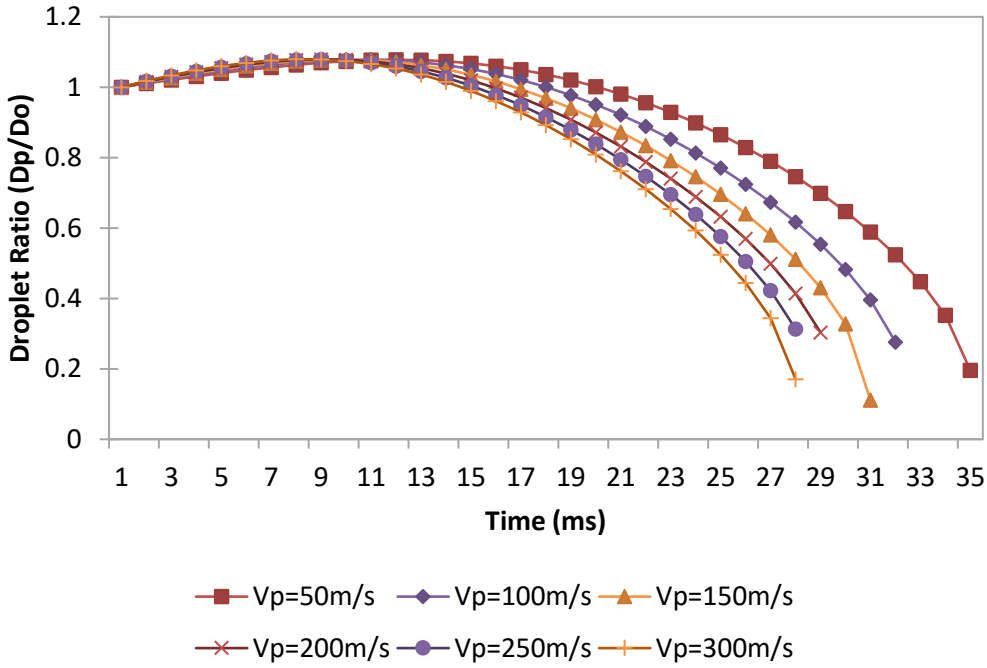

Figure 3-7 Transient condition of evaporation process for KE under different initial velocity

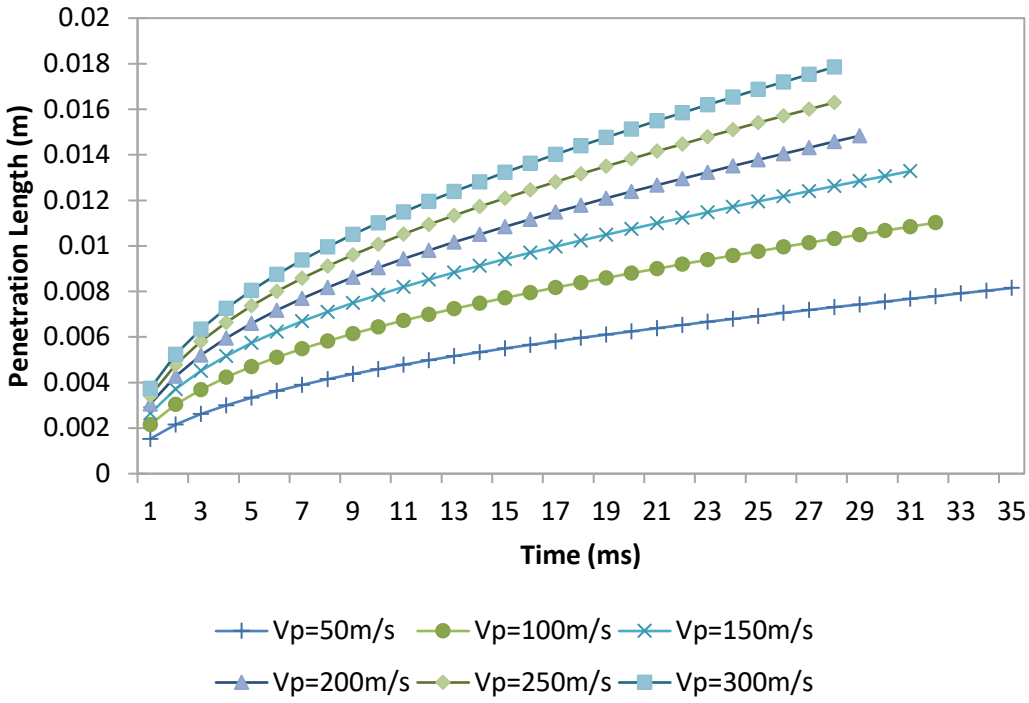

Figure 3-8 Transient condition of penetration process for KE under different initial velocity

Evaporation and penetration process of different alternative fuels are compared and presented in Figure 3-9 to Figure 3-12. First, it can be seen that effects of high initial temperature on both processes. Each fuel is heated to 500K and modelled in a transient condition. Behaviour of these fuels is found to be almost similar to the one obtained in Figure 3-1 and Figure 3-2. However, it should be highlighted, again, that higher initial temperature reduces the time for droplet to stop and enhances evaporation rate as the gradient is much larger. Only MTH fuel is almost completely vaporized when its droplet particle stops. Meanwhile, other fuels have their droplet diameter reduced by more than 50%, with BJ fuel has the highest reduction. The difference is that all fuels appear to have greater diameter reduction in a much shorter time at high initial temperature.

On another note, as the particles are accelerated to a higher velocity, evaporation rate remains the same. These can be seen in the plotted graphs in

Figure 3-11 as compared to Figure 3-1. Higher initial velocity may reduce time for droplet to stop due to increase of drag. Change of droplet diameter is much greater for KE, ETH and MTH fuels even in a short time. Other fuels, MA, BC and BJ show almost the same changes in droplet diameter as in lower initial velocity but, at a much shorter time. This allows droplet to penetrate more as inertial forces becomes a dominant factor.

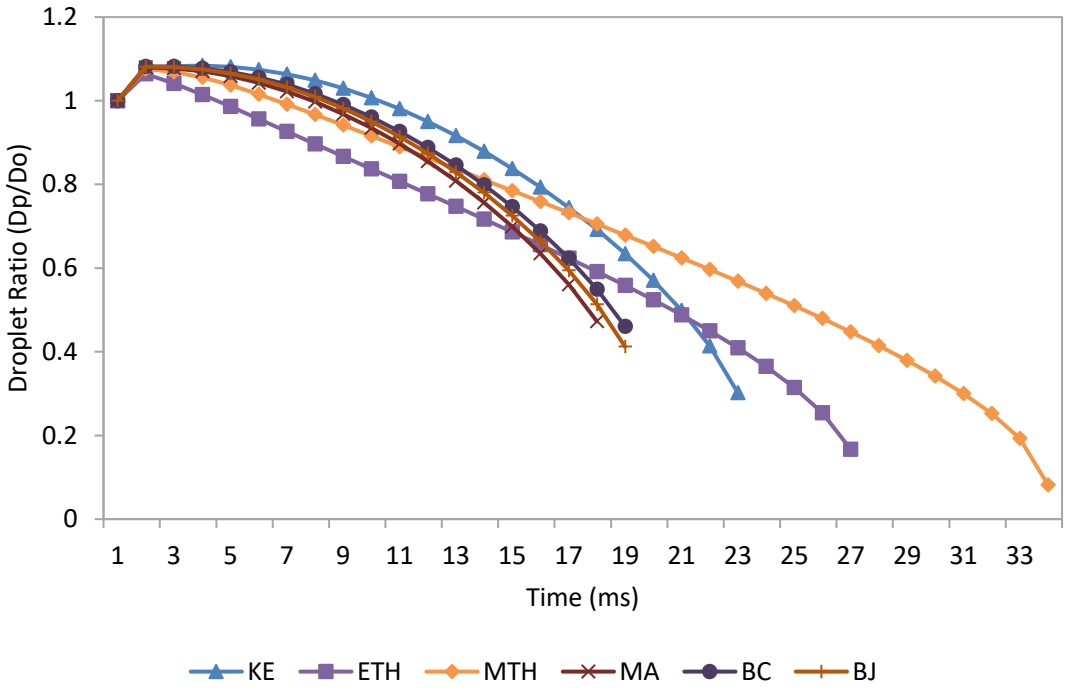

Figure 3-9 Comparison of evaporation process for alternative fuels at higher initial temperature (Tp=500K)

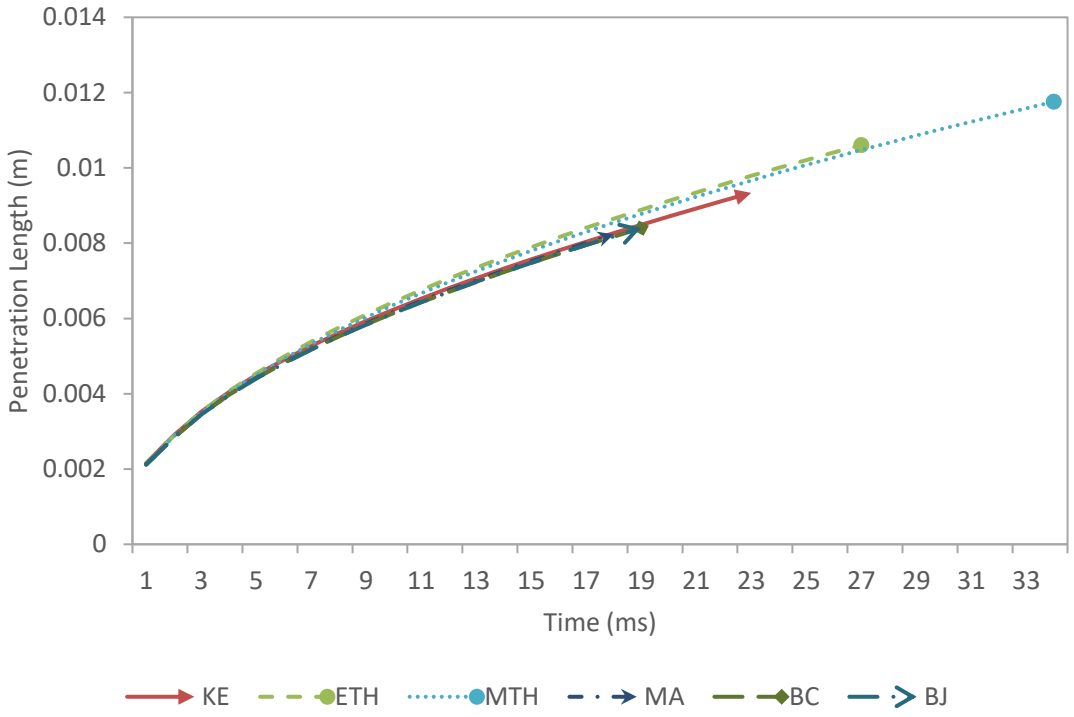

Figure 3-10 Comparison of penetration process for alternative fuels at higher initial temperature (Tp=500K)

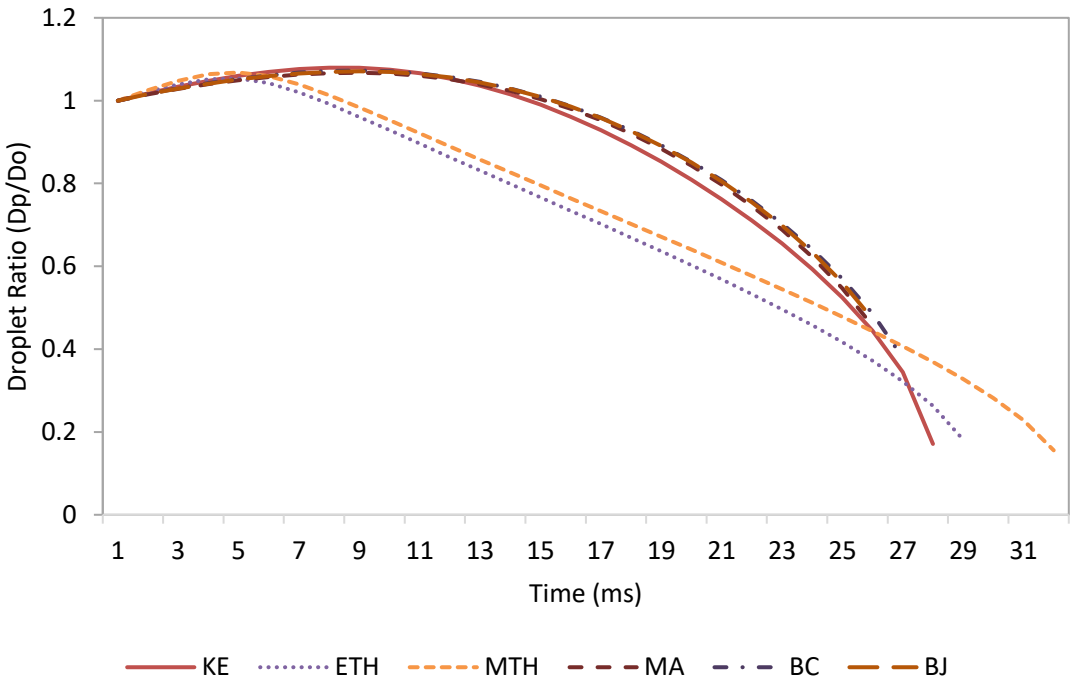

Figure 3-11 Comparison of evaporation process for alternative fuels at higher initial velocity (Vp=300m/s)

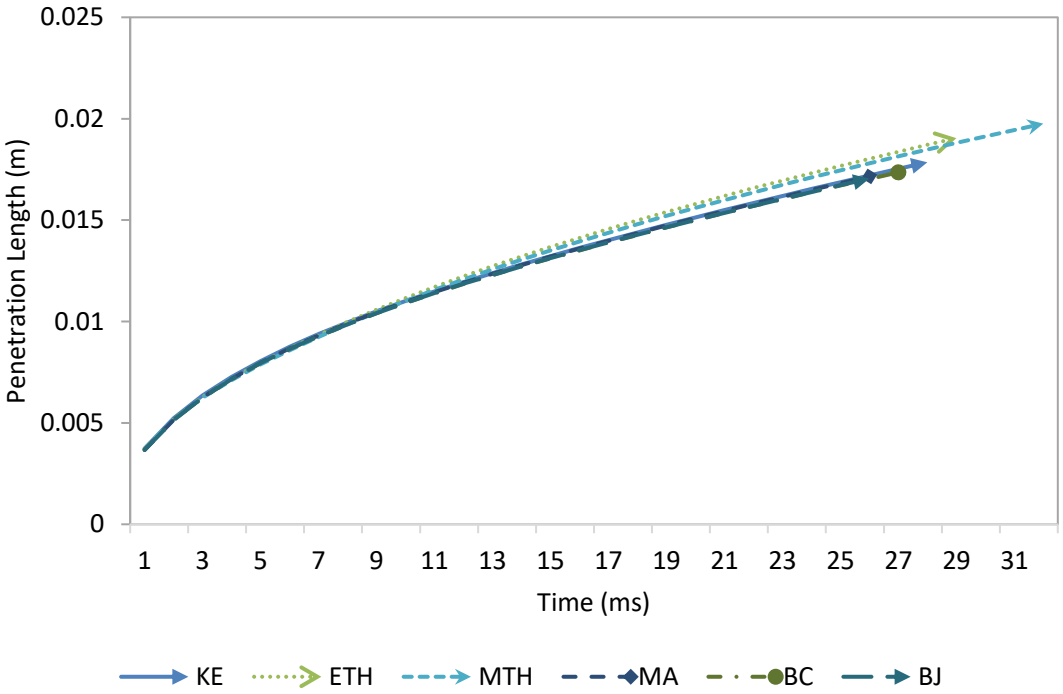

Figure 3-12 Comparison of penetration process for alternative fuels at higher initial velocity (Vp=300m/s)

3.5 Concluding Remarks

The focus of this chapter is the modelling of evaporation and spray penetration for alternative fuels. Detailed comparisons have been made to visualise the transient behaviour of these fuels. An approximate expression for evaporation modelling is derived from FLUENT and spray penetration modelling under the assumption of Mazlan (2012) and Sazhin et al. (2001) in a transient condition. It is worth to note that, this is the first attempt to model, evaluate, and compare alternative fuels especially the third generation of biofuels through evaporation and penetration process. The vapour pressure tendencies have significant effects on transient shape of the evaporation process. ETH fuel has the highest evaporation rate, followed by MTH, BC, MA, BJ, and KE at room temperature. At a given time, MTH droplet particle propagates the farthest distance followed by ETH and KE fuels. However, all biofuels have shorter penetration length in the given time. These give penalty costs to biofuels emissions formation. The

characteristic behaviour of temperature and density properties of droplet fuel is estimated under transient condition. Both parameters show a reverse pattern and they achieve constant values at a particular time. Each fuel has different constant value because of different thermochemical properties. The influence of initial conditions such as temperatures and velocity are also discussed. High initial temperature and velocity are preferable as they accelerate evaporation rate and exhibit greater changes to the droplet diameter resulting in much smaller droplet diameter in a shorter time. These initial conditions are shown to exhibit reduction of droplet particle's velocity in a much faster time. Nevertheless, high initial temperature also results in low penetration length, while high initial velocity allows further penetration.

4 EVALUATION OF BIOFUEL – ENGINE PERFORMANCE ANALYSIS (PYTHIA)

4.1 Introduction

This chapter presents the analysis of aircraft engine performance in terms of thrust, fuel flow and specific fuel consumption (SFC) at different mixing ratio percentages (20%, 40%, 50%, 60% and 80%) of alternative biofuel blends (Algae biofuel, Camelina biofuel and Jatropha biofuel) that have been used in flight test under different flight conditions. This study is a crucial step to understanding the influence of different blended alternative biofuels on the performance of aircraft engines at wide-range of flight cycles.

In-house computer software tools, PYTHIA & TURBOMATCH are used to analyse and model a three-shaft high-bypass-ratio engine that is similar to RB211 variant. Based on a few key assumptions that are discussed in section 4.5.4, our in-house computer software is used for the computational analysis and the results are compared with experiments conducted by Rahmes et al (2009). The PYTHIA programme has the ability to model and calculate various gas turbine engines for both design and off-design points by using a modified Newton-Raphson convergence technique in the zero-dimensional steady-state model (Igie and Minervino, 2014). It can also serve as a diagnostic tool for deterioration analysis to allow map scaling for off-design conditions. PYTHIA is integrated with the TURBOMATCH performance evaluation programme by iterating the mass and energy balance for each engine component. PYTHIA is user-friendly with novel interface for engine component selection (Mazlan, Savill and Kipouros, 2015). Its capability has been tested and validated for many years (Li *et al.*, 2011, 2012) across a wide range of turbomachinery from industrial gas to aero gas turbines. The latest version of PYTHIA has the capability to change fuel type and to vary blended mixing ratio percentage, while simultaneously maintaining the same engine design, with a

conventional kerosene fuel baseline. This is essential to evaluate fit-for-purpose fuels for real engines at various operating points.

In this chapter, a brief literature review on the process of the jet fuel and the application are presented, followed by the methodology for how the software is run to obtain design conditions. Next, engine model verification is made with open literature found in Bio-Synthetic Paraffinic Kerosene test programme in commercial aircraft. Later, the results are discussed and have shown that Lower Heating Value (LHV) has a significant influence on thrust, fuel flow and SFC under every flight condition and at all mixing ratio percentages. Wide LHV differences between two blended fuels also give a large variation on the engine performances. Meanwhile, blended Kerosene-Jatropha Biofuel and Kerosene-Camelina Biofuel show an improvement on gross thrust, net thrust, reduction of fuel flow and SFC at under every flight condition and at all mixing ratio percentages. Pure alternative of Jatropha Biofuel and Camelina Biofuel are found to result in much better engine performances. However, this is not the case for the Kerosene-Algae blended biofuel.

4.2 Literature Review

There are two types of biofuels that have been certified for use in aviation when they are blended with at least 50% of conventional kerosene, which are the Fischer-Tropsch (F-T), hydro processed Synthesized Paraffinic Kerosene (SPK), and the synthesized paraffinic kerosene from Hydro-processed Esters and Fatty Acids (HEFA) (Payan *et al.*, 2014). Three types of refining processes to convert bio-derived feedstock sources into bio-jet fuels are (Payan *et al.*, 2014):

1. Fischer-Tropsch (F-T) process

   This is a gas-to-liquid technology that involves a series of chemical conversion of a mixture of carbon dioxide and hydrogen, obtained from the burning of biomass feeds stocks, into synthetic liquid hydrocarbons.

2. Alcohol-To-Jet (ATJ) process

   It converts sugars or alcohols, derived from fermented sugar-rich or starchy biomass, into liquid jet fuel through a suite of catalytic reactions.

3. Fast pyrolysis (HEFA) process.

   Hydro-processing is a catalytic process that turns pyrolysis triglyceride oils, derived from oil-rich plant seeds and tree fruits, into liquid hydrocarbons that are used as jet fuels.

In present context, there have been three successful biofuel flights of commercial aircraft, which are Air New Zealand's Boeing 747-400 in 2008, Continental Airlines Boeing 737-800 and Japan Airline Boeing 747-300 in 2009. These flights used bio-SPK blends of up to 50% with conventional fuel and they found no abnormal impacts on different engine operations (Rahmes *et al.*, 2009). Payan et al. (2014) have addressed environmental studies on alternative fuels and analysed their relative greenhouse gas (GHG) emission reduction for biomass sources as compared to conventional jet fuel based on fossil sources and its blend. Results are summarized in Table 4-1.

Table 4-1 GHG Emission reduction with different feed stocks in relative to jet fuel (Payan *et al.*, 2014)

Feed stocks	GHG Emission Reduction (%)
Corn Stover	55
Sweet Sorghum	133
Canola	44
Camelina	86
Jatropha	42
Waste Fat	87
Wood Residues	148
Miscanthus	72
Switch grass	63
Algae	124

Payan et al. (2014) have described the possibility that the biomass-based fuel could contribute to GHG reduction and addressed its environmental concern. Therefore, focus of this study is on the effect of blended biofuels on aircraft engine performance especially on gross thrust, fuel flow and specific fuel consumption under different flight conditions and at different blended mixing ratio percentages. They are, in fact, equally important for engine performances to not be undermined. Three biofuels namely Algae Biofuel, Jatropha Biofuel, and Camelina Biofuel are evaluated as pure fuel and blended with kerosene ($C_{12}H_{24}$) at 20%, 40%, 50%, 60% and 80%. These biofuels are selected because of previous success in the test flight programmes. Their fuel properties are available in the published literature as listed in Table 4-2. A model of a three-shaft high-bypass-ratio engine RB211-524 is used throughout the analysis by using available engine parameters for verification. Validation is done for an RB211 variant, while comparisons with the work of Rahmes et al (2009) are also further conducted to examine the effects of different percentages of

blended fuel mixing ratios. This work may thus serve as an extension beyond Mazlan et al. (2015) work that used the earlier version of PYTHIA which could only provide strict comparisons for different pure fuels for a single designated condition only.

4.3 Methods

Configuration of the RB211-524 engine is specified in PYTHIA by using available library data and default settings configuration. These configurations are illustrated in Figure 4-1. At design point, kerosene fuel is selected. Each component of the engine model is described in terms of a 'brick' that denotes its own functionality. When the engine model is selected, 13 data blocks are arranged accordingly for INTAKE, COMPRE1, PREMAS, COMPRE2, COMPRE3, BURNER, MIXEES, TURBIN1, TURBIN2, TURBIN3, MIXFUL, DUCTER, and NOZCON. Most bricks are defined as an individual component treating thermodynamic processes independently. However, they have to be linked to perform a complete engine simulation. The properties and thermodynamic state of gasses at the entry of every brick can be collected as a Station Vector (SV) to connect each brick. Each SV consists of following eight items: 1) Fuel-air ratio, 2) Mass Flow, 3) Static Pressure, 4) Total Pressure, 5) Static Temperature, 6) Total Temperature, 7) Velocity, and 8) Area.

The ambient conditions (input) are ascribed according to the intended flight conditions such as altitude, flight speed, mass flow, pressure recovery, pressure deviation and relative humidity in the INTAKE brick. Meanwhile for compressors, the first compressor has the maximum pressure ratio of 2.0 with -10° stator angle. The subsequent high pressure (HP) compressors have maximum pressure ratio of 11.0 with -10° stator angles. In this case, however, only HP compressors are assumed to have bleeding air. The PREMAS brick is used to calculate outlet conditions from components such as a splitter, bleed,

bypass duct or jet pipe, with the given absolute relate changes of mass flow and total pressure. There is no water flow introduced to the burner.

MIXEES brick is used to calculate outlet conditions resulting from constant-area mixing of two flows with no allowance for total pressure loss. Its data is used after TURBINE brick data to calculate outlet conditions from constant-area mixing flows that has full allowance for total pressure change as a result from momentum balance. All turbines are set to have identical maximum enthalpy drop ratio of 0.04 and turbine inlet temperature (TIT) of 1580 K. These turbines also have -10° angle positions, and are choked at low speed. A convergent nozzle is later selected for NOZZLE brick. Results for engine parameters and performance for baseline fuel are tabulated in Table 4-3.

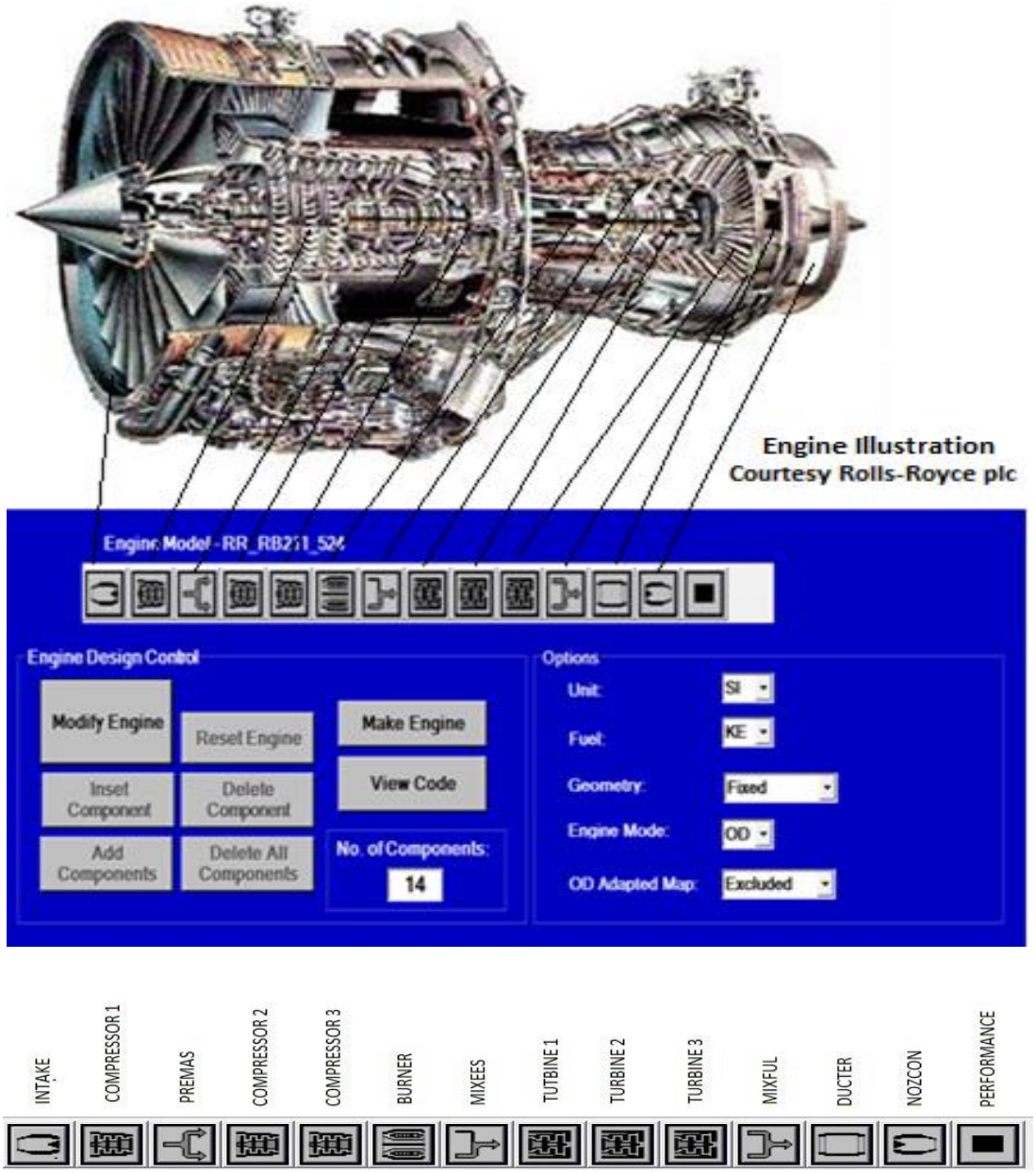

Figure 4-1 PYTHIA engine model schematic diagram.

Flowchart of the PYTHIA process is illustrated in Figure 4-2. It begins with the user defining inputs as previously mentioned in PYTHIA. TURBOMATCH is called for iterations in mass (equation (4-1)) and energy (equation (4-2)) balance relation. Equation (4-1) and equation (4-2) should be satisfied between successive components. New initial guess for pressure ratio, temperature (burner) and rotational speed must be made before iteration process.

TURBOMATCH is then coded by using FORTRAN. Compressor and turbine maps are needed for mass balance iteration process. NASA Chemical Equilibrium Analysis (CEA) is applied for evaluation of enthalpy, entropy, and specific heat with respect to temperature. These correlations are stored in the TURBOMATCH library data. The iteration process requires several initial guess values before they converge. All data are collected and imported into excel spreadsheet for analysis.

$$\frac{W_n\sqrt{T_n}}{P_n} = \frac{W_{n+1}\sqrt{T_{n+1}}}{P_{n+1}} \quad \textbf{(4-1)}$$

$$Turbine\ Work\ (TW) = Compressor\ Work\ (CW) \quad \textbf{(4-2)}$$

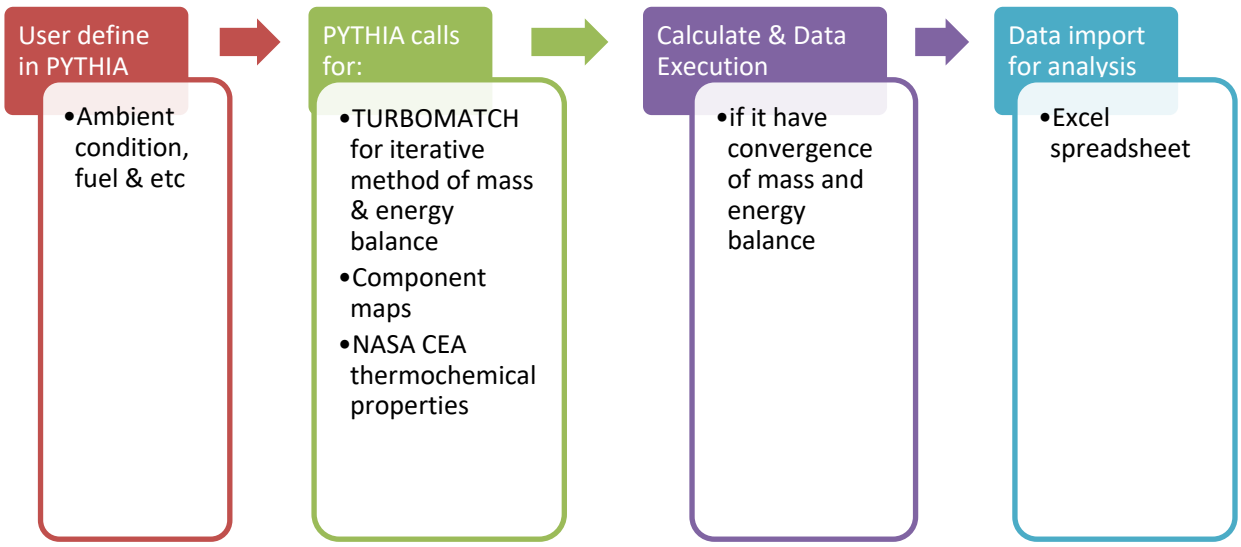

Figure 4-2 PYTHIA data process flowchart.

Table 4-2 Biofuel properties.

	Algae (AG)	Jatropha (BJ)	Camelina (BC)
Density (kg/m^3)	883.6	864-880	-
Cetane Number	85-92	46-55	50.4
Viscosity ($mm^2/s\ at\ 40℃$)	4.73	3.7-5.8	3.80
Pour Point (℃)	-21- -24	5	-7
Flash Point (℃)	179	163-238	136
Heating Value (MJ/kg)	43	44.4	44
CFPP (℃)	-	-1.2	-3
Acid Value (mg/KOH)	0.37	0.34	
Cloud Point (℃)	7	5	3
Oxidation Stability (h)	6.76	5.0	-
Iodine Value (I_2**/100g)**	97.12	109.5	152.8
Sulphur Content (ppm)	8.1	12.9	-
Specific Gravity (g/ml)	1.02	0.876	0.882
References	(Alcaine, 2007; Haik, Selim and Abdulrehman, 2011; Jena *et al.*, 2011; Makarevičienė *et al.*, 2014; Rinaldini *et al.*, 2014)	(Hoekman *et al.*, 2012; Giakoumis, 2013; Ashraful *et al.*, 2014)	(Hoekman *et al.*, 2012)

Table 4-3 Engine parameters and performance for baseline fuel.

INTAKE	
Altitude (m)	10588
Flight Mach Number	0.84
Mass flow intake (kg/s)	670
Relative Humidity (%)	60
Momentum Drag (kN)	189.72

COMPRESSORS			
	1	2	3
Z	0.7	0.8	0.8
PR	1.80	4.06	4.06
ETA	0.895	0.89	0.885
WA (kg/s)	670	126.4	126.4
P total (atm)	1.96	1.96	7.96

COMBUSTORS	
ETA	0.99
Pressure Drop (atm)	1.29
Fuel Flow (kg/s)	2.18
LHV (MJ/ kg fuel)	43.12
P total (atm)	31.04
FAR	0.02

TURBINES			
	1	2	3
ETA	0.91	0.92	0.92
T total (K)	1580	1499	1240
P total (atm)	31.04	31.04	12.44
WA (kg/s)	112.18	128.61	128.61

NOZZLE	
Area (m²)	2.25
Exit Velocity (m/s)	394.0
Nozzle Coefficient	0.98
T total (K)	464.39
P total (atm)	1.58

ENGINE PERFORMANCES	
BPR	4.3
Gross Thrust (kN)	293.38
Fuel Flow (kg/s)	2.18
SFC (kg/N.s)	21.07
Specific Thrust (N/kg.s)	154.71

4.3.1 Varying Flight Conditions

In order to describe the differences of flight conditions, an INTAKE block diagram are adjusted accordingly in the off-design performance analysis. This is done by varying Flight speed and altitude. End value should be given in a

prescribed number of steps, in which PYTHIA runs the data for off-design under different intended flight conditions.

4.3.2 Varying Mixing Ratio Percentages

These are conducted by repeating previously described procedures, except for burner block diagram. Three design, user-input parameters, fuel combination, second fuel type, and fuel-mixing rate, are adjusted accordingly. Fuel combination parameter represents condition of fuel mixing. Apparently, there are three options for selection, whether keeping the original, replacing the original or mixing the fuel. The second fuel type is based on the type of fuel used. There are 9 types of fuels to be chosen from data library. Fuel-mixing rate signifies blending mixing ratio percentages from 0-1, where 1 represents pure second fuel. Then, the off design (OD) condition is selected to calculate engine performance.

Several cases are put into tests. At first, fuel mixing and second fuel type are manipulated for the first blended fuel analysis. Second case focuses on the mixing blended ratio percentage that is later calculated. PYTHIA show results accordingly, while maintaining design condition at a constant. The resulting data are exported to excel sheet for analysis.

4.4 Results and Discussions

4.4.1 Engine performance comparison

Prior to the analysis, the engine model developed in PYTHIA was compared to experimental works carried out by Rahmes et al (2009) who conducted an off-wing engine ground test of an RB211-524 fuelled with 50% Jatropha / 50% Jet-A on a Boeing 747-400 of the Air New Zealand airline. Similar conditions have been applied in the model. It appears that fuel flow and percentage HV

differences are comparable to the engine model, with only slight difference as shown in Figure 4-3. In particular, Rahmes et al (2009) has shown a 1.07% reduction of fuel flow for the engine run on the blended Jatropha fuel while the model indicates a reduction of 1.11%. The small difference in the fuel flow shows that the model is not far off from the ground test conducted by Rahmes et al (2009). Unfortunately, there have not been any other resulted tests on blended biofuels for this type of engine (there are some for CFM56 engines). Differences observed are because of differences in the thermochemical properties of the fuel introduced. PYTHIA extrapolates these thermochemical properties when blended fuels are used in the model.

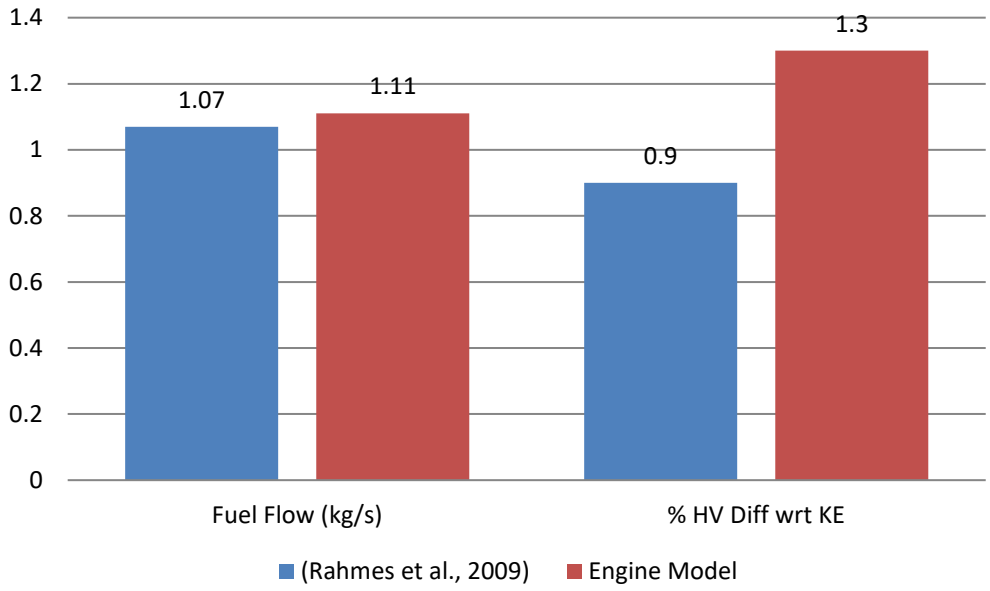

Figure 4-3 Performance comparison of blended KE+BJ

4.4.2 Influence of blended fuel on LHV

Thermochemical properties such as LHV are found to have major influence on the performance of aircraft engines. Other than that, blending ratio is found to significantly affect LHV which thus affects engine performance. Calorific value is measure of heat energy content of a fuel. A higher calorific value of fuel is desired because it releases higher heat, and consequently improves engine performance during combustion (Ashraful *et al.*, 2014). Lower, LHV and higher,

HHV heating values are measures of a fuel heat of combustion with the difference between them being the water heat of vaporization (Giakoumis, 2013).

Figure 4-4 shows LHV variation at different mixing ratio percentage blended with kerosene. KE+BJ has higher LHV, followed by KE+BC and KE+AG. As mixing ratio increases towards highly blended alternative fuels, LHV differences become larger. LHV results show up to 2.7% increase in KE+BJ combination and 2.03% increase in KE+BC as mixing ratio increases into a pure form. Meanwhile, KE+BJ blended fuel has higher LHV compared to KE+BC at every mixing ratio, as shown in Figure 4-5. However, KE+AG fuel shows a reduction of LHV as mixing ratio increases towards unity.

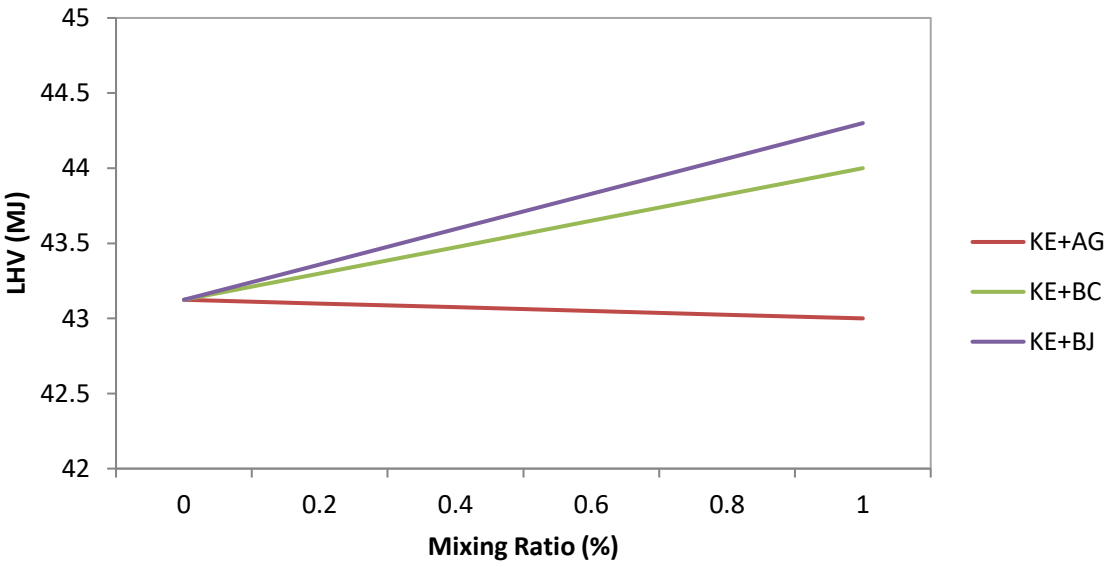

Figure 4-4 LHV variation at different mixing ratio percentage

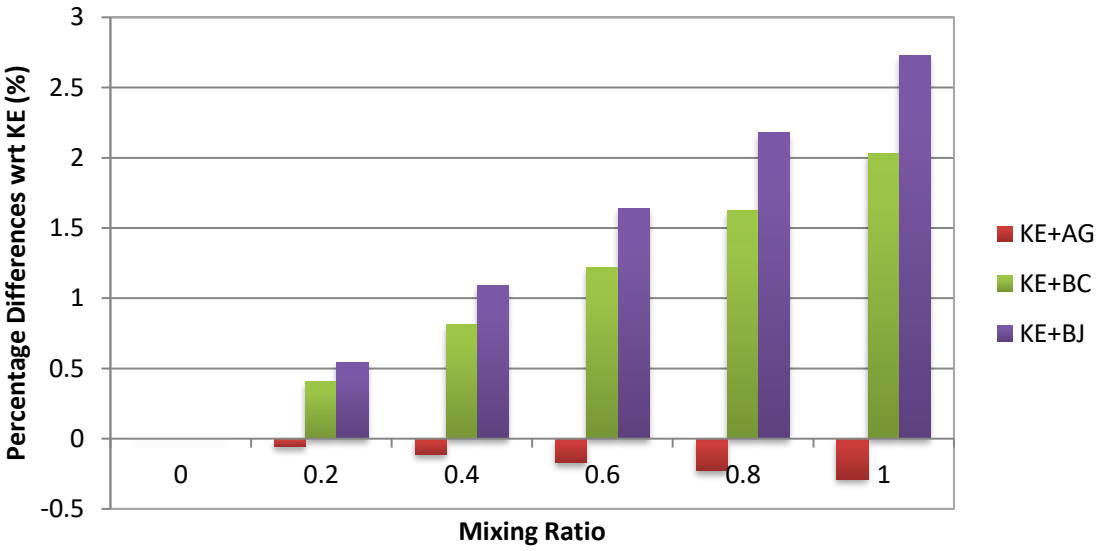

Figure 4-5 LHV percentage difference with respect to pure kerosene at different mixing ratio

4.4.3 Influence of 50% blended fuel on aircraft engine performance under different flight conditions

Blending of biofuels with conventional jet fuel is necessary to meet the current aviation requirement standard. 50% blended fuels are commonly used for flight testing as they are acceptable within the existing specifications. Two different flight conditions; take-off and climbing are chosen to be analysed. Kerosene fuel is used as baseline for comparison.

Take off Condition

Initially, aircraft is accelerated to a take-off velocity. The performance parameters for take-off condition are illustrated in Figure 4.6 – Figure 4-8. Line graphs in primary axis represent variation of performance parameters, while column graphs in secondary axis represent percentage differences, with respect to baseline. It appears that variations of gross thrust for alternative fuels are comparable with baseline fuel as illustrated in Figure 4-6. It shows very slight differences in overall gross thrust performance. However, positive percentage

indicates an increment in gross thrust at higher speeds. 50% of KE+BJ blended biofuel has larger percentage increment in gross thrust at every flight speed as compared to 50% of KE+BC and KE+AG. This indicates that 50% of KE+BJ blended biofuel can increase the gross thrust up to 0.22%, and 50% of KE+BC can increase it by 0.19% at 0.3 Mach number. Meanwhile, 50% of KE+AG blended biofuel has almost no significant difference in gross thrust as compared to baseline.

Fuel flow has positive variation at every flight speed for all fuels (Figure 4-7) and it increases more rapidly after 0.1 Mach number. However, there are more significant differences between these variations. Only 50% of KE+AG blended biofuel has a higher fuel flow than baseline. On the contrary, 50% of KE+BJ blended biofuel have the lowest fuel flow. These trends are also presented in the Figure 4-7, in which 50% of KE+BJ and KE+BC blended biofuels show some reductions. 50% of KE+AG blended biofuel also appear to show a nearly constant fuel flow percentage differences at every flight speed. These percentage trends seem to indicate that 50% of KE+BJ and KE+BC blended biofuels result in higher reduction in fuel flow at lower speed.

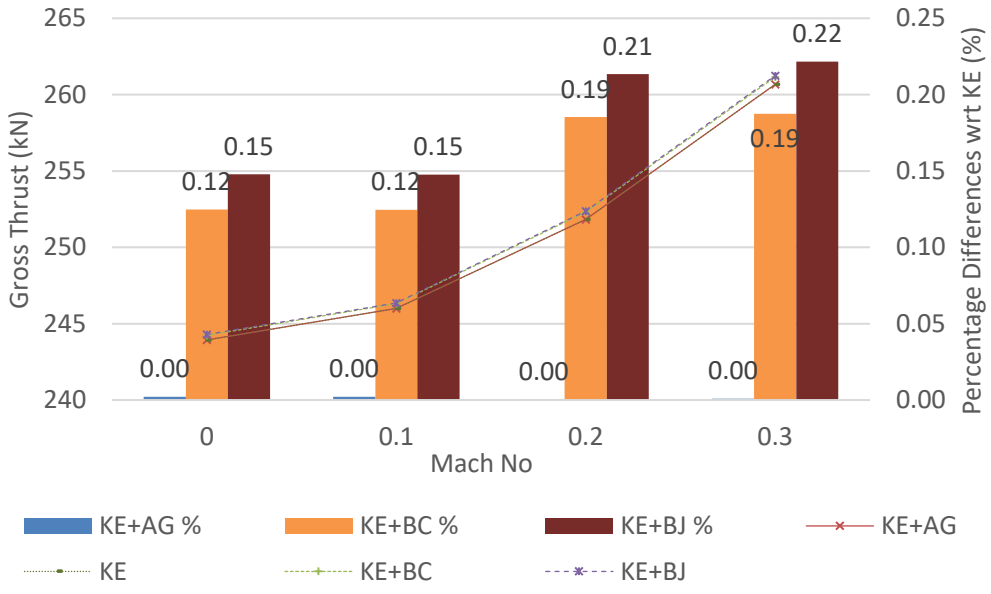

Figure 4-6 Variation of gross thrust at different Mach number

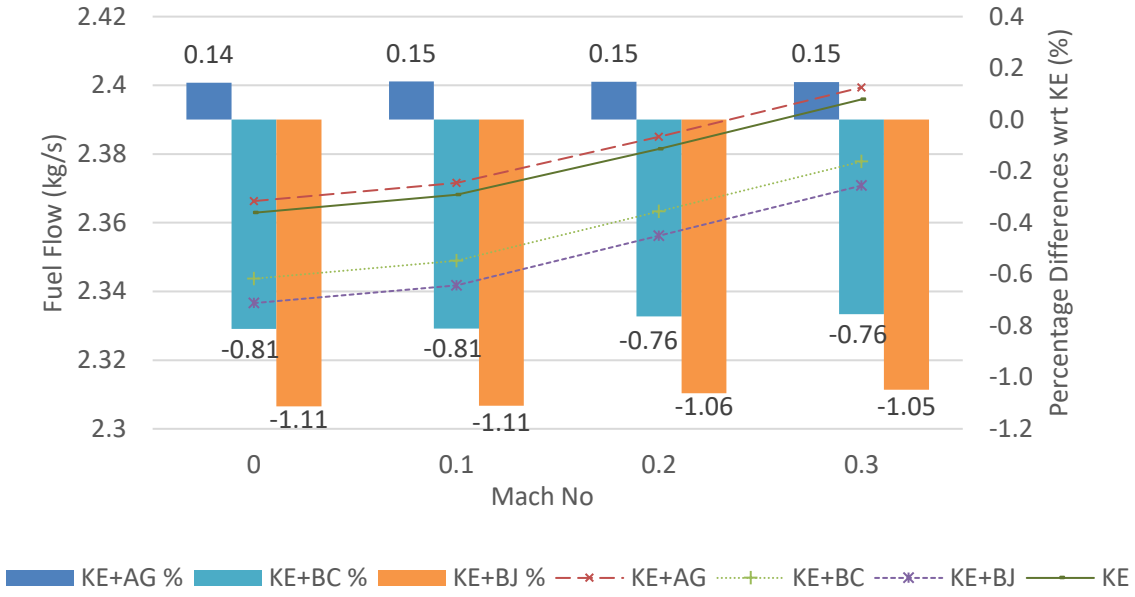

Figure 4-7 Variation of fuel flow at different Mach number

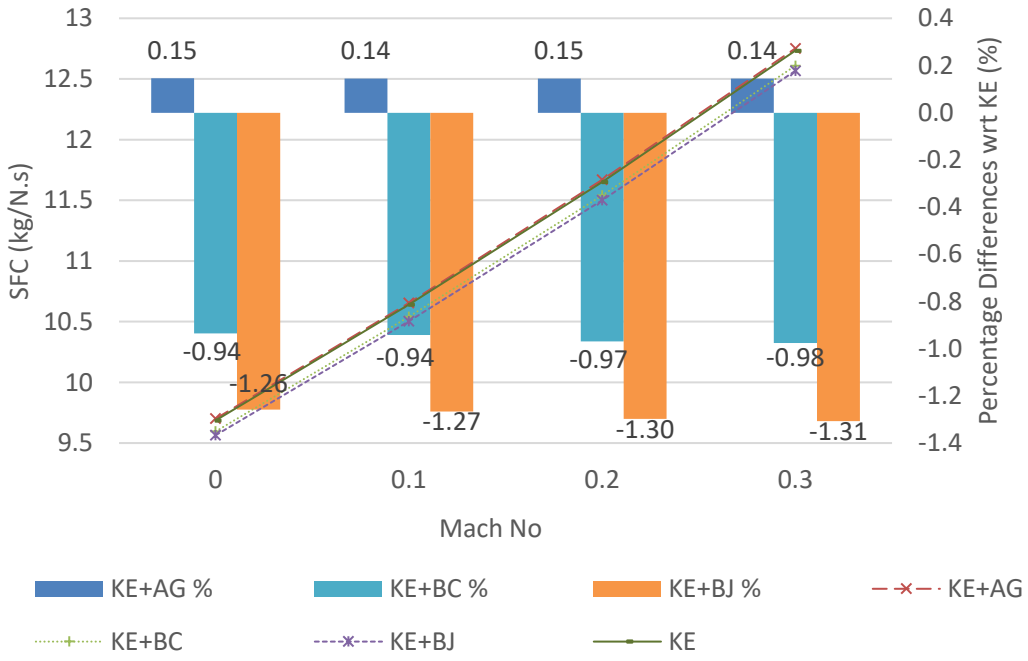

Figure 4-8 Variation of SFC at different Mach number

Figure 4-8 demonstrates positive linear variation of SFC of blended fuels at different flight speed. The 50% of KE+BJ and 50% of KE+BC blended biofuels

are shown to have a significantly lower SFC as compared to baseline fuel, while 50% of KE+AG blended biofuel is almost equivalent baseline. Nevertheless, these trends are slightly different with fuel flow. Percentage difference of SFC is much higher at high Mach number in both 50% of KE+BJ and KE+BC blended biofuels (Figure 4-8). As expected, SFC corresponds to fuel flow. At higher Mach number, both of these parameters demonstrate an increase. Nevertheless, differences of percentage from baseline fuel differ from the trends. Although fuel flow percentage differences are reduced at higher Mach number, SFC results in opposite effect. Despite an increase of Mach number, it results in more reduction in SFC as compared to baseline fuel at particular flight speed. These results have proven the influence of LHV of these fuels, in which fuels with higher LHV require more heat for burning, therefore more fuel flow. However, by using simplified SFC relations with LHV, it appears that LHV is inversely proportional with SFC as in equation 4-3 below.

$$\text{Specific Fuel Consumption, SFC } (kg/N.s) = \frac{v_a.3600}{\eta_P \eta_T LHV} \qquad \textbf{(4-3)}$$

It is to be noted that v_a,η_P, and η_T are flight velocity, propulsive efficiency and thermodynamic efficiency, respectively. Next section describes the effects of varying altitude for climbing flight conditions.

Climbing Condition

Climbing condition is conducted to analyse effects of blended biofuels performances at different altitudes, while keeping the flight speed constant at average of 240 knots (0.36M). Both gross thrust and net thrust result in negative and insignificantly different trends in all fuels as shown in Figure 4-9. Therefore, Figure 4-10 is plotted to visualize small changes in these fuels with respect to the baseline fuel. 50% of KE+AG blended biofuel has shown no differences in

gross and net thrusts as compared to baseline fuel. Conversely, both 50% of KE+BJ and KE+BC blended biofuels demonstrate a slight improvement in gross and net thrusts. This is similar to 50% of KE+BJ blended biofuel that has a significantly higher change in both gross and net thrusts.

Fuel flow shows negative linear variation at every altitude for all fuels (Figure 4-11). Likewise, 50% of KE+BJ and 50% of KE+BC blended biofuels have also result in lower fuel flow as compared to baseline. 50% of KE+AG blended biofuel, on the other hand, has an equivalent fuel flow as the baseline fuel and shows a constant percentage difference of fuel flow at different altitudes. It appears that only 50% of KE+AG blended biofuel shows a percentage increase of 0.15% in fuel flow at all altitudes as compared to baseline. 50% of KE+BJ and KE+BC blended biofuels result in a reduction of fuel flow up to 1.12% and 0.82%, respectively, as shown in column graphs on secondary axis.

Variations are, however, significantly different for SFC, where it is reduced at high altitude (Figure 4-12). Only 50% of KE+AG blended biofuel shows a higher SFC than baseline. 50% of KE+BJ and KE+BC blended biofuels reduce percentages of SFC (up to 1.28% and 0.96% respectively) as compared to baseline, while 50% of KE+AG blended biofuel displayed an increment of 0.14% in SFC. These results demonstrate that 50% of KE+BJ and KE+BC blended biofuels result in a significantly lower fuel flow and fuel consumption, regardless of changes in the altitude.

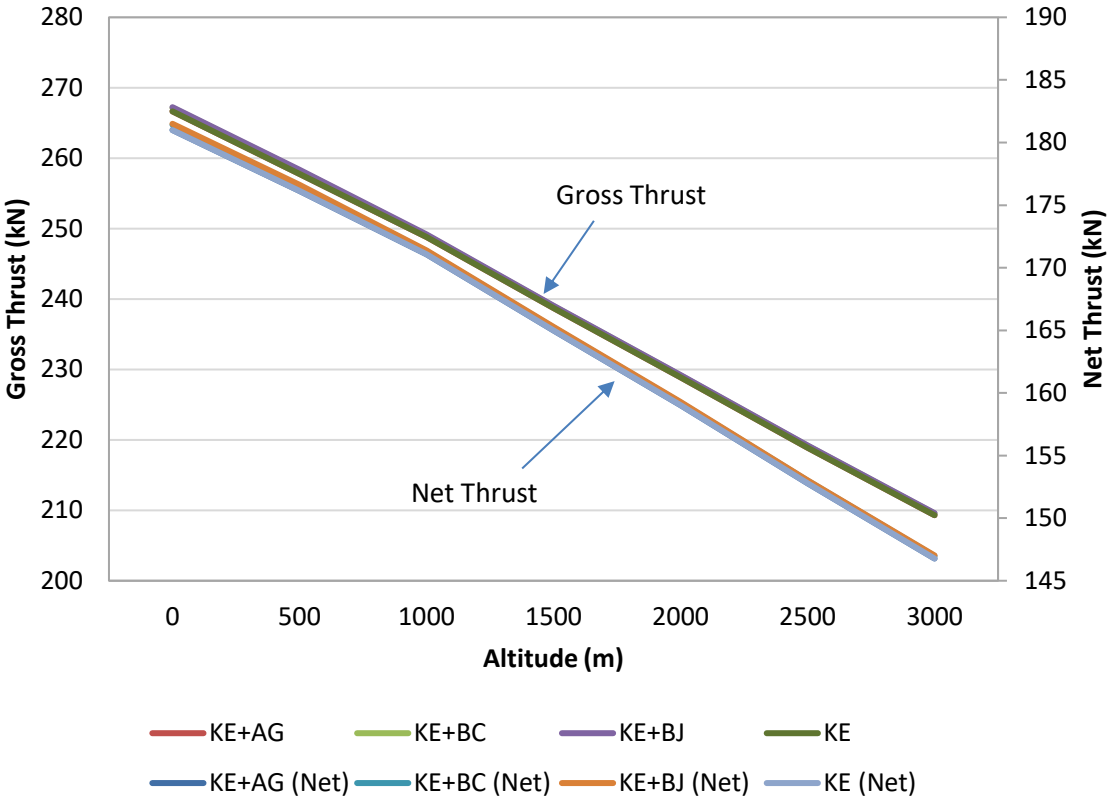

Figure 4-9 Variation of gross and net thrust at different altitude

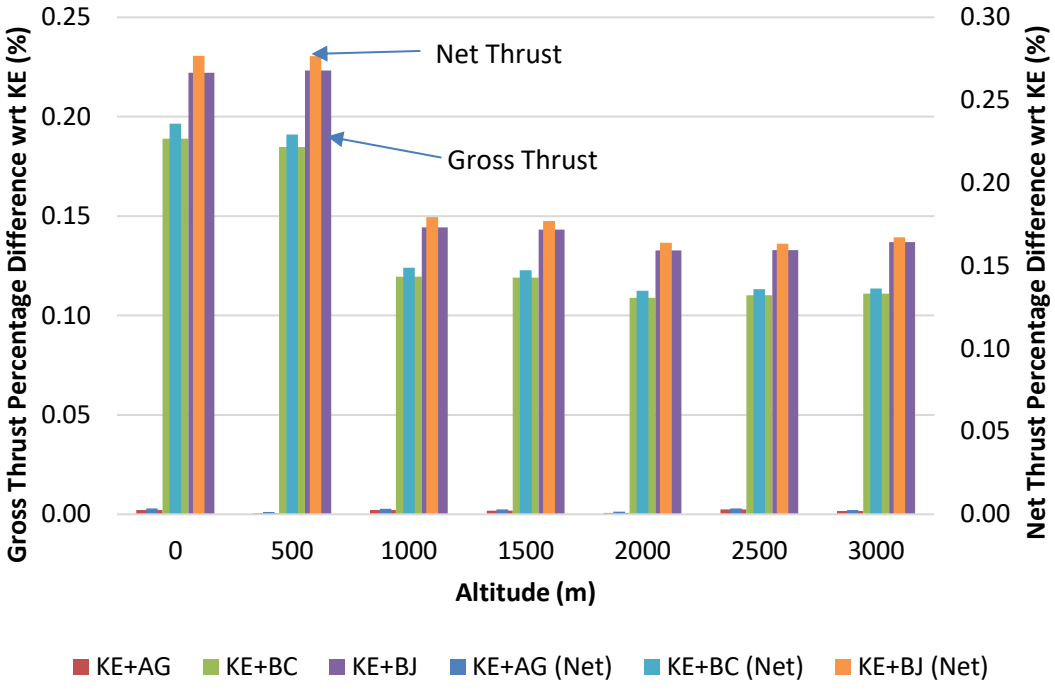

Figure 4-10 Gross and net thrust percentage difference with respect to pure kerosene at a different altitude

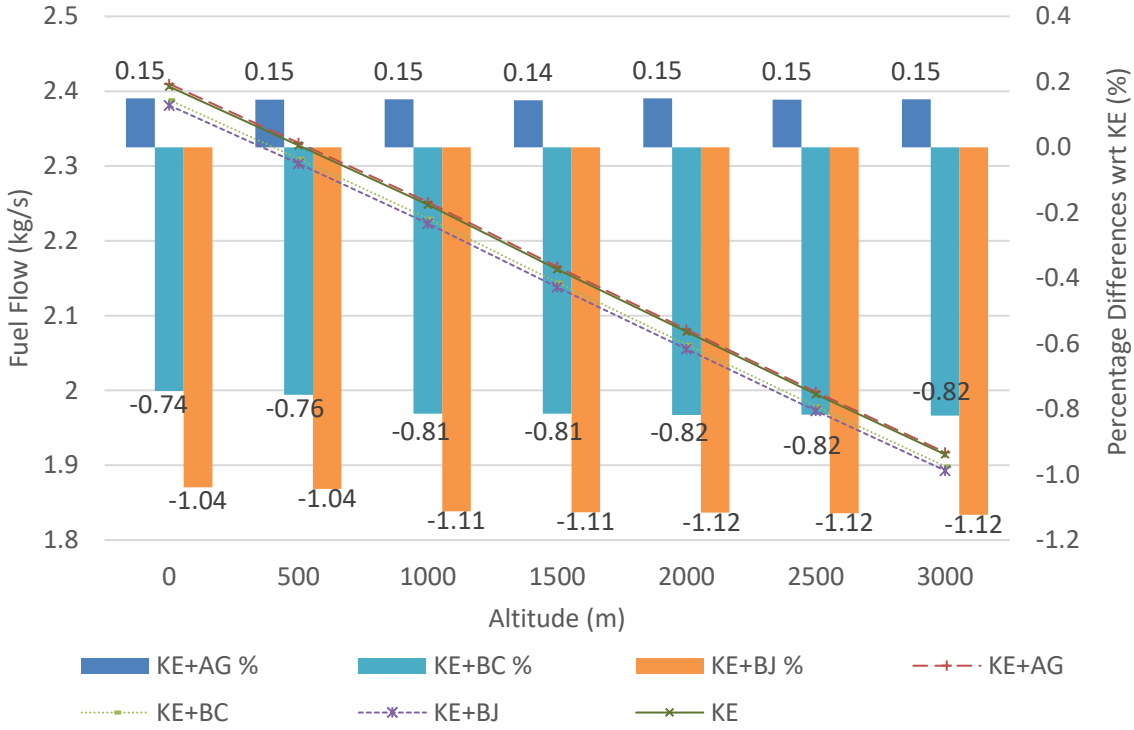

Figure 4-11 Variation of fuel flow at a different altitude

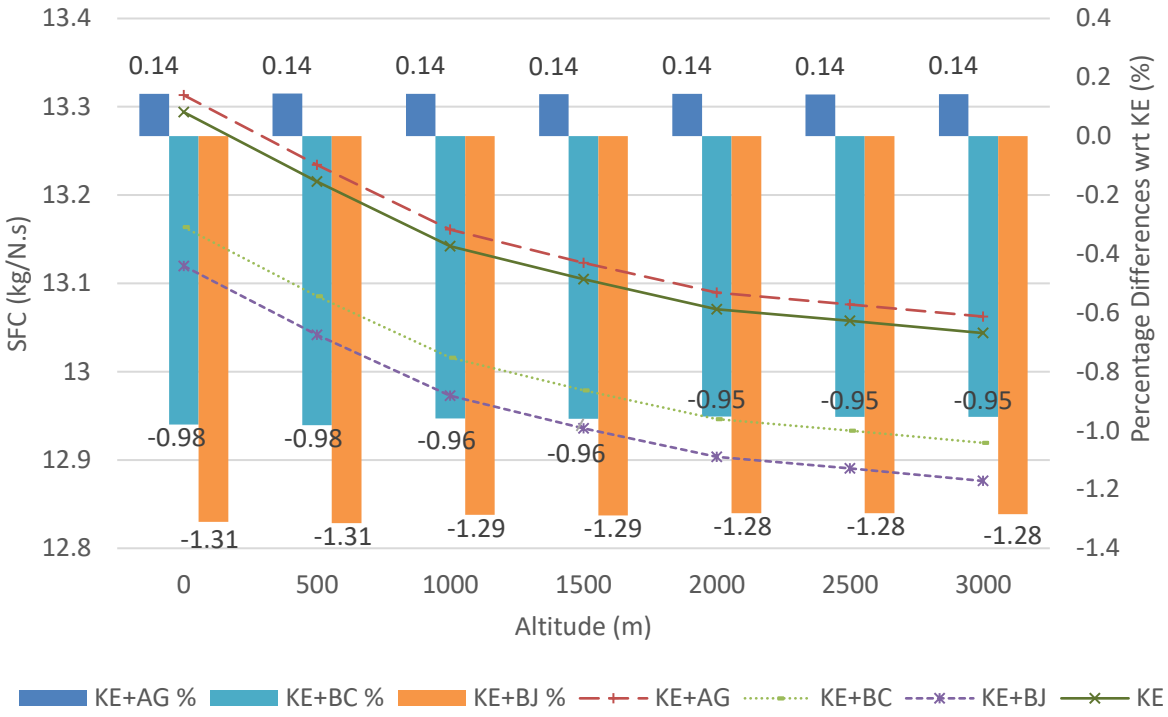

Figure 4-12 Variation of SFC at a different altitude

4.4.4 Influence of various mixing ratio blended fuel on aircraft engine performance at cruising condition

This section discusses effects of other blending mixing ratio percentages on engine performance at cruising flight condition. A selection of ambient and flight conditions are illustrated in Figure 4-13 which presents gross thrust variation and percentage difference as compared to baseline fuel. It is shown that there is an increase in gross thrust for all fuel combinations. KE+BJ blended biofuel results in higher increase in gross thrust, followed by KE+BC and KE+AG blended biofuels. BJ pure biofuel (mixing ratio of 1) has 0.23% increase in gross thrust, while BC pure biofuel has 0.18%. BJ pure biofuel 0.42% increase in net thrust, while BC pure biofuel has 0.35%. KE+AG blended biofuel, however, only has slight increase of only up to 0.01% in both gross and net thrusts.

KE+BJ and KE+BC blended biofuels demonstrate a linear fuel flow reduction as mixing ratio percentage increases as depicted in Figure 4-14. Data have shown a total reduction of 2.22% and 1.63% in the fuel flow for pure BJ and BC respectively. KE+AG blended biofuel shows an increment in fuel flow at about 0.29% at higher mixing ratio percentages. Similarly, KE+BJ and KE+BC blended biofuels exhibit a reduction in SFC as the mixing ratio increases (Figure 4-15). SFC is reduced by up to 2.63% and 1.96% for BJ pure biofuel and BC pure biofuel, respectively. Meanwhile, AG biofuel gives an increase of up to 0.28% on SFC in pure form. It should be noted that the use of BJ and BC can reduce the fuel flow and SFC for every percentage of blending ratio, but this is not the case for AG fuel.

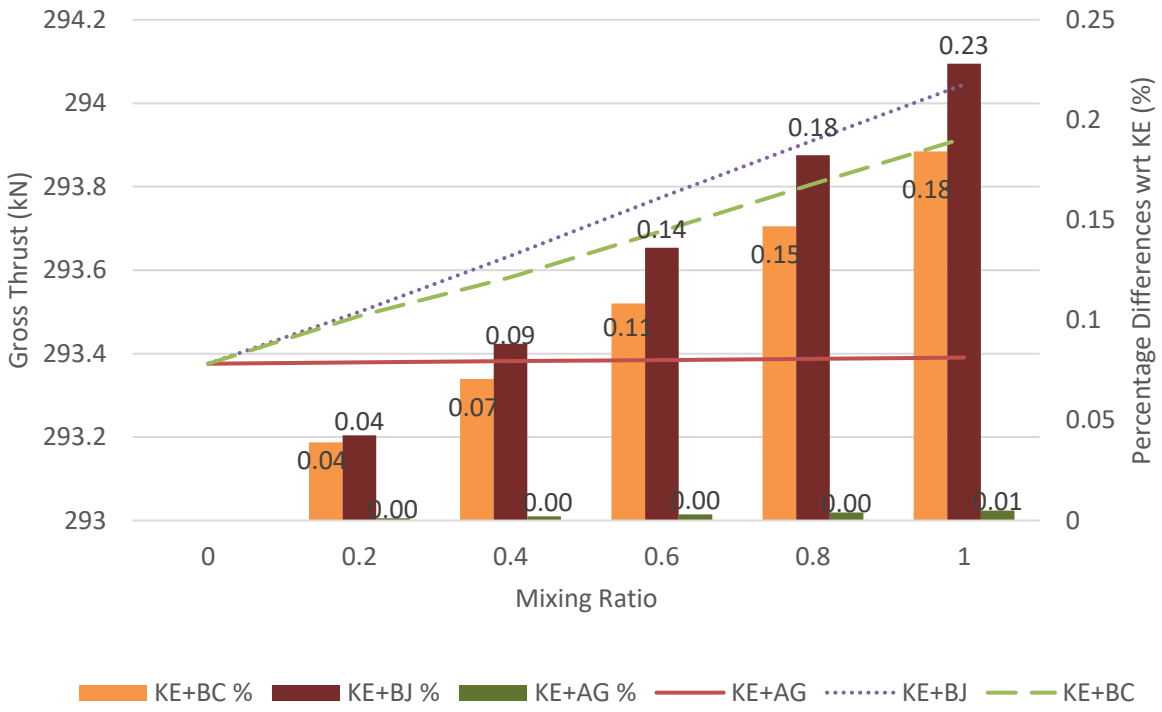

Figure 4-13 Variation of gross thrust at different percentage of mixing ratio

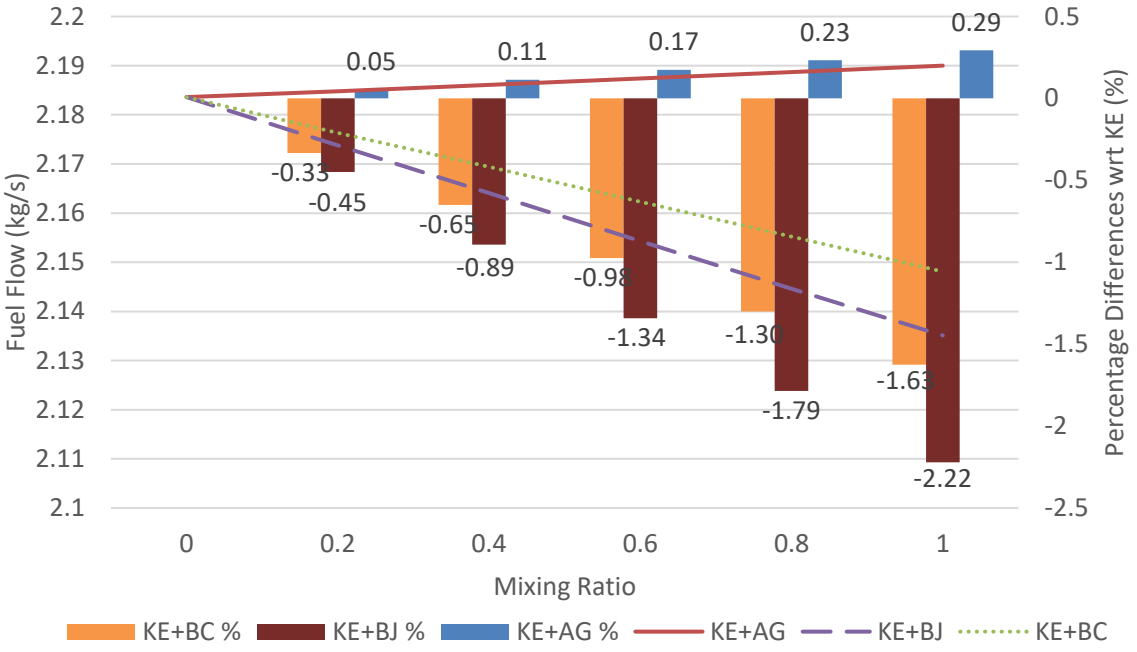

Figure 4-14 Variation of fuel flow at different percentage of mixing ratio

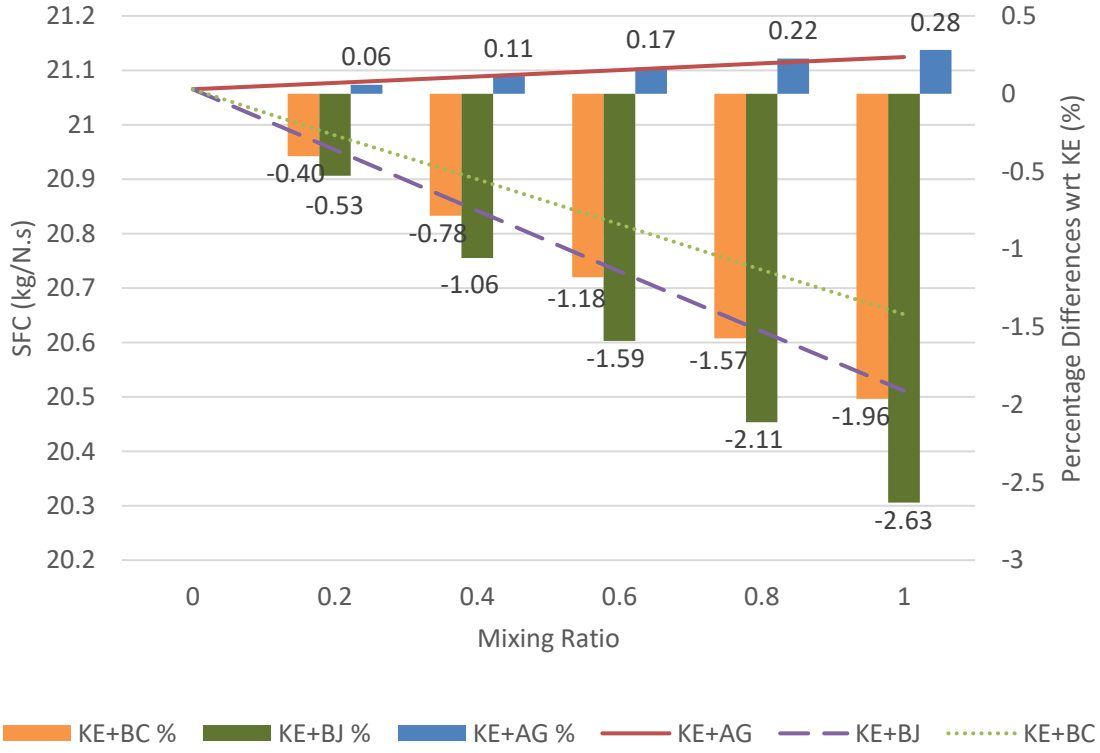

Figure 4-15 Variation of SFC at different percentage of mixing ratio

As previously discussed, performance of the aircraft engine can be deliberately enhanced by substituting kerosene with pure alternative fuels and thermochemical properties of the fuels affect the engine performance differently. These, however, in compliance with regulations enforced by authorised agencies. As alternative fuels are introduced into combustor, some assumptions should be addressed. Firstly, combustion efficiency remains the same for all fuels because it may vary in atomization due to differences in thermochemical properties. Secondly, properties of alternative fuels used are taken from the published literature, without taking consideration of ASTM approval and its processing method. Thirdly, since combustor with different of blended fuels is the primary focus, several results can be drawn out because of changed thermochemical properties. Results have shown that total pressure, mass flow and pressure drop increase slightly at higher percentage blended mixing ratio. As total pressure and mass flow rise, exit velocity increases, resulting in an increase in both gross thrust and pressure drop in the combustor. Reduction in fuel-to-air ratio (FAR) indicates that new equilibrium conditions are achieved; either more fuel or air is introduced in the combustor. Although large LHV fuel provides a better propulsive performance, it likely requires more air for combustion. Another crucial parameter is TIT as it determines the propulsive performance. TIT is then set to 1580K for all cases. Results show that high LHV fuel are able to sustain temperature longer, which is essentially important in the purpose to expand and convert high energy to useful work and kinetic energy.

In an objective comparison, Figure 4-16 and Figure 4-17 illustrate how these pure alternative fuels (AG, BC, and BJ) enhance performance at ground idle and cruising condition. At ground idle, BJ and BC fuels result in higher thrust, lower fuel flow and SFC as compared to kerosene fuel. AG fuel shows a slight increase in thrust, and a fair increase in fuel flow and SFC. However, at cruising condition, percentage differences with baseline are reduced for BJ and BC fuels for gross thrust. In contrast, AG fuel has a slight increment with improvement in fuel flow and SFC in cruising.

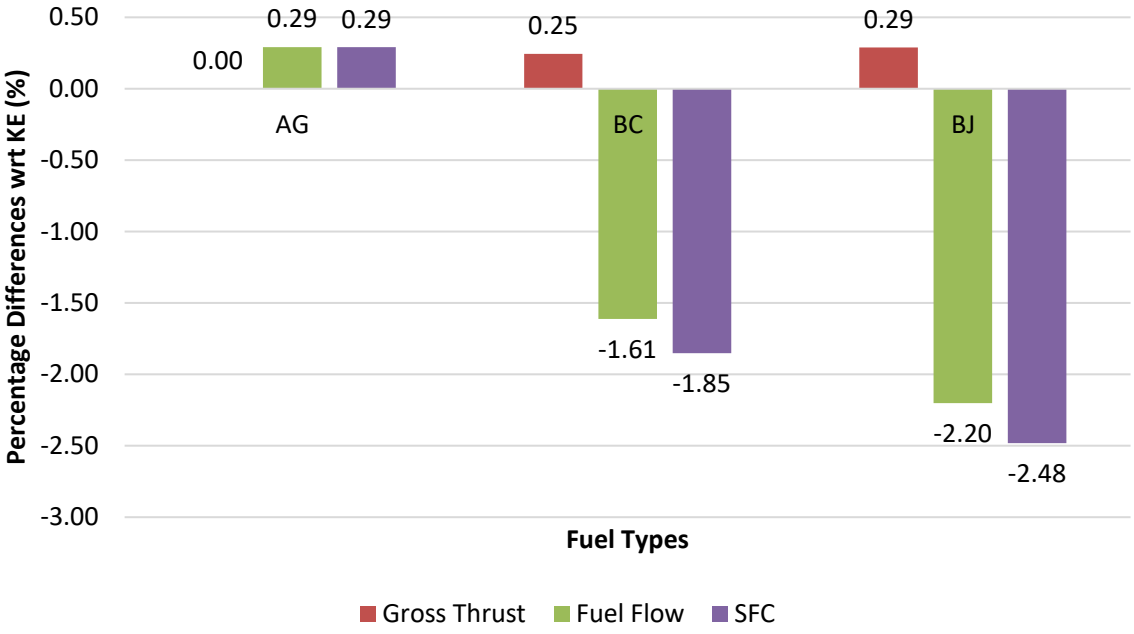

Figure 4-16 Performance comparison of pure alternative fuel at the ground condition

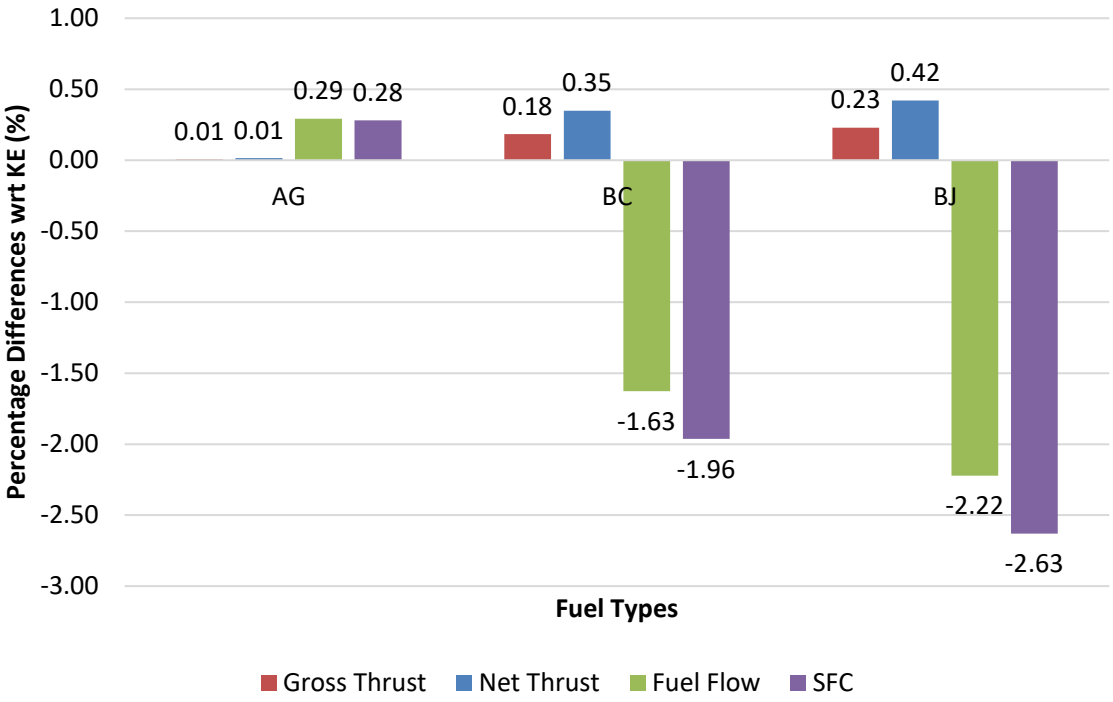

Figure 4-17 Performance comparison of pure alternative fuel at cruise condition

4.5 Concluding Remarks

Firstly, LHV of fuel poses significant effect on engine performance metrics in terms thrust, fuel flow and SFC under every flight condition and at different blended mixing ratio percentages. It is concluded that the greater the LHV difference between two fuels, the larger the change in the engine performance becomes. Secondly, performance analysis of 50% blended alternative biofuels is discussed thoroughly at two flight conditions, which are take-off at varying flight speed and climbing at varying altitude. 50% blended alternative biofuels are commonly used for flight-testing within the existing engine specifications. 50% of KE+BJ and KE+BC blended biofuel demonstrate an increase in gross thrust and net thrust, as well as improvements in fuel flow and SFC at a higher flight speed as compared to baseline kerosene fuel. However, 50% of KE+AG blended biofuel show no significant changes in gross and net thrusts, but an increase in fuel flow and SFC. At climbing conditions, however, both 50% of KE+BJ and KE+BC blended biofuels show an increase in gross and net thrusts and significantly more reductions in fuel flow and SFC as compared to baseline. On the other hand, 50% of KE+AG blended biofuel result in a higher fuel flow and SFC than baseline.

Finally, influence of various percentage mixing ratios is recorded and discussed at cruising condition. KE+BJ and KE+BC fuels, again, result in a much better engine performance as compared to the KE+AG fuel as the mixing ratio percentages increase. KE+BJ is also found to surpass KE+BC in terms of all engine performance metrics. However, KE+AG fuel has resulted in an increase in both fuel flow and SFC. All pure biofuels (AG, BC, and BJ) appear to offer slight improvements on gross thrust. BJ and BC fuels, on the other hand, show reductions in both fuel flow and SFC. Pure alternative fuels for both ground and cruising conditions are evaluated and reported accordingly. Under different conditions, AG fuel results in slight increase in gross thrust at cruise, while BJ and BC fuels show slight reduction as compared to ground condition.

Nevertheless, fuel flow and SFC are found to be significantly improving for BJ and BC fuels at cruising condition.

The present work may thus serve as an extension of Mazlan (2015) work using an earlier version of PYTHIA which could only provide strict comparisons for different pure fuels for single design conditions. The new results presented here show that previously reported results did capture the correct trends and were only subjected to relatively small offset errors. Conclusively, findings in this research do not only support earlier findings, but indeed, have gone beyond. Moreover, this work also has shown the capabilities to evaluate the engine performance utilizing the third generation of biofuel over wider flight cycles.

5 EVALUATION OF BIOFUEL - DETONATIVE COMBUSTION ANALYSIS

5.1 Introduction

Detonative combustion utilizes shocks and detonation waves by providing pressure-rise combustion and prominently result in higher thermodynamic efficiency as compared to conventional isobaric heat addition in a Brayton cycle combustor. Despite being unsteady, this combustion has already been in used in wave rotor, pulse detonation engine (PDE) and rotating detonation engine (RDE) configurations as alternative technologies for next generation of aerospace propulsion systems.

To enhance performance that it offers, environmental concerns shall be addressed as well. Following successful flights of many commercial aircraft running with different biofuels, they are now proven to be a viable choice to sustain the environment and energy demand. Biofuels with pressure-rise combustors are expected to perform better, while at the same time satisfy greener technology need. It is also believed that these alternative combustor technologies fuelled by alternative fuels could meet 2050 emissions targets plan for aviation. However, shortcomings associated with the use of biofuels alone in aircraft engine in terms of chemical, physical properties and also overall performance, that is dealt with in this research. The analysis utilizes PDE because is it relatively simple to model as it the first attempt to evaluate biofuels under detonative combustion.

This chapter presents an assessment for alternative fuels, which are Kerosene, Acetylene, Jatropha Biofuel, Camelina Biofuel, Algae Biofuel and Microalgae Biofuel under detonation combustion conditions. A wide literature review has been discussed briefly to gain insight the work done on detonative combustion. Theoretical and formulation frameworks are presented to describe how the model is developed. For simplicity, analysis is modelled by using an open-

ended tube geometry. The analysis applies Rankine-Hugoniot Equation, Rayleigh Line Equation, and Zel'dovich–von Neumann–Doering (ZND) model and takes into account species mole, mass fraction and enthalpies-of-formation of the reactants. Results and discussion on the minimum conditions for the detonation of each fuel are first determined before exploring pressure, temperature, and density ratios at each state of the combustion tube for different types systematically. Eventually, influence of different initial conditions is numerically calculated and compared.

5.2 Literature Review

Detonation is a mode of combustion that can provide an extremely efficient means of combusting a fuel-oxidizer mixture (Kailasanath, 2003). It produces kinetic energy of two orders of magnitude higher than slower-burning deflagration and of four orders of magnitude higher in terms of heat release (Frolov, 2014). It is thermodynamically more efficient and has real potential for next generation of aerospace propulsion systems (Li *et al.*, 2013) as detonative combustion utilizes shocks or detonation waves which act like a valve between the detonation product fresh charges (Eidelman, Grossmann and Lottati, 1991). It may, in fact, be the first practical application of non-isobaric heat addition in Humphrey cycle analysis (Vutthivithayarak, Braun and Lu, 2011).

The detonation wave is modelled as a normal shock wave or Zel'dovich–von Neumann–Doering (ZND) detonation wave, that advances into undisturbed fuel–air mixture of a uniform cross-sectional area tube, which is almost at rest for combustor entry condition (Heiser and Pratt, 2002), followed by Rayleigh type combustion (Kentfield, 2002b). The whole process satisfies Chapman–Jouguet (CJ) condition, which requires local Mach number at termination of the heat expansion region (Heiser and Pratt, 2002). CJ theory requires chemical reactions to be represented by heat discharge in an infinitesimally thin shock front that brings material from an initial state on inert Hugoniot line to a

subsequent CJ point state (Vutthivithayarak, Braun and Lu, 2011). The CJ point also forms a tangent from initial to final state on a Pressure-Volume diagram (p–v diagram) equivalent to the Rayleigh heating process. It is, however, difficult to evaluate relative performance of air-breathing PDEs in respect to conventional steady-flow propulsion systems without performing a full unsteady computational analysis because of intrinsically unsteady nature of the flow field due to detonation process (Brophy, Sinibaldi and Damphousse, 2002; Kailasanath, Patnaik and Li, 2002; Wintenberger and Shepherd, 2003).

In conventional Brayton cycle, heat injection process has maximum energy, which is fixed by compressor's delivered pressure and temperature limit. This means that the energy can be increased if heat injection process follows different thermodynamic cycle path (Blanco, 2014). The thermodynamic of Humphrey cycle is considered a modification to the Brayton cycle, where constant-pressure heat addition process is replaced by constant-volume heat addition process (Heiser and Pratt, 2002). Humphrey cycle appears much more efficient than the Brayton cycle (Kailasanath, 2000) since burning takes place rapidly. However, due to this speed, there is no enough time for pressure equilibration causing the overall process is thermodynamically closer to a constant volume process than constant pressure process that is typical of conventional propulsion systems (Kailasanath, 2000). On another note, thermodynamic efficiency of Chapmen–Jouget detonation has minimum entropy generation along Hugoniot curve as compared to other combustion modes, which appear to have potential thermodynamic advantage (Nikitin *et al.*, 2009; Li *et al.*, 2010).

Several devices utilize unsteady flow to achieve pressure-rise combustion, including pressure exchanger in wave rotor, Pulse Detonation Engine (PDE) and Rotating Detonation Engine (RDE). Wave rotor is a non-steady flow device that compresses combusted gas unsteady shock waves rather than curved blades (Chan and Liu, 2014) in the compressors. Its combustor is a combination

of pressure-wave compression and expansion confined combustion within the rotor channels (Akbari and Nalim, 2009). Shock waves are initiated as rotor channels are in open-and-close positions. Wave rotors have advantages to increase thermal efficiency by improving TIT, increasing output power and limiting NOx emission. This is done with rapid combustion and gas dynamic quenching, self-cooled machine and uniform exit velocity profile (Akbari and Muller, 2003; Akbari and Nalim, 2006, 2009). Despite that, its efficiency is reduced by friction and heat conduction, as well as expose to leakage problems of finite opening time of the channels (Chan and Liu, 2014). Alternatively, RDE attempts to improvise PDE in continuously detonation combustion. Detonation waves are continuously generated and propagated in azimuthal direction around an annular chamber at high frequency (Yi *et al.*, 2011; Lu and Braun, 2014). Further improvements in RDE from PDE include small geometry required to achieve detonation, dismissal of deflagration-to-detonation transition (DDT) devices, less time consumption for filling and purging process, low vibration and noise.

It is vital that environmental assurance shall be in parallel with better performance that the detonation mode of combustion offers. Unfortunately, to date, almost no efforts have been made to study the environmental effect of alternative fuels under detonative combustion conditions. Even though studies have been made on heavy-hydrocarbon fuel such as Jet Propellant (JP10), none have been made of other commercialized alternative fuels. Since alternative fuels are predicted to be in use in near future, it is certainly worth exploring their wider capability starting from now. Therefore, four biofuels, namely Jatropha Biofuel (BJ), Camelina Biofuel (BC), Microalgae Biofuel (MA) and Algal Biofuel (AG) have been evaluated as pure fuels, and are compared with conventional kerosene and acetylene (ACN) fuels. These particular biofuels are selected because of their reported successful use in conventional engine test flight programmes and availability on their fuel properties in the published literature, as listed in the Appendix A.1. This research is intended to

assess behaviour of these alternative fuels in terms of physical and chemical properties for changes in different initial conditions. This work only uses one-step chemistry reactions for a start in order to make a straight comparison between different fuels in order to assess if they were sufficiently accurate to be useful. It is noted that the remaining differences within the experiment are most likely due to not using full multi-step chemistry and this leaves opportunity open for further explorations.

5.3 Theoretical Formulation and Numerical Frameworks

The model utilizes ZND Theory and CJ Theory in a zero dimensional analysis under a few basic assumptions. In first attempt, the approach was to employ single tube, phase and cycle process. The model adopted here uses an open-ended constant-area tube geometry in a single cycle operation. It incorporates appropriate expressions, including Rankine-Hugoniot Equation, Rayleigh Line Equation, species mole and mass fraction of the reactants, enthalpies-of-formation and ideal-gas normal shock equations. Computational results from our analyses have been verified by using available limited published data from the literature to ensure the consistency of our model across an acceptable range of cases. Five key simplifying assumptions have been made in this work: upstream and downstream boundaries are included in the control volume, with no temperature or species concentration gradients; there is uniform zero-dimensional flow under adiabatic conditions; body forces, dissociation of products, and atomization of fuel are neglected; and only the normal shock relation is considered. In addition, although there are many variations in molecular structures of these alternative fuels, consideration of such variability in characteristics of the fuels is also neglected, and the analysis is based solely on the properties given in the Appendix A.1. Figure 5-1 illustrates different stages for the calculations below.

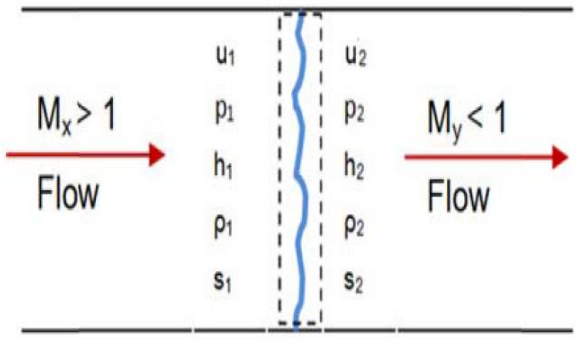

Figure 5-1 Illustrations of different states adapted from Blanco (2014)

For modelling, these assumptions are applied using the following relations:

1. Steady flow:

$$\dot{m}'' = \frac{\dot{m}}{A} \tag{5-1}$$

Conservation of mass:

$$\dot{m}'' = \rho_1 V_{x,1} = \rho_2 V_{x,2} \tag{5-2}$$

2. Ideal gas behaviour is applied.

$$P = \rho R T \tag{5-3}$$

3. Body forces are neglected.

Conservation of momentum:

$$P_1 + \rho_1 V_{x,1}^2 = P_2 + \rho_2 V_{x,2}^2 \tag{5-4}$$

Conservation of Energy:

$$h_1 + \frac{V_{x,1}^2}{2} = h_2 + \frac{V_{x,2}^2}{2} \tag{5-5}$$

Adopting heat addition ‘q’:

$$c_p T_1 + \frac{V_{x,1}^2}{2} + q = c_p T_2 + \frac{V_{x,2}^2}{2} \quad \textbf{(5-6)}$$

Given:

$$q \equiv \sum_{state\ 1} Y_i h_{f,i}^0 - \sum_{state\ 2} Y_i h_{f,i}^0 \quad \textbf{(5-7)}$$

Zero-dimensional analysis with variation of mass flux, initial temperature and pressure are calculated from conservation of mass and momentum, thus, Rayleigh line yields the following relationship:

$$\frac{P_2 - P_1}{\frac{1}{\rho_2} - \frac{1}{\rho_1}} = \frac{P_2 - P_1}{v_2 - v_1} = -\dot{m}''^2 \quad \textbf{(5-8)}$$

By combining conservation of mass, momentum and energy with heat addition:

$$\frac{\gamma}{\gamma - 1}(P_2 v_2 - P_1 v_1) - \frac{1}{2}(P_2 - P_1)(v_1 + v_2) - q = 0 \quad \textbf{(5-9)}$$

From Rayleigh Line, P_2 is:

$$P_2 = P_1 + \dot{m}''^2(v_1 - v_2) \quad \textbf{(5-10)}$$

By substituting into Rankine-Hugonoit Curve:

$$\frac{\gamma}{\gamma - 1}[(P_1 + \dot{m}''^2(v_1 - v_2))v_2 - P_1 v_1)] - \frac{1}{2}((P_1 + \dot{m}''^2(v_1 - v_2)) - P_1)(v_1 + v_2) - q = 0 \quad \textbf{(5-11)}$$

Then, by expanding and converting into quadratic equation:

$$av_2^2 + bv_2 + c = 0 \quad \textbf{(5-12)}$$

Where,

$$a = \frac{1+\gamma}{2(1-\gamma)}\dot{m}''^2 \quad \textbf{(5-13)}$$

$$b = \frac{\gamma}{\gamma-1}\left(P_1 v_1 + \dot{m}''^2 v_1\right) \quad \textbf{(5-14)}$$

$$c = \frac{\gamma}{1-\gamma}P_1 v_1 - 1/2\,\dot{m}''^2 v_1^2 - q \quad \textbf{(5-15)}$$

$$v_1 = \frac{R_1 T_1}{P_1} \quad \textbf{(5-16)}$$

And solve for v_2,

$$v_2 = \frac{-b \pm \sqrt{b^2 - 4ac}}{2a} \quad \textbf{(5-17)}$$

$P_2, V_{x,2}, T_2, c_2\ and\ M_2$ values for every v_2 are calculated accordingly. Next, detonation velocity in stoichiometric condition and gas mixture properties at the shock front (state 2') are estimated by applying stoichiometric relation:

$$C_x H_y + a(O_2 + 3.76N_2) \rightarrow xCO_2 + (y/2)H_2O + 3.76aN_2$$

Every species mole and mass fraction are calculated and thermochemical properties such as specific heat, gas constant, and specific heat ratio are obtained by using these relations:

$$c_{p,1} = \frac{\sum_{state\ 1} \chi_i \bar{c}_{p,i}}{MW_1} \text{ and } c_{p,2} = \frac{\sum_{state\ 2} \chi_i \bar{c}_{p,i}}{MW_2} \quad \textbf{(5-18)}$$

$$R_2 = \frac{R_u}{MW_2} \text{ and } \gamma_2 = \frac{c_{p,2}}{c_{p,2} - R_2} \quad \textbf{(5-19)}$$

Heat formation, q, is calculated by using enthalpies-of-formation in the tabulated table which is converted into a mass basis.

$$q \equiv \sum_{state\ 1} Y_i h_{f,i}^0 - \sum_{state\ 2} Y_i h_{f,i}^0 \quad \textbf{(5-20)}$$

Detonation velocity and temperature at state 2 are determined using:

$$v_D = \left[2\gamma_2 R_2 (\gamma_2 + 1) \left(\frac{c_{p,1}}{c_{p,2}} T_1 + \frac{q}{c_{p,2}} \right) \right]^{1/2} \quad \textbf{(5-21)}$$

$$T_2 = \frac{2\gamma_2^2}{\gamma_2 + 1} \left(\frac{c_{p,1}}{c_{p,2}} T_1 + \frac{q}{c_{p,2}} \right) \quad \textbf{(5-22)}$$

By using ideal-gas normal-shock and applying mixture specific heat ratio and Mach number at the initial state, these relations are used to find state 2':

$$\frac{P_{2'}}{P_1} = \frac{1}{\gamma + 1} [2\gamma M_1^2 - (\gamma - 1)] \quad \textbf{(5-23)}$$

$$\frac{T_{2'}}{T_1} = [2 + M_1^2(\gamma - 1)] \frac{2\gamma M_1^2 - (\gamma - 1)}{(\gamma + 1)^2 M_1^2} \quad \textbf{(5-24)}$$

$$\frac{\rho_{2'}}{\rho_1} = \frac{(\gamma + 1) M_1^2}{(\gamma - 1) M_1^2 + 2} \quad \textbf{(5-25)}$$

Then, $V_{x,2'}$ is calculated using conservation of mass:

$$\dot{m}'' = \rho_1 V_{x,1} = \rho_{2'} V_{x,2'} \quad \textbf{(5-26)}$$

$$M_{2,} = \frac{V_{x,2,}}{\sqrt{\gamma_{2,} R_{2,} T_{2,}}} \quad \textbf{(5-27)}$$

The state-2 Mach number should be equal to one (upper CJ-point).

5.4 Results & Discussions

5.4.1 Model Comparison

Before further analysis, the above model has been validated, first against a case study of Turns (2000) for acetylene fuel. The same procedures have then been used to evaluate other fuels by respecting chemical relations established by molecular formula of these fuels under stoichiometric combustion conditions. Experimental data for liquid hydrocarbon detonation suitable for comparison with our results are, however, quite scarce. Only limited data on a few comparisons can be made, except for biofuels. Most experiments have been carried out by using either hydrogen-oxygen or hydrogen-air reactions because of the ease in which detonation can be initiated. Nevertheless, a parametric validation, in terms of the detonation velocity and pressure gain in the burned state, is attempted. This causes the validation for only acetylene and kerosene fuels can be made. Model results for acetylene fuel are compared with the numerical data of Turns (2000) while comparisons for kerosene fuel are made with analytical study of Wintenberger et al. (2003), time-dependent Computational Fluid Dynamics (CFD) of Yungster and Breisacher (2005), experimental work conducted by Cheatham and Kailasanath (2005a) for a range of fuel droplet sizes. The detonation velocity is taken as the von Neumann spike, while pressure rise is taken as time-average. The literature findings are found to be generally comparable, falling within an acceptable range of results obtained from model calculations for both detonation velocity and pressure gained, most notably for acetylene experiments and kerosene

computations, as shown in Table 5-1. The differences are discussed in details in the following paragraphs.

Table 5-1 Model comparison with analytical and experimental studies

ACN	**Wintenberger et al.** (2003)	**Turns** (2000)	**Model**
$V_D\ (m/s)$	1879	1998	1997.95
$P_2\ (atm)$	19.20	20.6	25.97

KE	**Wintenberger et al. (2003)**	**Cheatham and Kailasanath** (2005a)	**Yungster and Breisacher (2005)**	**Model**
$V_D\ (m/s)$	1784	1786	2300	2398.9
$P_2\ (atm)$	18.40	10–33	16–44	28.98

Detonation is certainly sensitive to variations in the initial conditions under different temperature, pressure and mass flux, which are not always sufficiently specified to complete comparison. Initial sensitivity studies suggest that changes in initial conditions result in at most 10% uncertainty in predicted detonation velocity. Any dissociation effects are likely to have large effect on the detonation velocity. The detonation velocity is computed from Equation (5-21), which is based on the numerical approximation that pressure of burned state is significantly greater than pressure of unburned state. Detonation ratios of pressure calculated in burned state over the pressure in the unburned state are within the range identified by Turns (2000), so this approximation seems reasonable for the detonation case. However, dissociation also forms minor species, resulting in different mole and mass fractions of the products, alongside different values of heat addition, *q*, and total specific heat of the burned state (Equations (5-18) and (5-20)). Based on Equation (5-21),

detonation velocity is a square root function of these dependent variables, and, in the case of dissociation, total specific heat of the burned state increases, while heat addition (heat difference of reactant to product) decreases, resulting in lower detonation velocity as suggested by the published experiments and analytical results. In the worst case, a 35% discrepancy can be found between detonation speed predicted for Kerosene and current findings. However, it is to be noted that analytical results are based on a simplified method, while experimental results are subjected to error bars due to measurement and other uncertainties. The predicted detonation speed is also supported by published higher fidelity CFD results Yungster (2005). For acetylene, predicted detonation velocity exactly matches with a separate published analytical studies by Turns (2000) and falls within 6% of the same analytical analysis by Wintenberger (2003). This suggests that the adopted methodology is appropriate, at least for an initial investigation of biofuel alternatives, in which all predictions are closely similar (3% variation) for higher detonation velocity. Undoubtedly, other factors, such as dissociation of products, need to be addressed to fully confirm findings, but the trends manifested seem to be clear cut.

5.4.2 Conditions for Detonation

Based on model derived from previous section and chemical stoichiometric reaction (as tabulated in Table 5-2), three parameters have been analysed, in terms of the pressure ratios, density ratios and temperature ratios in respect to underlying initial conditions at different phases in the detonation tube. However, a number of essential steps need to be taken to initiate the analysis: first, all the fuels considered must achieve detonation velocity, either by raising mass flux or initial temperature before they can be detonated as shown in Table 5-3. Secondly, flow must be choked at State 2, and, finally, stoichiometric combustion has to be assured.

These minimum conditions were established as satisfying Equation (5-17), in which variables of *a*, *b*, and *c* function as pressure, mass flux, specific volume, temperature, heat addition and specific heat. Mathematically, the conditions for detonation have to satisfy both Rayleigh line and Rankine-Hugonoit Curve intersection. As the mass flux increases, the Rayleigh line becoming steeper (negative slope). It is note that heavy hydrocarbon fuels, KE and biofuels are hard to detonate, therefore need to be pre-heated or accelerated to a high velocity so that the both equations are satisfied. Microalgae fuel (MA), which requires the highest temperature and mass flux, is seen to be the most difficult to detonate, while Acetylene (ACN) the least because of the complex structure of the molecular and bond existed in the fuel. Practically, pre-detonator is used for pre-heating the fuel before it is ignited with higher energy initiation such as plasma, flame jet, or flash vaporization. The details are discussed in appendix A.4.2.

Table 5-2 Chemical equation used for stoichiometric condition

Fuels	Chemical Equation
ACN	$C_2H_2 + 2.5(O_2 + 3.76N_2) \rightarrow 2CO_2 + H_2O + 9.4N_2$
KE	$C_{12}H_{24} + 18(O_2 + 3.76N_2) \rightarrow 12CO_2 + 12H_2O + 67.68N_2$
MA	$C_{12}H_{20}O_5N_2 + 14.5O_2 + N_2 \rightarrow 12CO_2 + 10H_2O + 2N_2$
BJ	$C_{12}H_{26} + 18.5O_2 \rightarrow 12CO_2 + 13H_2O$
BC	$C_{12}H_{25.4} + 18.35O_2 \rightarrow 12CO_2 + 12.7H_2O$
AG	$C_{12}H_{19}O_3N + 15.25O_2 + N_2 \rightarrow 12CO_2 + 9.5H_2O + 1.5N_2$

Thermodynamic parameters are used to accurately predict detonation speed and other properties within range of minimum temperature and mass flux. Generally, given reactant pressure and temperature, thermochemical products

and detonation velocity can be estimated from NASA Chemical Equilibrium with Applications (CEA) analysis. However, this analysis uses a different analytical approach by allowing mole, mass fraction and enthalpy-of-formation of the reactants to use simple chemical relations in combustion. To estimate detonation velocity, estimation of heat addition, q, burned properties, and unreacted mixture specific heat are required. In order to obtain these, compositions of unreacted and reacted mixtures are first determined. After chemical relations of these fuels in stoichiometric combustion are well balanced, species mole and mass fractions can be determined. Thermochemical properties during the reaction are tabulated in Table 5-4. These properties are calculated based on summation of each species formed, in order to find its detonation velocity at arbitrary 2' state by using a ZND model. It is shown that all biofuels exhibit high heat release, q_2, (in order of 4 magnitudes) which is believed to be due to complex molecular structure of biofuels as heavy hydrocarbon requires significantly more heat to break intermolecular bonds to allow combustion. Further analysis shows that higher flame temperatures are recorded for these fuels.

Table 5-3 Minimum initial temperature & mass flux for detonation

	ACN	**KE**	**MA**	**BJ**	**BC**	**AG**
$\boldsymbol{T_1(K)}$	300	1467	2000	1700	1700	2000
G $\boldsymbol{(kg/s.m^2)}$	2612	3000	5800	4400	4400	4800
$\boldsymbol{\gamma_1}$	1.379	1.267	1.209	1.226	1.225	1.214
$\boldsymbol{Q_1(J)}$	3399.6	3648.4	12996.9	12744.9	127728.0	12622.4
$\boldsymbol{V_D(m/s)}$	1997.95	2398.9	3334.7	3244.2	3241.5	3289.5

Table 5-4 Thermochemical properties during the reaction

State 1 (Reactant)						
	ACN	**KE**	**MA**	**BJ**	**BC**	**AG**
c_{p1}	1.057	1.294	1.037	1.156	1.158	1.099
q_1	613.87	608.75	3412.21	2140.06	2147.67	2910.72
γ_1	1.379	1.267	1.209	1.226	1.225	1.214
State 2 (Product)						
c_{p2}	1.443	1.531	1.797	1.923	1.915	1.79
q_2	-2785.73	-3039.65	-9584.74	-10604.9	-10580.4	-9711.72
R_2	0.279	0.289	0.261	0.273	0.271	0.258
γ_2	1.24	1.232	1.17	1.165	1.165	1.168

5.4.3 Comparative detonation analysis of alternative biofuels using ZND model

Trend for pressure ratio achieved by various alternative fuels under minimum conditions of pressure, temperature, and mass flux is demonstrated in Figure 5-2. It is clearly seen that ACN fuel exhibits the highest pressure rise across the shock. This is believed due to its short molecular structure and energy contained between chemical bonds. All biofuels are also found to have moderate pressure rise. It should be highlighted, again, that each fuel has different initial temperature and mass fluxes to achieve detonative condition. All fuels result in initial increase in pressure ratio approaching shock, but diminish in the later phase. Strength from pressure gained weakens as wave propagates back upstream and cycles multiply. However, these effects are not considered in this study. Graphs have proven that by having a heavy molecular structure, biofuels and kerosene result in significantly lower pressure rise.

As presented in Figure 5-3, variation of temperature ratio takes a different trend. All fuels exhibit temperature increase along detonation tube. Temperature ratio rises rapidly before shock before relaxes downstream. After shock takes place, ACN achieves the highest change in temperature, followed by other heavy hydrocarbon fuels and biofuels. Thus, in addition to pressure-rise in detonative combustion, a temperature rise can also be achieved.

Density ratio patterns demonstrate a similar trend to pressure ratio, as shown in Figure 5-4. All biofuels (MA, AG, BC, and BJ) result in a significant change in density compared to other types of fuels, while KE shows the least variation in State 2. Compared to previously discussed pressure and temperature ratio variations, the changes seen in the final state are not largely significant. Molecular structure of fuel, enthalpy-formation of reaction and initial conditions have all contributed to these changes. Zero-dimensional physical parameters obtained are, indeed, consistent with structure of a detonation wave as highlighted in Kuo (2005). The spreadsheet of the analytical work using ZND model is included in Appendix C.1.

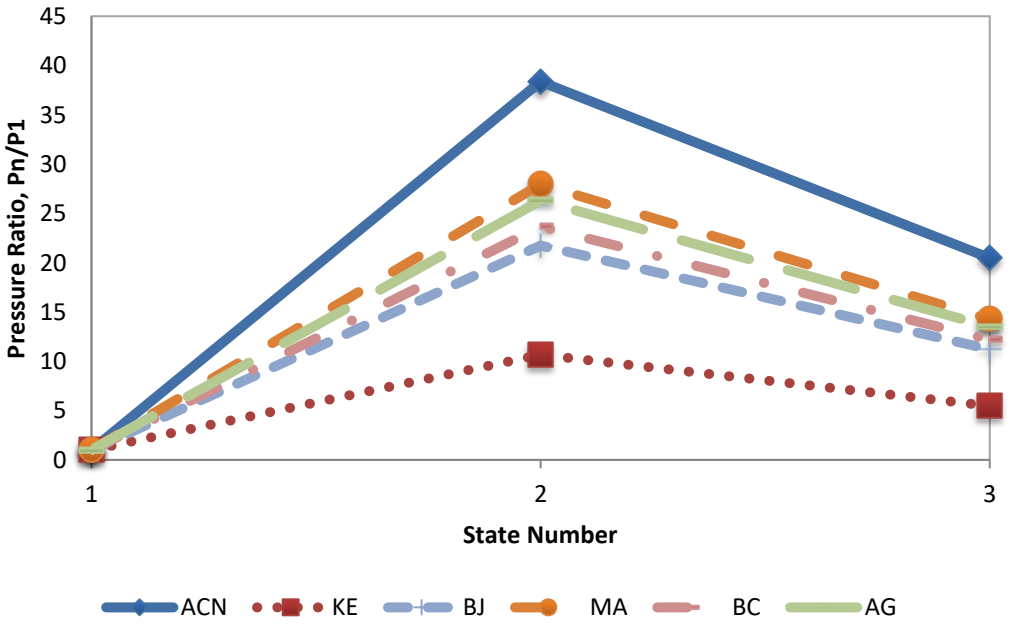

Figure 5-2 Pressure ratio at different state

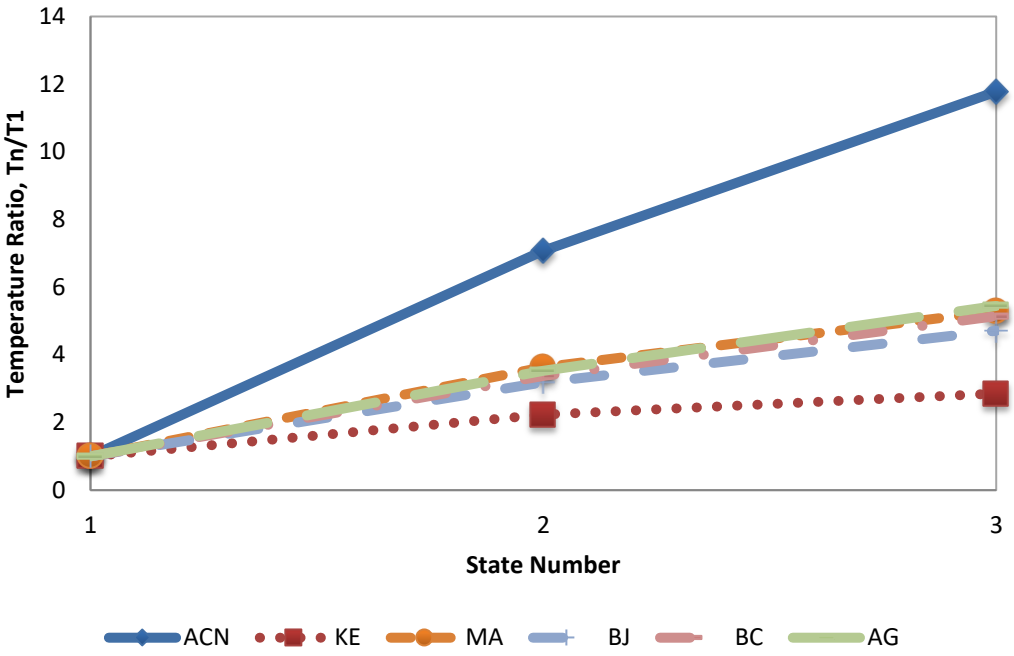

Figure 5-3 Temperature ratio at different state

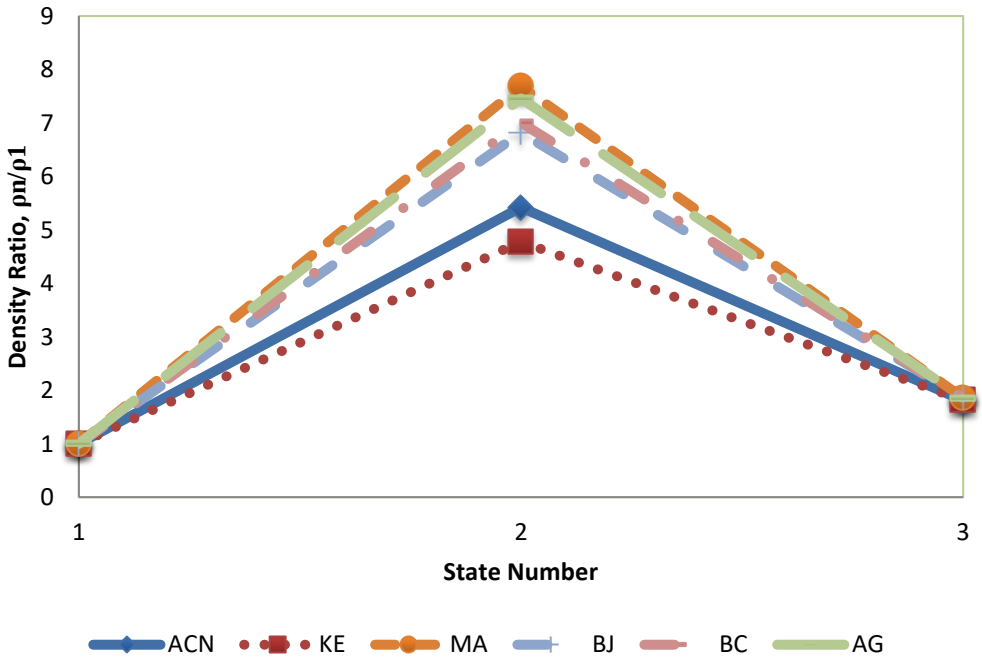

Figure 5-4 Density ratio at different state

5.4.4 Influence of various initial conditions

Initial conditions serve as critical factors for physical properties of burned gas at downstream locations. The impact on different upstream underlying conditions, such as temperature, mass flux, pressure, temperature, specific volume and Mach number ratios are discussed in this section to provide a broad insight into how initial conditions affect may downstream physical properties, presented as burned and unburned gas. Based on quadratic functions considered above, there are two distinct physical phenomena, which occur in the form of weak and strong detonations. Strong detonation is mathematically realizable but difficult to produce, while weak detonation requires a rapid reaction rate for it to occur. Both originate from the upper Chapman-Jouget point. Turns (2000) has described strong detonation occurrence as the burned gas velocity reaches a subsonic speed above the upper CJ point, while weak detonation occurs when burned gas velocity reaches supersonic speed below the upper CJ point. These conditions should satisfy both Rayleigh line and Rankine-Hugonoit Curve for them to occur. Generally, given the initial pressure and specific volume of unburned gas, the mass flux determines the type of shocks that will be produced as the Rayleigh line becomes steeper along the Rankine-Hugonoit Curve. The spreadsheets for calculating the influence of various initial conditions are attached in Appendix C.2 – C.4.

Effects of initial mass flux

Changes of pressure, temperature, specific volume and Mach number ratios for each fuel are recorded as mass flux increases. These are conducted when fuels achieved their detonation velocity under particular initial conditions. Figure 5-5 (a) illustrates pressure and temperature variations, while Figure 5-5 (b) shows variation of specific volume and Mach number ratio for ACN fuel as mass flux increases. Initial pressure and temperature remain constant at 1 atm and 300K respectively. Strong shocks appear to increase pressure and temperature ratio linearly as mass flux increases. On the contrary, weak shocks attempt to slightly decrease both ratios. Specific volume ratios and Mach number ratios, however,

show exponential trends. These trends are particularly identical for other fuels as well, except for rate of changes. Other fuels analysis is included in Appendix C.5. These trends are discussed in the following paragraphs.

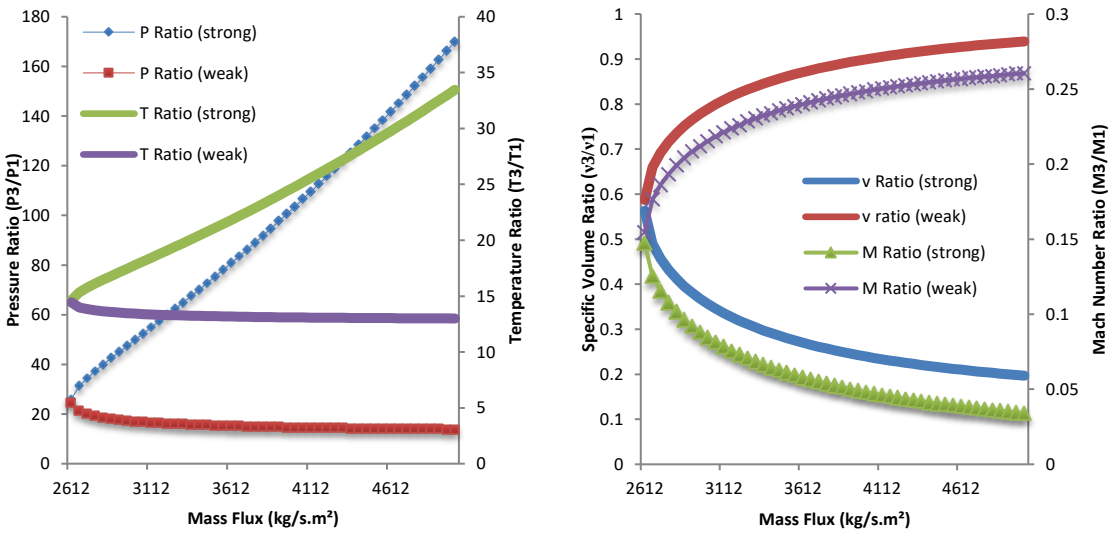

(a) (b)

Figure 5-5 Variation of (a) pressure and temperature ratios, and (b) specific volume and Mach number ratios for ACN fuel at different mass flux (P=1atm T=300K)

Further fuel comparisons have been made to investigate changes in physical properties as mass flux increases. Both weak and strong shocks influences are presented in Figure 5-6 and Figure 5-7. Due to its high sensitivity, ACN fuel analysis is excluded from the discussion. The initial conditions for the pressure and temperature are fixed at 1 atm and 2000 K, respectively. These parameters are selected to correspond when each fuel accomplishes its detonation velocity. In terms of influence of strong detonation wave, both temperature and pressure ratios result in linear increment for all fuels as mass flux increases, as presented in Figure 5-6 (a) and (b). KE fuel appears to have higher pressure ratios, while BJ and BC fuels have the highest temperature ratio. Due to their

similar molecular formulae, BJ and BC are, again, narrowly differentiated. Corresponding changes in specific volume and Mach number ratios are illustrated in Figure 5-6 (c) and (d). All the alternative fuels have a specific volume reduction after shock wave under strong detonation condition. Relatively small variation of these two ratios is seen as for KE fuel. In contrast, MA fuel shows significant changes in specific volume and Mach number ratios at low mass flux before these start to settle.

Meanwhile, under influence of weak detonation wave, variations of physical properties insignificantly differ as mass flux increases as depicted in Figure 5-7. Among all fuels, MA fuel largely affects changes of mass flux. It results in significantly higher pressure and temperature ratio as shown in Figure 5-7 (a) and (b), which are certainly useful to increase thermodynamic efficiency. However, other fuels remain constant without affecting mass flux. Difference in trends between strong and weak shock are mainly due to mathematical term of quadratic function in equation 5-17, in which heat formation q affecting the changes of the particular fuel. The heat formation is related to chemical properties from its molecular structure, such as in the case of enthalpy formation.

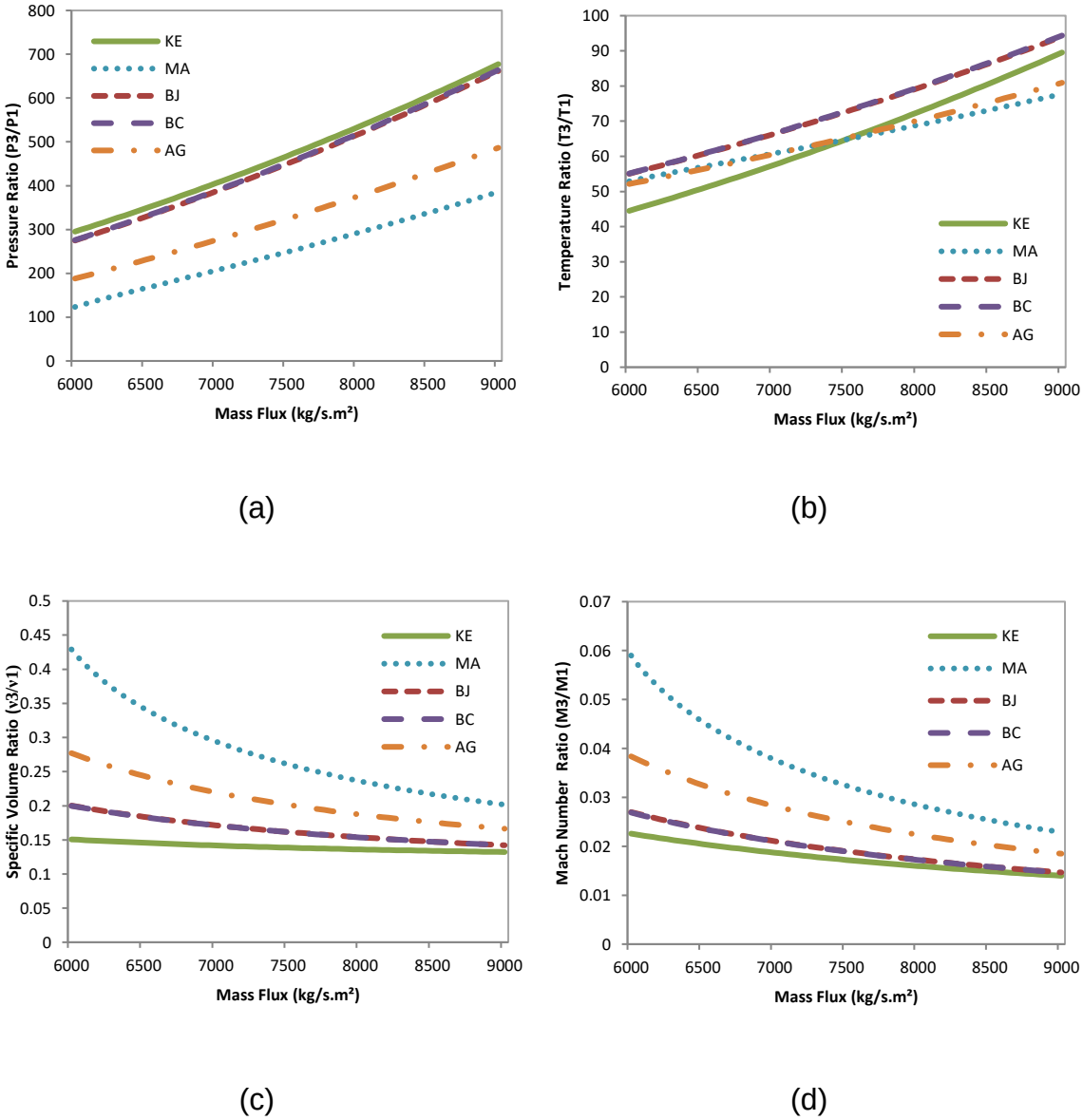

Figure 5-6 Comparison of (a) pressure ratios; (b) temperature ratios; (c) specific volume ratios; (d) and Mach number ratios at different initial mass flux under influence of strong detonation (P = 1 atm, T = 2000 K)

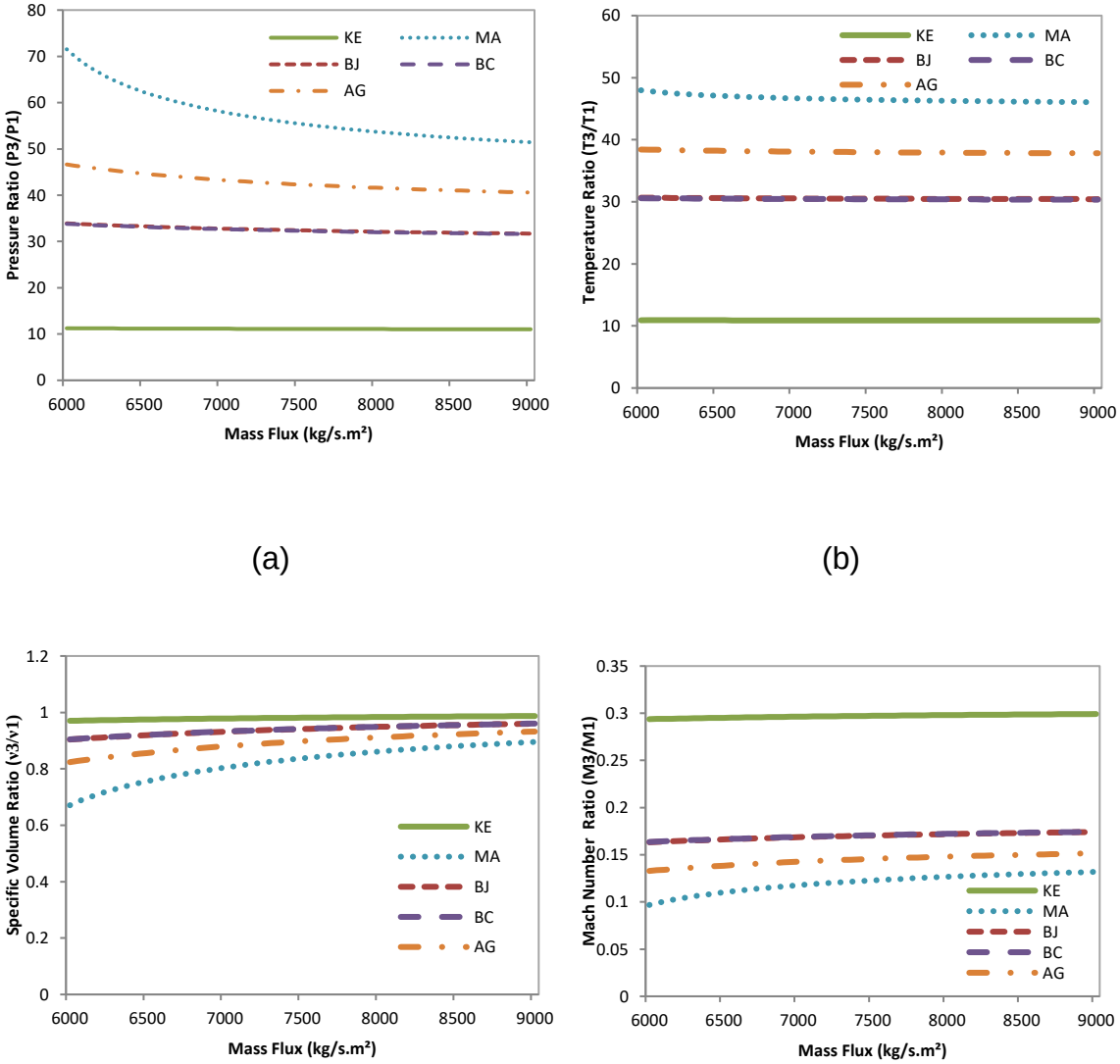

Figure 5-7 Comparison of (a) pressure ratios; (b) temperature ratios; (c) specific volume ratios; (d) and Mach number ratios at different initial mass flux under influence of weak detonation (P = 1 atm, T = 2000 K)

Effects of initial temperature

The effects of initial temperature to the physical properties ratios are discussed in this section. Initial conditions of pressure and mass flux remain constant, while manipulating initial temperatures. Figure 5-8 (a)-(c) demonstrates effects of initial temperature to pressure, temperature and density ratio of ACN fuel in each state. These figures show that high initial temperature results in lower pressure, temperature and density ratio during and after shock. It is also worth to mention two important findings due to initial temperature change; 1) higher initial temperature requires significantly lower initial Mach speed to achieve detonation, 2) higher initial temperature results in higher detonation velocity (refer to equation 5-21).

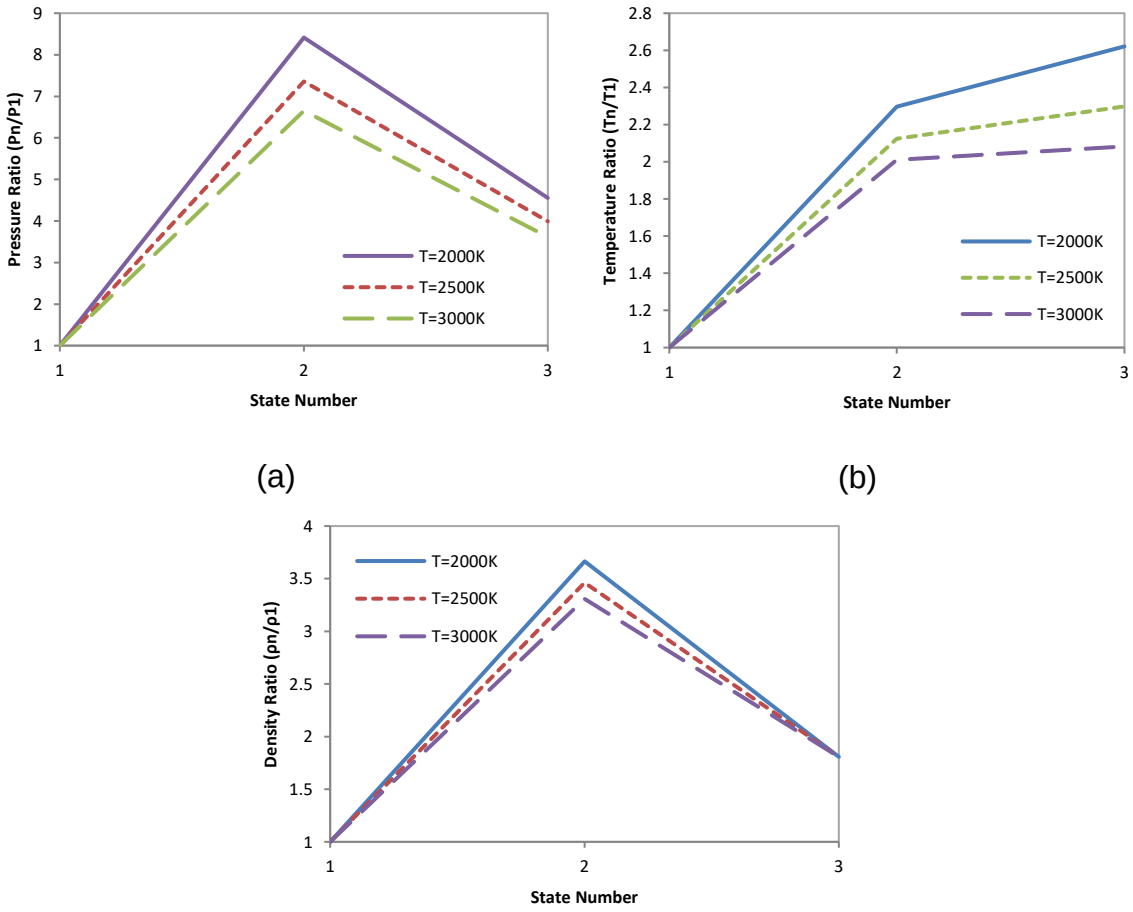

Figure 5-8 Influence of initial temperature to (a) pressure ratio, (b) temperature ratio, and (c) density ratio of ACN fuel in each state

Individual fuel is tested to observe changes of physical properties as initial temperature changes. Likewise, these analyses are conducted when fuels achieve their detonation velocity under particular initial conditions. Figure 5-9 (a) illustrates pressure and temperature variations, while Figure 5-9 (b) shows variation of specific volume and the Mach number ratio as initial temperature increases. Strong shocks appear to increase pressure and temperature ratio linearly. On the contrary, weak shocks seem to slightly decrease both ratios. However, specific volume and Mach number ratios show different trends. These trends are identical for other fuels as well, except rate of changes of physical properties. Other fuels analyses are included in Appendix C.6.

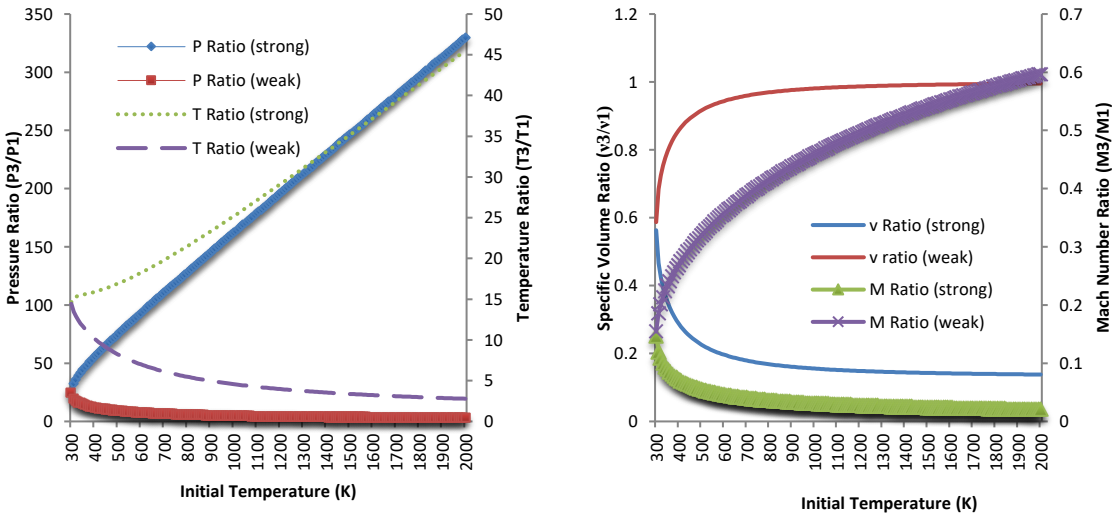

(a) (b)

Figure 5-9 Variation of (a) pressure and temperature ratios, and (b) specific volume and Mach number ratios for ACN fuel at different initial temperatures (P=1atm G=2612kg/s.m²)

Comparison between effect of initial temperature on the subsequent temperature of fuels, in terms of pressure, specific volume, and Mach number ratios are discussed in the next section. While initial temperature is manipulated, the other initial conditions of mass flux and pressure remain

constant at 1 atm and 6000 kg/s.m², respectively. The initial temperatures vary from 2000 K as this is the minimum temperature for MA and AG fuels to detonate. Figure 5-10 (a) and (b) demonstrate changes in pressure and temperature ratios, respectively. They show similar patterns with variations in mass flux, but although less significant. This suggests that mass flux has bigger impact on pressure and temperature ratios, as represented in the corresponding graphs gradient. Similarly, as initial temperature increases, significantly larger temperature ratio variations are seen for KE fuel, as compared to other fuels, as it requires lower temperature for detonation. Even though the impact of initial temperature on specific volume and Mach number ratios is almost identical as seen on the trends, the gradients are seen to be significantly higher (Figure 5-10 (c) and (d)). Initial temperature also appear to put more notable effects on specific volume and Mach number ratios compared to initial mass flux. It requires further modelling to explain the distinct changes to specific volume and Mach number ratios in KE, BJ, and BC fuels, but it appears that these fuels display more prominent gradient changes in specific volume and Mach number ratios at the lowest temperature for detonation.

Meanwhile, under the influence of weak detonation wave, variations of physical properties have significantly changed as initial temperature increases, as represented in Figure 5-11. Similarly, among all fuels calculated, MA fuel is most significantly influenced by initial temperature. MA fuel results in much higher pressure and temperature ratio as shown in Figure 5-11 (a) and (b), which directly has tendency to increase thermodynamic efficiency. KE fuel appears to have significantly lower pressure and temperature ratios, but the opposite occur specific volume and Mach number ratios. Other data also show that KE fuel is the least affected to initial temperature as compared to other fuels.

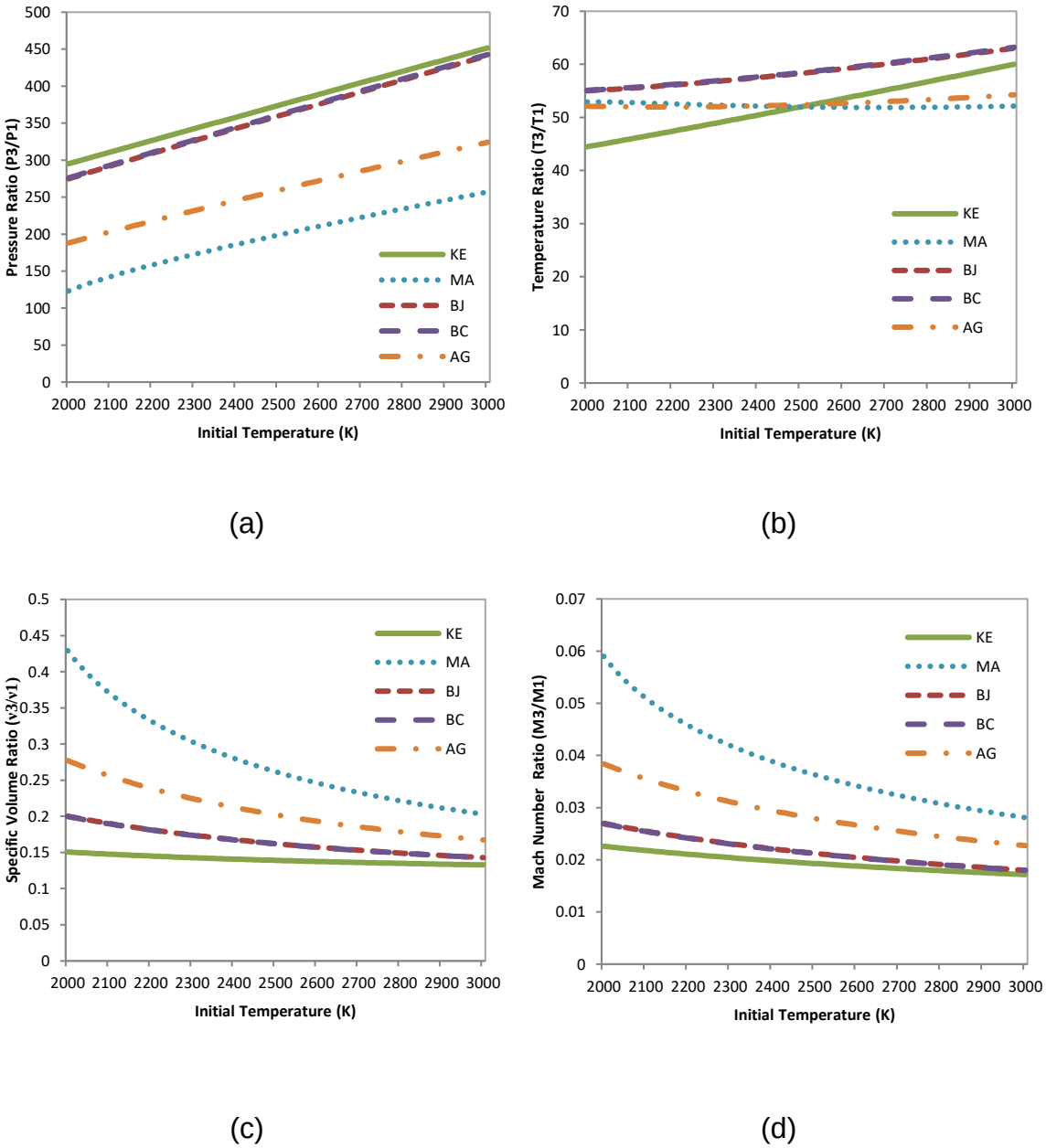

Figure 5-10 Comparison of (a) pressure ratios; (b) temperature ratios; (c) specific volume ratios; (d) and Mach number ratios at different initial temperature under influence of strong detonation (P=1 atm, G=6000 kg/s.m²)

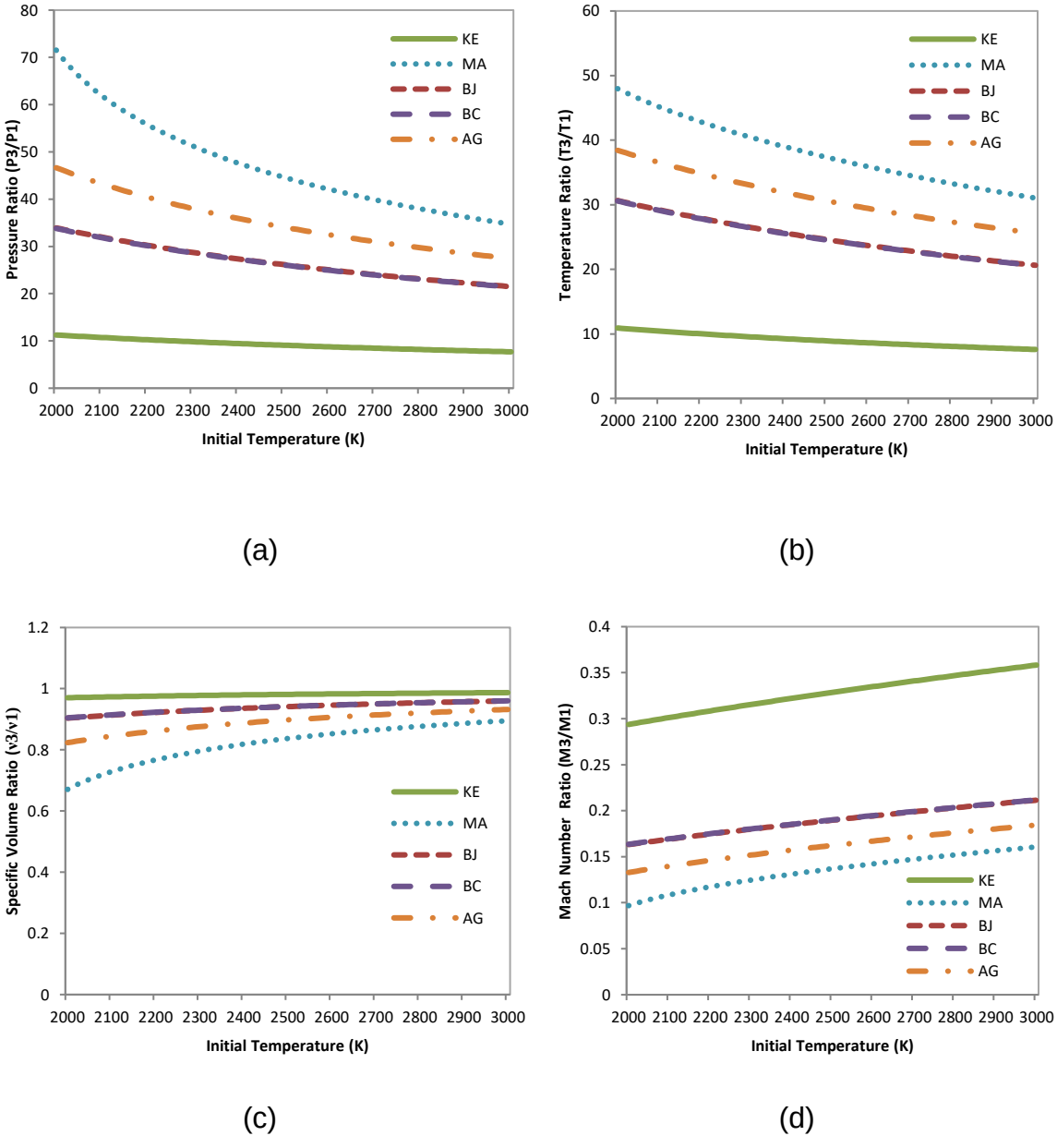

Figure 5-11 Comparison of (a) pressure ratios; (b) temperature ratios; (c) specific volume ratios; (d) and Mach number ratios at different initial temperature under influence of weak detonation (P=1 atm, G=6000 kg/s.m²)

Effects of initial pressure

Initial pressure puts a significant effect on flow speed at the end of tube and serves as limiting factor in its variation to allow detonation. To define the limitation, AG fuel is selected, whilst initial temperature is fixed to 2000 K and mass fluxes is varied between 5200 kg/s·m^2 to 5600 kg/s·m^2. These mass fluxes are used by taking into considerations for other fuels to achieve detonation as well. Other fuels are also being tested and results are recorded in Appendix C.7. Figure 5-12 plots results based on Mach number of burned gas under both strong and weak shock conditions. At high mass flux, initial pressure increases across a wider range as compared to low mass flux. As the initial pressure rises, with a given mass flux, burned gas Mach number increases during strong shock wave. Weak shock, in contrast, reduces burned gas flow. It is to be noted that all of the burned gas flows converge on choking condition. Due to these restrictions, higher mass flux is preferred from other alternative fuels as to avoid possible limitations on the modelling.

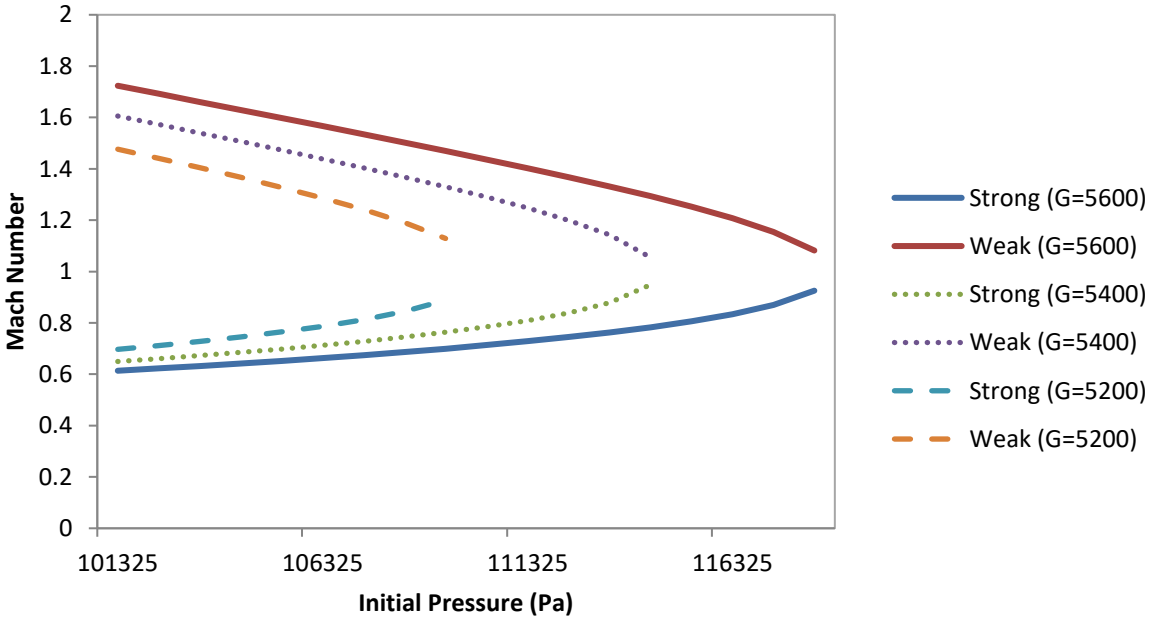

Figure 5-12 Influence of initial pressure and mass flux on the Mach number for AG fuel (T = 2000 K)

As shown in Figure 5-13 and Figure 5-14, other fuel options are compared based on temperature, pressure, Mach number, specific volume and Mach number ratios, under strong and weak detonation waves accordingly. It is found that pressure and temperature ratios are reduced as initial pressure increases (Figure 5-13 (a) and (b)). On the contrary, there is an exponential increase in burned gas Mach number, specific volume and Mach number ratios under strong detonation (Figure (a), (b) and (c)). For a given mass flux, this may provide a limitation on further reduction of temperature and pressure ratio changes, particularly for MA fuel. By referring to equation 5-17, it is believed that square root in the numerator restricts the modelling and physically indicates that the flow is choked. Since this analysis has constant initial temperature and mass flux for every fuel, specific volume thus becomes limiting factor. MA fuel is also seen to be more sensitive to changes of initial pressure than other fuel because of its heat formation, represented by q is significantly higher. This can be explained by thermochemical properties of molecular structure of the fuel as discussed in previous section.

Meanwhile, pressure and temperature ratios increases when initial pressure increases (Figure 5-14 (a) and (b), though changes in pressure ratios are noticeably more significant than temperature ratios. KE fuel appears to be least affected compared to other fuels under influence of weak shock. Specific volume, Mach number ratios and Mach number are reduced exponentially as initial pressure increases (Figure 5-14 (c), (d), and (e)). KE fuel is also found to result in higher speeds under these circumstances.

In summary, by comparing each fuel at its detonation condition, the following trends in physical properties with changes of initial mass flux, initial pressure, and initial temperature have been tabulated in Table 5-5.

Table 5-5 Effects of initial conditions to burned states

Properties	$G\uparrow$		$T\uparrow$		$P\uparrow$	
	Strong	**Weak**	**Strong**	**Weak**	**Strong**	**Weak**
P_2	↑	↓	↑	↓	↓	↑
T_2	↑	↓	↑	↓	↓	↑
v_2	↓	↑	↓	↑	↑	↓
M_2	↓	↑	↓	↑	↑	↓

↑ *represents increase while* ↓ *represents a decrease in the physical properties*

Based on results obtained, pressure ratio shows the most significant changes, followed by temperature ratio, specific volume ratio, and Mach number ratio to changes in initial conditions. Generally, physical properties influenced by strong and weak shock happens to apply inversely. Turns (2000) has suggested that influence of strong shocks are physically more practical for application that needs more attention. However, in multi-cycle application, these shocks are reduced every cycle. Even though sustainability and performance are the main challenges, but emission effect is deemed to be a more important issue. In the following chapter, detonation analysis is further investigated in terms of performance analysis. This analysis is needed to predict the formation of emission in detonation, especially in adopting biofuels.

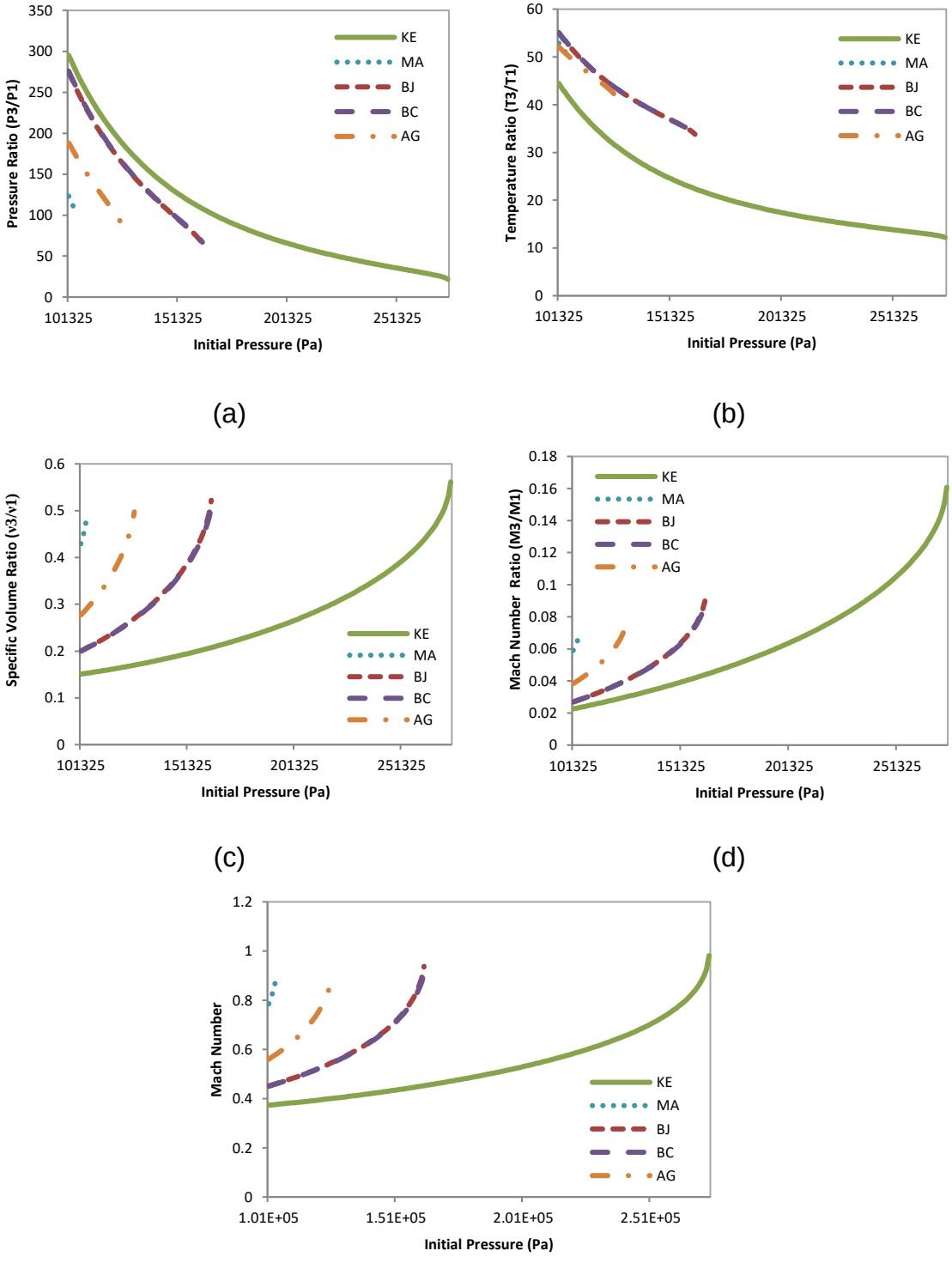

Figure 5-13 Comparison of (a) pressure ratios; (b) temperature ratios; (c) specific volume ratios; (d) Mach number ratios; and (e) Mach number at different initial pressure under influence of strong detonation (T = 2000 K, G = 6000 kg/s·m^2)

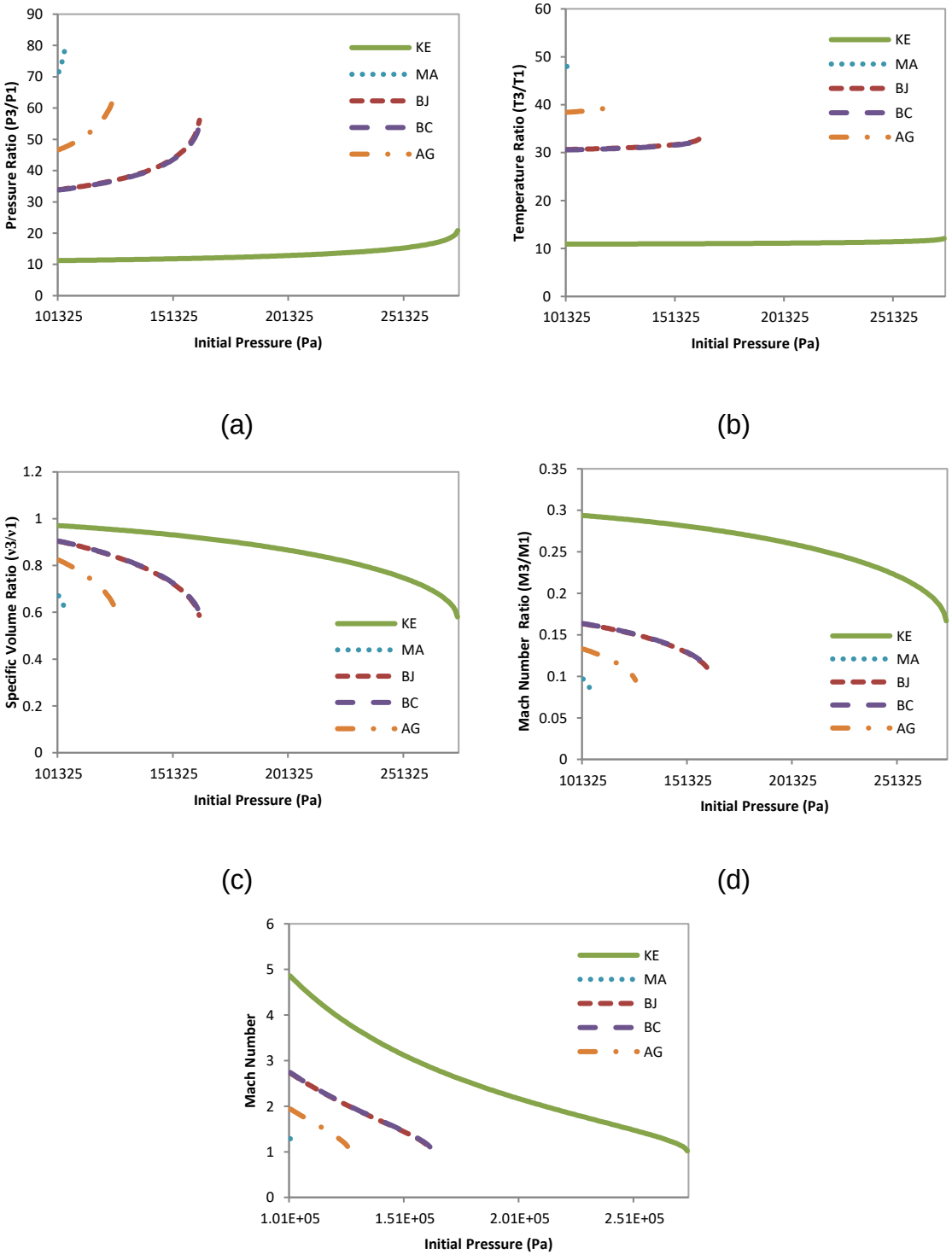

Figure 5-14 Comparison of (a) pressure ratios; (b) temperature ratios; (c) specific volume ratios; (d) Mach number ratios; and (e) Mach number at different initial pressure under influence of strong detonation (T = 2000 K, G = 6000 kg/s·m^2)

5.5 Concluding Remarks

The chapter focuses on assessment of detonative combustion by using alternative fuels, particularly biofuels which has not been done before. Concerning the energy and environmental crises whilst enhancing performance and thermodynamic efficiency to combustor, zero-dimensional models of biofuels in a detonative mode of combustion are thoroughly discussed and presented. A comprehensive review has been made to highlight work that has been done in this area including PDE process during operations. No research, so far, has been conducted to accommodate biofuels in detonative combustion. Therefore, the chapter has analysed the feasibility and effectiveness of various alternative fuels under PDE conditions. By systematically applying Rankine-Hugoniot Equation, Rayleigh Line Equation, and Zel'dovich–von Neumann–Doering models and involving both single-step chemistry and thermophysical properties for a stoichiometric mixture, the temporal effects of pressure, temperature, and density have been investigated under different initial conditions. The main conclusions of the work are as follow:

1. The effects of mass flux variation indication limitations to the changes in initial pressure, with higher mass flux allowing a wider range of initial pressure variations. The initial temperature has, indeed, a significant effect on the specific volume and Mach number ratios, while initial mass flux has even more significant effect on both pressure and temperature ratios.

2. As expected from chemistry knowledge, heavier and more complex hydrocarbons of biofuels molecular structure require heat energy to break intermolecular bonds, thus have greater molar specific heat. This is supported by thermochemistry evaluation of combustion flame temperature as each fuel exhibits different sensitivities when it is detonated. Since lighter fuels detonates more easily, further increase in initial conditions results in significantly faster chemical reaction rate as more free atoms are available to react.

3. Chemical and physical analyses presented above may be used to study thrust chamber dynamic and propulsive performance of a pulse detonation engine running on alternative biofuels in multi-cycle and multi-phase combustion. In order to sustain detonation, careful geometrical sizing of the tube design are necessary, alongside other important aspects, such as pulse detonation engine emissions and pollutant formation that require enormous attention to be evaluated in the near future. This aspect has also been covered in the following chapter.

6 EMISSION ANALYSIS

6.1 Introduction

This chapter discusses the emission of Nitrogen Oxides (NOx) for both conventional and pressure-rise combustors using biofuels (KE, BJ, BC, AG). This work provides a systematic prediction study of a simplified zero-dimensional stirred reactor model for NOx emissions for conventional and pressure-rise combustors using an in-house computer tool, HEPHAESTUS. HEPHAESTUS is an emission prediction software developed by Celis (2010) to predict pollutant emitted from gas turbine combustor. This software uses the Zeldovich equations (for NOx) and models the emission by implementing a partially-stirred reactor (PSR) model and perfectly stirred reactor (PSRS) models at different zones in the combustor. The basic assumptions involve a set of key parameters, but fuel injector parameters, fuel spray characteristics, pattern factor, flow recirculation, inhomogeneity of the mixture and flame unsteadiness have not been considered in order to maintain the universality and practical application of the emission model, the details of which are given in Celis (2010), Lokesh (2015) and Mazlan (2012).

This chapter presents a literature review on the formation of NOx, studies to reduce NOx, and an overview of other emission models predictions (It is important to note that NOx emission formation cannot be estimated directly because it depends on how the combustion is controlled). Next, a methodology section describes how the model in HEPHAESTUS can be validated based on thermochemistry analysis. Results shows that HEPHAESTUS is able to capture a reasonable prediction as compared to the International Civil Aviation Organization (ICAO) databank.

For a conventional combustor, the emissions from an aero gas turbine is evaluated at different power settings (30%-approaching, 80%-climbing, and 100%-take-off). The analysis is also extended to visualize the variations of

emission at different combustor inlet conditions such as different inlet temperature, pressure, total mass flow and fuel flow. For a pressure-rise combustor, the zero dimensional performance analysis from the previous chapter is incorporated for modelling the geometry tube design and to establish the initial conditions for detonation. The variations in emissions at various combustor tube conditions are also visualized for different air mass flow fraction in different zones, various fuel flows, combustion zone lengths, and different chamber pressures. Of all variations that are tested, NOx emission proves most sensitive to the fuel flow rate, which indicates that the effect of equivalence ratio is more significant for emission formation.

6.2 Literature Review

In recent years, air transportation has been growing rapidly (by an average of 1.9% per year from 2008-2025) more than any other transport mode, and the demand is still growing resulting in a high fuel consumption to about 5 million barrels of oil per day; accounting for about 5.8% of total oil consumption in the world (Zhang *et al.*, 2016). This high demand for fuel opens up two critical impacts which are the energy crisis and environmental problems as which have been addressed in the previous chapter. As environmental problem is the main concern here, future aircraft engines must offer low emissions with high efficiency at low cost, while maintaining the reliability and operability (DeLaat *et al.*, 2013).

Aircraft produce the same type of emissions as ground transportation vehicles, including carbon monoxide (CO), carbon dioxide (CO_2), sulphur trioxide (SO_3), sulphuric acid (H_2SO_4) and sulphur dioxide (SO_2) also called sulfur oxide (SOx), nitrogen dioxide (NO_2), nitrous oxide (N_2O), unburned hydrocarbons (UHC-C_nH_m), particulate matter (PM), water vapour (H_2O) and other condensable organic compounds (CH_2O, CH_3OH, and C_2HO) (Chandrasekaran and Guha, 2012; Mazlan, 2012; Starik *et al.*, 2013; Zhang *et al.*, 2016). Specifically, Levy,

Sherbaum and Arfi (2004) have addressed that the pollutant formation processes in a gas turbine that are associated with the combustor design and operational conditions as listed in Table 6-1.

Table 6-1 Aircraft turbine engine emissions formation based on operating conditions (Levy, Sherbaum and Arfi, 2004)

Emission type	Engine operation
H_2O, CO_2, SOx, Soot	All power settings
CO, UHC	Lower power, ground idle
NOx	All power settings, increase with power

Although emissions produced by aircraft are various, the aviation sector contributes relatively small amounts to air pollutants compared to other sectors (estimated 2–3% of total CO_2 emissions and less than 3% of the transportation NOx emissions) (Zhang *et al.*, 2016). Nevertheless, concerns are mounting because emissions produced by aircraft affects a wider part of the atmosphere including on the ground, and both lower and middle layers of the atmosphere directly through its flight cycles (Starik *et al.*, 2013). In addition to pollutant gases, radians, and cirrus clouds formations also contributes to air pollutions. Particles suspended in the atmosphere have various potential effects on humans in terms of health and the environment due to greenhouse effects. One can see that at cruising altitudes where aircraft has the most longer period, aircraft are directly depositing small non-volatile particles to the atmosphere (Wey *et al.*, 2007) which are very sensitive to various perturbations (Starik *et al.*, 2013)

For the emissions considered above, climate change occurs by two main routes: 1) direct greenhouse gas from CO_2, particulate matter (PM), and water

vapour H_2O, and 2) indirectly from NOx, Soot and H_2O emissions forming contrail and cirrus cloud. NOx leads to a change in methane and ozone levels has the most effects at low temperature for additional radiative forcing (Chandrasekaran and Guha, 2012). In the troposphere, emissions of NOx, which react with hydrocarbons to generate O_3 (Makida *et al.*, 2016), increase atmospheric ozone concentrations prohibiting the heat released by sunlight from being radiated back forming a greenhouse effect. Unfortunately, this greenhouse effect traps heat and caused the Earth temperature to rise which causes the climate change (Mazlan, 2012). For further elaborations on the consequences associated by these emissions to the human health are thoroughly discussed in Mazlan (2012). Emissions will thus definitely contribute to overall GHG. Improvements in engine thermal efficiency can reduce operating cost as well as the pollution. Payan et al. (2014) showed the relative GHG emission reduction for biomass sources compared to conventional jet fuel based on fossil sources and its blend. The results are shown in previous chapter (Table 4-1) and Figure 6-1. In the following context, algae biofuel can potentially reduce GHG emission and looks very promising.

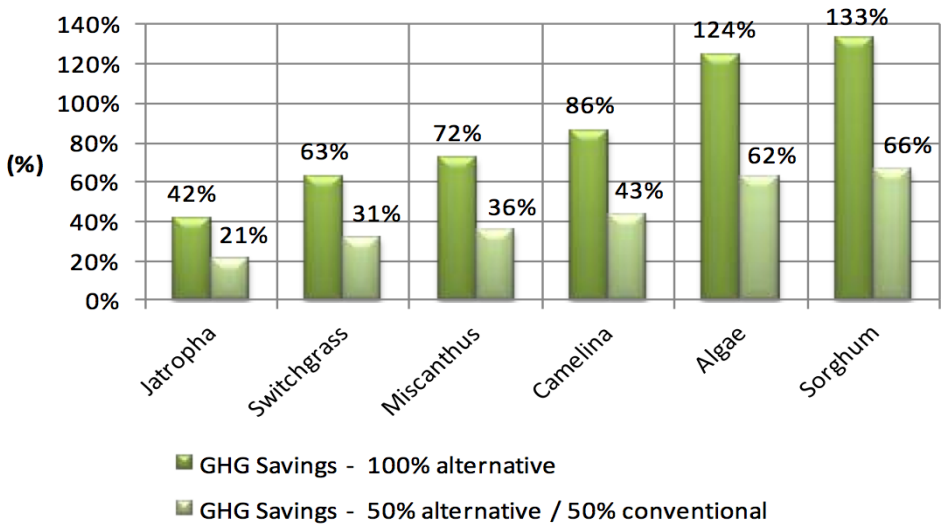

GHG Emission Savings From the use of Biomass Feedstocks Compared to Fossil fuel Sources

Figure 6-1 GHG Emission savings with 100% pure alternatives fuel and blended fuels (Payan *et al.*, 2014)

Since these emissions from aircraft affect both humans and the environment directly, it is expected that more stringent standards and regulations on emissions will be posed in the near future. This will certainly push the aviation industry further towards a more sustainable and greener aviation. Currently, the characteristics of aircraft particle emissions are one of the least understood and quantified relative to other major pollution sources (Wey *et al.*, 2007). Hence the focus have on NOx emissions only and briefly further investigate the NOx emission prediction in both conventional and pressure rise combustors.

6.2.1 Formation of NOx

Collectively, NOx refers to the oxides of nitrogen consisting of nitric oxide (NO), nitrogen dioxide (NO_2) and other nitric compounds. Among those, NO and NO_2 are the most common natural nitrogen oxides. In the combustion process, NO formed will oxidizing to NO_2 and the latter will dissociate to the former. However, at any elevated temperatures, NO_2 removal is rapid due to the presence of high radical concentrations, and NO_2 will be converted back to NO (Celis, 2010). As a consequence, the degree of conversion between NO and NO_2 varies at different pressure and temperature (Cheng, 2010). Cheng (2010) and Celis (2010) have addressed four mechanisms of NOx formation, which are: (i) thermal NO, (ii) nitrous oxide (N_2O) mechanism, (iii) prompt NO, and (iv) fuel NO.

Thermal NO

In a gas turbine, thermal NO plays a vital contribution to the formation of NOx. Thermal NO is produced by the oxidation of atmospheric (molecular) nitrogen in high-temperature regions of the flame (Khandelwal, 2012) and in the post-flame gasses which are predicted according to the extended Zeldovich mechanism (Celis, 2010; Mazlan, 2012) via the following reaction equation:

O_2= 2O

N_2 + O = NO + N

N + O_2 = NO + O

N + OH = NO + H

The process involved is endothermic reactions which is highly dependent on the temperature for above 1800K (Cheng, 2010) thus these thermal NO formations normally dominate at high power conditions (Khandelwal, 2012).

Nitrous oxide mechanism

Nitrous oxide mechanism is mentioned as follows (Cheng, 2010):

N_2 + O = N_2O

N_2O + O = NO + NO

N_2O + H = NO + NH

N_2O + CO = NO + NCO

Prompt NO

Prompt NOx is mostly formed at a low flame temperature (Cheng, 2010; Khandelwal, 2012) at the faster rate (Celis, 2010) than thermal NO. The mechanisms of such generation is very complex and are not very understood: nitrogen (N_2) reacts with CH to produce HCN, then HCN is oxides to CN, NCO and NO consequently as follows:

N_2 + CH = HCN + N

HCN → CN → NCO → NO

Three sources of prompt NO in hydrocarbon fuel combustion can be then identified (Celis, 2010):

(i) non-equilibrium O and OH concentrations, which accelerate the rate of formation of NOx through the thermal NO mechanism;

(ii) Fennimore prompt NO mechanism (reaction of hydrocarbon radicals with molecular nitrogen)

(iii) The reaction of O atoms with N_2 to form N_2O, and subsequently NO.

Fuel-bound NOx

Fuel-bound NOx refers to a nitric compound present in the fuel such as ammonia and leads to the conversion to NOx. Therefore, it is based on the type of fuel used because different fuel contains a different fraction of the nitrogen element. Unlike thermal NOx, the generation rate of fuel-bound NOx is not dependent on the temperature (Cheng, 2010). Lokesh (2015) has highlighted the influences on such NOx formation in combustion due to the following aspects:

1. Ambient temperature and pressure (Wey *et al.*, 2007).

2. Inlet and Outlet conditions (Engine power setting) at every reactor zone

3. Fuel composition and specifications

a. Thermo-physical properties - Stoichiometric flame temperature, caloric properties (Cp, γ, h, s, η), fuel density, bulk modulus, viscosity, flash point, boiling point, thermal conductivity, vapour pressure, LHV

b. Chemical properties – Thermal stability, aromatics, sulphur, and nitrogen content

4. Thermodynamic properties of the combustion products

5. Liner wall cooling characteristics

6. Fuel injector characteristics and location

7. Fuel spray characteristics

8. Equivalence ratio and degree of homogeneity of the fuel-air mixture

9. Combustor residence time.

6.2.2 Efforts of reducing NOx

Low emission combustors have long been proposed to mitigate issues of gas turbine emission. To describe the characteristics of these emissions a 'low-emission window' is described for conventional combustors as depicted in Figure 6-2. This figure shows the trend of NOx, CO, UHC and smoke with varying equivalence ratio from lean to rich. Since our focus is on NOx formation, it is observed that the NOx levels are maximum at an air to fuel ratio just below the stoichiometric ratio. One can identify that, for a fairly narrow band of temperatures the levels of both CO and NOx below mandated values; which region is called low-emission window (Levy, Sherbaum and Arfi, 2004). However, since the demand of current combustor technology which requires higher combustor temperature, NOx formation is becoming more prominent as shown in Figure 6-3. Based on the emission level required by regulations, the susceptible temperature should be met. Many methods have been proposed and are classified under wet or dry method for low NOx (Khandelwal, 2012).

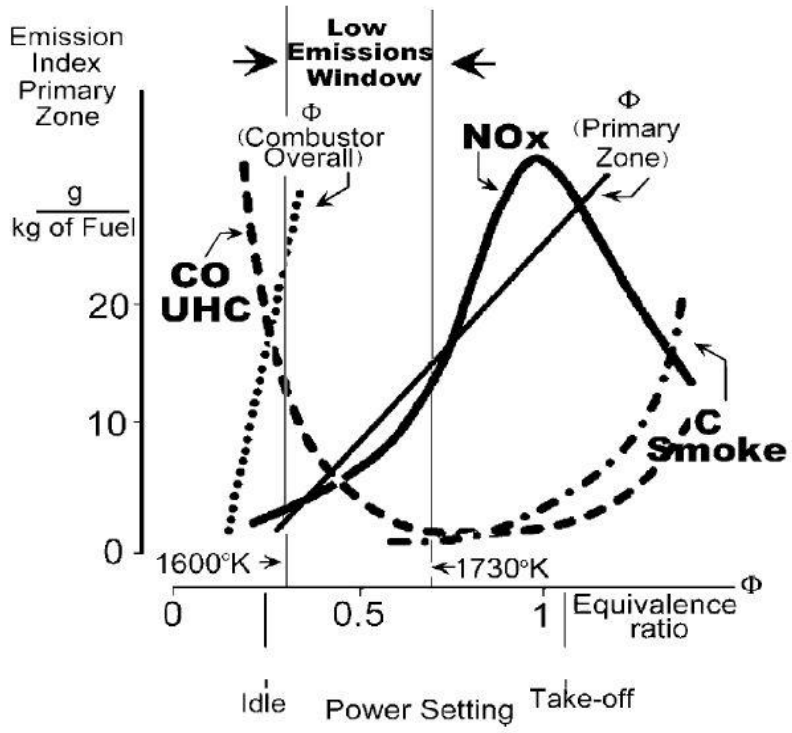

Figure 6-2 Low emission window (Levy, Sherbaum and Arfi, 2004)

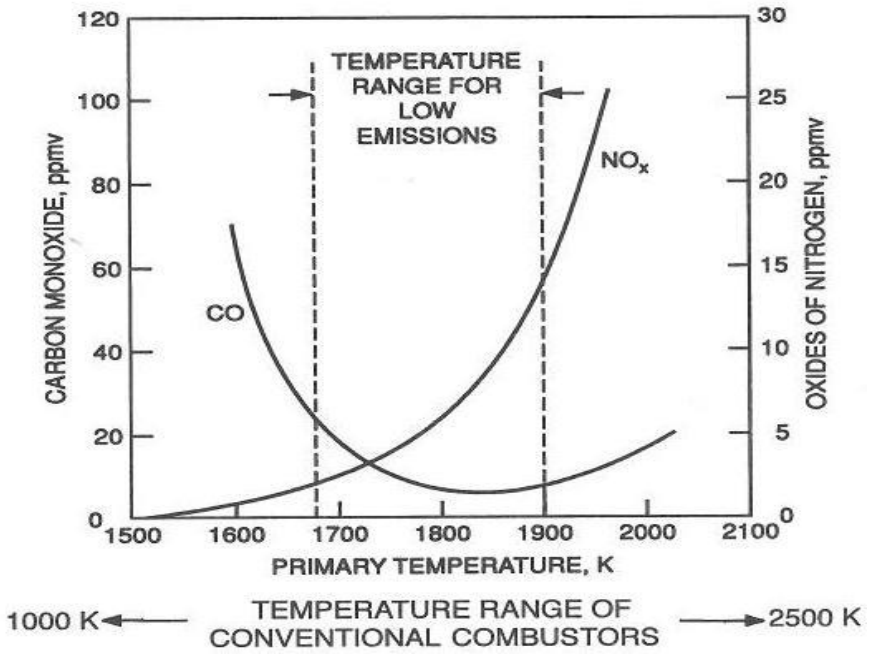

Figure 6-3 Range of permissible combustors temperature (Khandelwal, 2012)

Following increasing awareness of aircraft emissions due to more stringent regulations, demand for technologies to reduce NOx emissions are urgently needed especially to meet 2050 targets. Moreover, a combustion that can accommodate extremely low NO*x* emissions while maintaining high combustion efficiencies and a wide range of operational stability is desirable for most of the future energy systems, including aero gas turbines (Melo *et al.*, 2011). In 2004, a series of measurements of the trace gas and particulate emissions of aircraft has been done in APEX (Aircraft Particle Emissions Experiment) at NASA Dryden Flight Research Center (Wormhoudt *et al.*, 2007). It is worth to mention that Pratt & Whitney has developed the TALON combustor, which successfully reduced NOx emissions to 50% of CAEP/6 and General Electric developed the TAPS combustor, which was applied to GEnx and reduced NOx emissions to 30% of the CAEP/4 standard (Makida *et al.*, 2016).

There are many efforts to highlight the work done on NOx emissions reduction such as Levy, Sherbaum and Arfi (2004) have worked on lean burning to reduce thermal NOx. They have reduced the flame temperature and resident time by increasing the flow of air into the primary zone. They have also suggested that the prompt NOx can be reduced by the replacement of hydrocarbons by other fuels with lean combustion downstream but rich combustion in the primary zone. However, these consequences suffer combustion instability, as well as promoting more CO and UHC deposits. Thermal efficiency also can be reduced. Combustion instabilities happen due to the interaction of the fluctuating heat release of the combustion process with naturally occurring acoustic resonances. This large and high-frequency pressure oscillations in the combustor reduces the component life and premature mechanical failures. In the later work conducted by DeLaat et al. (2013), they have improved the lean-burning by adopting active control to handle the combustion instability concerns.

Sadanandan et al. (2011) have worked on the flameless combustion (FC) by intense mixing of recirculating burned gasses with fresh gas. Other variations which have been considered such as the exhaust gas circulation, high temperature air combustion, stagnation-point reverse flow, and moderate and intense low oxygen dilution combustion (MILD). Since high flame temperatures had a large effect on the NO*x* formation by enhancing both thermal-NO and N_2O mechanisms, they have suggested to increase the jet velocity to irrespective of the premixed or non-premixed configurations. They also further claimed that in flameless combustion, higher heat capacity of the products helps in lowering the flame heat and the temperatures locally which reduce NOx process.

Other works done by Makida et al. (2016) showed that enhancing the mixing in the primary combustion region can also be one of the solution to reduce NOx. This method can be done by tuning of the air mass flow ratio in the fuel nozzle, the primary and secondary combustion regions, and the wall cooling. In the other method used by Zhang et al. (2016), they have shown the practical used of hydrocarbon-based 'drop-in' alternative fuels through synthetic process of nature gas or coal (synthetic jet fuels) and hydro treating process of lipids (bio-jet fuels). These will benefits both economic and environmental sustainability.

To put all the criticisms on the mitigation measures mentioned above, Melo et al. (2009, 2011) also have the same arguments. Fuel staging involved mechanical complexity, controls problem and emission reduction are relatively low. In a catalytic combustion, practicability is the main concerns as it is limited for a non-stationary engine and has thermal instability. This will certainly reduce durability and fuel flexibility. Furthermore they further criticized that lean-premixed pre-vaporized (LPP) combustion has safety concerns due to auto-ignitions, combustion instability, and a lifetime issue, while rich burn-quick quench-lean burn (RQL) combustion requires separation chambers, more soot-forming in primary zone causing cooling problems and uniform quenching. A dry low NOx technology (DLN) combustors typically require the use of natural gas,

and not all turbine designs can accommodate such a combustor design. Finally, they have argued that in flameless combustion, requires to recirculate a lot of hot combustion products with low oxygen content, within a limited volume and over a wide range of operating conditions.

Wey *et al.* (2007) have conducted aircraft particle emission experiment at NASA Dryden Flight Research Centre over a wide range of power settings found that at low power settings, trace-species emissions were observed to be highly dependent on ambient conditions and engine temperature. They have also found good agreement with ICAO certification data that EICO has been increased when EINOx decreased. However, Wormhoudt *et al*. (2007) found that the NOx emission index increases with increasing engine thrust and due to an amount of fuel burned (Mazlan, 2012). These authors found that at higher powers aircraft NO*x* is dominated by NO, at low powers NO_2 can contribute more than 80% of the total NO*x*. HONO can also be significant (up to 7% of NO*x*). Novel combustor experiments adopting a large recirculation zone in the combustion chamber have demonstrated that the NO*x* emissions were extremely low for all models, generally below 10 ppm (Melo *et al.*, 2009).

While Starik *et al*. (2013), have conducted a numerical analysis using detailed reaction mechanism for modelling the process of both in the combustor and post-combustor flow. This is a vital study to take into account for the transformation of combustion exhaust during the expansion in the turbine and nozzle. Through an evolution of N-containing species, they found out that for all considered regimes, the concentrations of all *N*-containing species decrease when passing through the mixer. However, more NO_2 are produced from the conversion of NO in the engine exit. Turgut (2016) has conducted a separate study on the effects of ambient air temperature on gaseous emissions. He argued that different ambient conditions will tend to change fuel-air ratios in the combustor and therefore emission produced will also affect. He found that

affecting the combustor–inlet conditions, ambient air temperature leads to a tendency toward higher NOx and lower CO at higher ambient air temperatures.

The thermophysical and chemical properties of the fuels also play an important role on the NOx emission. As mentioned by Mazlan (2012), claimed that the flame temperature depends on the fuel properties, preheat temperature, and oxygen concentration. At higher combustion temperature fuel needs for bond breaking will lead to higher levels of dissociation (Lokesh, 2015). She further added that the formation of NOx increases as the density of the fuel increases. Higher density fuel leads to a larger mass of dense fuel at given speed and load in the fuel injector. These results more burning fuel and produce more NOx. In the meantime, Rahmes *et al.* (2009) studies showed that the differences in H/C ratio lower the flame temperature and accordingly reduce NOx (Mazlan, 2012).

6.2.3 Emission Models Prediction

Aero-engines operate at a wide range of operations which have a great influence on the pollutants formed. Therefore, a robust model is needed which takes into account variations in cycle parameters and a model that can accommodate other fuels for emission prediction is highly desirable. Most current models require engine-specific proprietary information (e.g. combustor dimensions, pressure coefficient, pressure loss factor, spray evaporation, pattern factor) are not always available and then lead to more uncertainty and less accuracy. Generally, elements such as CO_2 and H_2O emissions are directly estimated from chemistry (based on a number of moles and others) and fuel burn. On the contrary, NOx emission is predicted based on how the combustion is controlled and so generally requires more complex prediction methods that would require proprietary information from the manufacturer.

However, the work of Chandrasekaran and Guha (2012) brought out together many important prediction methods and made a clear comparison for their accuracy and practicability, as well as the advantages and disadvantages of using each method, before they proposed a new method called 'NOx: generic'. They have classified NOx emission prediction techniques into five general categories which are shown in Figure 6-4. Each method has its own advantages and disadvantages and the reader is highly recommended to refer to their article for further details.

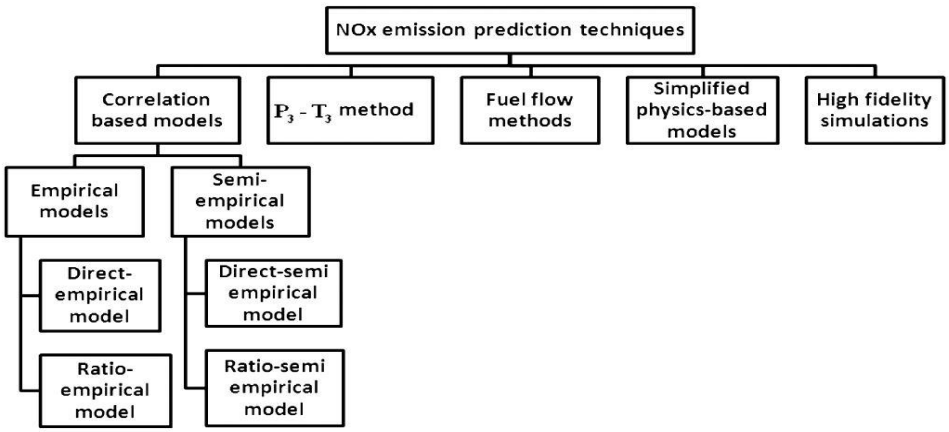

Figure 6-4 Classification of NOx emission prediction techniques (Chandrasekaran and Guha, 2012).

Among these techniques, a P3-T3 method is commonly used. This model is clearly described and explained in (Chandrasekaran and Guha, 2012). Based on this method, a physics-based stirred reactor approach was adopted to study the emission indices of Bio-SPKs (Lokesh, 2015) in our in-house code, HEPHAESTUS. This code uses the Zeldovich equations (for NOx) and models the emission by implementing a partially-stirred reactor (PSR) model; in the first part of combustor primary zone, and a series of perfectly stirred reactor (PSRS) models in the later part of the combustor primary zone, intermediate and dilution zones of a conventional combustor. This configuration of the divided zones in the reactor is illustrated in Figure 6-5 and the basic assumptions are given in Celis (2010), Lokesh (2015) and Mazlan (2012). To summarize, certain

parameters including fuel injector parameters, fuel spray characteristics, pattern factor, flow recirculation, inhomogeneity of the mixture and flame unsteadiness have not been considered in order to maintain the universality and practical application of the emission model. This is also to ensure that the requirement for much proprietary information can be avoided. The emission model is described in details by Celis (2010):

1. thermal NOx

$$\frac{dY_{NO}}{dt} = \frac{2\bar{M}_{NO}}{\rho}(1-\alpha^2)\left\{\frac{R_1}{1+\alpha K_1} + \frac{R_6}{1+K_2}\right\} \quad \textbf{(6-1)}$$

Where Y_{NO} is NO mass fraction, $\bar{M}$ is a molecular weight, $\alpha = [NO]/[NO]_e$ is calculated using actual values of NO concentration from previous step. R_i denotes in turn a 'one way equilibrium reaction rate. K_1 and K_2 rare defined as $K_1 = R_1/(R_2 + R_3)$ and $K_2 = R_6/(R_4 + R_5)$.

2. Prompt NOx

$$\frac{dY_{NO}}{dt} = \left(\frac{\bar{M}_{NO}}{\rho}\right) f_{pr} k'_{pr} ([O_2]_e)^a [N_2]_e [C_{12}H_{23}] exp\left(\frac{-36499.507}{T}\right) \quad \textbf{(6-2)}$$

Where,

$$f_{pr} = 4.75 + 0.0819x - 23.2\phi + 32\phi^2 - 12.2\phi^3 \quad \textbf{(6-3)}$$

$$k'_{pr} = 6.4 * 10^6 \left(\frac{0.0820575T}{P}\right)^{\alpha+1} \quad \textbf{(6-4)}$$

f_{pr} is a correction factor that incorporates the effects of fuel type, and α is the oxygen reaction order from mole fraction.

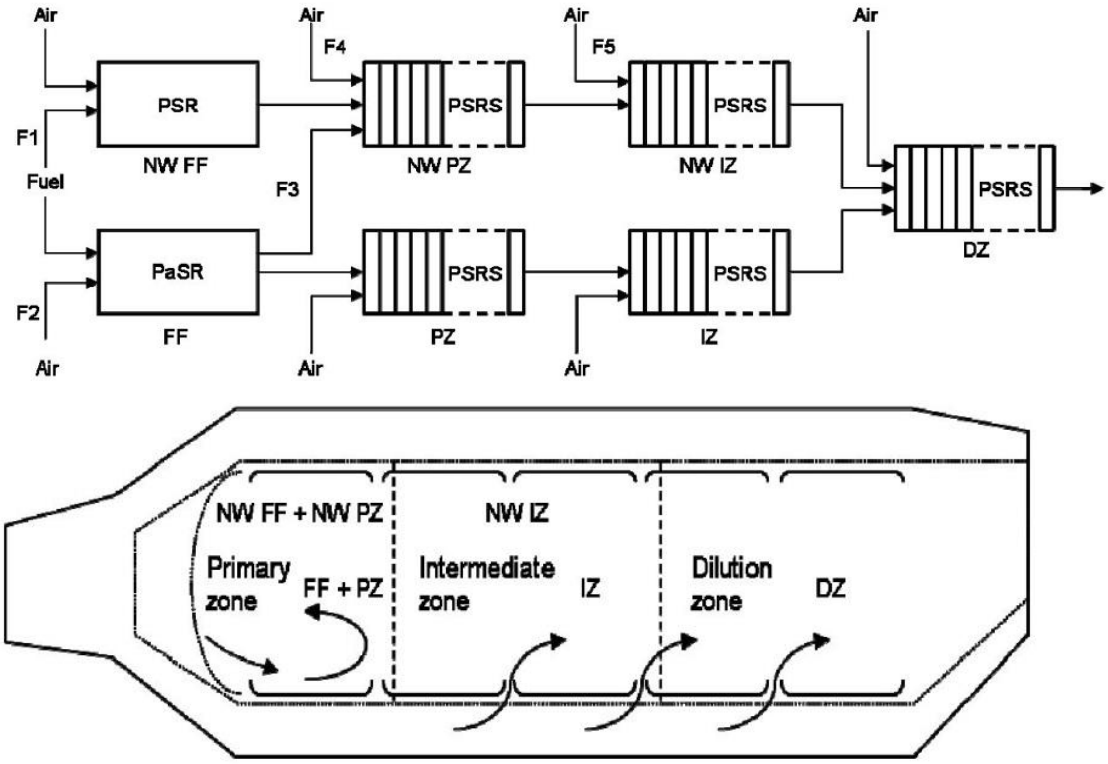

Figure 6-5 Configuration of divided zone in the reactor of the combustor (Mazlan, 2012).

6.3 Methods

6.3.1 Conventional combustor

Caloric properties for Jatropha biofuel (BJ), Camelina biofuel (BC) and Algae biofuel (AG) are evaluated using the NASA CEA code and comparisons have been made with the published Cranfield thesis by Lokesh (2015). There are relatively small differences (0.01%-0.03%) to the caloric properties calculated by Lokesh (2015). Further analysis has been conducted in NASA CEA to visualize and compare the caloric properties for these fuels. The results are consistent with her published thesis where again only small differences are observed in the caloric properties. Assuming both codes have been described in more detail earlier, the existing correlation in HEPHAESTUS can be used including the correlation of enthalpy, entropy and the specific heat at constant pressure.

PYTHIA code analysis for the engine performance has been conducted prior to the emission analysis at different flight cycles. Off-design parameters for different fuels obtained from PYTHIA are combustor inlet temperature, pressure, total mass flow, fuel flow and flame temperature at the turbine inlet and these are then used as inputs in HEPHAESTUS. Since it was not possible to obtain detailed engine/combustor data especially for the sizing, assumptions were made based on a comparison with the work done by Celis (2010), Mazlan (2012), and Lokesh (2015) as well as for the low emission combustor designs of Ye (2010), Hegde (2011), and Khandelwal (2012). The combustors data used for the emission analysis are tabulated in Table 6-2. Emission analysis is conducted using HEPHAESTUS by evaluating baseline conditions for different fuels at different power settings. Later, the variations of different combustor inlet conditions are evaluated at the different temperature, pressure, total mass flow and fuel flow.

Table 6-2 Input parameters

Zone		**Flame Front**	**Primary Zone**	**Intermediate Zone**	**Dilution Zone**
Flow Area (m^2)	In	0.1048	0.2599	0.2599	0.2606
	Out	0.2599	0.2599	0.2606	0.1467
Length (m)		0.0698	0.0698	0.0931	0.2328
Air inflow fraction		0.25	0.1	0.1	0.55

Firstly, HEPHAESTUS analysis of the model baseline conditions is validated using the ICAO databank of a particular engine at various engine operations. Next, the effects of various combustor initial conditions using HEPHAESTUS are validated using simple chemistry equations and thermochemistry of combustion for all fuels at different combustion conditions (lean, stoichiometric, and rich burning). These chemistry and thermochemistry analyses can also be used to validate the effects of increasing the fuel flow. Chemical equations for

hydrocarbon in combustion are used based on the book by Goodger and Ogaji (2011). For stoichiometric, lean and rich reactions, the following relations are used:

Stoichiometric:

$$C_aH_b + m_s(O_2 + 3.76N_2) \rightarrow n_1CO_2 + n_2H_2O + n_6N_2$$

Lean:

$$C_aH_b + m(O_2 + 3.76N_2) \rightarrow n_1CO_2 + n_2H_2O + n_5O_2 + n_6N_2$$

Rich:

$$C_aH_b + n(O_2 + 3.76N_2) \rightarrow n_1CO_2 + n_2H_2O + n_3CO + n_6N_2$$

Next, an adiabatic temperature is calculated. Adiabatic flame temperature is the temperature at which the combustion products reactions takes place where no heat is lost to the environment. There are two types of flame temperature conditions; 1) at constant pressure and 2) at constant volume. Based on the previous chemical reactions calculated in the previous section, an adiabatic flame temperature at constant pressure is calculated using the following relations:

$$H_{reac}(T_i, P) = H_{prod}(T_{ad}, P) \quad \textbf{(6-5)}$$

$$H_{react} = \sum_{react} N_i\bar{h}_i = H_{prod} = \sum_{prod} N_i\bar{h}_i \quad \textbf{(6-6)}$$

$$H = \sum N_i\left[\bar{h}^o_{f,i} + \bar{c}_{p,i}(T_{ad} - 298)\right] \quad \textbf{(6-7)}$$

Lastly, to verify the effects of initial pressure and temperature, other correlations published in the literature are used, as listed in Table 6-3. It should be noted that these correlations are based on particular engines only. However, there is

an attempt to adopt these correlation-based models through the use of an optimization study. A good ability to achieve successful correlation adjustment, which gives the best fit to a given set of experimental data, has been demonstrated in Tsalavoutas et al. (2007).

Table 6-3 List of correlation-based model (Chandrasekaran and Guha, 2012)

	Correlation-based Model
Rizk and Mongia	$EINOx = \dfrac{15 \times 10^{14}.\, t_{res}^{0.5}.\exp\left(\dfrac{-71100}{T_{fl}}\right)}{P_3^{0.03}\left(\dfrac{\Delta P_3}{P_3}\right)^{0.5}}$
Lipfert	$EINOx = 0.17282.\exp(0.00676593 T_3)$
AECMA	$EINOx = 2 + 28.5\sqrt{\dfrac{P_3}{3100}}\exp\left(\dfrac{T_3 - 825}{250}\right)$
GasTurb	$S_{NOx} = \left(\dfrac{P_3}{2965}\right)^{0.4} exp\left(\dfrac{T_3 - 826}{194} + \dfrac{6.29 - 100.WAR}{53.2}\right)$
Lefebvre	$EINOx = 4.59 \times 10^{-9}.P_3^{0.25}.F.t_{res}.exp\left[0.01(T_{fl} + 273)\right]$
NASA	$EINOx = 33.2.\left(\dfrac{P_3}{432.7}\right)^{0.4}.exp\left(\dfrac{t_3 - 459.67 - 1027.6}{349.9} + \dfrac{6.29 - 6.3}{53.2}\right)$
NPSS	$EINOx = 0.068.P_3^{0.5}.exp\left(\dfrac{t_3 - 459.67}{345}\right).\exp(H)$

6.3.2 Pressure rise combustor

The zero dimensional model of detonation analysis has been developed in the previous chapter. Values for the mass flux, fuel flow, pressure and temperature for detonation are used for the combustion tube geometry design and to set initial conditions. A simple single open-ended tube geometry design with a constant cross-sectional area is selected for simplicity. The geometry of conventional combustor used for the RB211 variant cannot be used in this emission analysis because of its irregular cross-sectional areas and the radius being much larger. As a consequence, it will not sustain detonation combustion and so would lead to errors in the HEPHAESTUS. Critically, the sizing should

be selected properly to sustain detonation in the tube analysis and establish the baseline condition. The constant parameters used in the analysis are listed in Table 6-4. The radius of the tube is designed based on a compromise between the experiment of hydrocarbon-fuelled pulse detonation engine conducted by Yungster and Breisacher (2005) and rotating detonation engines conducted by Schwer and Kailasanath (2016). To date, no efforts been made to study and predict pollutant formation within pressure-gain combustors other than these two efforts by Yungster and Breisacher (2005) and Schwer and Kailasanath (2016).

Prior to the emission analysis, caloric properties for kerosene (KE) are evaluated in NASA CEA under detonation combustion. Three calorific parameters: enthalpy, entropy, and the specific heat are investigated. Comparison of caloric properties under deflagration and detonation combustion needs to be made, so that this can be used in HEPHAESTUS emission modelling and justified. However, BJ, BC, and AG cannot be evaluated under detonation combustion in NASA CEA. Therefore, caloric properties of these biofuels are taken from the previous analysis model using the ZND modelling in a zero dimensional detonation analysis. Different fuels have different initial temperature and mass fluxes for detonation and these initial conditions resulted in variation of pressure rise across the shock for different fuels.

Next, the emission analysis is conducted using HEPHAESTUS by evaluating baseline conditions first for different fuels at the minimum detonation condition. Initially, parameters such as the temperature, pressure, and mass flux from ZND model obtained from detonation analysis (Chapter 5) are taken. Knowing the minimum mass flux required for detonation, the radius of the tube is calculated. Variables such as the air mass flow rate fractions, fuel flow, fuel temperature, and combustion zone lengths are assumed based on parametric study done by Ma, Choi, and Yang (2005) and Yungster and Breisacher (2005) experiments. These values are tabulated in Table 6-4. It should be noted that

the range of temperature Later, the variations for different conditions are evaluated at different air mass flow fractions introduced into each of the combustor zones (flame front, primary zone, intermediate zone, and dilution zone), as well as for variations in the fuel flow, combustion zone lengths, and chamber pressures.

Table 6-4 Constant parameters

Parameters	Values
Mass Air Fraction at Flame Front, FRAIRFF	0.05
Mass Air Fraction at Primary Zone, FRAIRP	0.35
Mass Air Fraction at Intermediate Zone, FRAIRI	0.35
Mass Air Fraction at Dilution Zone, FRAIRD	0.35
Fuel Flow, WF (kg/s)	7.5
Fuel Temperature, TF (K)	420
Cross Sectional Area (m^2)	0.0707
Flame Front Length, FFL (m)	0.05
Primary Zone Length, PZL (m)	0.15
Intermediate Zone Length, IZL (m)	0.15
Dilution Zone Length, DZL (m)	0.15

Verification of these different conditions is achieved through chemical and thermodynamic analysis of the flame temperature under detonation. Firstly, the same chemical equations are taken into consideration. Next, an adiabatic flame temperature at constant volume is calculated. Based on the chemical reactions calculated in the previous section, adiabatic flame temperatures at constant volume are calculated using the following steps:

1. In thermochemistry, the equation used in combustion of reactant-product mixtures is:

$$H_{reac}(T_i, P) - H_{prod}(T_{ad}, P) - R_u\left(N_{react}T_{init} - N_{prod}T_{ad}\right) = 0 \quad \textbf{(6-8)}$$

2. It can be expanded to:

$$\sum_{react} N_i\bar{h}_i - \sum_{prod} N_i\bar{h}_i - R_u\left(N_{react}T_i - N_{prod}T_{ad}\right) = 0 \quad \textbf{(6-9)}$$

3. Where H is defined as:

$$H = \sum N_i\left[\bar{h}^o_{f,i} + \bar{c}_{p,i}(T_{ad} - 298)\right] \quad \textbf{(6-10)}$$

4. The definition of enthalpy formation of reactant and product are:

$$H_{reac}(T_i, P) = H_{prod}(T_{ad}, P) + R_u\left(N_{react}T_{init} - N_{prod}T_{ad}\right) \quad \textbf{(6-11)}$$

$$H_{prod}(T_i, P) = \sum_{react} N_i\left[\bar{h}^o_{f,i} + \bar{c}_{p,i}(T_{ad} - 298)\right] - R_u\left(N_{react}T_{init} - N_{prod}T_{ad}\right) \quad \textbf{(6-12)}$$

5. Substitute equations (6-11) and (6-12) into equation (6-8).

The only unknown in the equation is T_{ad} and this appears on both sides of the equations. In order to determine this value, an initial T_{ad} guess has to be made. H_{prod} is determined from a NASA CEA computation, specifying detonation problem in the test case type tab. The effects of initial pressure and temperature to the emission formation can then be evaluated in NASA CEA.

6.4 Main Results and Discussion

6.4.1 Conventional combustor

Comparisons have been made with the ICAO databank for the RB211 engine at three different power settings as illustrated in Figure 6-6. Consistent with ICAO standard, cruising, climbing, and take-off have 30%, 85% and 100% power settings respectively. It is observed that emission prediction for the engine model predicted in HEPHAESTUS agrees fairly with ICAO databank for every power setting.

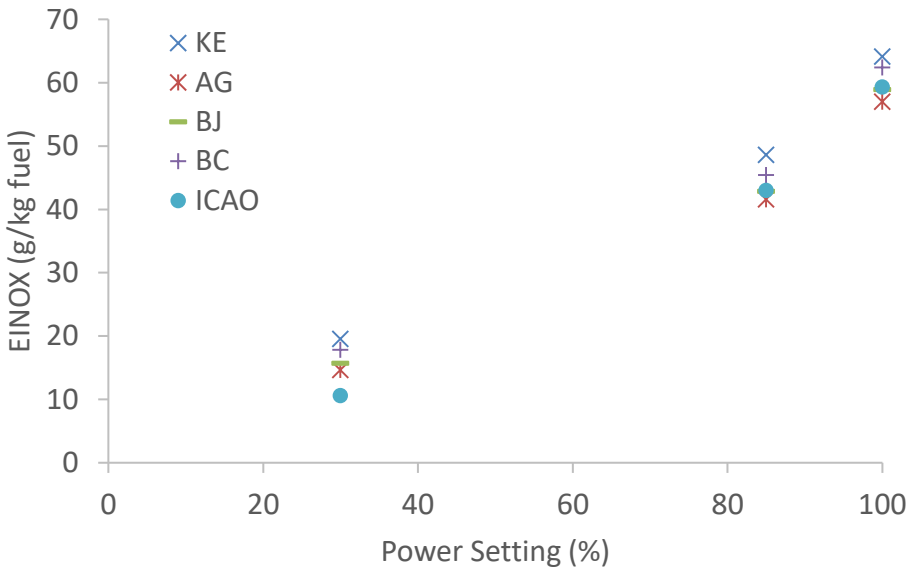

Figure 6-6 Comparison of the model using HEPHAESTUS with ICAO bank data

For a direct comparison of the baseline used in the emission analysis, Table 6-5 is tabulated to capture the biofuels NOx emission values as compared to KE and at different flight cycles. As mentioned in the Methods section, parameters such as inlet combustor temperature (T3), inlet combustor pressure (P3), mass flow (WA), and fuel temperature (TF) are obtained from PYTHIA analysis. As shown, all biofuels are capable of reducing NOx emission with respect to KE fuel at different engine operations; where AG fuel dominates emission reduction (up to 14%) followed by BJ and BC fuels.

Table 6-5 Baseline for emission index analysis

		T3 (K)	P3 (atm)	WA (kg/s)	WF (kg/s)	TF (K)	EINOx (g/kg fuel)	EINOx DIFF wrt KE (%)
CRUISE	KE	840.39	19.56	72.26	1.54	413.74	39.56	
	AG	840.38	19.56	72.26	1.55	413.74	34.68	-12.34
	BJ	841.37	19.60	72.44	1.51	413.90	35.70	-9.77
	BC	841.21	19.59	72.41	1.52	413.87	37.83	-4.37
CLIMB	KE	847.24	21.17	72.02	1.53	413.93	48.60	
	AG	845.46	20.94	71.23	1.52	413.92	41.59	-14.44
	BJ	846.51	20.98	71.43	1.48	414.08	42.86	-11.82
	BC	846.34	20.97	71.4	1.49	414.06	45.42	-6.55
TAKE-OFF	KE	852.08	30.69	113.62	2.43	414.28	64.15	
	AG	852.99	30.88	114.3	2.45	414.28	57.01	-11.14
	BJ	854.19	31.01	114.89	2.39	414.43	58.94	-8.13
	BC	854.01	30.99	114.79	2.40	414.41	62.40	-2.73

Based on the International Civil Aviation Organization (ICAO) for NOx certification standard, they are using the relation in equation 6-13 below which represents the total emission emitted for LTO cycle over kilo Newton of thrust. This relation shows the performance terms such as thrust produced and the fuel flow. Based on the emission index analysis above, it was found that these biofuels reduce NOx emission index and at the same time, it displayed better performances (as depicted in the previous chapter), such as a reduction of the fuel flow and the increase of thrust. Thus, for the overall NOx emission represented by the relation used, biofuels have the capability to reduce emissions as depicted in Table 6-6.

$$\frac{D_P}{F_{oo}}\left({}^{g}/_{kN}\right) = \sum_i EI_i \,.\, TIM_i . \frac{W_f}{RO} \qquad \textbf{(6-13)}$$

Table 6-6 Baseline NOx emission analysis

		EINOx (g/kg fuel)	WF (kg/s)	RO (kN)	TIM (s)	NOx (g/kN)	NOx Diff wrt KE (%)
CRUISE	KE	39.56	1.54	199.04	240	73.65	0.00
	AG	34.68	1.55	199.05	240	64.74	-12.09
	BJ	35.70	1.51	199.49	240	64.84	-11.96
	BC	37.83	1.52	199.42	240	69.16	-6.10
CLIMB	KE	48.60	1.53	161.35	132	60.77	0.00
	AG	41.59	1.52	162.74	132	51.25	-15.67
	BJ	42.86	1.48	163.22	132	51.36	-15.49
	BC	45.42	1.49	163.16	132	54.78	-9.87
TAKE-OFF	KE	64.15	2.43	254.00	42	25.74	0.00
	AG	57.01	2.45	254.13	42	23.04	-10.50
	BJ	58.94	2.39	254.54	42	23.24	-9.71
	BC	62.40	2.40	254.65	42	24.73	-3.90

Similarly, biofuels have potentially reduced the NOx as compared with KE fuel. AG fuel surpasses more reduction in NOx although it requires a higher fuel flow and lower gross thrust as calculated in the previous chapter. However, these results differ from published results by Lokesh (2015). Despite the type of engine she used in her performance analysis, the results differ because the older version of TURBOMATCH does not maintain the same engine design as for the conventional KE case. Moreover, she used an earlier version of PYTHIA which could only provide strict comparisons for different pure fuels for single design conditions only. The new and updated version of PYTHIA is capable of

analysing more alternative fuels options at different off-design conditions as mentioned in Chapter 4.

Off-design conditions are evaluated to visualize the effects of different combustor inlet conditions including different inlet temperature, pressure, mass flow, and the fuel flow. The variations are analysed separately for each power setting to capture the various trends as depicted in Figure 6-7 to Figure 6-9. It can be observed that the trends for different power settings are almost similar. The increase in initial combustor pressure and temperature would encourage NOx emission formations. A similar finding occurred when the mass flow was increased at the inlet of the combustor. However, increasing the fuel flow would tend to reduce more NOx emission formation. These trends are elaborated and verified in the following sections.

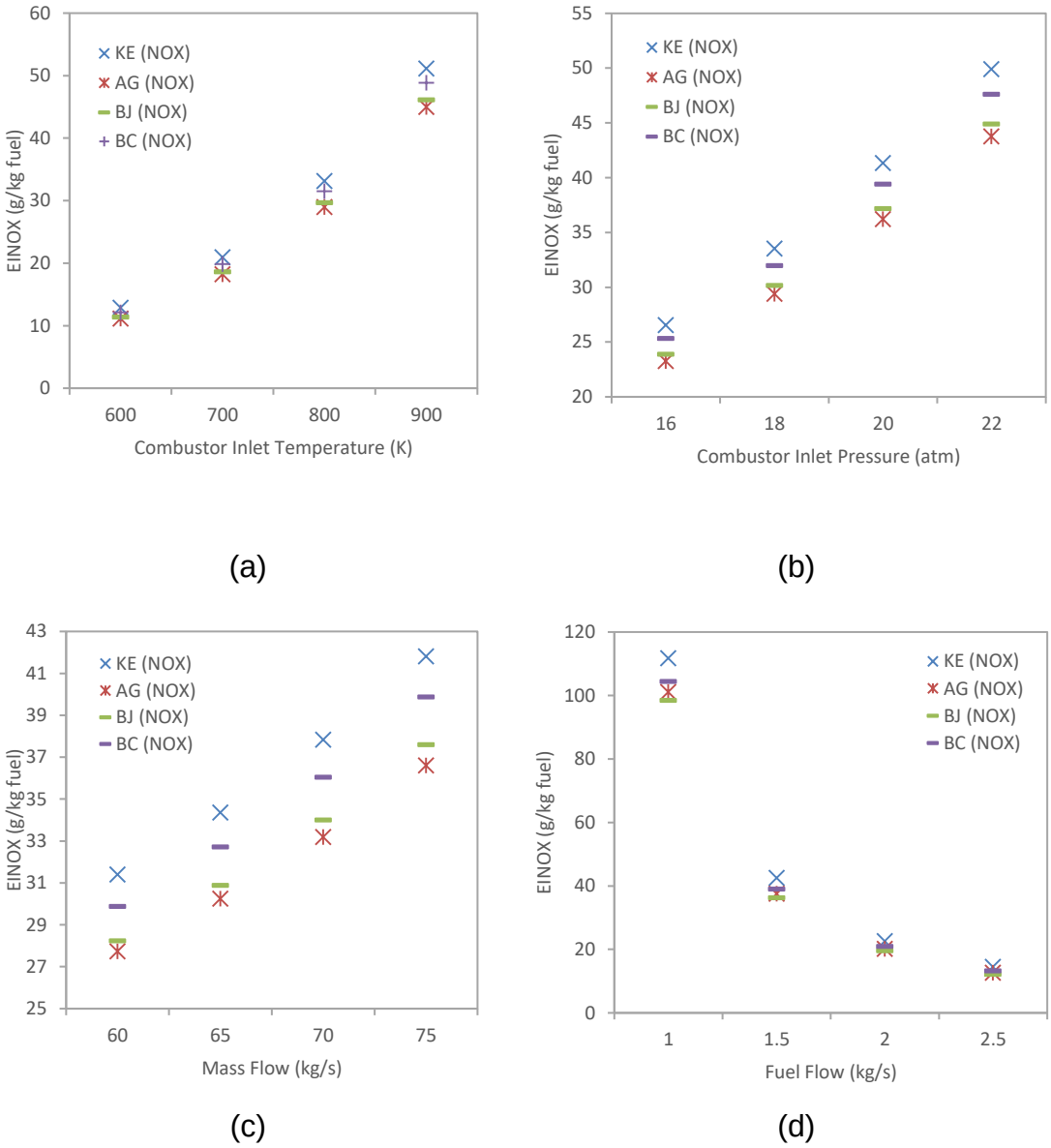

Figure 6-7 EINOx emission at different (a) combustor inlet temperature, (b) combustor inlet pressure, (c) mass flow, and (d) fuel flow for 25% Power setting

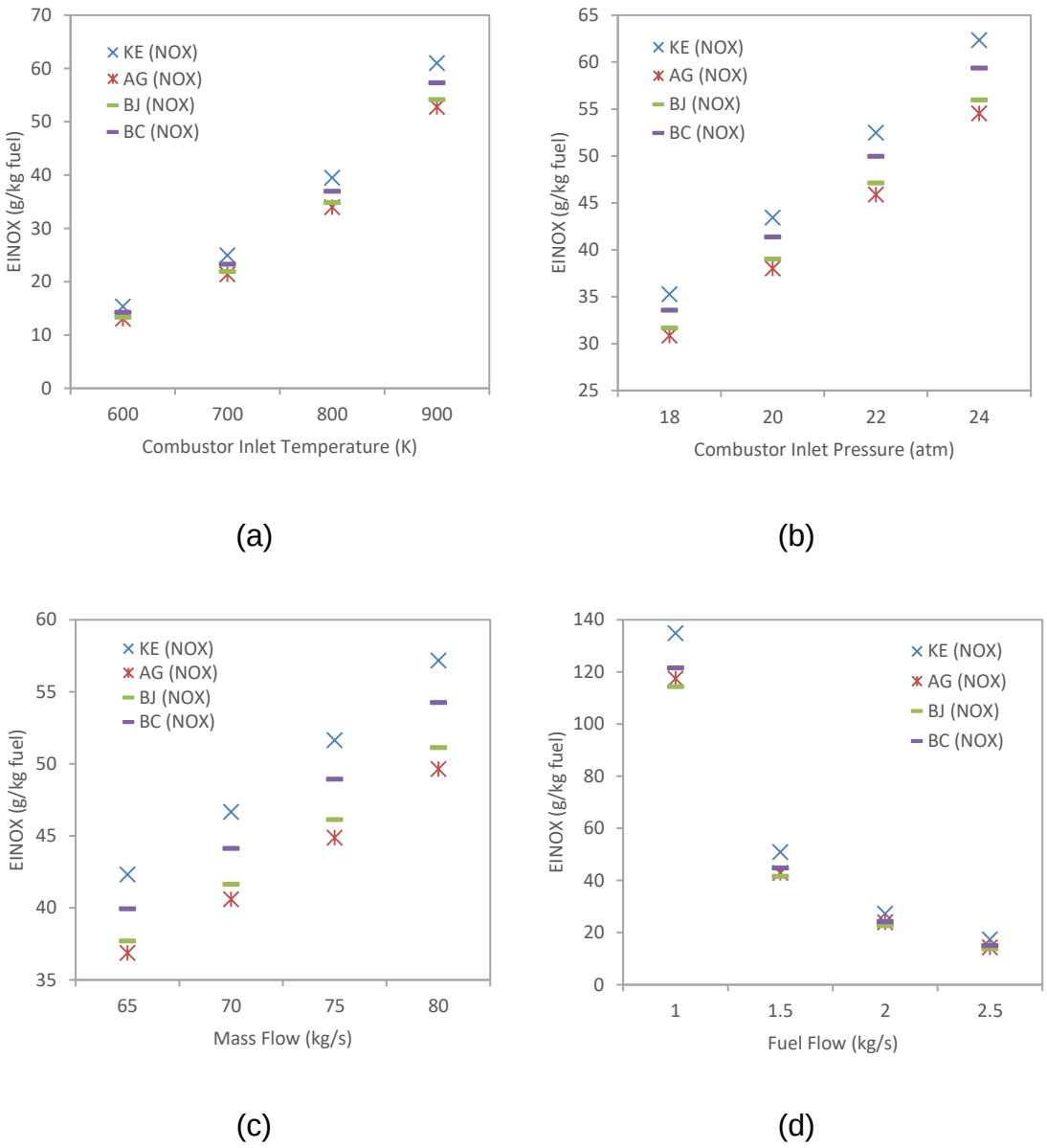

Figure 6-8 EINOx emission at different (a) combustor inlet temperature, (b) combustor inlet pressure, (c) mass flow, and (d) fuel flow for 85% Power setting

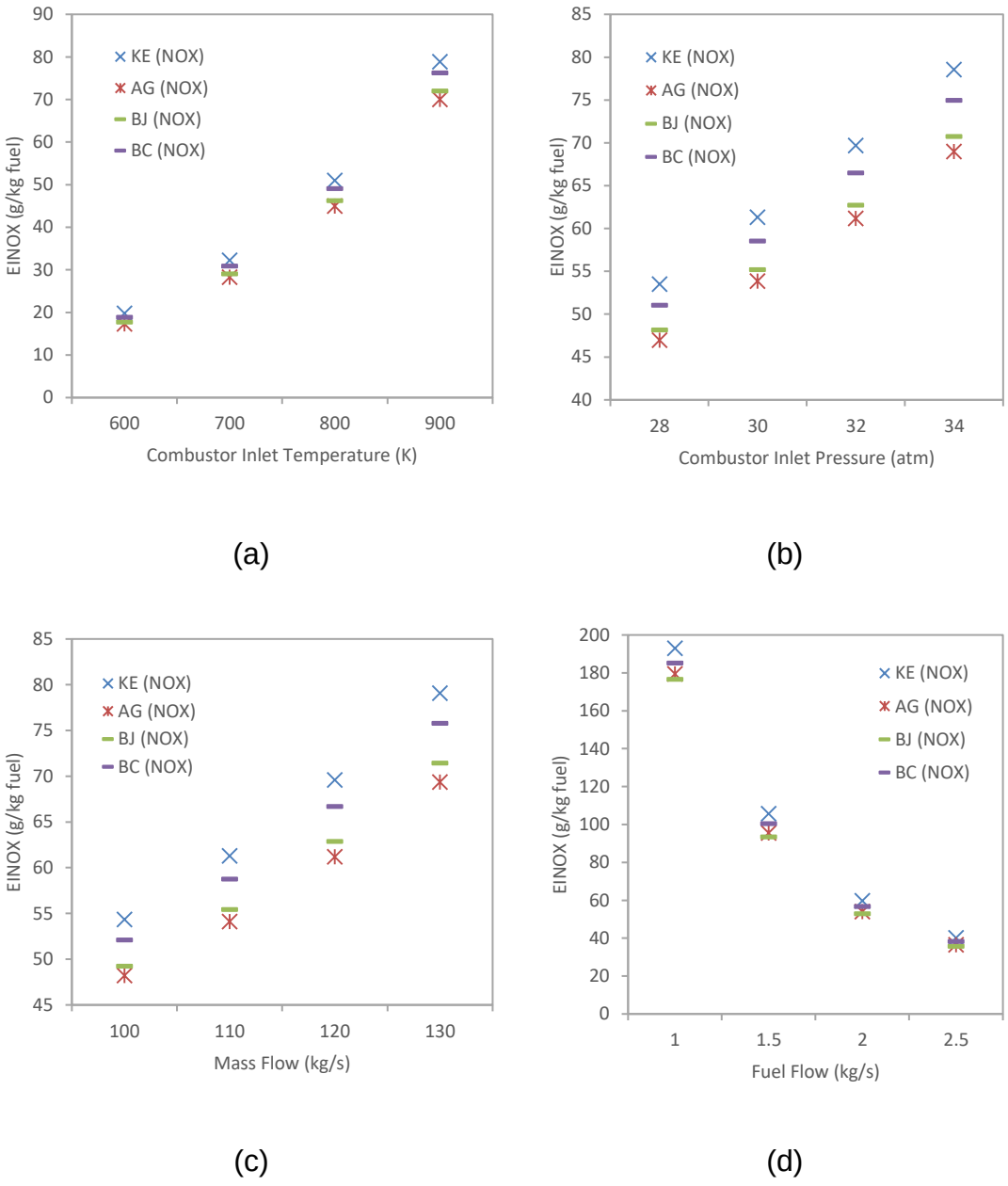

Figure 6-9 EINOx emission at different (a) combustor inlet temperature, (b) combustor inlet pressure, (c) mass flow, and (d) fuel flow for 100% Power setting

Effects of initial mass and fuel flow to the NOx formation

This section intended to support the findings for the effects on initial mass and fuel flow to the NOx formation. Increasing the mass flow in the combustor will tend to increase the NOx as depicted in Figure 6-7 until 6-9 part (c). This condition is well explained if the engine is throttling up where the more NOx emissions are produced as more fuel is burned with more air. On the contrary, increasing the fuel flow produces more reduction in the NOx emission as depicted in Figure 6-7 until 6-9 part (d). This situation is observed when we are trying to burn in rich combustion. As noted in the thermodynamic analysis later, burning fuel in rich conditions could tend to lower the flame temperature and produces less NOx. However, among all the effects of the combustor inlet conditions, it is observed that the fuel flow has the most significant effect on the emissions. Although higher fuel flow could reduce NOx but it is not an economical practice.

To examine this, firstly, chemical reactions in the combustion process are analysed manually using the equations in Goodger and Ogaji (2011) fuel reference book. Three different conditions are selected; stoichiometric, excess of air (lean), and fuel rich combustion. Further analysis is made to see how biofuels differ from kerosene fuel under combustion in terms of the product molar mass fraction. The chemical reaction equations are well-balanced and results for every fuel in different conditions are tabulated in Table 6-7 until Table 6-9. The species fractions of molar mass products for different combustion conditions are described by graphs in the table as well as included in the Appendix D.1. It is important to highlight that the NASA CEA program is not able to track all NOx species because there are often minor species formed. That is why, for the conventional combustor, the trace of N_2 products analyzed through thermochemistry and multistep chemistry is needed. Referring to the formation of NOx discussed in the previous section, N_2 products are among the main contributor to NOx formation. However, through chemical analysis, it is

shown that N_2 products are less for biofuel combustion. The differences in terms of percentage reductions are plotted in the Figure 6-10.

Table 6-7 Stoichiometry combustion

$$C_aH_b + m_s(O_2 + 3.76N_2) \rightarrow n_1CO_2 + n_2H_2O + n_6N_2$$

	KE	AG	BJ	BC
m_s	18.6	17.8	17.4	17.3
n_1	12.5	11.5	11.3	11.2
n_2	12.2	12.6	12.3	12.2
n_6	69.9	66.8	65.5	65.0
Molar (A/F)s	88.54	84.61	82.94	82.35
Mass (a/f)s	14.70	15.02	15.00	15.02
Molar (P/R)s	1.06	1.06	1.06	1.06
λN_2	0.612	0.609	0.610	0.609
% λN_2 wrt KE	-	-0.447	-0.441	-0.465
λH_2O	0.107	0.114	0.114	0.114
λCO_2	0.109	0.105	0.105	0.105

Table 6-8 Lean combustion (30%)

$$C_aH_b + m(O_2 + 3.76N_2) \rightarrow n_1CO_2 + n_2H_2O + n_5O_2 + n_6N_2$$

	KE	AG	BJ	BC
m	24.18	23.11	22.65	22.49
n_1	12.5	11.5	11.3	11.2
n_2	12.2	12.6	12.3	12.2
n_6	90.92	86.88	85.17	84.56
n_5	5.58	5.33	5.23	5.19
Molar (A/F)	115.10	109.99	107.83	107.05
Mass (a/f)	19.11	19.53	19.50	19.52
λN_2	0.621	0.619	0.619	0.619
% λN_2 wrt KE	-	-0.349	-0.344	-0.363
λO_2	0.038	0.038	0.038	0.038
λH_2O	0.083	0.089	0.089	0.089
λCO_2	0.085	0.082	0.082	0.082

Table 6-9 Rich combustion (30%)

$$C_aH_b + m(O_2 + 3.76N_2) \rightarrow n_1CO_2 + n_2H_2O + n_3CO + n_6N_2$$

	KE	AG	BJ	BC
m	13.02	12.44	12.20	12.11
n_1	1.34	0.835	0.845	0.82
n_2	12.2	12.6	12.3	12.2
n_3	11.16	10.67	10.46	10.38
n_6	48.96	46.78	45.86	45.53
Molar (A/F)	61.98	59.23	58.06	57.64
Mass (a/f)	10.29	10.52	10.50	10.51
λN_2	0.558	0.555	0.555	0.555
% λN_2 wrt KE	-	-0.581	-0.573	-0.605
λCO	0.127	0.127	0.127	0.127
λH_2O	0.139	0.149	0.148	0.149
λCO_2	0.015	0.010	0.010	0.010

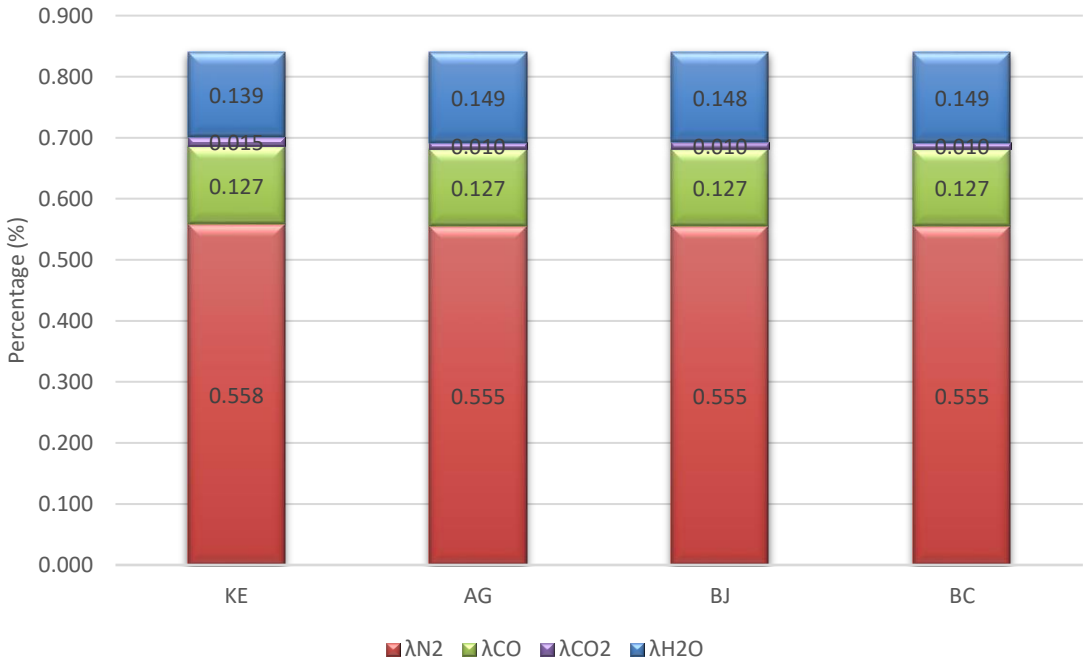

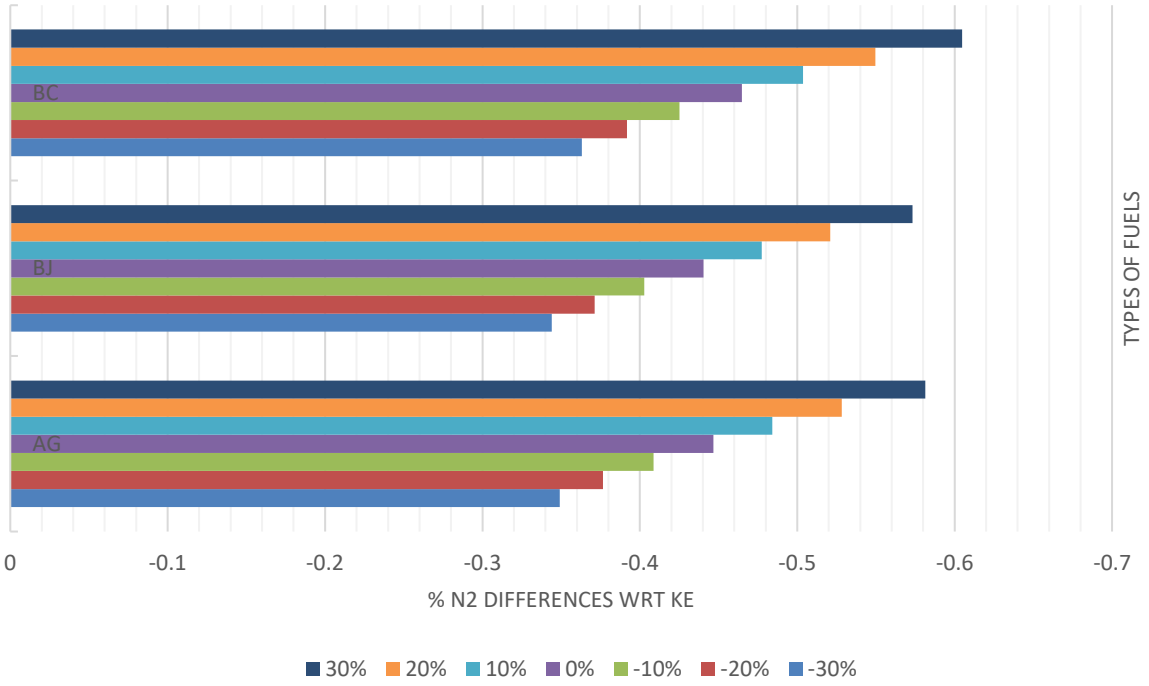

Figure 6-10 Molar mass fraction variations at different combustion types

Figure 6-10 shows that BC fuel has much lower molar mass fraction product of nitrogen compared to other fuels, but as mentioned in the previous section, the formation of NOx is highly dependable on temperature. Further evaluation is needed for thermochemistry to calculate the flame temperature. Flame temperature is a maximum at the stoichiometric condition for all fuels, as consistent with the thermodynamic analysis. However, there is a slight difference in the values for each fuel as different fuels have different levels of energy and molar constituents involved in breaking the bonds of these fuels. The variations of flame temperature for every fuel at different equivalence ratios are plotted in Figure 6-11 and the slight changes of the flame temperature with respect to kerosene are plotted in the bar graphs. The calculation of the flame temperature is included in Appendix D.3. BC fuel exhibits a slightly higher flame temperature compared to other biofuels, thus, encouraging more NOx formation. However, this analysis only considers a single step reaction chemistry, and does not therefore take into account the full chemical kinetics of

NOx formation. Accommodating multistep chemistry, dissociation and the minor species that will be formed, would mean the species mole and mass fractions of the products will be different, resulting from different values of flame temperature.

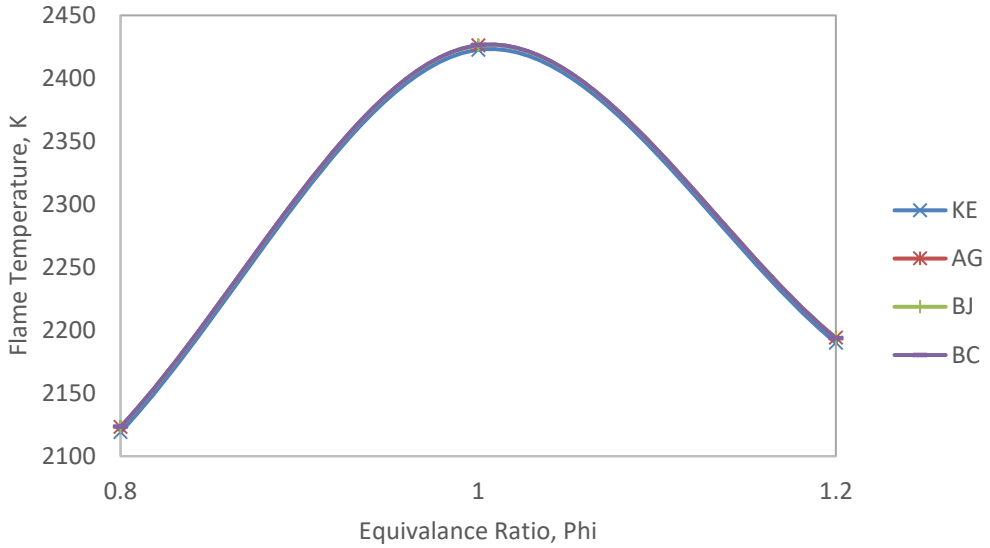

(a)

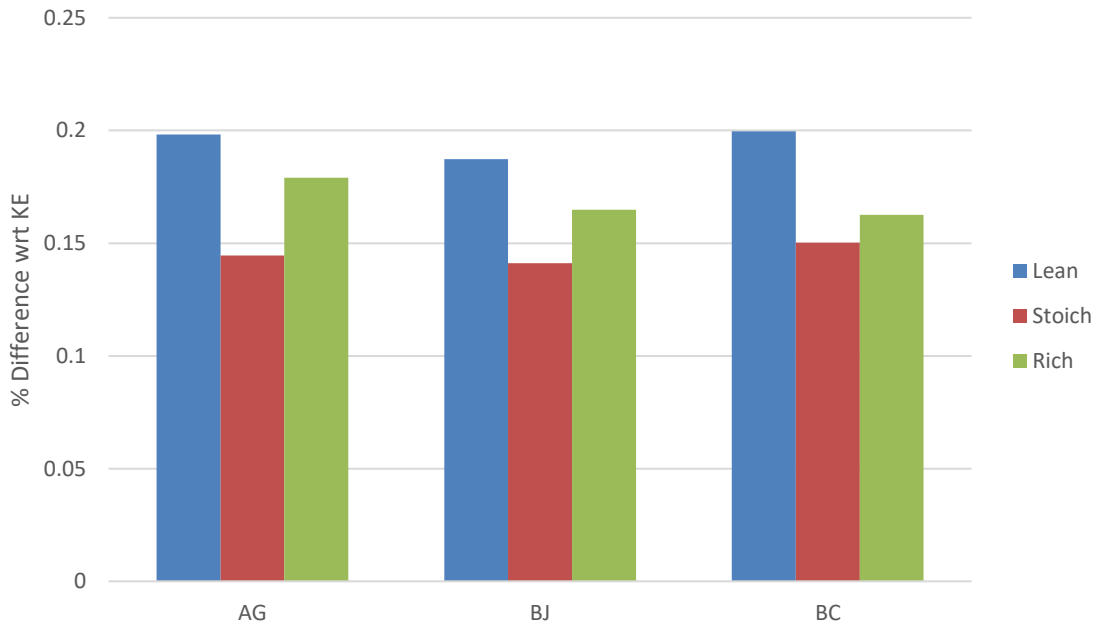

(b)

Figure 6-11 (a) Flame temperature variation of different fuels and (b) comparison with respect to KE Fuel.

Effects of temperature and pressure to the NOx formation

Increasing combustor inlet temperature and pressure can lead to increased NOx emissions for all engine operations. As proven by the present CEA analysis, and also published literature for correlation-based modelling, NOx formation is highly dependent on the combustor temperature and pressure. High pressure and temperature promote more NOx formation. In order to assess the effects of pressure and temperature to NOx formation, the same type of engine was used to accommodate the correlation-based models discussed in the methodology section in Table 6-4. Only kerosene fuel is evaluated at cruise condition and at stoichiometric combustion. This is because there are no existing correlation-based models for such alternative fuels. It has therefore been assumed that these correlation-based models can use constant parameters as listed in Table 6-10. Only P3 and T3 are varied to show how these two initial properties affect the NOx formation. Based on those six correlations shown in Table 6-4, it is clearly evidenced that the trends are consistent with the results using HEPHAESTUS in Figure 6-7 to Figure 6-9 part (a) and (b).

Table 6-10 Constant parameters for correlation-based model

	PARAMETERS
$(T_{flame})st$	2422.69K
$Fuel\ Flow$	1.5439 (kg/s)
t_{res}	0.5s
ΔP_3	99120.68 Pa
WAR	0.00168
$Air\ fraction\ in\ PZ$	0.1
$Humidity\ Factor$	0.1
$Time\ in\ mode$	240s

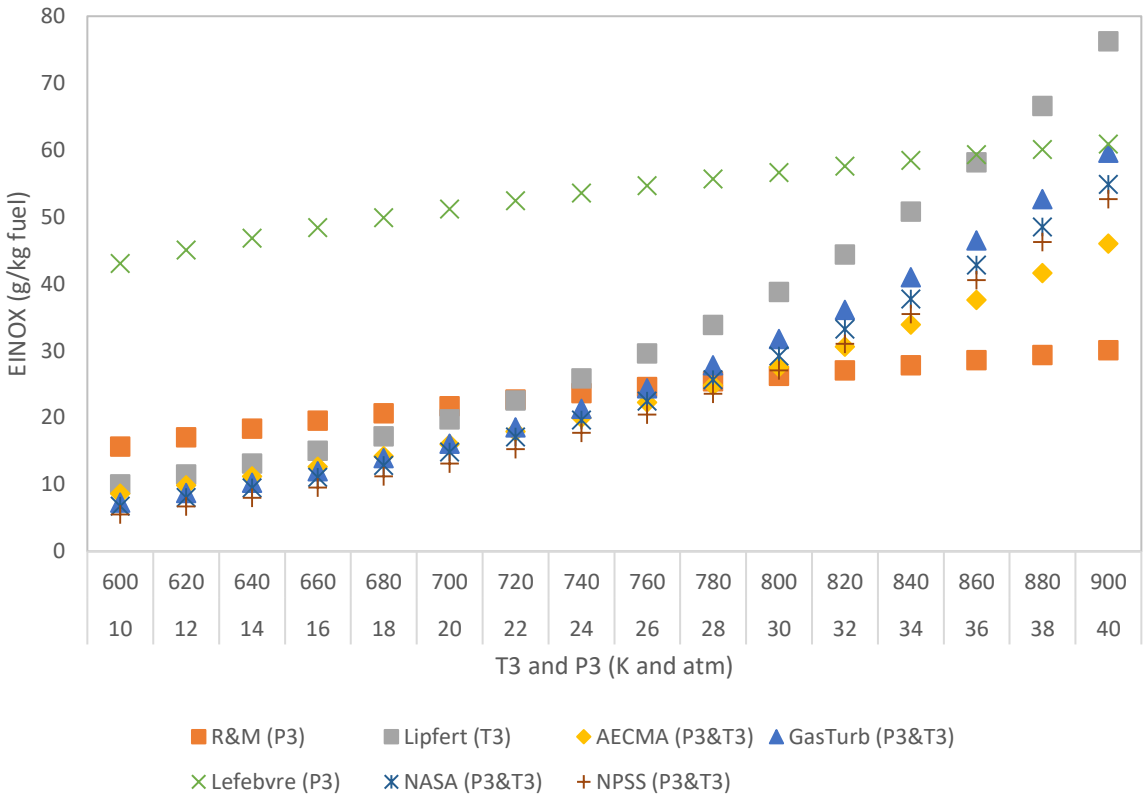

Figure 6-12 Effects of P3 and T3 variations on EINOx using correlation-based models

It is, however, observed that the HEPHAESTUS results are not presented and compare with the correlation models depicted in Figure 6-12. This is because of the difficulties to accommodate sufficient proprietary information required in PYTHIA. The graphs are presented only to view the consistency of the effects of pressure and temperature that encourage NOx formations. It is worth highlighting that most of the correlation-based models are not suitable for predicting pollutant emissions for a wide range of engines. This is because each model is valid for a particular engine only in which experiments are conducted.

6.4.2 Pressure-rise combustor

The use of HEPHAESTUS is extrapolated here to pressure-rise combustion with as two important assumptions despite the limitations that the correlations used in the code that are only strictly applicable to conventional combustors, which deal with constant pressure combustion. In addition to the assumptions previously discussed in section 6.2.3, and other assumptions addressed in Celis (2010), in order to attempt to apply HEPHAESTUS to the pressure rise combustor it was assumed that on the correlation of emissions with temperature and pressure remain valid under detonative combustion because HEPHAESTUS can handle the wider range of pressure and temperature that occurs. Then the geometrical sizing is assumed to be as in Chapter 5. The only other current solution to obtain an emission model prediction for pressure rise combustor now is to employ the thermodynamic model of N-mixture for each species and multistep kinetic model that was used by Yungster and Breisacher (2005) and Schwer and Kailasanath (2016). Fortunately, HEPHAESTUS was coded using the correlations of thermochemical properties over range of temperatures and pressures that at least allow same simple trends to be suggested. Therefore, further analysis has to be made to the code refinement by comparing the flame temperature in a conventional combustor and a pressure-rise combustor. Calculating the flame temperature is accurately essential as the other thermochemical properties such as enthalpy, specific heats, heat addition, calorific properties, and other parameters depend on this (see equations 6-8 to 6-12).

To adopt the mechanism, these properties must be comparable at reasonable temperature and pressure for the emission prediction in using HEPHAESTUS. In practice, it appears that the flame temperatures exhibit less than 10% differences when c_v is used and less than 1% differences when c_p is used for the two types of combustor in the analysis as shown in Table 6-11. The flame temperature calculation is included in Appendix D.4. These differences arise because the adiabatic flame temperature at constant volume depends on the

initial temperature. Both comparisons are made because ideally, designers used c_p instead of c_v in high-speed flow of air-breathing engines, including in pulse detonation engines propulsive performance prediction, even though there are series of shocks existing then in the combustor tube. Since the HEPHAESTUS codes uses c_p in the emission prediction as well, there are not many differences in the calorific properties. It is thus suggested that feasible HEPHAESTUS can be used for pressure gain combustor emission trend estimation for a range of temperatures, pressures and geometry size of the combustor. Again, it should be highlighted that the results are based on an extrapolation of the method and further experiments should be made to validate the data for these biofuels.

Table 6-11 Comparison of flame temperature of KE

Based on c_v	*Conventional*	*Detonation (T=1700K)*	*%Diff wrt Detonation*
T_f(Stoich)	2422.69K	2654.63K	-8.74
T_f (Lean)	2119.1K	2267.66K	-6.55
T_f (Rich)	2190.09K	2419.55K	-9.48
Based on c_p			
T_f(Stoich)	2422.69K	2425.47K	-0.11
T_f (Lean)	2119.1K	2121.87K	-0.13
T_f (Rich)	2190.09K	2210.45K	-0.93

As in the previous chapter has been discussed, each fuel has different minimum conditions for detonation because of the difference in its thermochemical properties. Several parameters from the previous detonation analysis are thus taken for emission analysis. Values such as the temperature and pressure are

taken directly, while the mass flux is specified for the geometrical design and the flow velocity. Given these parameters in Table 6-5, HEPHAESTUS is capable of evaluating the EINOx for every fuel and the baseline conditions are tabulated in Table 6-12. It is seen that BC and AG fuels exhaust more EINOx compared to KE fuel. This is due to higher pressure rise occur in these fuels. However, BJ fuel produces much less EINOx even at high pressure. The results for these biofuels are also due to the effect of the higher mass flow introduced in the tube, which is discussed later.

Table 6-12 EINOx emission in detonation combustion

	T	P	WA	EINOX	EINOX %DIFF WRT KE
	[K]	[atm]	[kg/s]	[g/kg fuel]	%
KE	1700	11.42	212.06	75.68	0
BJ	1700	26.06	311.02	75.54	-0.18
BC	1700	26.04	311.02	79.06	4.47
AG	1700	25.17	397.25	104.28	37.79

Performance evaluation of a pressure-rise combustor

To evaluate the NOx formation exhausted from a pressure-rise combustor, the ICAO relation is used as shown in equation (6-13). In order to use this relation, a performance analysis has to be made first. The simplified analytical model for a straight detonation tube, with single-pulse operation, uses the relations suggested by Ma, Choi and Yang (2005) in the present prediction procedure. The following relations are used in the analysis:

$$T_e = T_2 \left(\frac{P_\infty}{P_2}\right)^{\frac{\gamma-1}{\gamma}} \quad \textbf{(6-14)}$$

$$v_e = \sqrt{2\left[q - c_p(T_e - T_{t1})\right]} \quad \textbf{(6-15)}$$

$$F_{sp} = (1 + f)v_e - u_\infty \quad \textbf{(6-16)}$$

$$I_{sp} = \frac{F_{sp}}{fg} \quad \textbf{(6-17)}$$

The subscripts ∞, 1,2 and e used in equations 6-14 to 6-17 represent the states of freestream, unburned gas, CJ point, and exit plane, respectively. In the present case, seven parameters have fixed values and are listed in Table 6-13. It should also be noted that the fuel-to-air ratio, *f* is fixed and based on the stoichiometric condition of kerosene fuel combustion. This value is taken from the CEA analysis for kerosene fuel under detonation problem. The free stream and stagnation parameters are taken from Ma, Choi, and Yang (2005), for a single-tube pulse detonation propulsive performance. The purging process is not included in the analysis, but based on their analysis of the effect of valve timing, as the valve closing time increases, the specific thrust and specific impulse are reduced. However, the purging time has an opposite effects, where higher purging time increases specific impulse, but reduces the specific thrust. For an overall cycle, higher cycle time can also reduce both specific impulse and thrust.

Table 6-13 Constants used for propulsive performance evaluation

Constant parameters	
f	0.069
$P_\infty(kPa)$	29.384
$u_\infty(\frac{m}{s})$	636
$T_{t1}(K)$	428
$P_{t1}(kPa)$	214.81
$g(\frac{m}{s^2})$	9.81
M_∞	1.442

Given the minimum conditions for each fuel to be detonated, as analysed in the previous chapter, the performance results are tabulated in Table 6-14. From the equations, it is shown that higher pressure ratio in burned region over the unburned region results in an increase in the exit temperature. Exit velocity depends on the thermochemical properties of the fuel which means that every fuel has different heat release due to the in different molecular bonding. The equation also show that a higher exit velocity is needed to increase the specific thrust and at the same time increase the specific impulse. All biofuels tend to have higher exit temperature because they can only detonate at a higher temperature and mass flux. Thus, as expected, all biofuels have much higher specific impulse and thrust. However, at the same time more fuel is needed for the combustion, which reduces their advantage.

Table 6-14 Conditions for detonation and propulsive performance

	KE	BJ	BC	AG
$\frac{P_2}{P_1}$	12.56	26.06	26.04	25.17
$\frac{T_2}{T_1}$	2.46	3.63	3.62	3.42
$\frac{\rho_2}{\rho_1}$	5.11	7.18	7.20	7.37
γ	1.23	1.17	1.17	1.17
$q(\frac{kJ}{kg})$	3039.65	10604.9	10580.4	9711.72
$c_p\left(\frac{J}{mol.K}\right)$	1.531	1.923	1.915	1.79
$\dot{m}(\frac{kg}{s})$	23.56	34.56	34.56	45.55
$T_e(K)$	652.65	977.67	975.44	918.57
$u_e(\frac{m}{s})$	2466.13	4605.71	4600.39	4407.43
$F_{sp}(\frac{m}{s})$	1999.71	4286.42	4280.73	4074.50
$I_{sp}(s)$	2964.36	6354.17	6345.73	6040.02
$F(kN)$	47.127	148.13	147.93	185.61
$\dot{m}_f(\frac{kg}{s})$	1.62	2.38	2.38	3.13

Since all the performance parameters can be obtained, as above, the NOx produced per unit kilo Newton thrust can be evaluated using the ICAO relation (see again equation 6-13) and the results are tabulated in Table 6-15. As depicted in the table, although the biofuels tend to have a higher NOx emission index in detonation combustion compared to their conventional combustor application, due to high pressure, they have achieve much better propulsive performance. This then compensate to an extent for the amount of NOx exhausted per unit kilo Newton of thrust. In fact, the NOx produced by these biofuels can be reduced by up to half compared to kerosene fuel.

Table 6-15 NOx exhausted in a pressure-rise combustor

	EINOX	NOX	NOX %DIFF WRT KE
	[g/kg fuel]	[g/kN]	%
KE	75.68	624.59	0
BJ	75.54	290.84	-53.43
BC	79.06	304.80	-51.20
AG	104.28	422.38	-32.37

Thermodynamic efficiency is accounted for by further analysis with a compressor installed before the combustor. As is well established in the literature, a pressure-rise combustor utilizes a Humphrey cycle while a conventional combustor undergoes a Brayton cycle. By using the PYTHIA code results for pressure and temperature rise across the compressor for each particular fuel, the thermodynamic performances of both cycles can be calculated using equations 6-18 and 6-19 below. These numbering refer to the temperature-entropy graph of thermodynamic cycle. It should again be noted that the temperature rise across the combustor is taken from the conditions for these fuels to detonate. The results calculated are tabulated in Table 6-16.

$$\eta_H = 1 - \gamma \frac{T_2}{T_3} \left[\frac{\left(\frac{T_4}{T_3}\right)^{1/\gamma} - 1}{\frac{T_4}{T_3} - 1} \right] \quad \textbf{(6-18)}$$

$$\eta_B = 1 - \left(\frac{1}{\pi_c}\right)^{\frac{\gamma-1}{\gamma}} \left(\frac{1}{1 + M_\infty^2 \left(\frac{\gamma - 1}{2}\right)} \right) \quad \textbf{(6-19)}$$

As expected and verified here the Humphrey cycle exhibits much higher thermodynamic efficiency. However, we can now also see that the use of pressure rise combustor utilizing Humphrey thermodynamic cycle is capable of an increase in thermodynamic efficiency, of approximately 40%, over a Brayton cycle. This is because biofuels exhibit higher temperature rise across the shock waves established in the pressure-rise combustor.

Table 6-16 Thermodynamic efficiency of a pressure-rise combustor

	KE	BJ	BC	AG
$\boldsymbol{\pi_c}$	30.693	31.010	30.990	30.878
$\boldsymbol{\frac{T_2}{T_3}}$	0.364	0.363	0.363	0.364
$\boldsymbol{\frac{T_4}{T_3}}$	2.457	3.627	3.617	3.416
$\boldsymbol{\gamma}$	1.232	1.165	1.165	1.168
$\boldsymbol{\eta_H}$	0.669	0.674	0.674	0.672
$\boldsymbol{\eta_B}$	0.578	0.476	0.475	0.481
% $\boldsymbol{\eta_{Thermal}}$	15.89	41.75	41.80	39.83

Effects of different conditions

A parametric study was also performed to examine the NOx formation in four different zones; the flame front, primary zone, intermediate zone and dilution zone. It is well known that the wave travels along the tube. For this case, the flame front and primary zone are referred to where the wave initially formed, while intermediate and dilution zone referred to where the wave interacts with other expansion Taylor's waves and reflecting waves downstream. In order to gain insight into the range of emissions produced, different air mass flow fraction was introduced and different zone lengths are examined. Figure 6-13 presents a summary of all the computed results for these changes. Since the trends for kerosene has previously been very well explained and tested by experimental work of Yungster and Breisacher (2005), the focus of discussion is at the biofuels here. Since each fuel has different minimum conditions to detonate, they are prone to be more sensitive to the physical changes in the combustor tube. Therefore, as stability is the main concerns, the range of air mass flow fraction must be selected properly. It is clear from this figure that every zone has its own effect on the emission formation. However, NOx emission formation is more significant in the flame front zone. At the flame front and in the primary zone, NOx can be reduced at a higher air mass flow rate fraction because this can reduce the flame temperature, thus, potentially also reducing NOx formation. On the other hand, NOx formations increases downstream when more mass flow is introduced, due to the pressure rise by the interaction of reflection waves.

NOx emission is dramatically increased when the zone length increases in the upstream zones. Since these zones are expected to experience much higher temperature and longer residence time they promote more NOx formation. For the downstream zones, as the zone lengths are increased, NOx formation is reduced because the interaction waves have more time to settle and the pressure will drop. Many studies in the literature (E Wintenberger *et al.*, 2003; Cheatham and Kailasanath, 2005b; Ma, Choi and Yang, 2005; Rasheed,

Furman and Dean, 2011) have predicted the chamber dynamic behaviour of single tube pulse detonation engines. But, the present results offer a deeper insight for understanding the effect of thermodynamic behaviour in every zone on the NOx emission formation. The model for NOx emission predictions is strongly dependent to how the combustion is progresses. Next, we shall see how the fuel flow and equivalence ratios affect the NOx emission formation, using the chemical and thermochemical analysis to justify and explains the results.

Flame Front

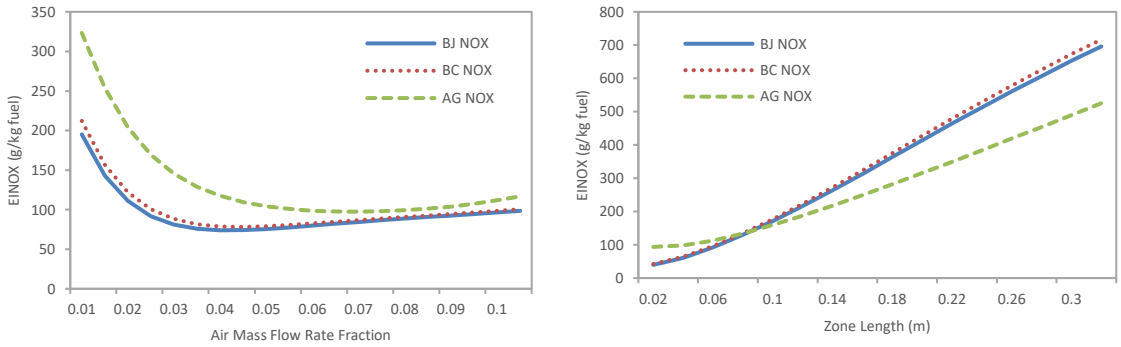

Primary Zone

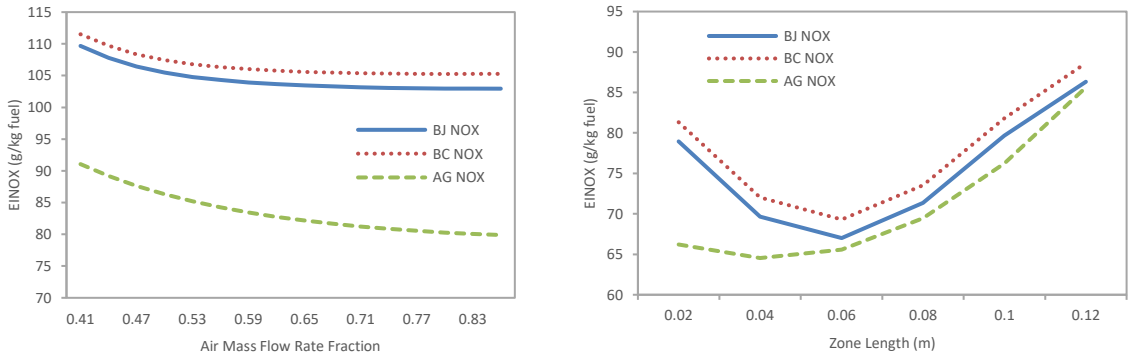

Intermediate Zone

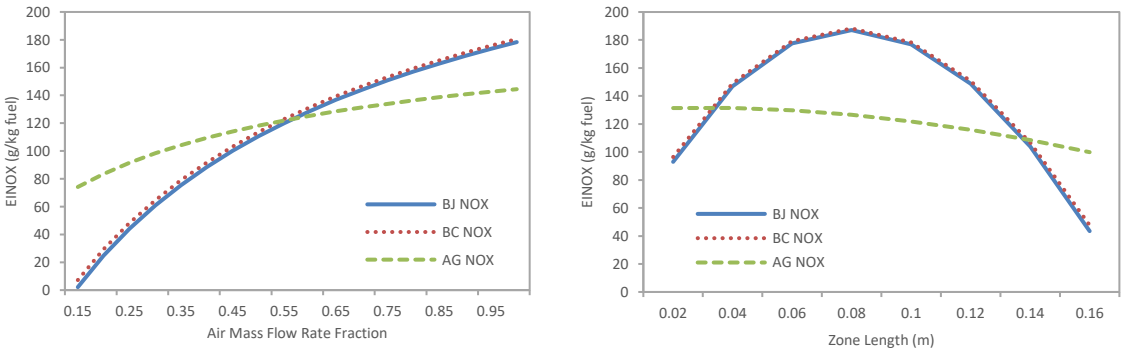

Dilution Zone

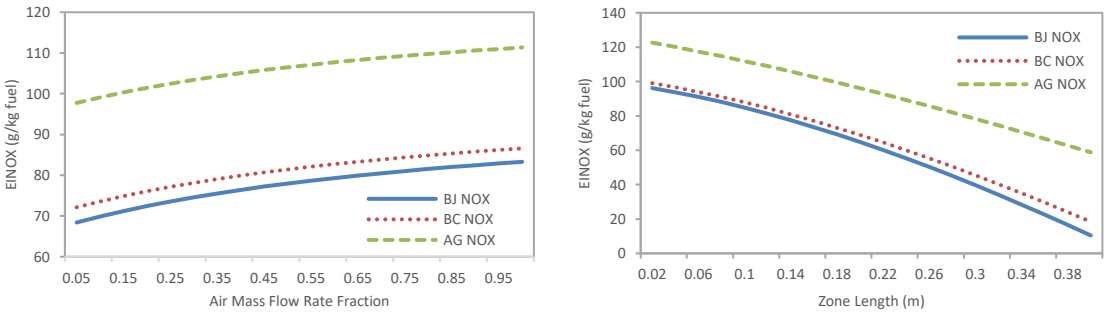

Figure 6-13 NOx emission at different zones; variations of introducing air mass flow fraction (left) and variations of combustion zone length (right)

In order to assess the effects of equivalence ratio on NOx emission, variations of fuel flow are taken into consideration. Note that every fuel exhibits different fuel flow measurement to achieve stoichiometric combustion. Fuel flow of KE fuel is presented in Figure 6-14 while the other results for other fuels are included in the Appendix D.2. These fuels capture similar parabolic trends in which fuel-rich and fuel-lean mixtures showed less NOx formation. For fuel-rich mixtures (at higher fuel flow), the NOx emission index can be decreased exponentially. The observed trends are supported by Yungster and Breisacher (2005) experimental results which suggested that these are due to the competition between fuel and nitrogen for the available oxygen. The peak of the NOx formation is occurs at the nearly the stoichiometric mixture, where the flame temperature is maximum. The thermochemistry analysis is described next.

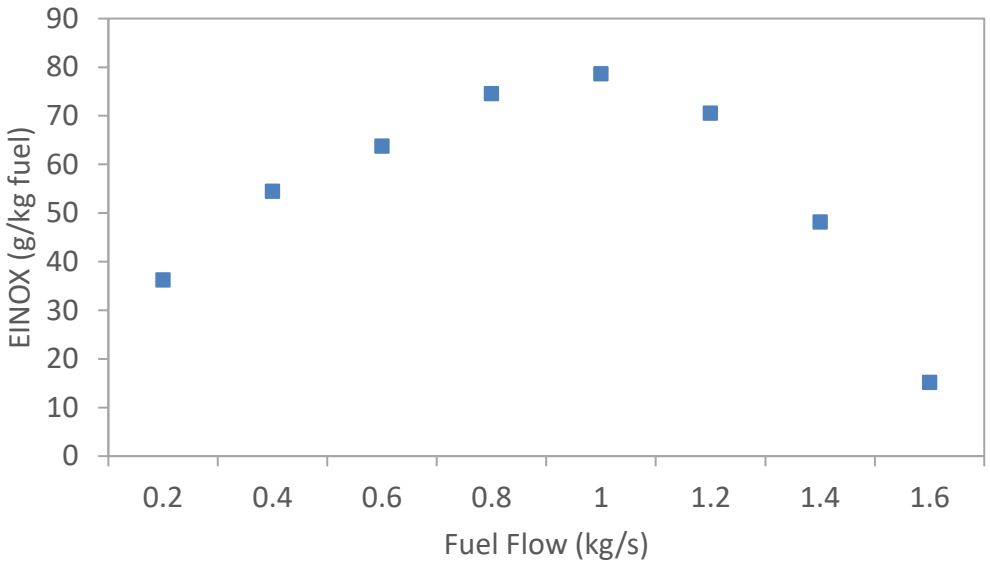

Figure 6-14 Influence of KE fuel flow on NOx emission

Further analysis is carried out to find the adiabatic flame temperature using the thermochemistry relations as discussed in the methodology section. It should be noted that only kerosene fuel is being analysed because the CEA approach could not evaluate fuels other than this for a detonation case. The variation of

flame temperature at different combustion mixtures is plotted in Figure 6-15. The initial pressure and temperature are fixed to 11 atm and 1700K respectively. The maximum flame temperature occurred again at nearly stoichiometric condition. As expected, for lean and rich combustion, flame temperatures are reduced. At higher temperature more bond breaking occurs and more effective collisions are expected that will promote NOx formation. The calculation of the flame temperature is included in Appendix D.4.

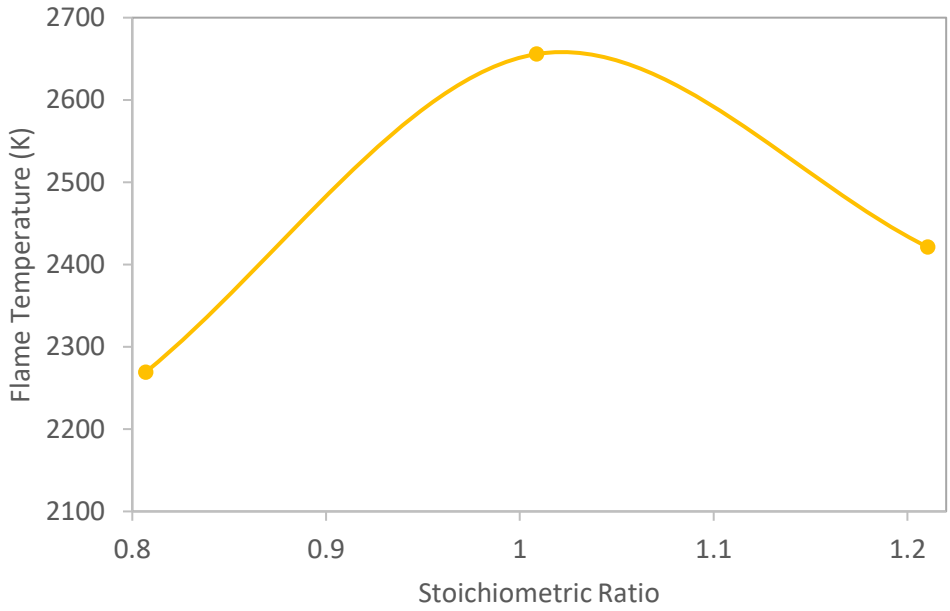

Figure 6-15 Flame temperature variations at different combustion mixtures

The effects of chamber pressure are illustrated in Figure 6-16. A higher chamber pressure produced more NOx formation. As expected from the literature studies, high pressures and temperatures occurring within the detonation waves result in higher emission, while a quick drop-off of these parameters implies much lower emission. The results obtained using HEPHAESTUS emission model prediction did capture correct trends compared to both experimental and numerical studies conducted by Yungster and Breisacher (2005) and Schwer and Kailasanath (2016) respectively. The production of NOx is based on the non-equilibrium reactions, so its formation is

affected by the rate constant and the law of mass action within the NOx reaction while other species maintain nearly equilibrium value. Therefore, higher pressure pushes the build-up of atomic nitrogen reactions and later produces more NOx formation because they have more energy for effective collision. If multiple detonations events occur, the chamber pressure will start to fall and the shocks becoming weaker which provides better condition for NOx emission reduction. However, as consequences, the combustor performance in terms of specific impulse will tend to reduce as well which is not preferable.

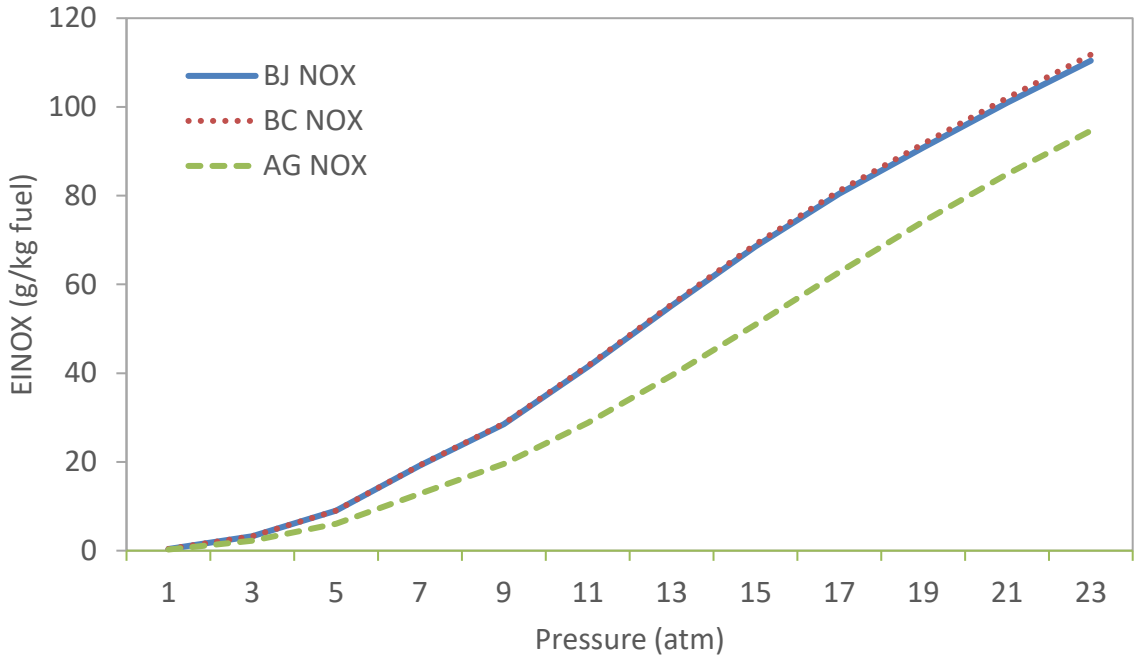

Figure 6-16 Influence of chamber pressure on NOx

The emission model results are primarily assessed against numerical and experimental works by Yungster and Breisacher (2005) for hydrocarbon-fuelled pulse detonation engine. It should be noted that experimental data on liquid hydrocarbon detonation suitable for comparison with the present results are quite scarce. Limited data exists with which only a few comparisons can be made and none are data available for alternative fuels. Most of the experiments have been carried out using either hydrogen-oxygen or hydrogen-air reactions

because of the easiness to initiate detonation. In order to validate the present modelling through parametric studies as well as experiment, the analysis was made in terms of its NOx emission index. But again, only kerosene fuel could be validated.

Yungster and Breisacher (2005) have conducted a variety of tests to evaluate the effects of pressure, temperature, length of the tube, equivalence ratios of the mixtures, and various stratified charges on the NOx emission indices under transient conditions. Their important findings support and are comparable to the present emission model prediction results:

1. High initial pressures and temperatures will encourage more NOx emission indices.
2. Long detonation tubes will exhibit more NOx emission is because of longer residence time across the Taylor waves and plateau region. The fuels will also experience high pressure and temperature for longer time.
3. More NOx emission is also observed under stoichiometric conditions, but are reduce for both lean and rich mixtures. At the stoichiometric condition, the flame temperature reaches its peak, thus, promoting more NOx. While a fuel-rich mixture reduces NOx, mainly due to the competition between fuel and nitrogen for available oxygen.
4. Rich mixtures are preferable at the early stage and lean mixtures downstream to reduce more NOx emissions, as in a so-called stratified charges. Rich mixtures at the upstream also boost the easiness for the fuel to be detonated.
5. Open-end ignition promotes more NOx formation because of the detonation wave reflection from the thrust wall which creates short, but very strong, temperature and pressure spikes.

The HEPHAESTUS computed NOx emission prediction were thus in good agreement with Yungster and Breisacher (2005) experiments. It should be noted, however, that the HEPHAESTUS emission prediction still requires a degree of proprietary information, and it is difficult to acquire all the necessary input parameters needed in the model. For instances, the length of each zone, the total mass flow through the tube, air mass fraction being introduced at each zone and others. Such information is essential for accuracy because it influences the NOx formation significantly. In the present validation study, the sizing of the tube, amount of air introduced, pressure and temperature remained the same. The best HEPHAESTUS emission prediction comparison is thus the stratified charges experiment. The NOx emission indices obtained through the experiment varies from 25 to 90 g/kg fuel. The effects of other tests is described in Table 6-17.

Table 6-17 Estimated range of EINOx obtained by Yungster and Breisacher (2005)

Varying parameters	Range	Estimated range of EINOx obtained (g/kg fuel)
Length of the tube	50-200cm	38-60
Initial pressure and temperature	14.7-125 psi 77°F-800°F	40-148
Equivalence ratios	0.6-1.4	13-150
Stratified charges (rich-to-lean)	0.7-1.4 ϕ at closed-end 0.4-0.6 ϕ at opened-end	25-90
Method of ignition	Opened-end Closed-end	140-180 130-140

Among all the predictions made, it can be concluded that most fall within the range obtained in the Yungster and Breisacher (2005) experiments. Some discrepancies are associated with the over simplified physics model and one-

step chemistry analysis. Nevertheless, this work shows that the HEPHAESTUS approach for emission prediction can be used in a pressure-rise combustor. In view of the very few methods available for the prediction of NOx emission in detonation combustion, it would be a very useful practice for further investigation and development.

6.5 Concluding Remarks

Many other important computational tools for the prediction of EINOx are available in the published literature and in the public domain. A systematic study has been carried out to compare the present computational tools with the most dependable and preferred tools for NOx prediction. It is observed in this work that HEPHAESTUS provides a comparable parametric study for NOx prediction, and at the same time, its capabilities are extended to another mode of combustion; detonation. However, the present work still needs the application of a gas turbine performance software like PYTHIA for a conventional combustor and the NASA CEA scheme for a pressure-rise combustor. To date, almost no effort has been made to predict NOx emission in a pressure-rise combustor using biofuels. And these studies attempt to provide explorative approach in predicting NOx formation in a pressure-rise combustor. Validation has been made for both combustors which satisfy reasonable trends. A simplified thermochemistry analysis has been adopted to support the results. Important findings are highlighted as follows:

Conventional combustor

1. Each of the biofuel studied in the present work has a different capability to reduce NOx emission. It is difficult to decide which fuel has the most emission reduction for all power settings. For NOx reduction, BJ fuel can reduce this by up to 15.85% and 20.73% for an engine on approach and climbing conditions. While AG fuel can reduce NOx up to 12.61% during take-off.

2. Almost all NOx emission can be reduced when the fuel flow is increased moving to rich combustion condition although there could be a penalty cost from economical point of view.

3. It is not beneficial to increase combustor pressure as it will increase NOx emission at the highest power setting. Increasing combustor temperature will also increase NOx formation.

Pressure rise combustor:

1. Emission analysis for detonation combustion is demonstrated successfully. Prior to the emission analysis, a ZND model was used to study the performance and obtain necessary initial parameters to be used for sizing purposes. HEPHAESTUS has shown its capability to predictively estimate NOx emission effectively of a pressure-rise combustor with certain modifications. The geometry of combustor in RB211 variant cannot be used in predicting emission for detonation because of its irregular cross-sectional areas and the radius is much larger. As a consequence, it will not sustain detonation combustion and errors occur in using HEPHAESTUS.

2. In high-speed combustion, stability becomes a major concern and very parameter is very sensitive to initial variations. Therefore, establishing the correct baseline conditions are difficult.

3. Generally, some biofuels contribute an increase in EINOx relative to kerosene at their minimum temperature for detonation by at least 4% for BC fuel, but not for BJ fuel. However, in terms of NOx produced over a unit of kilo Newton thrust, biofuels exhibit better reduction by up to 50%. This is because biofuels has much higher thermal efficiencies.

4. Pressure-rise combustor produces more NOx formation due to its nature of higher pressure and temperature involved during the combustion process as compared to conventional combustor (refer to Table 6-6 and

Table 6-12). But, understanding which factors produces more NOx is important to minimize the impact.

5. NOx can be reduced at a higher air mass flow rate fraction at the flame front and in the primary zone, because this can reduce the flame temperature. On the other hand, NOx formations increases downstream when more mass flow is introduced, due to the pressure rise by the interaction of reflection waves.

6. NOx emission is dramatically increased when the zone length increase in the upstream zones because experiencing much higher temperature at a longer residence time. At downstream zones, NOx formation is reduced because the interaction waves have more time to settle and the pressure will drop.

7 TRADE-OFF ASSESSMENT

7.1 Introduction

This work provides a systematic trade-off solution to address the final objective of this research. Although there is a number of engineering software tools that can be used for optimization purposes, its capabilities of commercially used software in statistics to accommodate problems in aerospace propulsion are certainly worth exploring. The unique ability of factorial design problems in statistics allows interactions between factors given at different levels of the designs and most importantly, assesses the optimal trade-off in a pressure-rise combustor.

Some earlier relevant optimisation studies such as performed by Mazlan (2012), the present work attempts to evaluate the trade-off between performance and emission using biofuels under different modes of combustion by applying an explorative Design of Experiment (DoE) method rather than a strict design optimization approach. It follows an explorative approach, offering an alternative solution to the practicability in this field since there are very limited number of studies published. The general factorial problem in the Minitab software is used to capture the main effects between the factors and to obtain a trade-off between the performance and emissions matrices. Such a factorial experiment problem is most effective way to discover the interaction between variables in which one-factor-at-a-time approach may fail, be inefficient and produce incorrect results (Montgomery and Runger, 2011).

This chapter firstly discussed on the work done on optimization in the literature review. The approach used in this work is shown in the method section, and finally the results are discussed for separate combustors. As an initial analysis, a parametric study was made to investigate the behaviour of main decision variables for particular types of combustor namely, conventional combustor and pressure-rise combustor using different biofuels (KE, BJ, BC, AG, and MA). Each combustor design involves a complex separate analysis because methods used to assess each combustor has a different approach. This evaluation has been studied and discussed

in the previous chapter. Every combustor is analysed at different designated case at different factors and levels. The discrete variables trade-off are presented for every case. It is important to stress that the configurations identified are not optimal but are best configurations from the set evaluated in DoE and allow any specific trends that develop between input parameters to be identified. Pareto optimally criteria could then be applied to this information.

7.2 Literature Review

In recent years, optimization method arose as an essential tool to ensure design system operates at optimal condition under certain constraints. Aviation industry has done tremendous efforts in optimization work ranging from aerodynamics (see Antunes and Azevedo (2014) and Buckley and Zingg (2013)), shapes and structural designs (see Schmidt et al. (2013) and Elham and van Tooren (2014)), dynamic and trajectories/routes (see Xu et al (2014), engine performance (see Berton and Guynn (2011) and Boulkeraa and Ghenaiet (2010) for turboprop), technology and economic perspectives (see Curran et al. (2009). Some of the works are very specific on the field but at least in the last four decades, the field of multidisciplinary design optimization (MDO) has been more attractive due to its advances in theory, algorithms, software frameworks and applications.

The main attraction of MDO is interaction between individual discipline (Martins and Lambe, 2013). MDO decomposes into two or several levels of sub-problems with upper or system level and lower or subsystem level, that is categorized into two types: hierarchical (parent-childhood relationship) and non-hierarchical (same-level children sub-problems) (Gunawan *et al.*, 2003). A complete survey of all architectures in MDO is explained in-depth by Martins and Lambe (2013) covering optimization problem statements, diagrams and detailed algorithms for non-specialists and future references. This certainly pushes aerospace industry in the design of complex system as a whole. Early work of MDO only covers fundamental design formulation, optimization methods, and sensitivity analysis, but now it advances to topics of surrogate modelling, visualization, multi-objective optimization

and optimization under uncertainty (Willcox and Haftka, 2014). Willcox and Haftka (2014) further added that MDO communities are struggling with issues related to the efficient sensitivity calculation, surrogate modelling, Pareto frontiers, visualization, and implementations in the industries.

During mid 20th century, Schmit, Haftka and collaborators introduced MDO and built its application around other branches of engineering. For aerospace in particular, Sobieski and Haftka (1997) made a complete survey for interaction of structures with other discipline, Rallabhandi and Mavris (2008) as well as Bijewitz et al. (2016) made studies on the airframe with propulsion cycle, Ghoman et al. (2012) focuses on wing shape, structure, and aerodynamics MDO, last but not least, Toal et al. (2014) focuses on optimization of a whole engine thermochemical design.

Environmental and performance aspect has emerged as an essential trade-off in the design phase of novel engines. From design's point of view, not only engine performance requirements, external factors such as cost and environmental issues are all required to be in place. At present, there are myriad works on optimization and trade-off performance and environmental impacts are being done, including Antoine and Kroo (2005) on aircraft designing within environmental (noise) and cost constraints, Mazlan (2012) on optimization assessment on biofuel to find the trade-off between emission (NOx and CO) and thrust and Cavalca et al. (2015) on micro turbine performance with consideration of pollutant emission. Much recently, Jimenez and Mavris (2017) studied selections of aircraft technologies in response to environmental impacts in the future and put a broader perspective on the performance trade-off between fuel burns, LTO NOx and noise. It is found to be less distinctive in the overall reduction. It seems that these results are, indeed, comparable to this work and discussed later in the section.

Nonetheless, this work excludes an economical viewpoint. Optimization methods select the best set and variables in each case by using iterative numerical calculation (Aldheeb, 2012). There are many optimization techniques involved although two

main approaches are non-evolutionary and evolutionary methods. Each approach is divided into several techniques as presented in Figure 7-1. Aldheeb (2012) has described each technique thoroughly and is not repeated here. To provide a meaningful insight on the selection of most preferred optimization techniques, genetic algorithms, differential evolution and particle swarm optimization are often the best choices. Evolutionary optimization techniques are preferred due to their flexibility, robustness and capability of solving complex problems. This is advantageous since complexity of optimization problems dramatically increased as more design variables and objective functions involved (Kipouros, 2013). Kipouros (2013) further added that not only appropriate selection of optimizations are essential, but modelling and optimization algorithm tuning play important role to capture execution and exploration design problem successfully.

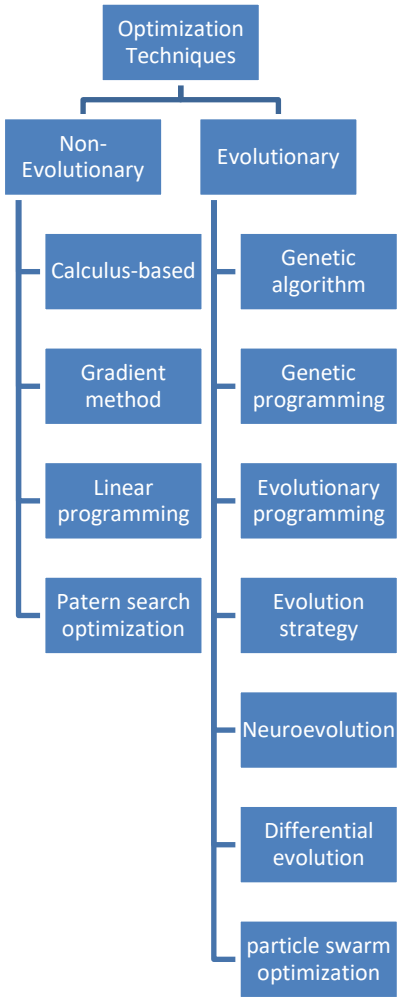

Figure 7-1 Optimization techniques

7.3 Methods

7.3.1 Conventional combustor

Prior to the trade-off assessment, data from performance analysis (PYTHIA) and emission analysis (HEPHAESTUS) are compiled to first identify the necessary parameters needed in each computer tool subsequently. Among all parameters calculated, the best solutions are selected from discrete variables by using trade-off assessment in order to achieve targeted objectives of the research. The process flow and parameters needed are illustrated in Figure 7-2.

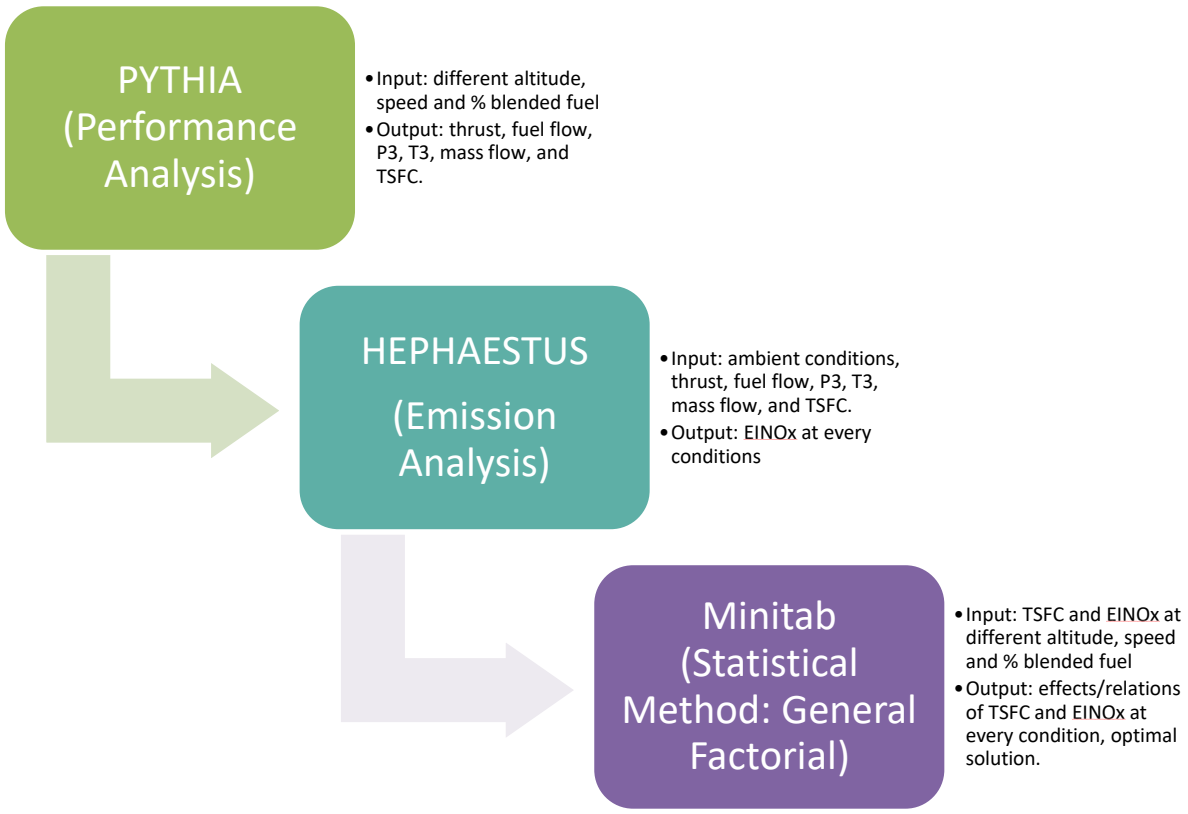

Figure 7-2 Flow process of conventional combustor trade-off assessment

In performance analysis, assessments are made according to designated case study, as presented in Table 7-1. Off-design conditions are calculated at different factors such as different ranges of altitudes, speeds and blended ratio percentages. These factors' variations are designed to accommodate HEPHAESTUS requirements. Parameters output from PYTHIA such as mass flow rate of fuel, total mass flow rate through combustor chamber, total pressure and temperature of

combustion chamber are put into the emission analysis of EINOx. Thrust specific fuel consumption (TSFC) is also calculated from PYTHIA output. A design of experiment using general factorial is used in Minitab software. General factorial design suits well in case study as the analysis is conducted at factors of different levels. With given number of factors and its' levels, Minitab adjusts case study randomly in a worksheet. Two responses, TSFC and EINOx, are re-arranged according to the factors. All data are, then, entered manually for individual factor.

Table 7-1 Case study of conventional combustor

<table>
<tr><th>Case No</th><th>Description</th><th>Factors (No of Levels)</th><th>Range []</th><th>Objectives</th></tr>
<tr><td>1</td><td>KE+AG
KE+BC
KE+BJ</td><td>Altitude
(3 levels)
Speed
(4 levels)
% Blend
(3 levels)</td><td>Altitude
[500m-1500m]
Speed
[0.2M-0.8M]
% Blend
[0.2-1.0]</td><td rowspan="4">Minimum TSFC
Minimum EINOx</td></tr>
<tr><td rowspan="2">2</td><td>Cruise (50% blend)</td><td rowspan="2">Type of Fuels
(4 levels)
Speed
(7 levels)</td><td>Type of Fuels
[KE, KE+AG,
KE+BC, KE+BJ]
Speed
[0-0.8M]</td></tr>
<tr><td>Ground (50% blend)</td><td>Type of Fuels
[KE, KE+AG,
KE+BC, KE+BJ]
Speed
[0-0.3M]</td></tr>
<tr><td>3</td><td>All Blended Fuels</td><td>Type of Fuels
(3 levels)
Altitude (3 levels)
Speed (4 levels)
% Blend (3 levels)</td><td>Type of Fuels
[KE+AG, KE+BC,
KE+BJ]
Altitude
[500m-1500m]
Speed
[0.2M-0.8M]
% Blend
[0.2-1.0]</td></tr>
</table>

7.3.2 Pressure-rise combustor

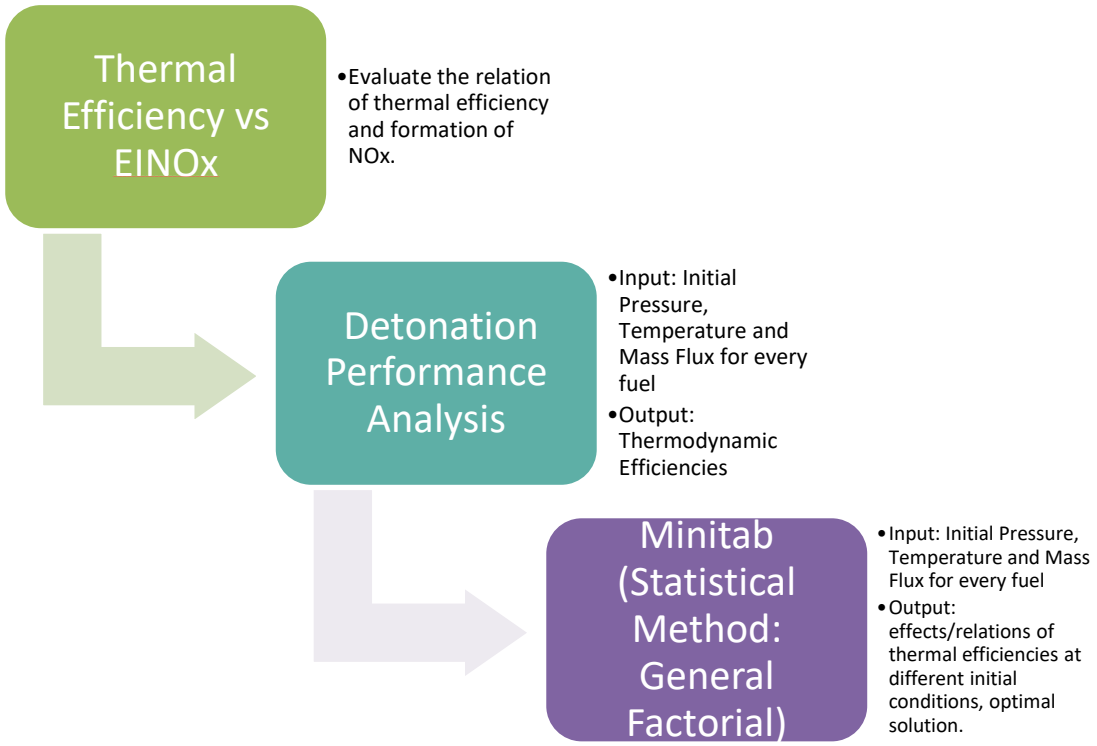

Figure 7-3 Flow process of pressure-rise combustor trade-off assessments

A separate trade-off assessment for pressure-rise combustor is conducted differently due to HEPHAESTUS' incapability to accommodate such extreme intensity of conditions and higher temperatures, pressures and mass fluxes. The flow process of this analysis is described in Figure 7-3. Notably, HEPHAESTUS captures reasonable trends as discussed in previous emission analysis with very limited range. In order to conduct a systematic trade-off assessment, every fuel is given similar factors for every case of study. Since each fuel has different thermochemical properties that mainly affect stability and sensitivity of its physical properties, it is difficult to sustain detonation and accommodate them in HEPHAESTUS. Therefore, relation of thermal efficiency and formation of NOx is investigated first by assigning the same parameters assumed in previous emission chapter (see Table 6-15). Based on these assigned parameters, emission analysis is evaluated for each fuel and described in the following section where consistent trends are observed for every fuel.

By the virtue of fact that thermal efficiency has an indirect relation to emission formation as well as to limited capability of HEPHAESTUS, trade-off assessment for this combustor are evaluated based on its' thermodynamic efficiencies. It is worth nothing that, these are not necessarily always true in all cases as higher thermodynamic efficiency can reduce NOx formation depending on the control of combustion. In previous emission analysis, results have shown pressure-rise combustor does contribute to significantly higher NOx formation due to high pressure rise and temperature. Studies of gas turbine performance have notably agreed that increasing thermal efficiency may proficiently reduce fuel consumption, leading to less pollutant formation. Since interests of this work derive from a very limited number of published literatures, it focuses, in particular, to the indirect emission formation in pressure-rise combustor alongside with the relation of thermal efficiencies on NOx formation is on the particular initial physical conditions of pressures, temperatures and mass fluxes.

As thoroughly discussed in Chapter 5, two conflicting waves, strong and weak are calculated, evaluated and optimized separately for each case study. These cases are designed and tabulated in Table 7-2. In this particular context, it is not practical to vary combustion zone lengths and air mass fraction in each zone due to complexity of many variables involved. Nevertheless, the analysis is still relevant as a design agreement within all requirements.

Table 7-2 Case study of pressure-rise combustor

Case No	Description	Factors (No of Levels)	Range []	Objectives
1	KE Fuel	Pressure (4 levels) Temperature (4 levels) Mass Flux (4 Levels)	Pressure [1-2.5 atm] Temperature [2000-5000K] Mass Flux [6000-9000kg/s.m^2]	Maximum Strong and Weak Waves Thermal Efficiencies
	MA Fuel		Pressure [1.01-1.04 atm] Temperature [2000-5000K] Mass Flux [6000-9000kg/s.m^2]	
	BJ Fuel		Pressure [1-1.6 atm] Temperature [2000-5000K] Mass Flux [6000-9000kg/s.m^2]	
	BC Fuel		Pressure [1-1.6 atm] Temperature [2000-5000K] Mass Flux [6000-9000kg/s.m^2]	
	AG Fuel		Pressure [1.01-1.15 atm] Temperature [2000-5000K] Mass Flux [6000-9000kg/s.m^2]	
2	All Fuels	Type of Fuels (5 levels) Temperature (4 levels) Mass Flux (4 Levels)	Type of Fuels [KE, MA, BJ, BC, AG] Temperature [2000-5000K] Mass Flux [6000-9000kg/s.m^2]	

7.4 Main Results and Discussion

7.4.1 Conventional combustor

This section discusses results obtained in conventional combustor based on two responses of TSFC and EINOx, which are analysed with different factors such as types of fuels, operating conditions, altitudes (in metres), speeds (in Mach number) and blended ratio percentages. The analysis compares their main effects from the mentioned factors and trade-off that is the presumed solution of the desired objective to the factors given. Note that the minimum constraints for particular flight conditions, such as thrust and fuel flow required are fulfilled and have been taken into considerations.

Different fuels used (Case 1 - Individual Fuel)

The main effects on TSFC and EINOx and their interactions for Case 1 are illustrated in Table 7-3. Since the results are almost similar, AG fuel is presented in the text while other fuels are attached in the Appendix E.2.1 as reference. It is shown that the effects of altitude are less significant (the trends has no gradient) on TSFC (shown in Table 7-3 (a) and (c)) than EINOx. On the other hand, speed has the most significant changes (large gradient), in which TSFC has opposite trends (refer to Table 7-3 (a) and (b)) compared to EINOx. As previously discussed, this behaviour is easily explained by taking into account throttling actions from the consumption of burned fuel producing more NOx. TSFC also simultaneously reduces as rate of changes in thrust is higher than fuel flow. Similarly, effect of blending percentage ratios has also resulted in the same trends but is, however, less significant.

The results are further analysed by considering combined effects of the three factors; altitude, speed and percentage blending ratios as depicted in Table 7-3 (c) and (d). The effects on TSFC for AG fuel illustrate that speed has contributed to the most significant changes, while for EINOx, both altitude and speed affect equally. EINOx emission is shown to result to higher NOx formation at higher speed regardless of blended ratio percentages. The greatest improvement in the TSFC is attained at higher speed, which is contradicting with NOx emission analysis. The results of DoE

method interaction lead to identifying a best trade-off solution, which is discussed later. For a clear visualization, the interactions of the factors are contour plotted and presented in Table 7-4 (a) and (b) for EINOx response and (c) and (d) for TSFC response. Contrasting results of EINOx and TSFC were observed due to the speed factor which require an appropriate trade-off. Again, the contour plots for other fuels are included in Appendix E.2.1.

Table 7-3 Main and combined effects of TSFC and NOx for Case 1

TSFC	**EINOx**
AG fuel	
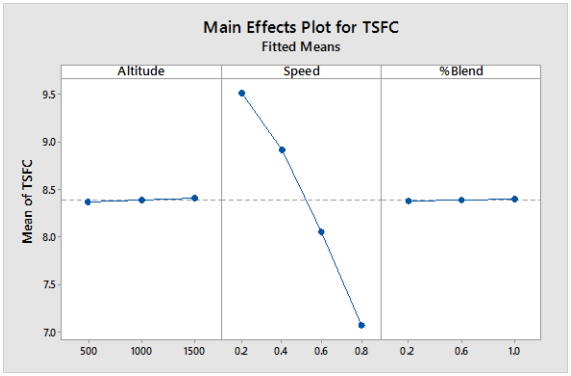	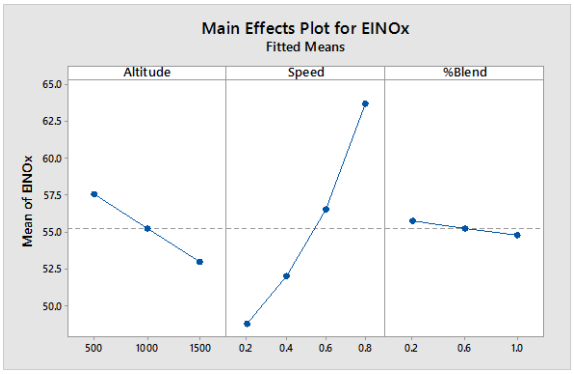
(a)	(b)
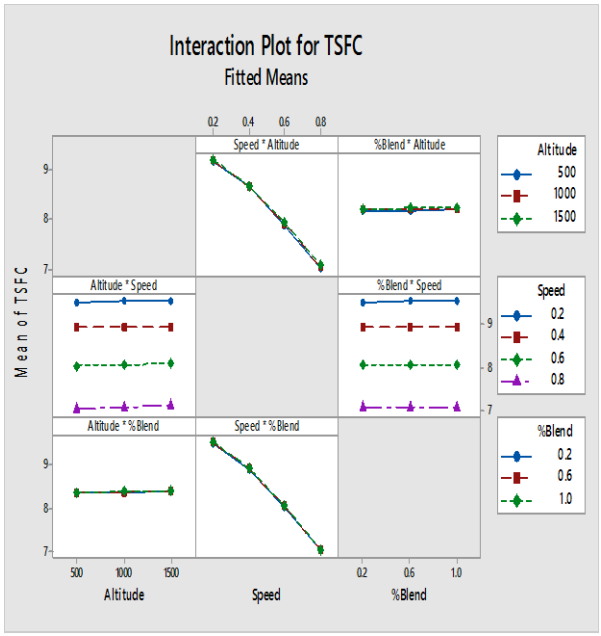	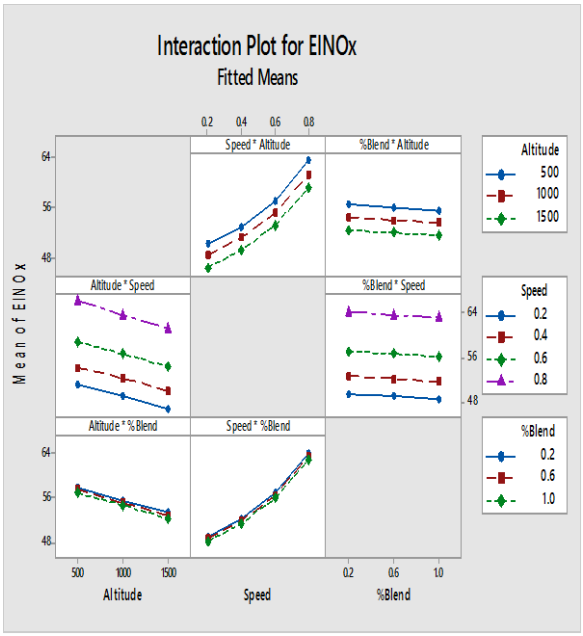
(c)	(d)

Table 7-4 Contour plots for the interactions of responses and the factors for Case 1

EINOx	TSFC
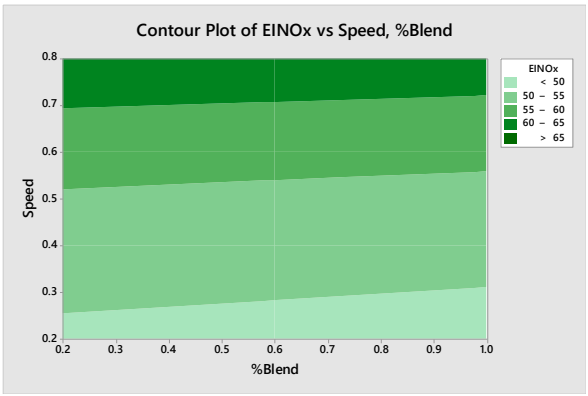	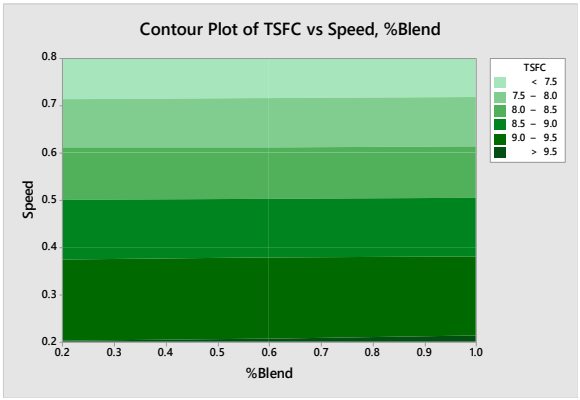
(a)	(c)
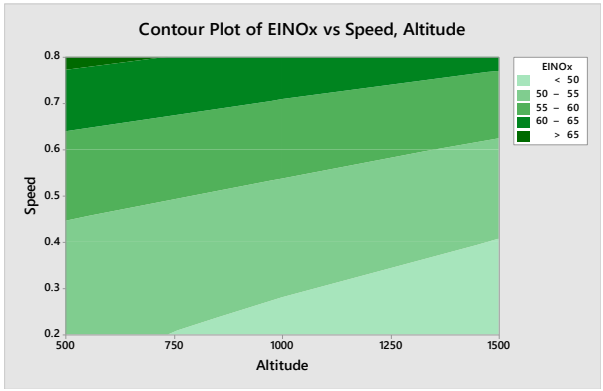	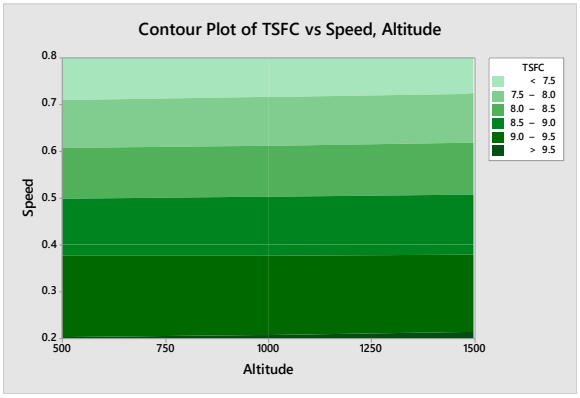
(b)	(d)

Trade-off (Case 1- Individual Fuel)

Based on the two conflicting responses, a further analysis has been made to obtain the trade-off. Table 7-5 summarizes the findings, where it can be seen that all fuel types should operate at high altitude of 0.6 Mach number. The best configuration suggests that pure AG fuel is the one to be considered, but not BC and BJ fuels. It is worth noting that the lowest TSFC is preferred, as it reduces other emission as well and is economically sustainable. Figure 7-4 illustrates distributed compromise plots for each case. The arrows represent the best compromise point for particular fuel.

Table 7-5 Trade-off solutions for Case 1

Type of Fuel	*Altitude (m)*	*Speed (Mach)*	*%Blend*	*EINOx Fit*	*TSFC Fit*
KE+AG	1500	0.6	1	53.8916	8.09443
KE+BC	1500	0.6	0.2	57.2532	8.04146
KE+BJ	1500	0.6	0.2	53.2849	8.03109

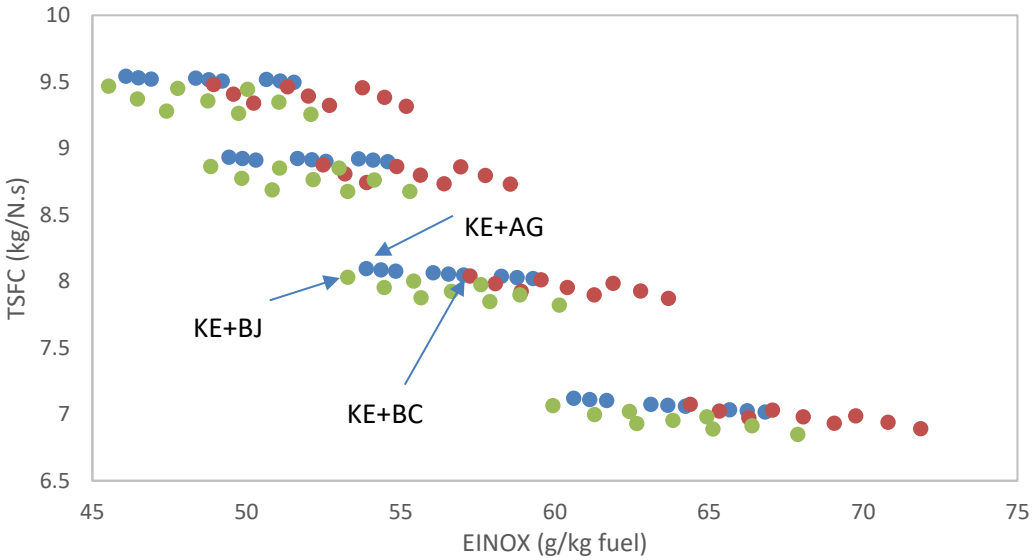

Figure 7-4 Trade-off plots for Case 1

Different operating conditions (Case 2)

In Case 2, further analysis is conducted to evaluate a certified 50% blended ratio fuel at two operating conditions: cruise and ground level, by using KE fuel is used as reference. Similarly, two responses (EINOx and TSFC) with two factors (a type of fuel and speed) are considered. Notably, some performance parameters are not presented because diverging results for biofuels are obtained. The main effects results can be seen in Table 7-6. The cruise effects are shown on the left side while the effect on ground are shown on the right side of the table. The mean of EINOx for KE+AG fuel is shown to be the lowest in both flight operations (Table 7-6 (a) and (b)), while KE fuel remains as the highest among all fuels. On the contrary, KE fuel has better TSFC in cruise (Table 7-6 (c)), but not on the ground (Table 7-6 (d)). The influence of speed factors is found to be significant and put opposite effects on

EINOx and TSFC responses. This proves the consistency of these results altogether.

The trends for overall interaction between factors are illustrated in Table 7-7 (left: for the effects on cruise, right: effects on the ground). At cruise, results have shown that there is a crossover in the mean of EINOx between KE with KE+BJ (Table 7-7 (a)), as well as KE+BC at higher speeds for TSFC (Table 7-7 (c)). KE+AG fuel consistently shows the lowest mean EINOx at every speed. However, KE fuel has significantly improved in TSFC at cruise (Table 7-7 (c)). In terms of speed, changes of TSFC between the types of fuels are found to be significant, in which KE has the lowest TSFC for speed-type of fuel interaction. On the ground, the trends for EINOx and TSFC have depicted that the change is more gradual for all interaction factors (Table 7-7 (b) and (d)). Similarly, KE+AG fuel has the lowest EINOx, but KE+BJ fuel has significantly improved in TSFC.

Table 7-6 Main effects of TSFC and EINOx for Case 2

Cruise	Ground
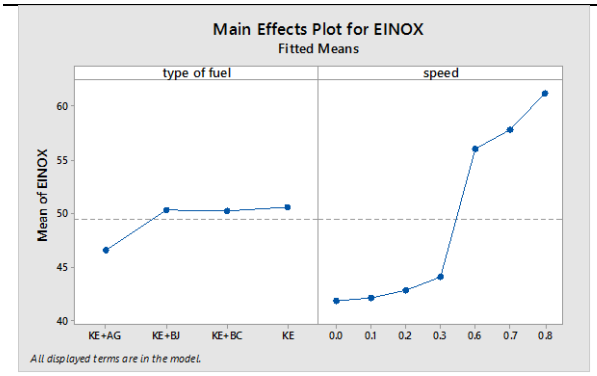	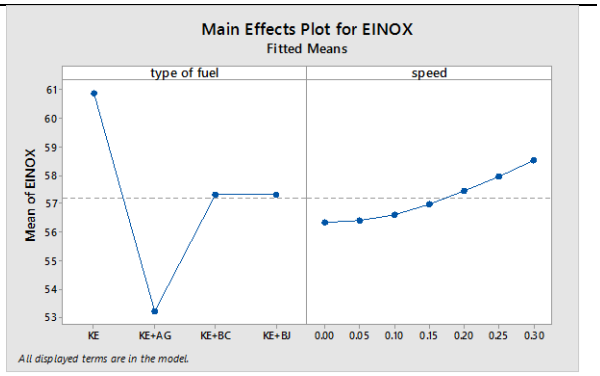
(a)	(b)
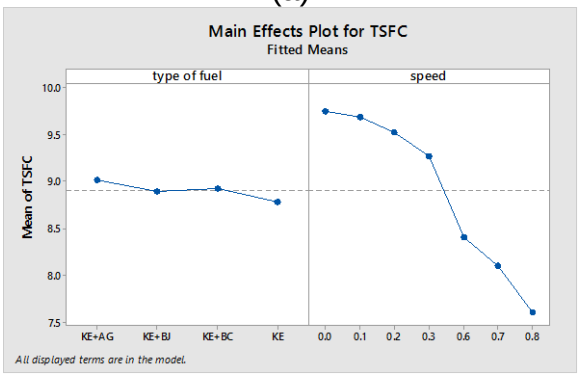	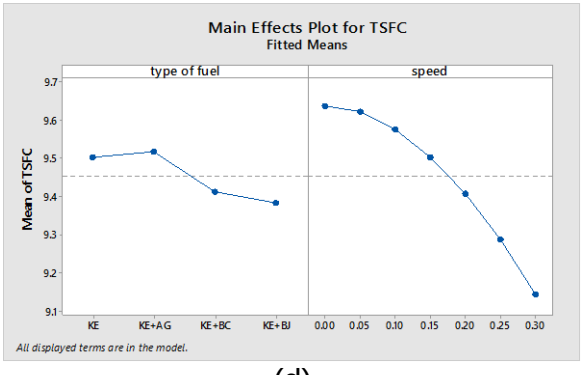
(c)	(d)

Table 7-7 Interaction plot of TSFC and EINOx for Case 2

Cruise	Ground
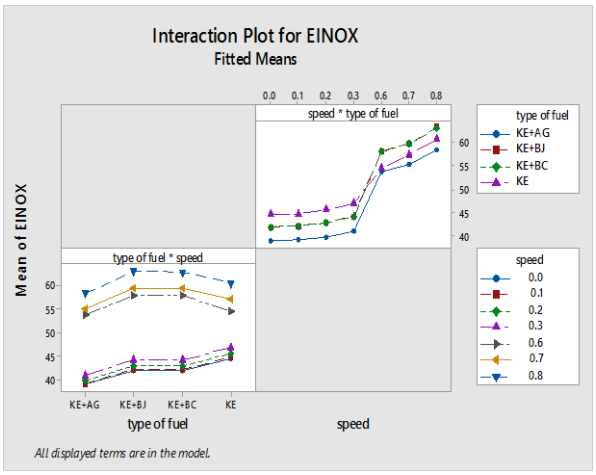 (a)	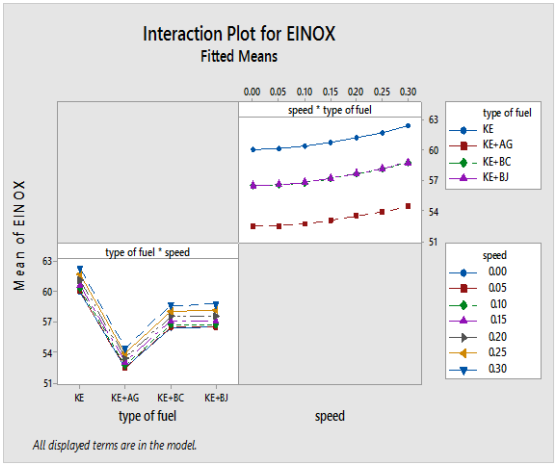 (b)
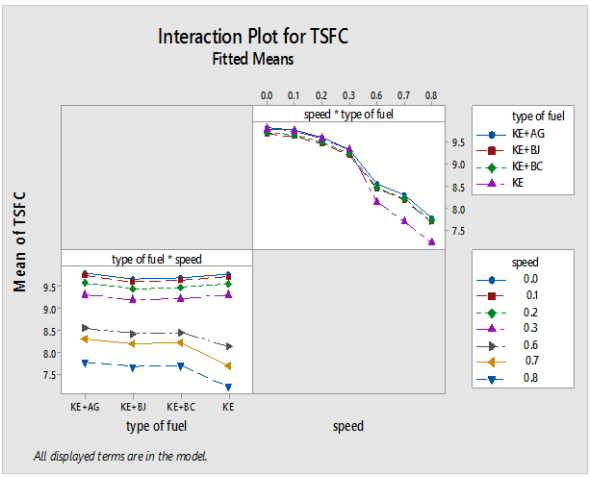 (c)	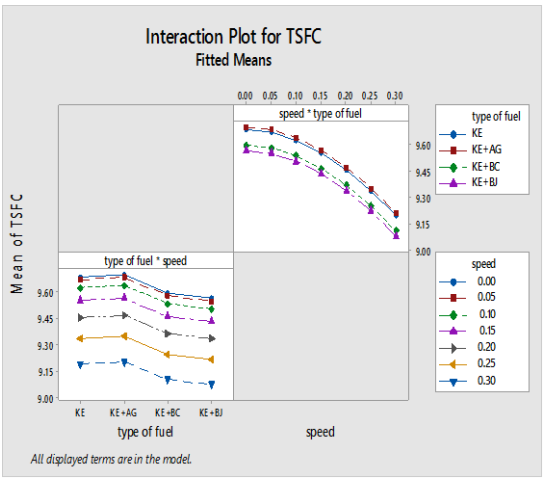 (d)

Trade-off (Case 2)

Similar conflicting trends are observed between TSFC and EINOx at different speeds. To compare the trade-off between those two, the same approach is conducted. The trade-off solutions are tabulated in Table 7-8. At cruise, KE fuel has better trade-off between EINOx (54.51 g/kg fuel) and TSFC (8.14 kg/N.s) at 0.6 Mach number, while at ground, KE+AG fuel has much better trade-off in EINOx (54.42 g/kg fuel) and TSFC (9.2 kg/N.s) at 0.3 Mach number. A scattered plot for visualizing the compromise point for both cases is illustrated in Figure 7-5 represented by arrows.

Table 7-8 Trade-off solutions for Case 2

	Type of Fuel	Speed	EINOx Fit	TSFC Fit
Cruise				
	KE	**0.6**	**54.507**	**8.142**
Ground				
	KE+AG	**0.3**	**54.416**	**9.205**

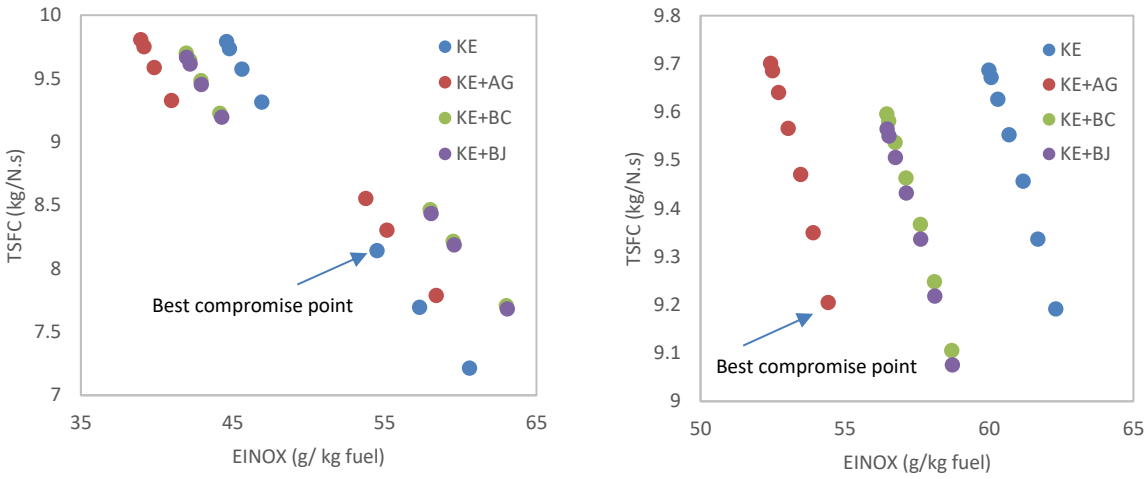

(a) (b)

Figure 7-5 Trade-off plots for (a) Cruise and (b) Ground

All fuels at different operating conditions (Case 3)

A whole assessment for all fuels using this type of combustor is described in Case 3. Three types of fuel are analysed with three factors such as altitudes, speeds and blended percentage ratios. By using the similar approach as in the previous cases, results for the main effects ((a) and (b)) and interaction plots ((c) and (d)) are illustrated in Table 7-9. Both KE+AG and KE+BJ fuels have EINOx below the mean value (Table 7-9 (a)). On the contrary, KE+AG fuel has significantly higher TSFC compared to the mean value. To compare, the three factors (altitude, speed and blended ratio percentage) show opposite effects and trade-off assessment is required.

Table 7-9 Main effects plots for Case 3

EINOX	TSFC
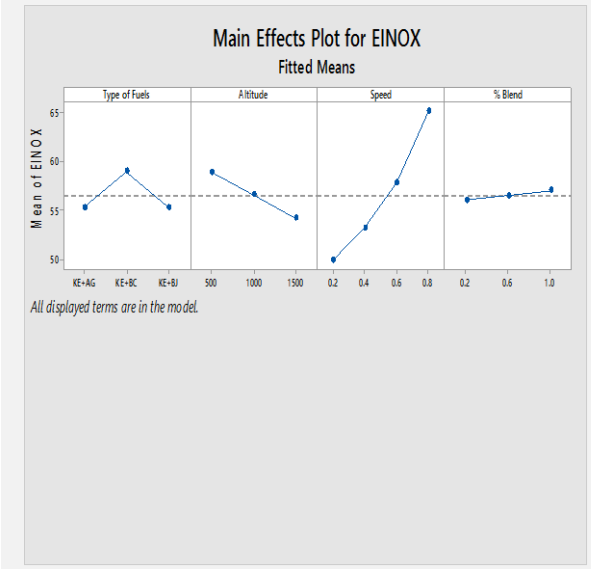	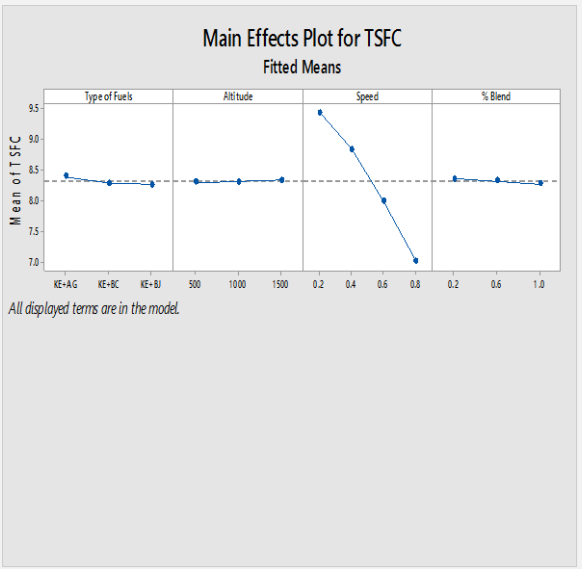
(A)	(b)
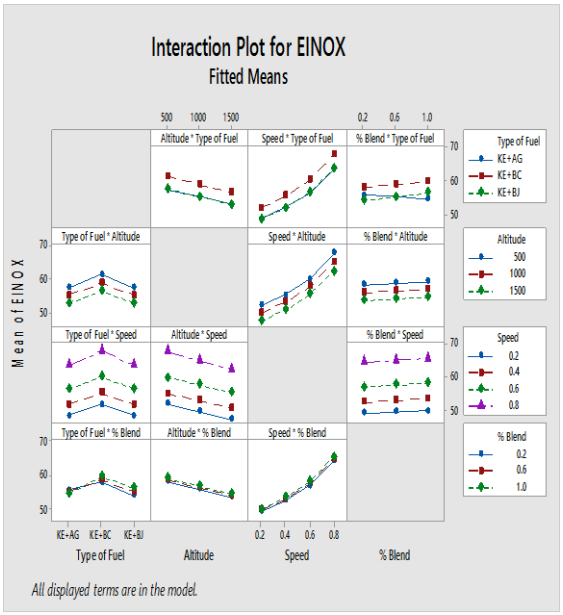	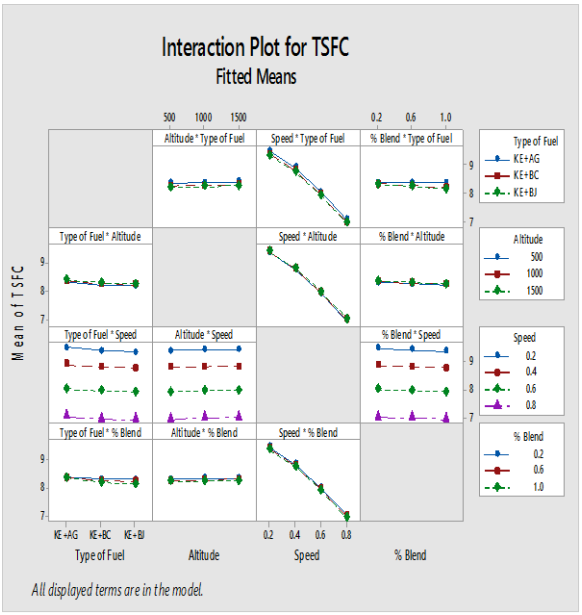
(C)	(d)

Interaction plots show a wider view on the effects of these factors described. The discussion begins with the matrix of mean EINOx in the first column (Table 7-9 (c)), which is the interaction of type of fuel to other factors. KE+BC fuel produces more EINOx at every blended ratio percentage. In contrast, other factors of interactions (a type of fuel-speed and type of fuel-altitude) have shown a gradual change. As depicted in the second column, generally, EINOx is less produced at higher altitude.

KE+AG fuel and KE+BJ fuel produce less EINOx as compared to KE+BC fuel. Meanwhile, in the third column, EINOx has increased exponentially due to the increase in speed. In fourth column, a crossover trend shows between KE+AG and KE+BJ fuels. The matrix interaction in the mean of TSFC (Table 7-9 (d)) shows different behaviours. There are no significant changes being observed in most of the interactions except for speed, in which a negative is observed. All factors have shown that TSFC can be reduced at higher speed. By comparing both response matrices, the results show that speed is the main contributor compared to other factors involved.

Trade-off (Case 3)

Similarly, further analysis is carried out to obtain trade-off solutions in Case 3. In comparison with other case, Case 3 involves four factors simultaneously. There are five solutions given in DoE and those results are tabulated in Table 7-10 while Figure 7-6 illustrates how the solutions are distributed with the circles indicating the best trade-off solutions identified. It is worth highlighting that KE fuel is excluded initially, to keep the number of factors and its levels equally distributed. In short, this case analysis was initially intended to identify the best trade-off between all biofuels and the work is progressing to carry out the comparison with KE fuel. The same conditions as proposed by the solutions are used to analyse KE fuel. As a result, KE+BJ fuel dominates the top three solutions. All suggested solutions have shown better trade-off at higher altitude. KE+BJ fuel at higher speed with lower blended percentage ratio has a better trade-off.

To evaluate on how the biofuels can benefit both trade-off, the comparison with KE fuel is further analysed. The same approach is conducted separately using the same conditions as in the optimal solutions. KE+BJ fuel has shown that high speed with lower blended ratio percentages has the reduction of EINOx and TSFC by 1.07% and 2.06% respectively. However, it seems that the second solution gives a much further reduction of EINOx (2.24%) and TSFC (1.36%). In characterizing the broader, underlying the trade-off between performance and NOx emission, we can find that

there is no distinct reduction between those two. This has been noted earlier in one of the literature surveys by Jimenez and Mavris (2017).

Table 7-10 Trade-off solutions for Case 3

Solution	*Type of Fuels*	*Altitude*	*Speed*	*% Blend*	*EINOx Fit*	*TSFC Fit*	*% Diff wrt KE for EINOx*	*% Diff wrt KE for TSFC*
1	KE+BJ	1500	0.8	0.2	59.9426	7.06502	-1.07	-2.06
2	KE+BJ	1500	0.6	0.2	53.2849	8.03109	-2.24	-1.36
3	KE+BJ	1500	0.6	0.6	54.4631	7.95248	-0.08	-2.32
4	KE+AG	1500	0.8	1.0	60.6121	7.11996	0.03	-1.29
5	KE+BJ	1500	0.6	1.0	55.6570	7.87544	2.11	-3.27

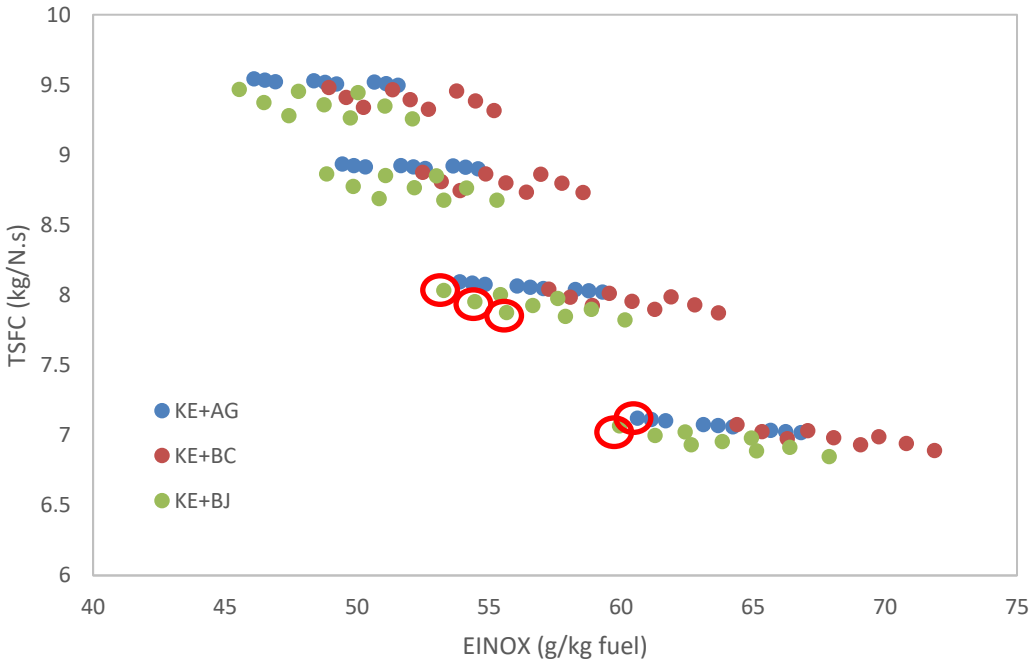

Figure 7-6 Trade-off plots for Case 3

7.4.2 Pressure-rise combustor

Analysis of the main effects, their interactions and trade-off assessment in a pressure-rise combustor uses a different approach. A significant difference to the conventional combustor is that HEPHAESTUS is not used in the analysis, but instead, a comparison of thermal efficiencies variations of both strong and weak waves is done. Its' reasoning is discussed in method section. Regarding methodological and practical considerations of the responses, the results predicted for NOx in pressure-rise combustor required proprietary information that does not comply with the detonation analysis that results in uncertain effects. In fact, the examination of predicted NOx has many fluctuations over a range of initial conditions. By referring back to equation 6-14 in previous chapter, temperature ratio between burned over unburned fuel determines the effectiveness of thermal efficiency in a Humphrey cycle is. It is also shows that temperature and specific heat ratio have a direct relation to thermal efficiency.

To provide a meaningful insight in relation of thermal efficiency and NOx emission, a range of temperatures between 1700K-1900K is given for every fuel. EINOx has a unit of g/kg of fuel while NOx in g/kN of thrust. However, apart from discrete choices available and also a restriction in HEPHAESTUS analysis, the design space is also explicitly included in Appendix E.2.1, taking into account thermochemistry parameters, physical properties and other variables. Constant parameters used in the analysis are similar to Table 6-15. Note that MA fuel is excluded in the analysis. The relation between NOx emission and thermal efficiency is plotted in Table 7-7 for KE fuel, while other fuels are included in Appendix E.2.1. Every fuel shows a dramatic reduction in NOx emission as thermal efficiencies increases. From the results, it shows that NOx emission formation is sensitive to thermal efficiency. Again, it is noted that these trends are observed at particular conditions only and do not define solution over a wide range of operations entirely. The rationale for doing this short analysis is to show the sensitivity of thermal efficiency to the discrete configuration of NOx variables. Several extensions of this work are possible and the most obvious novelty is the inclusion complexity models over wider design space.

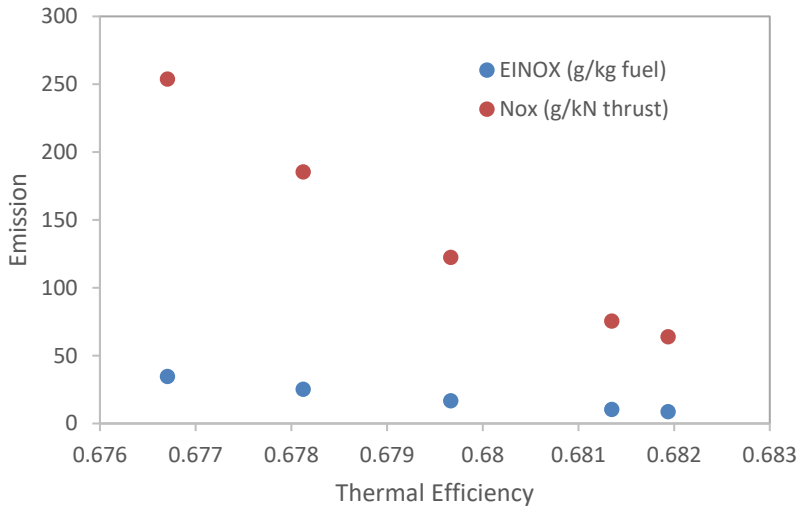

Figure 7-7 Relation of thermal efficiencies and NOx emission for KE fuel

Different fuels used (Case 1 – Individual Fuel)

Case 1 in this analysis comprises of the assessments of all fuels. The assessment is conducted separately as these fuels have different detonation initial conditions. Five different fuels are considered: KE, BJ, BC, AG, and MA fuel with different sets of range. Three factors such as pressure, temperature and mass flux are considered. By using the same approach as in conventional combustor, the main effects are analysed and results are illustrated in Table 7-11. The overall results for all fuels have shown almost similar trends, therefore AG fuel is presented in the text while other fuels are attached in Appendix E.2.2. Notably, 'etha 1' and 'etha 2' represent the thermodynamic efficiency of strong and weak shock waves as shown in Table 7-11 (a) and (b) respectively. Under influences of strong waves, variation of pressure has a negative relation with thermal efficiency for all fuels analysed as higher initial pressure reduces pressure ratio thus reduces temperature rise (Table 7-11 (a)). On the contrary, it is shown that both mass flux and temperature factors have positive relations for all fuels because higher initial mass fluxes and temperatures have a tendency to increase temperature ratio across shocks (see Figure 5-6 and Figure 5-10) thus increase thermal efficiency.

These factors under the influence of weak detonation capture diverse trends of effects (Table 7-11 (b)). Initial pressure (see Figure 5-14 (b)) and initial mass flux (see Figure 5-7 (b)) to the change of temperature ratio result in an unchanged effect observed in weak shock waves as discussed in Chapter 5. Nevertheless, it is also indicated that initial temperature has negatively affected thermal efficiency under influence of weak detonation for all fuels.

Table 7-11 Main effects plot for Case 1 under influences of strong and weak waves (AG Fuel)

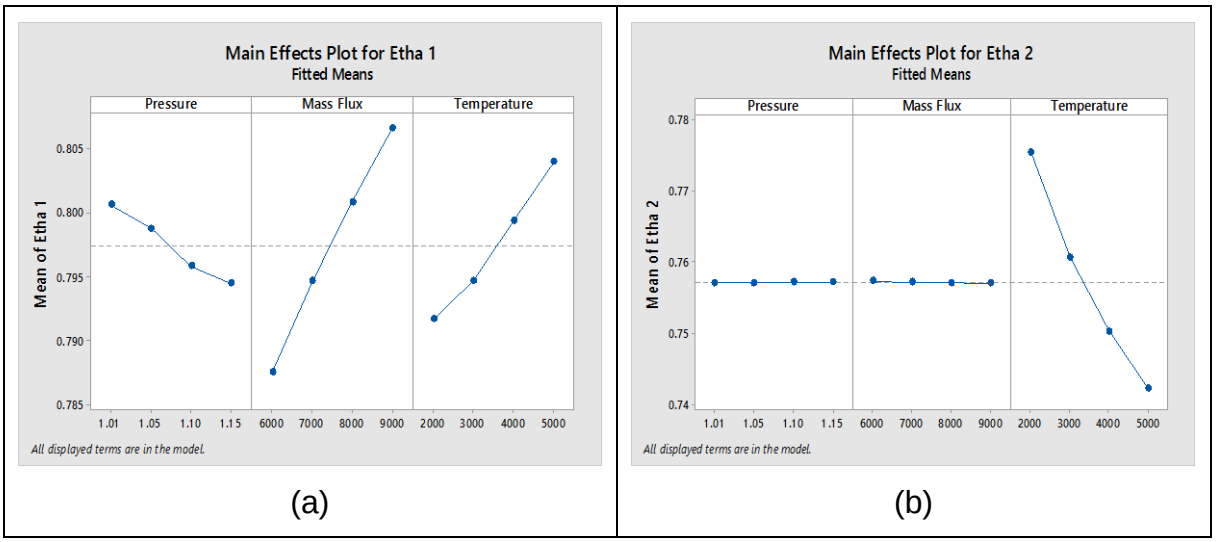

(a) (b)

Further analysis is conducted to identify interactions between factors as tabulated in Table 7-12 for AG fuel, while other fuels analysis is included in Appendix E.2.3. In strong detonation wave, interactions of pressure-temperature and pressure-mass flux have shown a negative relationship as depicted in first column of Table 7-12 (a). A higher pressure reduces thermal efficiency, but higher mass fluxes with the same pressure can increase thermal efficiency gradually. Meanwhile, higher temperature with lower pressure has shown much higher thermal efficiency, but then reduces as pressure increases. Generally, these trends are observed for all fuels. Higher mass flux with lower initial pressure and higher mass flux with higher temperature are desirable to obtain higher thermal efficiency. Similar trends are observed in the interaction of temperature with other factors as well.

The interactions of these factors under weak detonation wave are illustrated in Table 7-12 (b). There are undistinguishable trends observed on pressure-mass flux interactions. In pressure-temperature interaction, changes in pressure have no effects on thermal efficiency but low temperature exhibits significantly higher thermal efficiency. Similar trends are observed in mass flux-temperature interaction for all fuels. In response to a strong influence of temperature on the thermal efficiency, contour plots are illustrated in Figure 7-8 while other fuels are included in Appendix E.2.4. Again, contour plots displays conflicting results between thermal efficiencies under influence of both waves. All fuels have shown higher thermal efficiency is obtained at higher initial temperature for strong waves, but weak waves have shown opposite outcomes and requires trade-off between those two.

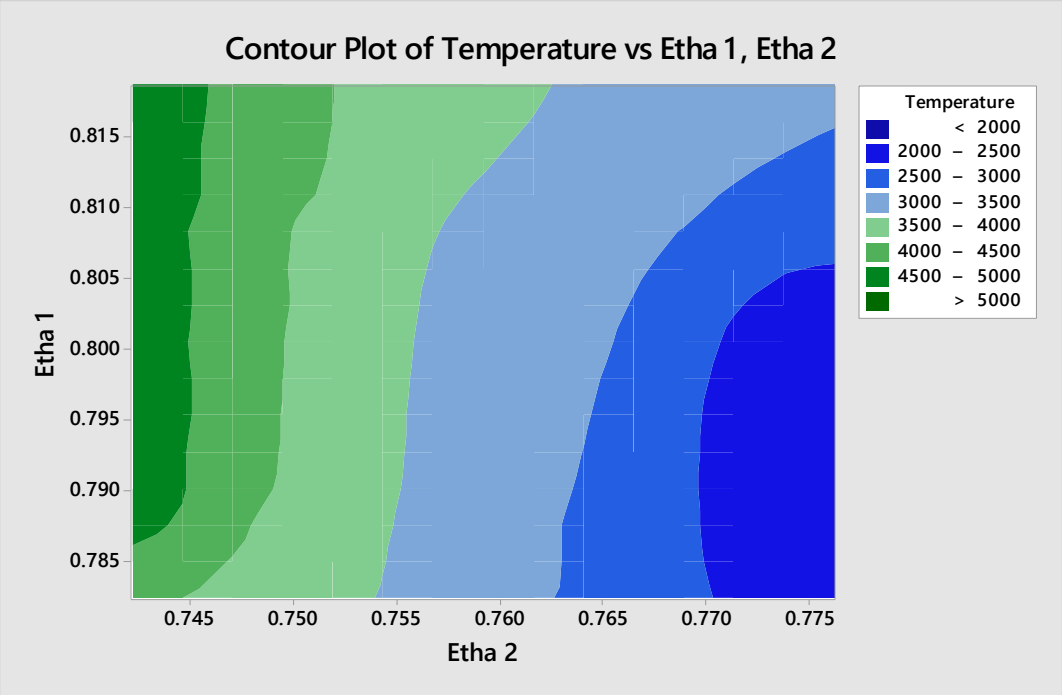

Figure 7-8 Effects of initial temperatures for Case 1 (AG fuel)

Table 7-12 Interaction plots for Case 1 under influences of strong and weak waves

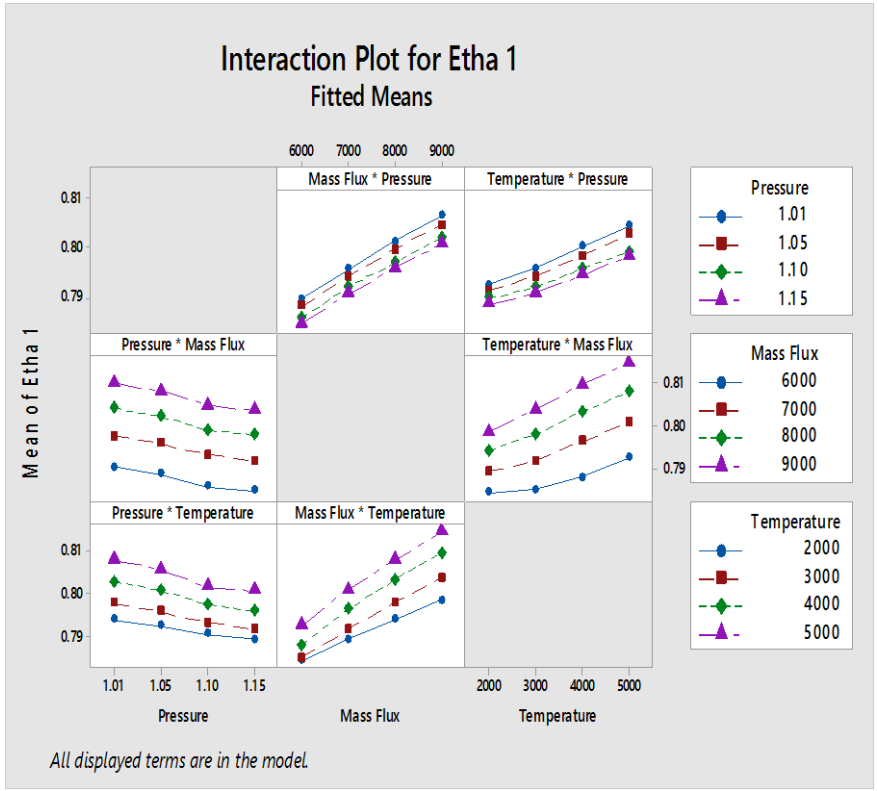

(a)

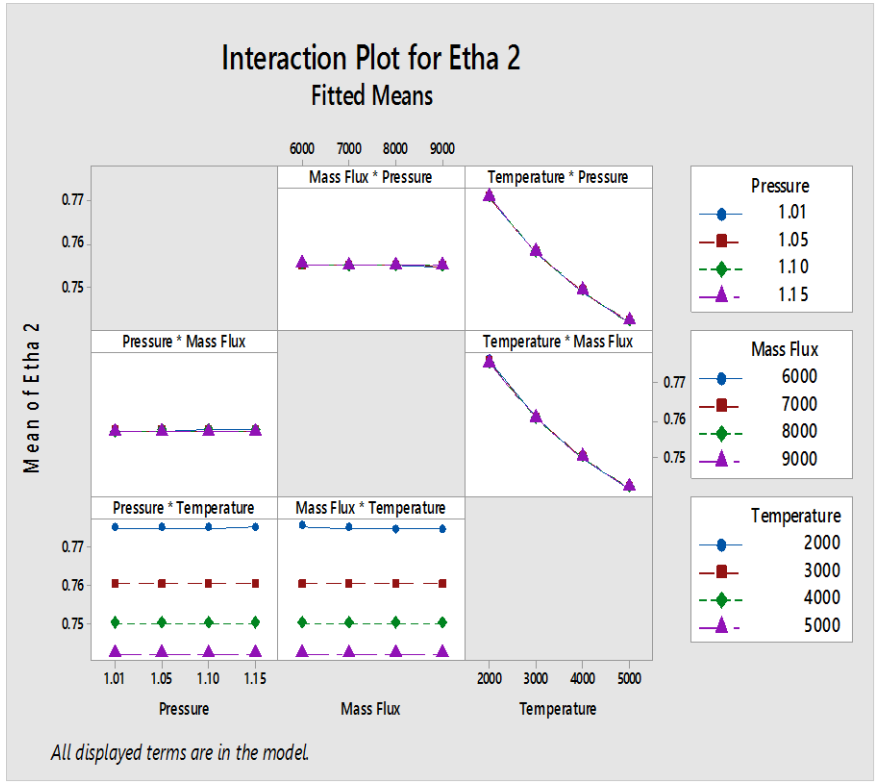

(b)

Trade-off (Case 1 – Individual Fuel)

Trade-off assessment is conducted to find the best solutions between two shock waves formed with respect to their thermal efficiencies. Results and two proposed solutions for each fuel are tabulated in Table 7-13. In summary, all fuels have shown that low initial pressures and temperatures with high initial of mass flux are preferred. A further comparison of compromise solutions are brought together in one diagram and is shown in Figure 7-9. The arrows indicate the best trade-off solution for particular fuels.

Table 7-13 Trade-off solutions for Case 1 – Individual Fuel

	No of Solution	Pressure (atm)	Mass Flux (kg/s.m^2)	Temperature (K)	Etha 1	Etha 2
KE Fuel	1	1	9000	2000	0.826325	0.742510
	2	1	8000	2000	0.818928	0.742533
MA Fuel	1	1.01	9000	2000	0.797936	0.780184
	2	1.02	9000	2000	0.797588	0.780195
BJ Fuel	1	1	9000	2000	0.810964	0.771223
	2	1	8000	2000	0.805325	0.771276
BC Fuel	1	1	9000	2000	0.811282	0.771305
	2	1	8000	2000	0.805628	0.771359
AG Fuel	1	1.01	9000	2000	0.801320	0.775101
	2	1.05	9000	2000	0.799725	0.775128

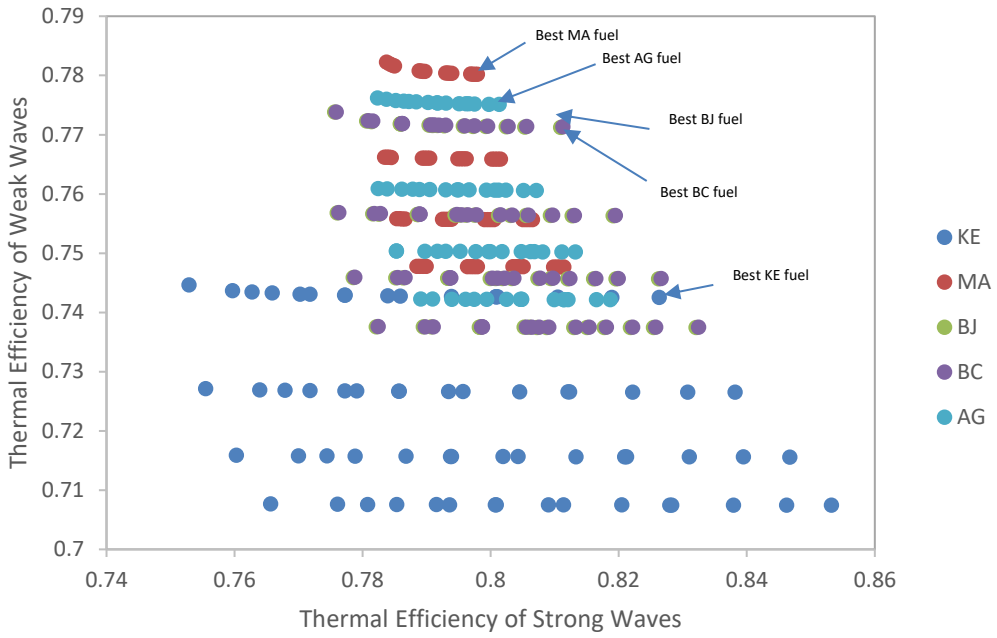

Figure 7-9 Trade-off plots for Case 1 – Individual Fuel

All fuels at different initial conditions (Case 2)

In Case 2, three factors are considered: types of fuel used, mass flux and temperature. Given the similar approach as previous case, results are shown in Table 7-14. Pressure factor is excluded to minimise complexity of the analysis. As an additional note, the abbreviation used for MA and AG fuels are presented as BMA and BA, respectively. A comparison of thermal efficiency between both waves, KE, MA, and AG fuels depict opposing results as shown in Table 7-14 (a) and (b). BJ and BC fuels have shown higher thermal efficiency for both waves than the average. Likewise, mass flux and temperature effects result in similar trends as previous analysis of strong shock wave, whereas thermal efficiency increases as mass flux and temperature increase. Weak wave has shown mass flux has no effects on thermal efficiency but has negative effects on temperature (Table 7-14 (b)).

As a comparison with main effects plots (Table 7-14 (c) and (d)), trends are found to be similar but interactions of other factors are also considered. In strong shock wave, higher mass flux and temperature enhance thermal efficiency gradually as shown in first column in (c). KE fuel has the highest thermal efficiency as the mass flux and the temperature increase, followed by BC, BJ, AG and MA fuels. In weak waves, mass flux interactions with other factors are less effective as shown in (d). In contrast with strong wave, KE fuel has shown significantly lower thermal efficiency, but it can be increased by lower temperature.

Table 7-14 Main effects and the interaction of the factors for Case 2

Thermal Efficiency of a Strong Wave *Thermal Efficiency of a Weak Wave*

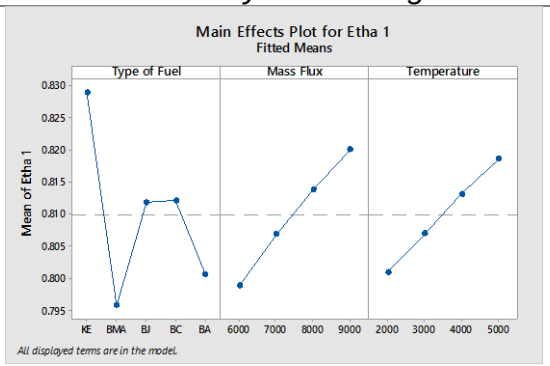

(a)

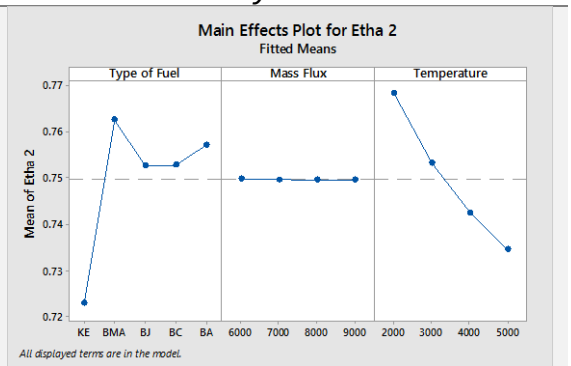

(b)

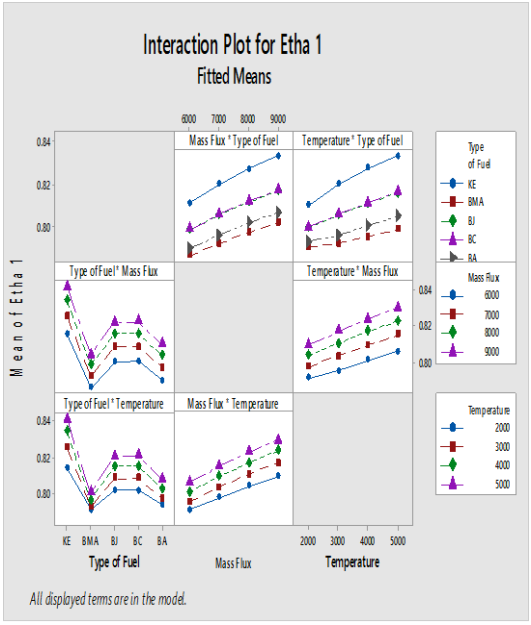

(c)

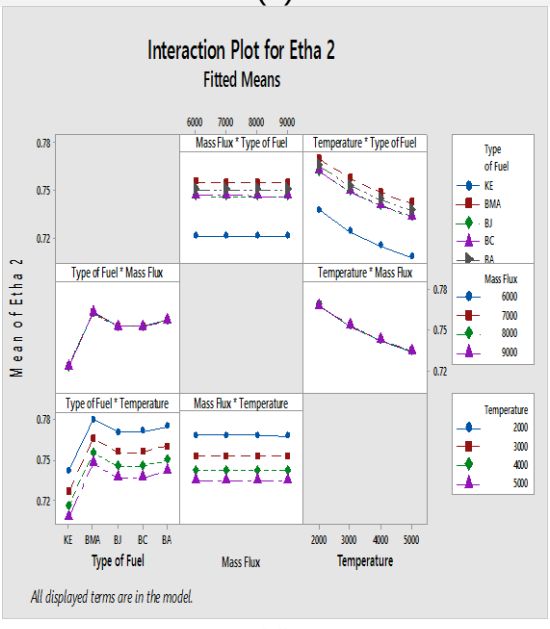

(d)

Trade-off (Case 2)

Finally, all fuels are assessed to find a trade-off between those three factors mentioned. To compare objectively, initial pressure was held to 1 atm and range of temperatures and mass fluxes are given by 2000K-5000K and 6000-9000 kg/s.m², respectively. As previously described, at these conditions, HEPHAESTUS may not be able to capture correct emission prediction thus making evaluation of thermal efficiency is the only option to find the trade-off assessment. Results of overall trade-off assessment for Case 2 with five solutions are identified and tabulated in Table 7-15. Surprisingly, BC fuel has resulted in the best two trade-off between two thermal efficiencies, followed by BJ fuel with all solutions suggesting for higher mass flux. However, it shows that higher temperature does not guarantee maximum thermal efficiencies. A similarly distributed plot compromise between the two efficiencies is illustrated in Figure 7-10, where the best compromise point in Case 2 can be identified.

Table 7-15 Trade-off solutions for Case 2

No Solution	*Type of Fuels*	*Mass Flux (kg/s.m^2)*	*Temperature (K)*	*Etha 1*	*Etha 2*
1	BC	9000	3000	0.819509	0.756359
2	BC	9000	2000	0.811282	0.771305
3	BJ	9000	3000	0.819158	0.756292
4	BJ	9000	2000	0.810964	0.771223
5	BC	9000	4000	0.826616	0.745703

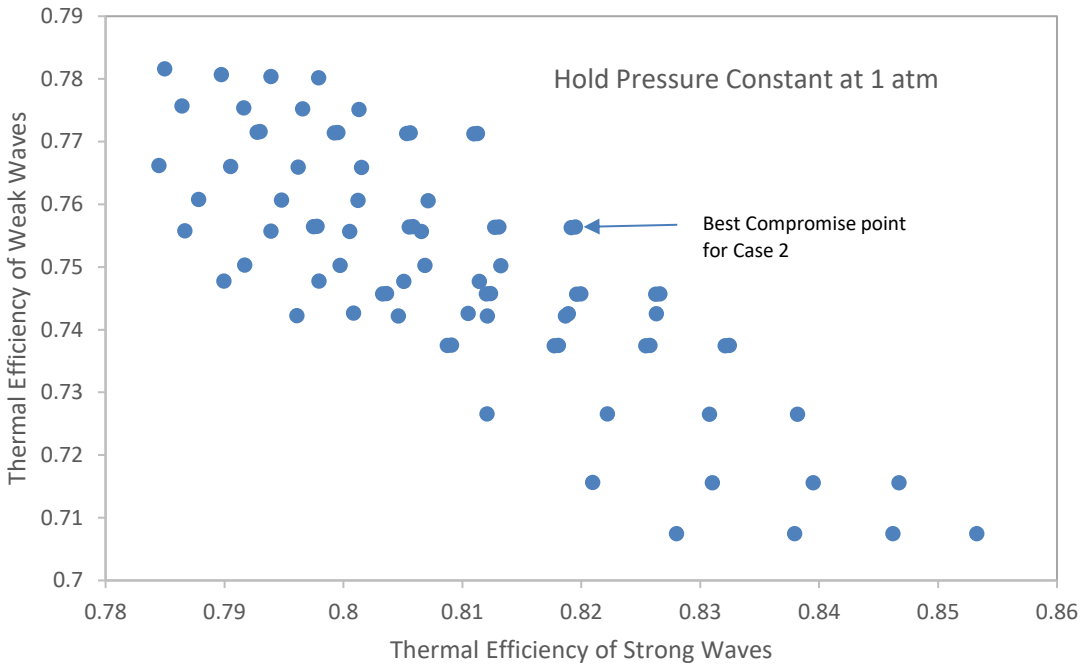

Figure 7-10 Trade-off plots for Case 2

7.5 Concluding Remarks

This work aims to identify a trade-off between performance and emission of conventional and pressure-rise combustors which has not been attempted so far. By applying Design of Experiment (DoE) method into Minitab tools, main effects, interactions of factors and best solutions are discussed and presented. Two types of the combustors are analysed separately due to difference in parameterization analysis involved. As previously clarified, DoE tests are used because of its capability to evaluate factors with different sets of levels and factors interactions. Furthermore, several important conceptual trade-off can be carried out using DoE methods. Based on the designated case study, results of this work conclude that:

For conventional combustor:

1. Contrasting effects of EINOx and TSFC due to speed factor require a trade-off evaluation. High speed results in reduction in TSFC, but not EINOx.
2. All fuels (Case 1) have better EINOx and TSFC trade-off at high altitude, with KE+BJ fuel dominates the solution suggested in DoE.
3. For 50% blended fuel (Case 2), KE fuel has better trade-off between EINOx (54.51 g/kg fuel) and TSFC (8.14 kg/N.s) at 0.6 Mach number in cruise, while KE+AG fuel has significantly better trade-off in EINOx (54.42 g/kg fuel) and TSFC (9.2 kg/N.s) at 0.3 Mach number on the ground.
4. For an overall analysis (Case 3), KE+BJ fuel has shown that higher speed with lower blended ratio percentages (20%) has better trade-off. A reduction of 1.07% and 2.06% of EINOx and TSFC, respectively, is obtained as compared to KE fuel.
5. In identifying trade-off between performance and NOx emission, no significant difference is found between them in the context of design space being considered.

For pressure-rise combustor:

1. A short analysis is presented to observe the relation of thermal efficiency and EINOx formation. However, it is found to be limited to a narrow range of initial conditions as discussed above.
2. The contrasting results of thermal efficiencies involving strong and weak waves require a trade-off with the respect to pressure, temperature and mass flux variations. These efficiencies are evaluated because it indirectly measures the emission.

3. Temperature poses the largest effect to thermal efficiencies of both waves. All fuels (Case 1) result in high thermal efficiency at high initial temperature for strong waves, but opposite result is shown for weak waves. In order to get better trade-off in Case 1, it is found that lower temperature with higher mass flux are preferred.

4. For an overall assessment (Case 2), BC fuel is proven to have the best trade-off between the two thermal efficiencies, followed by BJ fuel with all solutions suggested for high initial mass flux with low temperature.

8 GENERAL CONCLUSION AND RECOMMENDATIONS

8.1 Conclusion

A primary motivation of this research work is to address two vital issues: environment crisis due to global warming caused by fossil fuels and energy crisis, which is related to the overdependence of crude oil. Both drive the interest in aviation industries to use alternative fuels based on biofuels. The present research is aimed at quantitatively evaluate the feasibility of biofuels in conventional and pressure-rise combustors to allow best trade-off configuration in engine and power plant performance, and at the same time reduce the environmental impacts. To inform the methodological and practical consideration of this research work, a wide literature review has first been presented to highlight opportunities and potentials of biofuels in aerospace propulsion technologies. This background research also provides a meaningful insight for the selection of a novel combustor technology and a conventional combustor for environmental goals in the coming future.

In order to characterize the broader, underlying aim of this research, six objectives are highlighted as a focus for the research work and it is argued that these objectives have successfully been met. The research work comprises three main stages: biofuel evaluations, emission analysis, and trade-off assessment. The biofuel evaluation work is subdivided into three parts, which are spray analysis, engine performance analysis, and detonation analysis. Particular, the spray analysis was intended to serve as an extension to work by Mazlan (2012), with third generation biofuels introduced and transient conditions adopted for the modelling of evaporation and spray penetration. Additional initial conditions are also included in the analysis to give different perspectives. The results reported indicate all biofuels have shorter penetration length than kerosene, and certainly provide a penalty cost to biofuels emissions, especially where soot formation and therefore, necessary engine design geometry considerations need to be made carefully to overcome this drawback.

Engine performance analysis was the successfully demonstrated using a new version of the in-house computer tool: PYTHIA, again extending the work done by Mazlan (2015). These latest findings not only support earlier findings, but also go beyond them especially by integrating the newer biofuels that can now be considered in the new version of PYTHIA together with consistent off-design conditions. An engine model similar to a RB211 variant is used for the analysis. Performance parameters such as thrust, fuel flow and specific fuel consumption (SFC) are considered at different blended ratio percentages of the biofuels with kerosene, over different flight cycles. To compare objectively, kerosene was set as the reference fuel for the other three, biofuels considered namely Algae biofuel, Camelina biofuel, and Jatropha biofuel. The results indicated that the Lower Heating Value (LHV) of each fuel had a significant influence on engine performances over different flight cycles. Blended Kerosene-Jatropha Biofuel and Kerosene-Camelina Biofuel showed an improvement in the engine performance, but this was not the case for the Kerosene-Algae blended biofuel.

A zero-dimensional detonation combustion analysis is then conducted. In order to address emissions reduction and at the same time to promote performance enhancement to the combustor, the assessment was carried out with biofuels. The work thus intended to examine the feasibility and effectiveness of various biofuels under detonation combustion. Almost no previous efforts have been made to study such biofuels under such extreme conditions and it is certainly therefore worth exploring the wider capability of these fuels in this way. A theoretical model framework is adopted in the analysis, with several reasonable assumptions outlined as necessary steps for preliminary results. The evaluation of both physical properties and thermochemistry are considered at different initial conditions. Consistent results are observed with the limited available published works and comparable trends are compared to experimental results for heavy hydrocarbon analyses. The present results have shown lighter fuels detonated more easily, while heavier hydrocarbons in the form of the biofuels need higher heat addition and mass flux. The influence of strong and weak

detonation waves varies with physical properties for every fuel and due to their thermochemical properties.

The research is then further advanced to perform an emission analysis. Although many other important and reliable computational tools for emission predictions are available in the published literature and in the public domain, it was deemed worth exploring the use of another in-house computer tools: HEPHAESTUS. Focusing on NOx emission, two separate analyses of the two different types of combustors are conducted. In a conventional combustor, outputs from PYTHIA at various operating conditions are required prior to the analysis. Results for this type of combustor have shown that BJ fuel can reduce NOx by 15.85% and 20.73% for the engine under approach and climb conditions respectively while for AG fuel NOx is reduced by 12.61% during take-off. Several initial conditions are considered to observe this effects on NOx formation. Higher temperatures, pressures, and mass flow promote NOx formation, while increases fuel flow has negative effects. These variations have been validated through thermochemistry evaluation, using the NASA CEA approach, and engine model-based correlations. Among all initial conditions, the fuel flow rate produced the most significant effects on the NOx formation. In a pressure-rise combustor, further thermochemistry evaluation is needed to accommodate high-speed combustion in HEPHAESTUS. In high-speed combustion, stability in sustaining the detonation is a major concern, and geometrical sizing of the combustor is more challenging. In general, a pressure-rise combustor exhibits more NOx as compared to conventional combustor due to the higher pressures and temperatures involved in the process. However, as compared to KE fuel, it seems that biofuels offer more NOx reduction (up to 53.43% reduction), but not for EINOx where there is at most a 37.7% increase for AG fuel. The differences because biofuel has better performance in thrust produced as where the ICAO relations were considered. Similarly, the fuel flow rate for the pressure-rise combustor significantly influenced the EINOx formation.

Finally, trade-off assessment is conducted taking account of all the findings in the previous chapters. Several important trade-off can be carried out using the DoE method. Because of the many different level design variables involved, and their wide interaction of those variables, a general factorial problem in Minitab is utilized. Again, in previous chapter, the two different types of combustor are analysed separately. In conventional combustor, two objectives are underlined, which are EINOx formation and TSFC. Six different cases are studied comprising different factors and levels. The results of the DoE method application lead to the identification of the best trade-off between the two objectives. With respect to the factor of speed, opposite effects have been observed which demand a trade-off. Results suggested that all fuels have better trade-off at higher altitudes with KE+BJ fuel dominating the optimal solutions. It is although worth to mention that there is no distinct reduction in those objectives over the design space considered. The assessment of the pressure-rise combustor, involved a different approach, as it is impractical to accommodate all the design variables without significantly adding the complexity to the analysis. By virtue of fact that the thermal efficiency has an indirect relation to the emission formation (not focusing on NOx only) as well as the limited capability of HEPHAESTUS, the trade-off assessment for this combustor is based on thermal efficiencies only. The two waves formed during the detonation combustion have been mathematically realized in a zero-dimensional analysis. Based on the assumptions made, the two waves have conflicting thermal efficiencies, which require trade-off considerations under several factors prescribed such as pressure, temperature, and mass flux. Results from the DoE indicate that the temperature has the most influence on the interaction between the factors. BC fuel appeared to have the best trade-off between the two thermal efficiencies followed by BJ fuel with all the best solutions suggested for higher initial mass flux. As no other work has been done on the trade-off of the pressure-rise combustor with biofuels, these results will have to be validated by future experimental tests. Moreover, the quality of the DoE application suggests the possibility to apply the same methodology with wider design space under considerations.

8.2 Recommendations and future works

This work has covered an analytical and preliminary study of biofuels under different modes of combustion. Future research aiming to further assess, evaluate, and optimize the trade-off between performance and emission is highly recommended, especially for the practical application of third generation of biofuels. As biofuel is the main concerns of the present research, several extensions of this work are possible, via either analytical studies or experimental works, both directly or indirectly. Moving forward, there are a number of key direction in which the present study could be expanded upon or improved, and there are arranged below according to the topics covered in the thesis:

Spray Analysis

1. Despite the considerable progress in developing models of spray analysis involving evaporation of droplets, adopting the temperature gradient inside the droplets is often neglected for simplicity. As suggested by Sazhin (2017), the validity of these assumptions is far from obvious. Considering a temperature gradient in the droplets is highly recommended for future work.

2. In the present context of evaluating biofuels in spray analysis, it is worth also to consider other shapes of droplets, in addition to spheroidal droplets, for engineering applications.

3. Most of the present spray analysis is tied to the simplified assumptions and it is beneficial to consider such other effects, and their further extension to biofuels. (Sazhin, 2017) highlights several effects including the interaction between droplets, droplet heating and evaporation in near- and super-critical conditions, and quantum-chemical effects as well as kinetic modelling of biofuels using a CFD approach.

Performance Analysis

1. Further evaluation of engine performance should introduce the option to consider Microalgae biofuel in PYTHIA, since the required properties are well gathered in this work. Moreover, introducing Microalgae biofuel in PYTHIA could add variety to the choice of the fuel blend selections.
2. It is also suggested that the new version of PYTHIA should accommodate design cases like a decision tree simultaneously. These could cover a wider range of off-designs operations concurrently at each run.

Detonation Analysis

1. As future directions for detonation research, a full multi-step chemistry of biofuel is encouraged for better comparison with experimental work.
2. Further work on biofuel under high-speed combustion should be directed to the thrust chamber dynamics, and propulsive performance, involving multiple-tubes, multi-phase flow, and multi-cycle operation by adopting full flow path-based performance prediction.
3. For practical purposes in an air-breathing engine, the unsteady operations of the manifold should be considered to provide more accurate flow conditions at the aft and downstream of the combustor, especially since this unsteadiness will eventually degrade the performance of a pressure-rise combustor.
4. Provide a solution to initiate biofuel detonation and enhance DDT for biofuels.

Emission Analysis

1. Considering a pressure-rise combustor type in HEPHAESTUS is highly recommended. Since the NASA CEA can accommodate a detonation problem, the required thermochemical properties such as correlations for enthalpy, specific heat, and entropy as the function of temperature can be identified. Thus, HEPHAESTUS can be extended as well.
2. Modification of HEPHAESTUS is needed to accommodate microalgae fuel as well. This also can be achieved from thermochemistry evaluation in NASA CEA first, even for just conventional type of combustor.
3. The present analysis only studies single step chemistry of reaction and does not take into account chemical kinetics of NOx formation. Accommodating multistep chemistry with chemical kinetics analysis is highly recommended to track the dissociation and minor species formed resulting from different values of flame temperature.

Trade-off Assessment

1. A best trade-off between the performance and emission impact for pressure-rise combustor has not been made so far. Referring to a wide literature survey, the emission exhausted by a pressure-rise combustor is hardly understood. Too many variables have to be considered which then requires complex design space. The robustness of optimization method used is highly desirable to handle and provide innovative solutions. Taking this into consideration, a development of hybrid optimization is probably one of the best solutions in future.
2. The trade-off assessment by DoE preferred here is based on discrete variables. Continuous variables could potentially offer wider solutions. This can be addressed by integrating the software codes PYTHIA-HEPHAESTUS and then executing the results and obtain the fitness function. In particular, the present work has prepared the ground for

more detailed design optimization studies in the future and suggest how such an optimization should be formulated. Later, MATLAB Optimization tools could be utilized for different optimization methods.

REFERENCES

A, A., Padmanaban, V. and Subramaniam, T. (2013) 'A Comparison of Fuel Properties Between Fractionated and Non-Fractionated Composition of Micro Algae Based Biodiesel', in *SAE Technical Papers*. doi: 10.4271/2013-01-2814.

Akbari, P. and Muller, N. (2003) 'Performance Investigation of Small Gas Turbine Engines Topped with Wave Rotors', in *39th AIAA/ASME/SAE/ASEE Joint Propulsion Conference and Exhibit*. Huntsville, Alabama: American Institute of Aeronautics and Astronautics, pp. 1–11.

Akbari, P. and Nalim, R. (2006) 'Analysis of Flow Processes in Detonative Wave Rotors and Pulse Detonation Engines', in *44th AIAA Aerospace Sciences Meeting and Exhibit*. Reno, Nevada: American Institute of Aeronautics and Astronautics, pp. 1–13.

Akbari, P. and Nalim, R. (2009) 'Review of Recent Developments in Wave Rotor Combustion Technology', *Journal of Propulsion and Power*, 25(4), pp. 833–844. doi: 10.2514/1.34081.

Alcaine, A. A. (2007) *Biodiesel from microalgae*, *Biotechnology Advances*. Kungliga Tekniska Hogskolan, Sweden.

Aldheeb, M. . (2012) *Optimization of Micro Air Launch Vehicle for Micro and Nano Satellite*. International Islamic University Malaysia.

Amin, S. (2009) 'Review on biofuel oil and gas production processes from microalgae', *Energy Conversion and Management*. Elsevier Ltd, 50(7), pp. 1834–1840. doi: 10.1016/j.enconman.2009.03.001.

Antoine, N. E. and Kroo, I. M. (2005) 'Framework for Aircraft Conceptual Design and Environmental Performance Studies', *AIAA Journal*, 43(10), pp. 2100–2109. doi: 10.2514/1.13017.

Antunes, A. P. and Azevedo, J. L. F. (2014) 'Studies in Aerodynamic Optimization Based on Genetic Algorithms', *Journal of Aircraft*, 51(3), pp. 1002–1012. doi: 10.2514/1.C032095.

Ashraful, A. M., Masjuki, H. H., Kalam, M. A., Fattah, I. M. R., Imtenan, S., Shahir, S. A. and Mobarak, H. M. (2014) 'Production and comparison of fuel properties , engine performance , and emission characteristics of biodiesel from various non-edible vegetable oils : A review', *Energy Conversion and Management*. Elsevier Ltd, 80, pp. 202–228. doi: 10.1016/j.enconman.2014.01.037.

Atabani, A. E., Silitonga, A. S., Badruddin, I. A., Mahlia, T. M. I., Masjuki, H. H. and Mekhilef, S. (2012) 'A comprehensive review on biodiesel as an alternative energy resource and its characteristics', *Renewable and Sustainable Energy Reviews*. Elsevier Ltd, 16(4), pp. 2070–2093. doi: 10.1016/j.rser.2012.01.003.

Austin, J. M. and Shepherd, J. E. (2003) 'Detonations in hydrocarbon fuel blends', *Combustion and Flame (Elsevier)*, 132(February 2002), pp. 73–90.

Ballal, D. R. and Zelina, J. (2004) 'Progress in Aeroengine Technology (1939–2003)', *Journal of Aircraft*, 41(1).

Berton, J. J. and Guynn, M. D. (2011) 'Multi-Objective Optimization of a Turbofan for an Advanced, Single-Aisle Transport', *Journal of Aircraft*, 48(5), pp. 1795–1805. doi: 10.2514/1.C031333.

Bijewitz, J., Seitz, A., Isikveren, A. T. and Hornung, M. (2016) 'Progress in Optimizing the Propulsive Fuselage Aircraft Concept', *54th AIAA Aerospace Sciences Meeting*, pp. 1–11. doi: 10.2514/6.2016-0767.

Blanco, G. M. (2014) *Numerical Modelling of Pressure Rise Combustion for Reducing Emissions of Future Civil Aircraft*. Cranfield University.

Boulkeraa, T. and Ghenaiet, A. (2010) 'Turboprop Cycle Optimization Using Repulsive Particle Swarm Algorithm', *Journal of Propulsion and Power*, 26(4), pp. 882–892. doi: 10.2514/1.46491.

Braun, E. M., Lu, F. K., Wilson, D. R. and Camberos, J. a. (2010) 'Detonation Engine Performance Comparison Using First and Second Law Analyses', in *46th AIAA/ASME/SAE/ASEE Joint Propulsion Conference & Exhibit*. Nashville, TN: American Institute of Aeronautics and Astronautics.

Brennan, L. and Owende, P. (2010) 'Biofuels from microalgae-A review of technologies for production, processing, and extractions of biofuels and co-products', *Renewable and Sustainable Energy Reviews*, 14(2), pp. 557–577. doi: 10.1016/j.rser.2009.10.009.

Brophy, C. M. (2009) 'Initiation Improvements for Hydrocarbon / Air Mixtures in Pulse Detonation Applications', in *47th AIAA Aerospace Sciences Meeting Including The New Horizons Forum and Aerospace Exposition*. Orlando, Florida: American Institute of Aeronautics and Astronautics, pp. 1–10.

Brophy, C. M., Sinibaldi, J. O. and Damphousse, P. (2002) 'Initiator Performance for Liquid-Fueled Pulse Detonation Engines', in *40th AIAA Aerospace Sciences Meeting & Exhibit*. Reno, NV: American Institute of Aeronautics and Astronautics.

Buckley, H. P. and Zingg, D. W. (2013) 'Approach to Aerodynamic Design Through Numerical Optimization', *AIAA Journal*, 51(8), pp. 1972–1981. doi: 10.2514/1.J052268.

Caldwell, N. and Gutmark, E. (2007) 'A Review of Pulse Detonation Engine Research at the University of Cincinnati', in *43rd AIAA/ASME/SAE/ASEE Joint Propulsion Conference & Exhibit*. Cincinnati, OH: American Institute of Aeronautics and Astronautics, pp. 1–21.

Carter, J. D. and Lu, F. K. (2011) 'Experiences in Testing of a Large-Scale, Liquid-Fueled, Air-Breathing, Pulse Detonation Engine', in *47th*

AIAA/ASME/SAE/ASEE Joint Propulsion Conference & Exhibit. San Diego, California: American Institute of Aeronautics and Astronautics, pp. 1–14.

Cavalca, D. F., Bringhenti, C., Tomita, J. T. and Silva, O. F. R. (2015) 'Microturbine Design Point Evaluation and Optimization Considering Pollutant Emissions and Thermoeconomic Approach', *Journal of Propulsion and Power*, 31(4), pp. 1107–1116. doi: 10.2514/1.B35511.

Celis, C. (2010) *Evaluation and Optimisation of Environmentally Friendly Aircraft Propulsion System*. Cranfield University. doi: 10.1017/CBO9781107415324.004.

Chan, S. and Liu, H. (2014) 'Experimentally modified unsteady shock wave model for wave rotor design', *50th AIAA/ASME/SAE/ASEE Joint Propulsion Conference*. Reston, Virginia: American Institute of Aeronautics and Astronautics, pp. 1–12. doi: 10.2514/6.2014-3730.

Chandrasekaran, N. and Guha, A. (2012) 'Study of Prediction Methods for NOx Emission from Turbofan Engines', *Journal of Propulsion and Power*, 28(1), pp. 170–180. doi: 10.2514/1.B34245.

Cheatham, S. and Kailasanath, K. (2005) 'Single-Cycle Performance of Idealized Liquid-Fueled Pulse Detonation Engines', *AIAA Journal*, 43(6), pp. 1276–1283. doi: 10.2514/1.11799.

Chen, P.-C., Wang, W.-C., Roberts, W. L. and Fang, T. (2013) 'Spray and atomization of diesel fuel and its alternatives from a single-hole injector using a common rail fuel injection system', *Fuel*. Elsevier Ltd, 103(x), pp. 850–861. doi: 10.1016/j.fuel.2012.08.013.

Cheng, B. (2010) *Gas Turbine Technology - Preliminary Design Study of a Low Emission Combustor for Open Rotor Engine*. Cranfield University, UK.

Chisti, Y. (2007) 'Biodiesel from microalgae.', *Biotechnology advances*. Elsevier Inc., 25(3), pp. 294–306. doi: 10.1016/j.biotechadv.2007.02.001.

Curran, R., Castagne, S., Rothwell, A., Price, M., Murphy, A. and Raghunathan, S. (2009) 'Uncertainty and sensitivity analysis in aircraft operating costs in structural design optimization', *Journal of Aircraft*, 46(6), pp. 2145–2155. doi: 10.2514/1.21751.

Dairobi, G., Wahid, M. A. and Inuwa, I. M. (2013) 'Feasibility Study of Pulse Detonation Engine Fueled by Biogas', *Advances in Thermofluids*, 388, pp. 257–261. doi: 10.4028/www.scientific.net/AMM.388.257.

DeLaat, J. C., Kopasakis, G., Saus, J. R., Chang, C. T. and Wey, C. (2013) 'Active Combustion Control for a Low-Emissions Aircraft Engine Combustor Prototype : Experimental Results', *Journal of Propulsion and Power*, 29(4). doi: 10.2514/1.B34653.

Demirbas, A. (2010) 'Use of algae as biofuel sources', *Energy Conversion and Management*. Elsevier Ltd, 51(12), pp. 2738–2749. doi:

10.1016/j.enconman.2010.06.010.

Demirbas, A. and Fatih Demirbas, M. (2011) 'Importance of algae oil as a source of biodiesel', *Energy Conversion and Management*. Elsevier Ltd, 52(1), pp. 163–170. doi: 10.1016/j.enconman.2010.06.055.

Ebrahimi, H. B. and Merkle, C. L. (2002) 'Numerical Simulation of a Pulse Detonation Engine with Hydrogen Fuels', *Journal of Propulsion and Power*, 18(5).

Eidelman, S., Grossmann, W. and Lottati, I. (1991) 'Review of propulsion applications and numerical simulations of the pulsed detonation engine concept', *Journal of Propulsion and Power*, 7(6), pp. 857–865. doi: 10.2514/3.23402.

Ejim, C. E., Fleck, B. a. and Amirfazli, a. (2007) 'Analytical study for atomization of biodiesels and their blends in a typical injector: Surface tension and viscosity effects', *Fuel*, 86, pp. 1534–1544. doi: 10.1016/j.fuel.2006.11.006.

Elham, A. and van Tooren, M. J. L. (2014) 'Weight Indexing for Wing-Shape Multi-Objective Optimization', *AIAA Journal*, 52(2), pp. 320–337. doi: 10.2514/1.J052406.

Epstein, A. H. (2013) 'Aeropropulsion for Commercial Aviation in the 21st Century and Research Directions Needed', in *51st AIAA Aerospace Sciences Meeting including the New Horizons Forum and Aerospace Exposition*. Grapevine (Dallas/Ft. Worth Region), Texas: American Institute of Aeronautics and Astronautics, pp. 1–17.

Fortier, M.-O. P., Roberts, G. W., Stagg-Williams, S. M. and Sturm, B. S. M. (2014) 'Life cycle assessment of bio-jet fuel from hydrothermal liquefaction of microalgae', *Applied Energy*. Elsevier Ltd, 122(July 2011), pp. 73–82. doi: 10.1016/j.apenergy.2014.01.077.

Frolov, S. M. (2014) 'Natural-Gas-Fueled Pulse-Detonation Combustor', *Journal of Propulsion and Power*, 30(1), pp. 41–46. doi: 10.2514/1.B34920.

Ghassemi, H., Baek, S. W. and Khan, Q. S. (2006) 'Experimental Study on Evaporation Ofkerosene Droplets At Elevated Pressuresand Temperatures', *Combust.Sci.and Tech*, 178(October), pp. 1669–1684. doi: 10.1080/00102200600582392.

Ghoman, S. S., Kapania, R. K., Chen, P. C., Sarhaddi, D. and Lee, D. H. (2012) 'Multifidelity, Multistrategy, and Multidisciplinary Design Optimization Environment', *Journal of Aircraft*, 49(5), pp. 1255–1270. doi: 10.2514/1.C031507.

Ghosh, S. and Hunt, J. C. R. (1994) 'Induced Air Velocity within Droplet Driven Sprays', in *Proceedings: Mathematical and Physical Sciences, Vol 444, No. 1920*. The Royal Society, pp. 105–127.

Giakoumis, E. G. (2013) ‘A statistical investigation of biodiesel physical and chemical properties , and their correlation with the degree of unsaturation’, *Renewable Energy*. Elsevier Ltd, 50, pp. 858–878. doi: 10.1016/j.renene.2012.07.040.

Giakoumis, E. G., Rakopoulos, C. D., Dimaratos, A. M. and Rakopoulos, D. C. (2012) ‘Exhaust emissions of diesel engines operating under transient conditions with biodiesel fuel blends’, *Progress in Energy and Combustion Science*. Elsevier Ltd, 38(5), pp. 691–715. doi: 10.1016/j.pecs.2012.05.002.

Goodger, E. and Ogaji, S. O. T. (2011) *Fuels and Combustion in Heat Engines*. Bedford: Cranfield Design + Print.

Gu, X., Basu, S. and Kumar, R. (2012) ‘Dispersion and vaporization of biofuels and conventional fuels in a crossflow pre-mixer’, *International Journal of Heat and Mass Transfer*. Elsevier Ltd, 55(1–3), pp. 336–346. doi: 10.1016/j.ijheatmasstransfer.2011.09.025.

Gunawan, S., Azarm, S., Boyars, a. and Wu, J. (2003) ‘Quality-Assisted Multi-Objective Multidisciplinary Genetic Algorithms’, *AIAA Journal*, 41(9), pp. 1752–1762. doi: 10.2514/2.7293.

Haik, Y., Selim, M. Y. E. and Abdulrehman, T. (2011) ‘Combustion of algae oil methyl ester in an indirect injection diesel engine’, *Energy*. Elsevier Ltd, 36(3), pp. 1827–1835. doi: 10.1016/j.energy.2010.11.017.

Harris, P. G., Guzik, S., Farinaccio, R., Stowe, R. A., Whitehouse, D., Josey, T., Hawkin, D., Ripley, R., Link, R., Higgins, A. . and Thibault, P. . (2002) ‘Comparative Evaluation of Performance Models of Pulse Detonation Engines’, in *38th AIAA/ASME/SAE/ASEE Joint Propulsion Conference & Exhibit*. Indianapolis, Indiana: American Institute of Aeronautics and Astronautics.

Hathaway, M. D., DelRosario, R. and Madavan, N. K. (2013) ‘NASA Fixed Wing Project Propulsion Research and Technology Development Activities to Reduce Thrust Specific Energy Consumption’, in *49th AIAA/ASME/SAE/ASEE Joint Propulsion Conference*. San Jose, CA: American Institute of Aeronautics and Astronautics, pp. 1–20.

Hegde, G. B. (2011) *Design, Evaluation and Performance Analysis of Present, Novel and Low Emission Combustors*. Cranfield University, UK.

Heiser, W. H. and Pratt, D. T. (2002) ‘Thermodynamic Cycle Analysis of Pulse Detonation Engines’, *Journal of Propulsion and Power*, 18(1).

Hinkey, J., Williams, J., Henderson, S. and Bussing, T. (1997) ‘Rotary-valved, multiple-cycle, pulse detonation engine experimental demonstration’, in *33rd Joint Propulsion Conference and Exhibit*. Reston, Virigina: American Institute of Aeronautics and Astronautics. doi: 10.2514/6.1997-2746.

Hitch, B. (2002) ‘An Analytical Model of the Pulse Detonation Engine Cycle’, in *40th AIAA Aerospace Sciences Meeting & Exhibit*. Reno, NV: American

Institute of Aeronautics and Astronautics.

Hoekman, S. K., Broch, A., Robbins, C., Ceniceros, E. and Natarajan, M. (2012) 'Review of biodiesel composition , properties , and specifications', *Renewable and Sustainable Energy Reviews*. Elsevier Ltd, 16(1), pp. 143–169. doi: 10.1016/j.rser.2011.07.143.

Huang, G., Chen, F., Wei, D., Zhang, X. and Chen, G. (2010) 'Biodiesel production by microalgal biotechnology', *Applied Energy*. Elsevier Ltd, 87(1), pp. 38–46. doi: 10.1016/j.apenergy.2009.06.016.

Hughes, C. E. (2011) 'Aircraft Engine Technology for Green Aviation to Reduce Fuel Burn', in *3rd AIAA Atmospheric Space Environments Conference*. Honolulu, Hawaii: American Institute of Aeronautics and Astronautics, pp. 1–18.

Hutchins, T. E. and Metghalchi, M. (2003) 'Energy and Exergy Analyses of the Pulse Detonation Engine', *Journal of Engineering for Gas Turbines and Power*, 125(4), p. 1075. doi: 10.1115/1.1610015.

Igie, U. and Minervino, O. (2014) 'Impact of Inlet Filter Pressure Loss on Single and Two-Spool Gas Turbine Engines for Different Control Modes', *Journal of Engineering for Gas Turbines and Power*, 136(9), p. 91201. doi: 10.1115/1.4027216.

Jena, U., Vaidyanathan, N., Chinnasamy, S. and Das, K. C. (2011) 'Evaluation of microalgae cultivation using recovered aqueous co-product from thermochemical liquefaction of algal biomass', *Bioresource Technology*. Elsevier Ltd, 102(3), pp. 3380–3387. doi: 10.1016/j.biortech.2010.09.111.

Jiang, X., Siamas, G. a., Jagus, K. and Karayiannis, T. G. (2010) 'Physical modelling and advanced simulations of gas–liquid two-phase jet flows in atomization and sprays', *Progress in Energy and Combustion Science*. Elsevier Ltd, 36(2), pp. 131–167. doi: 10.1016/j.pecs.2009.09.002.

Jimenez, H. and Mavris, D. (2017) 'Pareto-Optimal Aircraft Technology Study for Environmental Benefits with Multi-Objective Optimization', *Journal of Aircraft*, pp. 1–17. doi: 10.2514/1.C033688.

Jiminez, H., Pfaender, H. and Mavris, D. (2012) 'Fuel Burn and CO2 System-Wide Assessment of Environmentally Responsible Aviation Technologies', *Journal of Aircraft*, 49(6), pp. 1913–1930. doi: 10.2514/1.C031755.

Kaemming, T. (2003) 'Integrated Vehicle Comparison of Turbo-Ramjet Engine and Pulsed Detonation Engine', *Journal of Engineering for Gas Turbines and Power*, 125(January), pp. 257–262. doi: 10.1115/1.1p-496116.

Kailasanath, K. (2000) 'Review of Propulsion Application of Detonation Waves', *AIAA Journal*, 38(9).

Kailasanath, K. (2003) ‘Recent Developments in the Research on Pulse Detonation Engines’, *AIAA Journal*, 41(2), pp. 145–159. doi: 10.2514/2.1933.

Kailasanath, K. (2006) ‘Liquid-Fueled Detonations in Tubes’, *Journal of Propulsion and Power*, 22(6), pp. 1261–1268. doi: 10.2514/1.19624.

Kailasanath, K. and Patnaik, G. (2000) ‘Performance estimates of pulsed detonation engines’, in *Proceedings of the Combustion Institute*, pp. 595–601. doi: 10.1016/S0082-0784(00)80259-3.

Kailasanath, K., Patnaik, G. and Li, C. (2002) ‘The flowfield and performance of pulse detonation engines’, in *Proceedings of the Combustion Institute*, pp. 2855–2862. doi: 10.1016/S1540-7489(02)80349-2.

Kentfield, J. A. C. (2002a) ‘Fundamentals of Idealized Airbreathing Pulse-Detonation Engines’, *Journal of Propulsion and Power*, 18(1).

Kentfield, J. A. C. (2002b) ‘Thermodynamics of Airbreathing Pulse-Detonation Engines’, *Journal of Propulsion and Power*, 18(6), pp. 1170–1175.

Khandelwal, B. (2012) *Development of Gas Turbine Combustor Preliminary Design Methodologies and Preliminary Assessments of Advanced Low Emission Combustor Concepts*. Cranfield University, UK.

Kipouros, T. (2013) ‘Stochastic optimisation in computational engineering design’, *Advances in Intelligent Systems and Computing*, 175, pp. 475–490. doi: 10.1007/978-3-642-31519-0.

Kostas, J., Honnery, D. and Soria, J. (2009) ‘Time resolved measurements of the initial stages of fuel spray penetration’, *Fuel*. Elsevier Ltd, 88(11), pp. 2225–2237. doi: 10.1016/j.fuel.2009.05.013.

Kumar, P., Suseela, M. R. and Toppo, K. (2011) ‘Physico-Chemical Characterization of Algal oil : a Potential Biofuel’, *ASIAN Journal of EXP. BIOL.SCI.VOL2(3),2011 493-497*, 2(3), pp. 493–497.

Kuo, K. . (2005) *Principles of Combustion 2nd Edition*. New Jersey: John Wiley & Sons.

Lam, M. K. and Lee, K. T. (2012) ‘Microalgae biofuels: A critical review of issues, problems and the way forward.’, *Biotechnology advances*. Elsevier Inc., 30(3), pp. 673–90. doi: 10.1016/j.biotechadv.2011.11.008.

Lee, C. S. and Park, S. W. (2002) ‘An experimental and numerical study on fuel atomization characteristics of high-pressure diesel injection sprays’, *Fuel*, 81, pp. 2417–2423. doi: 10.1016/S0016-2361(02)00158-8.

Lefebvre, H. A. and Ballal, D. R. (2010) *Gas Turbine: Alternative Fuels and Emissions*. 3rd edn. Florida: CRC Press.

Levy, Y., Sherbaum, V. and Arfi, P. (2004) ‘Basic thermodynamics of

FLOXCOM , the low-NOx gas turbines adiabatic combustor', *Applied Thermal Engineering*, 24(x), pp. 1593–1605. doi: 10.1016/j.applthermaleng.2003.11.022.

Li, C. and Kailasanath, K. (2001) 'A Numerical Study of Reactive Flows in Pulse Detonation Engines', in *37th AIAA/ASME/SAE/ASEE Joint Propulsion Conference & Exhibit*. Salt Lake City, Utah: American Institute of Aeronautics and Astronautics.

Li, C. and Kailasanath, K. (2003) 'Detonation Initiation in Pulse Detonation Engines', in *41st Aerospace Sciences Meeting and Exhibit*. Reno, Nevada: American Institute of Aeronautics and Astronautics.

Li, J.-M., Teo, C. J., Lim, K. S., Wen, C.-S. and Khoo, B. C. (2013) 'Deflagration to Detonation Transition by Hybrid Obstacles in Pulse Detonation Engines', in *49th AIAA/ASME/SAE/ASEE Joint Propulsion Conference AIAA*. San Jose, CA: American Institute of Aeronautics and Astronautics, pp. 1–12. doi: 10.2514/6.2013-3657.

Li, J., Fan, W., Qiu, H., Yan, C. and Wang, Y.-Q. (2010) 'Preliminary study of a pulse normal detonation wave engine', *Aerospace Science and Technology*. Elsevier Masson SAS, 14(3), pp. 161–167. doi: 10.1016/j.ast.2009.12.002.

Li, J., Fan, W., Yan, C. and Li, Q. (2009) 'Experimental Investigations on Detonation Initiation in a Kerosene-Oxygen Pulse Detonation Rocket Engine', *Combustion Science and Technology*, 181(3), pp. 417–432. doi: 10.1080/00102200802612310.

Li, Y. G., Abdul Ghafir, M. F., Wang, L., Singh, R., Huang, K., Feng, X. and Zhang, W. (2012) 'Improved Multiple Point Nonlinear Genetic Algorithm Based Performance Adaptation Using Least Square Method', *Journal of Engineering for Gas Turbines and Power*, 134(3), p. 1-. doi: 10.1115/1.4004395.

Li, Y. G., Ghafir, M. F. A., Wang, L., Singh, R., Huang, K. and Feng, X. (2011) 'Nonlinear Multiple Points Gas Turbine Off-Design Performance Adaptation Using a Genetic Algorithm', *Journal of Engineering for Gas Turbines and Power*, 133(July 2011), pp. 1–9. doi: 10.1115/1.4002620.

Lokesh, K. (2015) *Techno-Economic Environmental Risk Analysis of Advanced Biofuels for Civil Aviation*. Cranfield University, UK.

Lu, F. K. and Braun, E. M. (2014) 'Rotating Detonation Wave Propulsion: Experimental Challenges, Modeling, and Engine Concepts', *Journal of Propulsion and Power*, 30(5), pp. 1125–1142. doi: 10.2514/1.B34802.

Lu, F. K., Carter, J. D. and Wilson, D. R. (2011) 'Development of a Large Pulse Detonation Engine Demonstrator', in *47th AIAA/ASME/SAE/ASEE Joint Propulsion Conference & Exhibit*. San Diego, California: American Institute of Aeronautics and Astronautics, pp. 1–15.

Lü, J., Sheahan, C. and Fu, P. (2011) 'Metabolic engineering of algae for fourth generation biofuels production', *Energy & Environmental Science*, 4(7), p. 2451. doi: 10.1039/c0ee00593b.

Ma, F., Choi, J.-Y. and Yang, V. (2005) 'Thrust Chamber Dynamics and Propulsive Performance of Single-Tube Pulse Detonation Engines', *Journal of Propulsion and Power*, 21(4), pp. 681–691. doi: 10.2514/1.8182.

Ma, F., Choi, J.-Y. and Yang, V. (2006) 'Propulsive Performance of Airbreathing Pulse Detonation Engines', *Journal of Propulsion and Power*, 22(6), pp. 1188–1203. doi: 10.2514/1.21755.

Ma, F., Choi, J. and Yang, V. (2004) 'Thrust Chamber Dynamics and Propulsive Performance of Single-Tube Pulse Detonation Engines', in *42nd AIAA Aerospace Sciences Meeting and Exhibit*. Reno, Nevada: American Institute of Aeronautics and Astronautics, pp. 1–21.

Maity, J. P., Bundschuh, J., Chen, C.-Y. and Bhattacharya, P. (2014) 'Microalgae for third generation biofuel production, mitigation of greenhouse gas emissions and wastewater treatment: Present and future perspectives – A mini review', *Energy*. Elsevier Ltd, 78, pp. 104–113. doi: 10.1016/j.energy.2014.04.003.

Makarevičienė, V., Lebedevas, S., Rapalis, P., Gumbyte, M., Skorupskaite, V. and Žaglinskis, J. (2014) 'Performance and emission characteristics of diesel fuel containing microalgae oil methyl esters', *Fuel*, 120, pp. 233–239. doi: 10.1016/j.fuel.2013.11.049.

Makida, M., Kurosawa, Y., Yamada, H., Shimodaira, K., Yoshida, S., Nakamura, N. and Hayashi, A. K. (2016) 'Emission Characteristics Through Rich – Lean Combustor Development Process for Small Aircraft Engine', *Journal of Propulsion and Power*, pp. 1–10. doi: 10.2514/1.B35970.

Martins, J. R. R. A. and Lambe, A. B. (2013) 'Multidisciplinary Design Optimization: A Survey of Architectures', *AIAA Journal*, 51(9), pp. 2049–2075. doi: 10.2514/1.J051895.

Mata, T. M., Martins, A. A. and Caetano, N. S. (2010) 'Microalgae for biodiesel production and other applications: A review', *Renewable and Sustainable Energy Reviews*, 14(1), pp. 217–232. doi: 10.1016/j.rser.2009.07.020.

Mazlan, N. M. (2012) *Assessing/Optimising Bio-Fuel Combustion Technologies for Reducing Civil Aircraft Emissions*. Cranfield University.

Mazlan, N. M., Savill, M. and Kipouros, T. (2011) 'Computational Evaluation and Exploration of Combustion Performance for Liquid Jet Fuels Derived from Biomass', in *3rd CEAS Air & Space Conference*. Venice.

Mazlan, N. M., Savill, M. and Kipouros, T. (2015) 'Effects of biofuels properties on aircraft engine performance', *Aircraft Engineering and Aerospace Technology*, 87, pp. 437–442. doi: 10.1108/AEAT-09-2013-0166.

Melo, M. J., Sousa, J. M. M., Costa, M. and Levy, Y. (2009) 'Experimental Investigation of a Novel Combustor Model for Gas Turbines', *Journal of Propulsion and Power*, 25(3). doi: 10.2514/1.35173.

Melo, M. J., Sousa, J. M. M., Costa, M. and Levy, Y. (2011) 'Flow and Combustion Characteristics of a Low-NOx Combustor Model for Gas Turbines', *Journal of Propulsion and Power*, 27(6). doi: 10.2514/1.B34033.

Montgomery, D. C. and Runger, G. C. (2011) *Applied Statistics and Probability for Engineers*. 5th edn. New Jersey: John Wiley & Sons (Asia) Pte Ltd.

Morsi, S. and Alexander, A. (1972) 'An investigation of particle trajectories in two-phase flow systems', *J. Fluid Mech*, 55, pp. 193–208. doi: 10.1017/S0022112072001806.

New, T. H., Panicker, P. K., Lu, F. K. and Tsai, H. M. (2006) 'Experimental Investigations on DDT Enhancements by Shchelkin Spirals in a PDE', in *44th AIAA Aerospace Sciences Meeting and Exhibit*. Reno, Nevada: American Institute of Aeronautics and Astronautics, pp. 1–10.

New, T., Panicker, P., Chui, K., Tsai, H. and Lu, F. (2006) 'Experimental Study on Deflagration-to-Detonation Transition Enhancement Methods in a PDE', in *14th AIAA/AHI Space Planes and Hypersonic Systems and Technologies Conference*. Reston, Virigina: American Institute of Aeronautics and Astronautics, pp. 1–13. doi: 10.2514/6.2006-7958.

Nikitin, V. F., Dushin, V. R., Phylippov, Y. G. and Legros, J. C. (2009) 'Pulse detonation engines: Technical approaches', *Acta Astronautica*, 64(2–3), pp. 281–287. doi: 10.1016/j.actaastro.2008.08.002.

Padmanabhan MR, A. and Stanley, S. A. (2012) 'Microalgae as an Oil Producer for Biofuel Applications', *Research Journal of Recent Sciences*, 1(3), pp. 57–62.

Panicker, P. K., Li, J.-M., Lu, F. K. and Wilson, D. R. (2007) 'Development of a Compact Liquid Fueled Pulsed Detonation Engine with Predetonator', in *45th AIAA Aerospace Sciences Meeting and Exhibit*. Reno, Nevada: American Institute of Aeronautics and Astronautics, pp. 1–13.

Panicker, P. K., Wilson, D. R. and Lu, F. K. (2006) 'Operational Issues Affecting the Practical Implementation of Pulsed Detonation Engines', in *14th AIAA/AHI Space Planes and Hypersonic Systems and Technologies Conference*. Canberra, Australia: American Institute of Aeronautics and Astronautics, pp. 1–18.

Payan, A. P., Kirby, M., Justin, C. Y. and Mavris, D. N. (2014) 'Meeting Emissions Reduction Targets : A Probabilistic Lifecycle Assessment of the Production of Alternative Jet Fuels', in *AIAA/3AF Aircraft Noise and Emissions Reduction Symposium*. Atlanta, GA: American Institute of Aeronautics and Astronautics, pp. 1–17.

Qiu, H., Xiong, C., Yan, C. and Fan, W. (2012) 'Propulsive Performance of Ideal Detonation Turbine Based Combined Cycle Engine', *Journal of Engineering for Gas Turbines and Power*, 134(8), p. 81201. doi: 10.1115/1.4006483.

Rahmes, T. F., Kinder, J. D., Henry, T. M., Crenfedlt, G., LeDuc, G. F., Zombanakis, G. P., Abe, Y., Lambert, D. M., Lewis, C., Juenger, J. A., Andac, M. G., Reilly, K. R., Holmgren, J. R., McCall, M. J. and Bozzano, A. G. (2009) 'Sustainable Bio-Derived Synthetic Paraffinic Kerosene (Bio- SPK) Jet Fuel Flights and Engine Tests Program Results', in *9th AIAA Aviation Technology, Integration, and Operations Conference (ATIO)*. Hilton Head, South Carolina: American Institute of Aeronautics and Astronautics, pp. 1–19. doi: doi:10.2514/6.2009-7002.

Rakitin, A. E. and Starikovskii, A. Y. (2010) 'Gradient Mechanism of Detonation Initiation for PDE Applications', in *48th AIAA Aerospace Sciences Meeting Including the New Horizons Forum and Aerospace Exposition*. Orlando, Florida: American Institute of Aeronautics and Astronautics, pp. 1–11.

Rallabhandi, S. K. and Mavris, D. N. (2008) 'Simultaneous Airframe and Propulsion Cycle Optimization for Supersonic Aircraft Design', *Journal of Aircraft*, 45(1), pp. 38–55. doi: 10.2514/1.33183.

Rasheed, A., Furman, A. H. and Dean, A. J. (2011) 'Experimental Investigations of the Performance of a Multitube Pulse Detonation Turbine System', *Journal of Propulsion and Power*, 27(3). doi: 10.2514/1.B34013.

Rawat, I., Kumar, R. R., Mutanda, T. and Bux, F. (2013) 'Biodiesel from microalgae : A critical evaluation from laboratory to large scale production', *Applied Energy*. Elsevier Ltd, 103, pp. 444–467. doi: 10.1016/j.apenergy.2012.10.004.

Rinaldini, C. A., Mattarelli, E., Magri, M. and Beraldi, M. (2014) 'Experimental Investigation on Biodiesel from Microalgae as Fuel for Diesel Engines', *SAE Technical Paper*. doi: 10.4271/2014-01-1386.Copyright.

Roisman, I. V., Araneo, L. and Tropea, C. (2007) 'Effect of ambient pressure on penetration of a diesel spray', *International Journal of Multiphase Flow*, 33, pp. 904–920. doi: 10.1016/j.ijmultiphaseflow.2007.01.004.

Roy, G. D., Frolov, S. M., Borisov, A. a. and Netzer, D. W. (2004) 'Pulse detonation propulsion: challenges, current status, and future perspective', *Progress in Energy and Combustion Science*, 30(6), pp. 545–672. doi: 10.1016/j.pecs.2004.05.001.

Ryu, J., Kim, H. and Lee, K. (2005) 'A study on the spray structure and evaporation characteristic of common rail type high pressure injector in homogeneous charge compression ignition engine', *Fuel*, 84, pp. 2341–2350. doi: 10.1016/j.fuel.2005.03.032.

Sadanandan, R., Luckerath, R., Meier, W. and Wahl, C. (2011) 'Flame

Characteristics and Emissions in Flameless Combustion Under Gas Turbine Relevant Conditions', *Journal of Propulsion and Power*, 27(5). doi: 10.2514/1.50302.

Sazhin, S. S. (2017) 'Modelling of fuel droplet heating and evaporation: Recent results and unsolved problems', *Fuel*. Elsevier Ltd, 196, pp. 69–101. doi: 10.1016/j.fuel.2017.01.048.

Sazhin, S. S., Feng, G. and Heikal, M. R. (2001) 'A model for fuel spray penetration', *Fuel*, 80(15), pp. 2171–2180. doi: 10.1016/S0016-2361(01)00098-9.

Schmidt, S., Ilic, C., Schulz, V. and Gauger, N. R. (2013) 'Three-Dimensional Large-Scale Aerodynamic Shape Optimization Based on Shape Calculus', *AIAA Journal*, 51(11), pp. 2615–2627. doi: 10.2514/1.J052245.

Schutte, J. S., Jimenez, H. and Mavris, D. N. (2011) 'Technology Assessment of NASA Environmentally Responsible Aviation Advanced Vehicle Concepts', in *49th AIAA Aerospace Sciences Meeting including the New Horizons Forum and Aerospace Exposition*. Orlando, Florida: American Institute of Aeronautics and Astronautics, pp. 1–12.

Schwer, D. A. and Kailasanath, K. (2016) 'Modeling NOx Emissions for Air-Breathing Rotating Detonation Engines', in *52nd AIAA/SAE/ASEE Joint Propulsion Conference*. Salt Lake City, Utah: American Institute of Aeronautics and Astronautics, pp. 1–13. doi: 10.2514/6.2016-4779.

Shimada, T., Hayashi, A. K., Yamada, E. and Tsuboi, N. (2011) 'Numerical Study on Detonation Characteristics Using a Bio-Fuel', in *49th AIAA Aerospace Sciences Meeting including the New Horizons Forum and Aerospace Exposition*. Orlando, Florida: American Institute of Aeronautics and Astronautics. doi: 10.2514/6.2011-582.

Singh, J. and Gu, S. (2010) 'Commercialization potential of microalgae for biofuels production', *Renewable and Sustainable Energy Reviews*. Elsevier Ltd, 14(9), pp. 2596–2610. doi: 10.1016/j.rser.2010.06.014.

Singleton, D. R., Sinibaldi, J. O., Brophy, C. M., Kuthi, A. and Gundersen, M. A. (2009) 'Compact Pulsed-Power System for Transient Plasma Ignition', *IEEE Transactions on Plasma Science*, 37(12), pp. 2275–2279. doi: 10.1109/TPS.2009.2024672.

Sobieski, J. S.- and Haftka, R. . (1997) 'Multidisciplinary aerospace design optimization : survey of recent developments', *Structural Optimization*, 14, pp. 1–23. doi: 10.1007/BF01197554.

Starik, A. M., Lebedev, A. B., Savel'ev, A. M., Titova, N. S. and Leyland, P. (2013) 'Impact of Operating Regime on Aviation Engine Emissions : Modeling Study', *Journal of Propulsion and Power*, 29(3). doi: 10.2514/1.B34718.

Suali, E. and Sarbatly, R. (2012) ‘Conversion of microalgae to biofuel’, *Renewable and Sustainable Energy Reviews*. Elsevier Ltd, 16(6), pp. 4316–4342. doi: 10.1016/j.rser.2012.03.047.

Suder, K. L. (2012) ‘Overview of the NASA Environmentally Responsible Aviation Project’s Propulsion Technology Portfolio’, in *48th AIAA/ASME/SAE/ASEE Joint Propulsion Conference & Exhibit*. Atlanta, Georgia: American Institute of Aeronautics and Astronautics, pp. 1–23.

Toal, D. J. J., Keane, A. J., Benito, D., Dixon, J. A., Yang, J., Price, M., Robinson, T., Remouchamps, A. and Kill, N. (2014) ‘Multifidelity Multidisciplinary Whole-Engine Thermomechanical Design Optimization’, *Journal of Propulsion and Power*, 30(6), pp. 1654–1666. doi: 10.2514/1.B35128.

Tsalavoutas, A., Kelaidis, M., Thoma, N. and Mathioudakis, K. (2007) ‘Correlations Adaptation for Optimal Emissions Prediction’, in *ASME Turbo Expo 2007: Power for Land, Sea, and Air*. Montreal, Canada: ASME, pp. 545–555. doi: 10.1115/GT2007-27060.

Tüccar, G. and Aydın, K. (2013) ‘Evaluation of methyl ester of microalgae oil as fuel in a diesel engine’, *Fuel*, 112, pp. 203–207. doi: 10.1016/j.fuel.2013.05.016.

Tucker, K. C., King, P. I. and Schauer, F. R. (2008) ‘Hydrocarbon Fuel Flash Vaporization for Pulsed Detonation Combustion’, *Journal of Propulsion and Power*, 24(4), pp. 788–796. doi: 10.2514/1.28412.

Turgut, E. T. (2016) ‘Effects of Ambient Air Temperature on Gaseous Emissions of Turbofan Engines’, *Journal of Propulsion and Power*, 32(3). doi: 10.2514/1.B35916.

Turns, S. (2000) *Introduction to Combustion: Concepts and Application*. McGraw-Hill.

Vutthivithayarak, R., Braun, E. M. and Lu, F. K. (2011) ‘Examination of the Various Cycles for Pulse Detonation Engines’, in *47th AIAA/ASME/SAE/ASEE Joint Propulsion Conference & Exhibit*. San Diego, California: American Institute of Aeronautics and Astronautics, pp. 1–11.

Wahlen, B. D., Morgan, M. R., McCurdy, A. T., Willis, R. M., Morgan, M. D., Dye, D. J., Bugbee, B., Wood, B. D. and Seefeldt, L. C. (2013) ‘Biodiesel from microalgae, yeast, and bacteria: Engine performance and exhaust emissions’, *Energy and Fuels*, 27(1), pp. 220–228.

Wey, C. C., Anderson, B. E., Wey, C., Miake-Lye, R. C., Whitefield, P. and Howard, R. (2007) ‘Overview on the Aircraft Particle Emissions Experiment’, *Journal of Propulsion and Power*, 23(5). doi: 10.2514/1.26406.

Willcox, K. and Haftka, R. (2014) ‘Special Section on Multidisciplinary Design Optimization’, *AIAA Journal*, 52(4), p. 669. doi: 10.2514/1.J052182.

Wintenberger, E., Austin, J. M., Cooper, M., Jackson, S. and Shepherd, J. E. (2003) 'Analytical Model for the Impulse of Single-Cycle Pulse Detonation Tube', *Journal of Propulsion and Power*, 19(1), pp. 22–38. doi: 10.2514/2.6099.

Wintenberger, E. and Shepherd, J. E. (2003) 'A Model for the Performance of Air-Breathing Pulse Detonation Engines', in *39th AIAA/ASME/SAE/ASEE Joint Propulsion Conference and Exhibit*. Huntsville, Alabama: American Institute of Aeronautics and Astronautics, pp. 1–16.

Wormhoudt, J., Herndon, S. C., Yelvington, P. E., Miake-lye, R. C. and Wey, C. (2007) 'Nitrogen Oxide (NO/NO2/HONO) Emissions Measurements in Aircraft Exhausts', *Journal of Prop*, 23(5). doi: 10.2514/1.23461.

Wu, Y., Ma, F. and Yang, V. (2002) 'System Performance and Thermodynamic Cycle Analysis of Air-Breathing Pulse Detonation Engines', in *40th AIAA Aerospace Sciences Meeting & Exhibit*. Reno, NV: American Institute of Aeronautics and Astronautics.

Xu, J., Andrew Ning, S., Bower, G. and Kroo, I. (2014) 'Aircraft Route Optimization for Formation Flight', *Journal of Aircraft*, 51(2), pp. 490–501. doi: 10.2514/1.C032154.

Ye, L. (2010) *The NOx Emission Optimization in the Preliminary Design of Low Emission Combustor for a Civil Turbofan Engine*. Cranfield University, UK.

Yi, T.-H., Lou, J., Turangan, C., Choi, J.-Y. and Wolanski, P. (2011) 'Propulsive Performance of a Continuously Rotating Detonation Engine', *Journal of Propulsion and Power*, 27(1), pp. 171–181. doi: 10.2514/1.46686.

Yule, A. J. and Filipovic, I. (1992) 'On the Break-Up Times and Lengths of Diesel Sprays', *International Journal of Heat and Fluid Flow*, 13, pp. 197–206. doi: 10.1016/0142-727X(92)90028-8.

Yungster, S. . and Breisacher, K. . (2005) 'Study of NOx Formation in Hydrocarbon-Fuelled Pulse Detonation Engines', in *41st AIAA/ASME/SAE/ASEE Joint Propulsion & Exhibit*. Tucson, Arizona: American Institute of Aeronautics and Astronautics. doi: 10.1080/13647830600876629.

Zhang, C., Hui, X., Lin, Y. and Sung, C. (2016) 'Recent development in studies of alternative jet fuel combustion : Progress , challenges , and opportunities', *Renewable and Sustainable Energy Reviews*. Elsevier, 54, pp. 120–138. doi: 10.1016/j.rser.2015.09.056.

Zhu, L. D., Hiltunen, E., Antila, E., Zhong, J. J., Yuan, Z. H. and Wang, Z. M. (2014) 'Microalgal biofuels: Flexible bioenergies for sustainable development', *Renewable and Sustainable Energy Reviews*. Elsevier, 30, pp. 1035–1046. doi: 10.1016/j.rser.2013.11.003.

APPENDICES

Appendix A (Literature Surveys)

A.1 Fuels properties

	MICROALGAE	ALGAE	JOJOBA	JATROPHA	CAMELINA	CANOLA	PALM	RAPESEED	SOY	WCO
Density (kg/m3)	886	883.6	863-866	864-880	-	881.6	874.7	882.2	882.8	880.6
Cetane Number	48.31	85-92	63.5	46-55	50.4	53.7	61.9	53.7	51.3	56.2
Viscosity (mm2/s @ 40 o celcius)	4.47	4.73	19.2-25.4	3.7-5.8	3.80	4.38	4.61	4.5	4.26	4.75
Pour Point (o celcius)	-12	-21- -24	-6-6	5	-7	-6	13	-10	-4	-0.3
Flash Point (o celcius)	165.5	179	61-75	163-238	136	153	163	169	159	161.7
Heating Value (MJ/kg)	40.045	40.72	42.76-47.38	38.5-42	45.2	36.55-40.5	38.73-40.39	36.55-40.5	39.6	30.83
Cold filter plugging point (o celcius)	18	-	-	-1.2	-3	-9	9	-12	-4	-2.8
Acid value (mg/KOH)	0.13	0.37	0.71	0.34		0.22	0.27	0.24	0.32	0.41
Cloud point (o celcius)	-5.2	7	6-16	5	3	-2	14	-3	0	5.3
C (%)	61.52	68.30	-	76.57	-	-	76.09	77.07	77.03	76.90
H (%)	8.50	8.30	-	12.21	-	12.84	12.44	11.84	11.90	12.02
O (%)	20.19	16.40	-	11.32	-	11.04	11.27	10.93	10.95	10.77
N (%)	9.79	6.20	-	-	-	-	-	-	-	-
Kinematic viscosity (mm/s2 @ 40 o celcius)	33.06	-	24.05	4.75	-	-	4.3-4.5	4.2	4.0	19.24
Oxidation stability (h)	8.83	6.76	-	5.0	-	11.0	11.4	7.4	5.0	5.0
Iodine Value (g I2/100g)	119.1 g	97.12	43.80-56.55	109.5	152.8	108.8	54	116.1	125.5	85.1
Sulfur Content (ppm)	-	8.1	-	12.9	-	2.2	3.1	4.6	2.7	8.6
specific gravity	-	1.02 g/mL	0.865-0.869 at 15celcius	0.876	0.882	0.883	0.873	0.879	0.882	-

A.2 Biofuels Mind Map

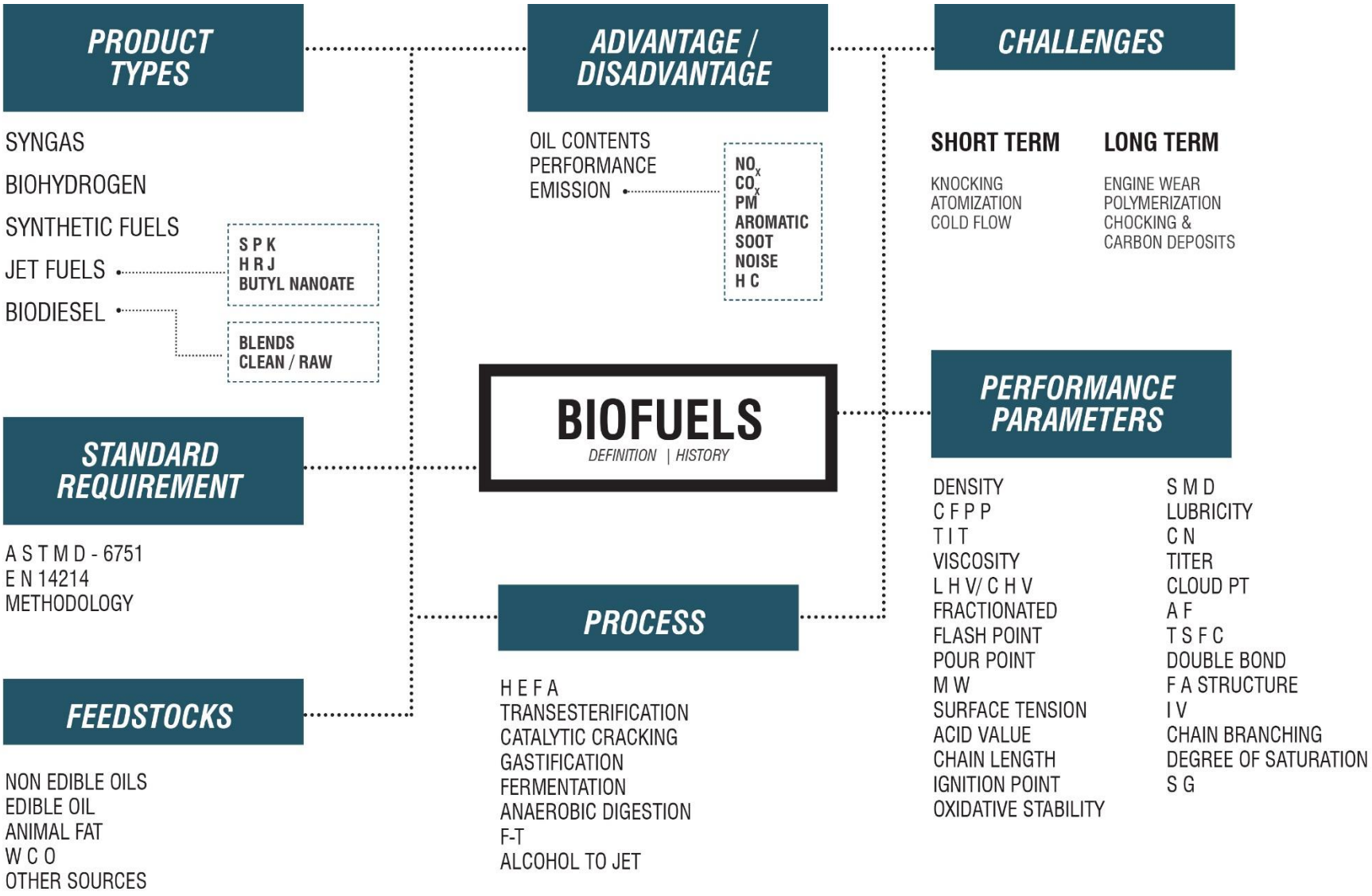

A.3 Microalgae Biofuel Mind Map

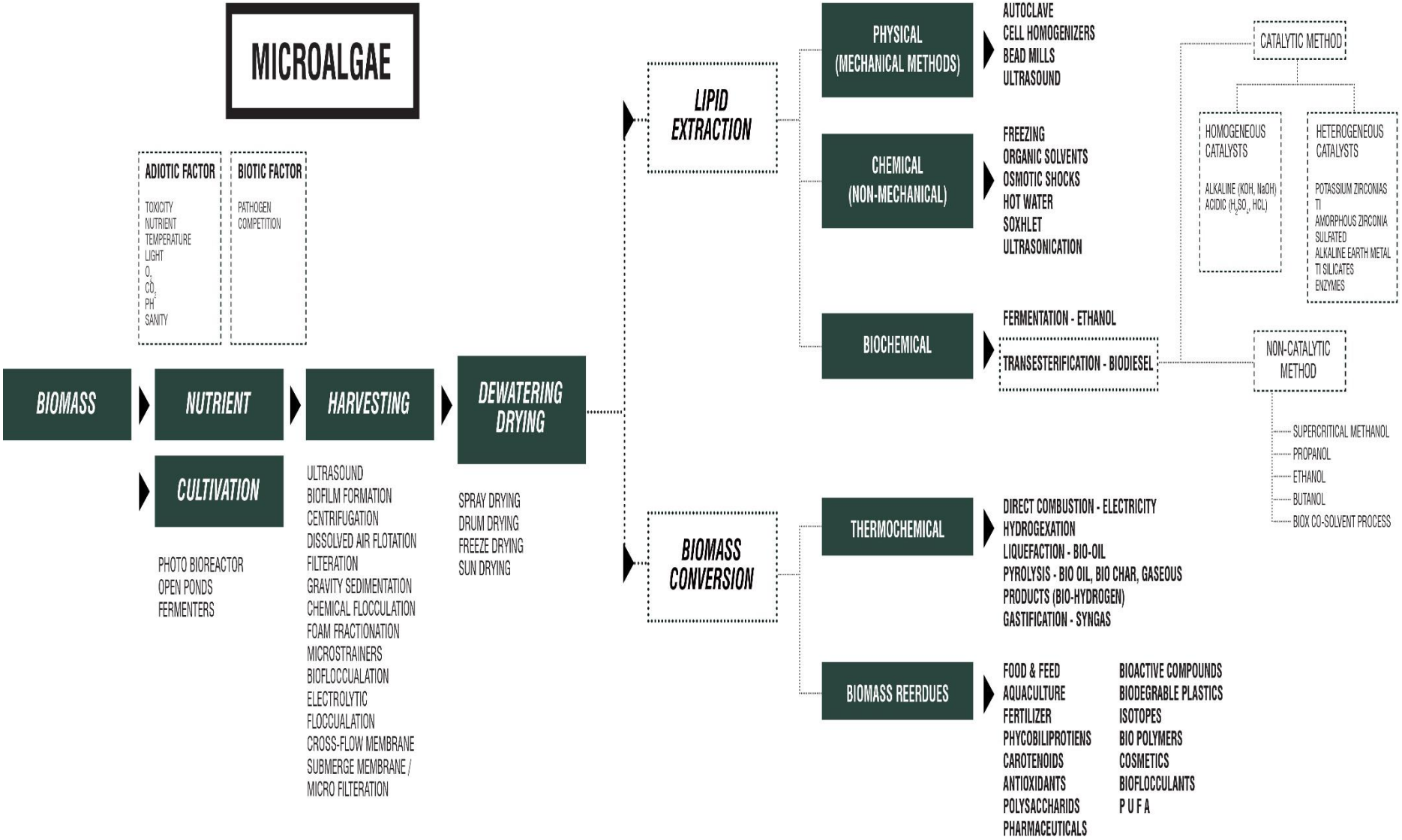

A.3.1 Advantages of Microalgae Biofuels

Advantage	References
Sustainability: **Renewable resource of energy that could be sustainably supplied.**	(Huang *et al.*, 2010)
Environmental friendly: **No net increased release of carbon dioxide.** **Very low or no sulphur content.** **Carbon monoxide would be cut down by 10%, NOX by 9.3% due to its high oxygen content.** **No aromatic compounds and other chemical substance (herbicides/pesticides), which are harmful.** **Algae biofuel is non-toxic and biodegradable.** **Greenhouse-gas emissions cut half.** **Reducing emissions (PM & UHC) up to 73% compared to petroleum diesel.**	(Brennan and Owende, 2010; Huang *et al.*, 2010; Mata, Martins and Caetano, 2010; Demirbas and Fatih Demirbas, 2011; Rawat *et al.*, 2013; Tüccar and Aydın, 2013; Wahlen *et al.*, 2013; Maity *et al.*, 2014; Zhu *et al.*, 2014)
Economy: **Transportation and harvesting costs are relatively low compared to other oil crops.** **More cost effective farming.**	(Demirbas, 2010; Huang *et al.*, 2010; Rawat *et al.*, 2013)
Properties: **Better flash point.** Low freezing point & high density for aviation. Saturated fatty acids result in esters with higher cetane number, higher oxidative stability & better lubrication. Unsaturated fatty acids result in esters with better cold flow **properties.** **Contain additional oxygen to enhance complete combustion.**	(Brennan and Owende, 2010; Huang *et al.*, 2010; A, Padmanaban and Subramaniam, 2013; Tüccar and Aydın, 2013)
Growing capabilities: **High growth rates (100 times faster).** **Easy (anywhere) and simple to grow with very little nutrients supply (N, P, and K) and harvest with little attention.**	(Brennan and Owende, 2010; Demirbas, 2010; Huang *et al.*, 2010; Mata, Martins and Caetano, 2010; Singh

Needless water than terrestrial crops. **Allowing multiple and continuous harvesting of biomass year round, unlike oilseed crops.** **The dual potential for treatment of organic effluent from the agro-food industry.**	and Gu, 2010; Demirbas and Fatih Demirbas, 2011; Kumar, Suseela and Toppo, 2011; Lam and Lee, 2012; Tüccar and Aydın, 2013; Wahlen *et al.*, 2013; Rawat *et al.*, 2013; Maity *et al.*, 2014)
Lipids/Oil Contents: **Microalgae lipids contain twice the energy stored per carbon atoms than carbohydrates.** **Microalgae have much more oil than macro algae.** **Produce an oil yield higher than other vegetable crops (25 times higher than oil palm and 250 times than soybeans- up to 100000 L/ha) in a shorter time.** **Oil content in microalgae can exceed 80% by weight of dry biomass.** **Microalgae have the potential to produce 25–220 times higher triglycerides than terrestrial plants.**	(Amin, 2009; Brennan and Owende, 2010; Singh and Gu, 2010; Kumar, Suseela and Toppo, 2011; Atabani *et al.*, 2012; Padmanabhan MR and Stanley, 2012; Suali and Sarbatly, 2012; A, Padmanaban and Subramaniam, 2013; Tüccar and Aydın, 2013; Rawat *et al.*, 2013; Maity *et al.*, 2014)
Land acquisition: **Requires the least land area (Up to 49 or 132 times less when compared to rapeseed or soybean crop) than other biodiesel feed stocks and can produce in large volume.** **Does not require fertile land or food crops.**	(Brennan and Owende, 2010; Demirbas, 2010; Demirbas and Fatih Demirbas, 2011; Lam and Lee, 2012; Tüccar and Aydın, 2013; Maity *et al.*, 2014)
Fixation of CO2 **High-efficiency CO2 mitigation to fix CO2 from the atmosphere, flue gasses or soluble carbonate into their cells and simultaneously capturing solar energy with efficiency 10–50 times greater than terrestrial plants. 1 kg of dry algal biomass utilizes about 1.83 kg of CO2.**	(Amin, 2009; Brennan and Owende, 2010; Demirbas, 2010; Mata, Martins and Caetano, 2010; Demirbas and Fatih Demirbas, 2011; Lam and Lee, 2012)
Water treatment: **The growth of microalgae can effectively remove NH4+,**	(Mata, Martins and Caetano, 2010;

NO3-, PO43- from wastewater.	Rawat *et al.*, 2013)
Co-products: **Produce valuable co-products such as proteins and residual biomass after oil extraction that may be used as feed or fertilizer, or fermented to produce ethanol or methane.**	(Brennan and Owende, 2010; Mata, Martins and Caetano, 2010; Singh and Gu, 2010)
Photosynthesis: **High photosynthetic rate and efficiency (up to 50 times higher).**	(Amin, 2009; Suali and Sarbatly, 2012; Rawat *et al.*, 2013)

A.3.2 Disadvantages of Microalgae Biofuels

Disadvantages	References
Harvesting, extraction, and filtration: **Harvesting microalgae can be difficult because of their small cell size.** **Lipid extraction from microalgae is a complicated task.** **Large amounts of free fatty acids (FFA) are difficult to convert to biodiesel through transesterification.** **Unicellular lipids are found in suspension making separation (filtration) difficult.**	(Huang *et al.*, 2010; Lam and Lee, 2012; Suali and Sarbatly, 2012; Rawat *et al.*, 2013)
Capital costs: **Cultivation, extraction and production cost (effective large-scale facilities-bioreactors) and energy-intensive were higher compared to the final yield of the product.** **The price of biodiesel is approximately twofold that of the conventional diesel at present.**	(Demirbas, 2010; Huang *et al.*, 2010; Atabani *et al.*, 2012; Padmanabhan MR and Stanley, 2012; Suali and Sarbatly, 2012; Zhu *et al.*, 2014)
Properties & Performance: **Relatively new technology and performs poorly compared to its mainstream alternative.** **Produces unstable biodiesel with many polyunsaturated.** **Highly viscous and not suitable for direct use which**	(Amin, 2009; Huang *et al.*, 2010; Demirbas and Fatih Demirbas, 2011; Rawat *et al.*, 2013; Tüccar and

requires conversion to meet regulatory standards. **Low density and cetane number lead to power reduction and incomplete combustion of the engine (even in blended).** **Torque output values reduced with the increasing concentration of microalgae biodiesel.** **Lower fuel value than diesel fuel.** **High water contents (80– 90%); not all energy conversion processes of biomass can be applied to microalgae.**	Aydın, 2013)
Susceptible to bacterial oxidation subsequently causing internal corrosion of the storage tanks.	(Rawat *et al.*, 2013)
Lack of data for large-scale plants.	(Brennan and Owende, 2010)

A.4 Pulse Detonation Engine Mind Map

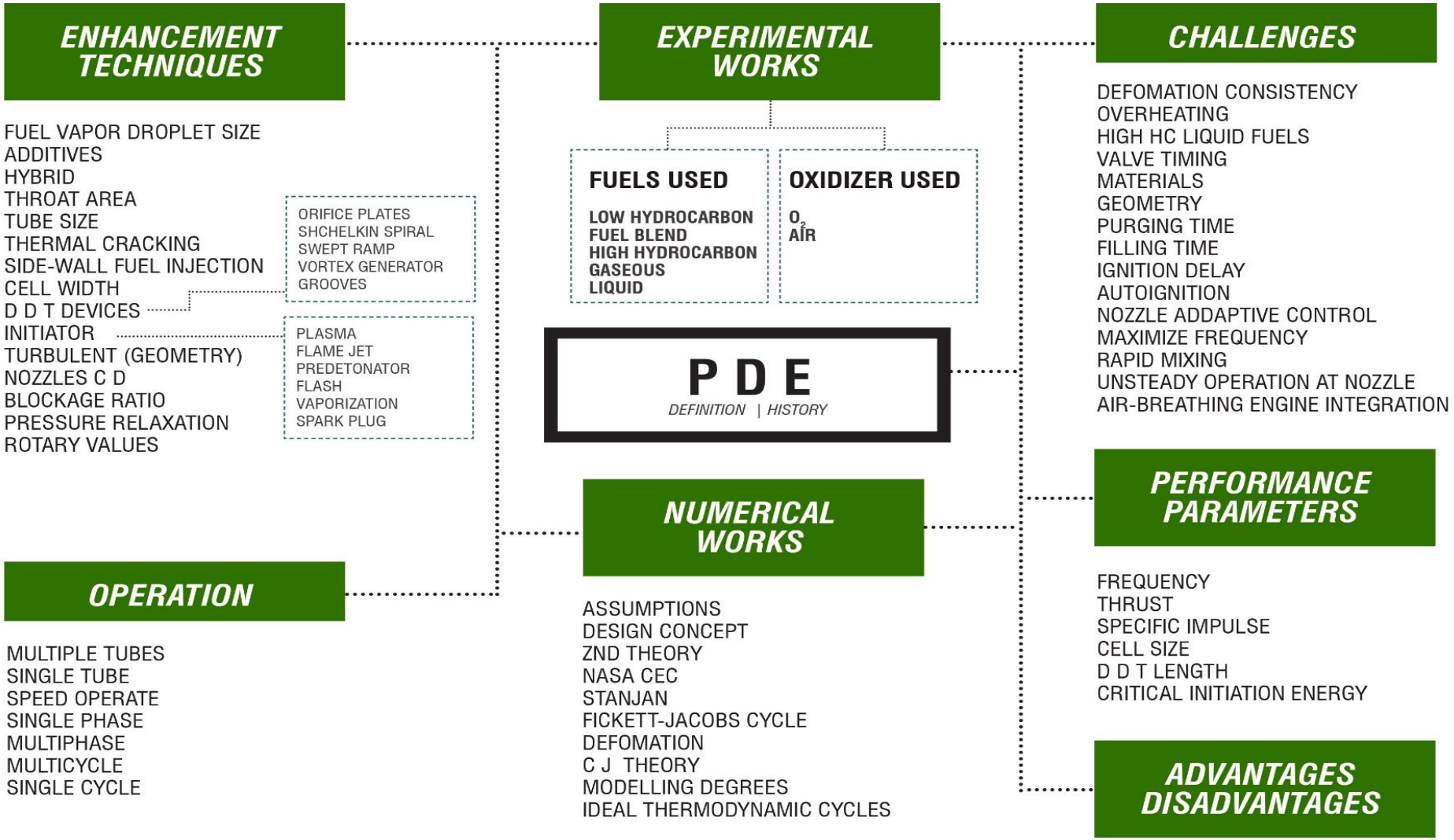

A.4.1 PDE Works

Themes	Findings	Sources
Performances • **Specific Impulse** • **Thrust** • **Thermodynamic Efficiency**	• Optimizing the internal geometry could increase 2% of performance. • The larger the percentage of the fuel in the vapour state, the better the overall performance of the PDE. • Specific impulse can be improved through gradual relaxation to ambient condition using different nozzles designs and partially filling the tube with a non-reactive mixture, and is reduced to the increase refilling period, ignition delay and velocity. • The thrust of the engine is found to be the sum of three terms representing the detonation tube impulse, the ram momentum, and the unsteady mass transfer. • The interface expansion waves play a role, equally important to that played exit expansion waves, in the pressure evolution and thrust production. • Thrust is proportional to the frequency of detonation, the area of the detonation tube, the initial pressure, and the number of tubes. • Use of orifice plates with more than 50% blockage, constant plasma field, variable speed rotary valve system and sidewall injection of fuel is intended to maximize thrust output. • The ideal thermodynamic cycle efficiency of the PDE is in the range of 0.4 to 0.8 for typical hydrocarbon fuels corresponding to specific impulse in the range of 3000 to 5000 s. • Real PDE cycle has better performance, in terms of specific impulse and thrust than the real Brayton cycle only for flight Mach numbers less than about 3, or cycle static temperature ratios less than about 3. • The embedded PDE turbofan could provide 2% higher thrust and an 11% reduction in the thrust specific fuel consumption over the baseline turbofan.	(Kailasanath and Patnaik, 2000; Li and Kailasanath, 2001; Wu, Ma and Yang, 2002; Ebrahimi and Merkle, 2002; Harris *et al.*, 2002; Heiser and Pratt, 2002; Wintenberger and Shepherd, 2003; Ma, Choi and Yang, 2004; Caldwell and Gutmark, 2007; Tucker, King and Schauer, 2008; Carter and Lu, 2011; Qiu *et al.*, 2012)
Operations • **Flight**	• PDE has superiority, compared with conventional subsonic combustion ramjet and Scramjet at about 3-7 Mach number.	(Heiser and Pratt, 2002; Kailasanath,

Speed • **Initiation** • **Ambient Condition** • **Cycle**	• Higher initiation pressures led to shorter transition distances, whereas lower pressures failed to initiate a detonation. • The flow inside the chamber responds to changes outside and no general solution to this problem since it depends on the specific system configuration at the open end of the tube that one is attempting to mimic. • An optimum cycle frequency achieved with improved valve close-up time. • A larger purge time decreases the specific thrust but increases the specific impulse for a given cycle period and valve close-up time. • Direct initiation of detonation is impractical for multi-cycle PDE due to difficulties resulting from the energy requirement and time response, thus DDT devices needed. • The presence of droplets in a fuel–air mixture has negatively affect ignition, DDT and detonation wave propagation through the mixture. • Rapid initiation of detonation was achieved in a short distance with the flame jet ignition. • The higher efficiency of the nanosecond initiating system in terms of DDT length and time. • The effectiveness of the DDT enhancement configurations is dependent on the operation frequency.	Patnaik and Li, 2002; Wu, Ma and Yang, 2002; Ma, Choi and Yang, 2004; Tucker, King and Schauer, 2008; Li *et al.*, 2009, 2010, 2013; Braun *et al.*, 2010; Rakitin and Starikovskii, 2010)
Modelling	• The 0D model offers a good approximation to the time-averaged performance while 1D model provides a good approximation of transient performance of PDE cycle.	(Harris *et al.*, 2002)
Designs • **Valves** • **Combustor** • **Nozzles** • **Fuels**	• Delaying the opening of this valve decrease the average level of thrust. • The performance of the short engines with no exhaust nozzle is relatively poor but improve slightly with decreasing combustor diameter due to the increasing combustor pressure. • Nozzle throat area affects both the flow expansion process and chamber dynamics. Convergent section preserves the chamber pressure during the blowdown and refilling processes while divergent section improves the performance due to the	(Hitch, 2002; Austin and Shepherd, 2003; Li and Kailasanath, 2003; Ma, Choi and Yang, 2004; T. New *et al.*, 2006; Panicker *et al.*, 2007)

increase in the effective thrust wall area. Convergent-divergent throat configurations have a tendency to destabilize the coupling between the flame and shock fronts.

- Smaller throat improves the performance by up to 6%, whereas the nozzle length has minor effects on the performance. But, an exceedingly small throat jeopardizes the engine performance due to the relatively longer blowdown process and larger internal flow losses.
- Several loss mechanisms in combustor and nozzle due to viscous damping, wall heat transfer, refilling process, nozzle flow expansion, and divergence, and chamber interior ballistics.
- Gaseous fuels and light hydrocarbons are easy to create uniform fuel-air mixtures with liquid hydrocarbon fuels and can initiate detonation. Smaller molecular weight products act as “sensitizers” to the parent fuel, reducing the critical energy required to initiate a detonation. Critical initiation energy is linearly proportional to the cell width.
- The cell width decreases with increasing pressure, the fraction of additives, increasing amounts of hydrogen or hydrocarbon.
- The cell width is directly proportional to the reaction zone thickness.
- The cell sizes are strongly correlated to the difficulty to initiate detonations.
- Most liquid hydrocarbon fuel/air mixtures, the cell sizes are close to 40-50 mm.

A.4.2 PDE Enhancement Techniques

Methods	Descriptions	Effects	References
DDT Enhancement **Shchelkin Spiral, tabs, grooves, orifice plates, swept-ramp obstacles, smaller tube and fluidic obstacles along the path**	Using DDT devices rapidly to accelerate detonation with the use of wall turbulence devices. Promote flame turbulent mixing and increases the flame velocity Orifice plates also create wave reflections between themselves and with the closed end of the detonation tube	Thrust & specific impulse losses Blockage in Shchelkin Spirals Destruction from high heat load Increase in the flame surface area and the energy release rate contribute to the higher acceleration rate and thus detonation transition is attained earlier Swept-ramp obstacles very low total pressure loss, attractive thermal management characteristics, and effective initiation over short distances	(Brophy, Sinibaldi and Damphousse, 2002; Hutchins and Metghalchi, 2003; T. H. New *et al.*, 2006; Brophy, 2009; Rakitin and Starikovskii, 2010; Lu, Carter and Wilson, 2011; Li *et al.*, 2013)
Initiation **High-energy arc discharges, lasers, explosives, plasmas, corona discharge, distributed photo ignitions, flame jet ignition**	Arc discharges impart more energy to the gas mixture than conventional spark ignition systems. Non-equilibrium transient plasma discharges are produced by applying high-voltage nanosecond pulses that generate streamers,	Not efficient and the associated circuitry is heavy and bulky Wear away or destroy the electrodes. To overcome is to array them inward around the circumference of the detonation tube Transient plasma reduce ignition delay and ignite leaner mixtures reducing specific fuel consumption, high-repetition rates, high-altitude operation, and reduced NOx emissions The cell sizes are strongly correlated to difficulty to initiate detonations	(Singleton *et al.*, 2009; Lu, Carter and Wilson, 2011) (Kailasanath, 2003)
Hybrid or two-stage system	Smaller amount of fuel and oxidizer mixture may be used to create a hot turbulent jet which continues into another chamber filled with the main	Have extra chamber which adds to weight	(T. H. New *et al.*, 2006)

	fuel- oxidizer mixture to create detonations		
Flash vaporization	Pressurize and heat the liquid fuel prior to mixing with air. Flash vaporization is then accomplished by injecting the liquid fuel into the hot air.	Shorter ignition time and high ignition energy associated with liquid fuels. Benefit of thermal management	(Lu, Carter and Wilson, 2011)
End wall fill process	Sidewall injection to speed up the process. Numbers of ports along the side of the tube are used to fill it with the premix and another set of ports diametrically opposite is used to purge.	Preventing auto-ignition by purging with cool inert gas Sustainability of the detonation wave front.	(Carter and Lu, 2011; Lu, Carter and Wilson, 2011)
Geometric focalization devices	Shock focusing by reflection from concave surfaces, and the interaction between supersonic jets for promoting detonation initiation		(Li and Kailasanath, 2003)
Multiple combustors	Allows continual flow from inlet into the open combustor(s),	Preventing thrust loss from inlet air stagnation and/or expulsion.	(Hinkey *et al.*, 1997)
Bell-shaped nozzle	The converging sections of nozzles introduced shock wave reflections whereas diverging sections generated a negative thrust for a portion of the cycle due to over expansion	Affected the flow dynamics and, hence, the timing of the various phases of the engine cycle	(Kailasanath, 2000)

Appendix B (Spray Analysis)

B.1 Spray Analysis Spreadsheet

EVAPORATION ANALYSIS																							
Rep	**Cd**	**dVp/dt**	**Nu**	**h**	**Ap**	**mp**	**Sc**	**Di,m**	**kc**	**T(kelvin)**	**Pv(MPa)**	**Ci,s**	**Ni**	**dmp/dt**	**mdot**	**Vp**	**dTp/dt**	**Tp(K)**	**Tp(celcius)**	**rhop**	**rp**	**dp**	**dp/do**	**s**
9.878	4.294	-1610203	4.246	31845.66	1.25664E-09	3.39E-12	1.690	1.2E-06	0.254	294.15	0.330	0.000	3.4E-05	-7.9E-12	0.00010179	100.000	4141642	294.150	21.000	810	0.00001	0.00002	1.000	0.002158
8.078	4.964	-1293771	4.031	29850.47	1.28914E-09	3.39E-12	1.690	1.25E-06	0.248	296.15	2.252	0.001	2.0E-04	-4.7E-11	0.00010179	83.898	3747503	335.566	62.416	779.545	1.01E-05	2.03E-05	1.013	0.003034
6.674	5.720	-1054106	3.846	28150.68	1.31956E-09	3.39E-12	1.690	1.29E-06	0.242	298.15	8.865	0.003	6.9E-04	-1.7E-10	0.00010179	70.960	3409408	373.041	99.891	752.6379	1.02E-05	2.05E-05	1.025	0.003689
5.558	6.576	-869039	3.685	26677.76	1.34853E-09	3.39E-12	1.690	1.33E-06	0.237	300.15	24.764	0.007	1.7E-03	-4.3E-10	0.00010179	60.419	3113851	407.136	133.986	728.1584	1.04E-05	2.07E-05	1.036	0.00423
4.659	7.547	-723764	3.542	25392.83	1.37571E-09	3.39E-12	1.690	1.38E-06	0.233	302.15	55.038	0.015	3.5E-03	-8.8E-10	0.00010179	51.729	2850377	438.274	165.124	705.8009	1.05E-05	2.09E-05	1.046	0.004696
3.926	8.649	-608169	3.416	24267.77	1.40053E-09	3.38E-12	1.690	1.42E-06	0.229	304.15	104.132	0.027	6.1E-03	-1.6E-09	0.00010179	44.491	2611501	466.778	193.628	685.3352	1.06E-05	2.11E-05	1.056	0.00511
3.322	9.906	-515137	3.302	23281.9	1.42226E-09	3.36E-12	1.690	1.46E-06	0.226	306.15	175.059	0.043	9.7E-03	-2.5E-09	0.00010179	38.409	2392057	492.893	219.743	666.5847	1.06E-05	2.13E-05	1.064	0.005484
2.820	11.343	-439524	3.200	22419.69	1.44004E-09	3.34E-12	1.690	1.49E-06	0.223	308.15	269.043	0.063	1.4E-02	-3.7E-09	0.00010179	33.258	2188606	516.813	243.663	649.4097	1.07E-05	2.14E-05	1.070	0.005828
2.398	12.995	-377522	3.107	21669.12	1.45301E-09	3.3E-12	1.690	1.53E-06	0.221	310.15	385.535	0.086	1.9E-02	-5E-09	0.00010179	28.863	1998914	538.699	265.549	633.6955	1.08E-05	2.15E-05	1.075	0.006146
2.043	14.902	-326267	3.021	21020.72	1.46033E-09	3.25E-12	1.690	1.57E-06	0.220	312.15	522.479	0.112	2.5E-02	-6.6E-09	0.00010179	25.088	1821548	558.689	285.539	619.3433	1.08E-05	2.16E-05	1.078	0.006443
1.740	17.118	-283562	2.943	20466.84	1.46124E-09	3.18E-12	1.690	1.6E-06	0.218	314.15	676.698	0.141	3.1E-02	-8.2E-09	0.00010179	21.825	1655567	576.904	303.754	606.2646	1.08E-05	2.16E-05	1.078	0.006724
1.481	19.712	-247710	2.870	20001.28	1.45514E-09	3.1E-12	1.690	1.63E-06	0.218	316.15	844.314	0.171	3.7E-02	-9.9E-09	0.00010179	18.989	1500316	593.460	320.310	594.3776	1.08E-05	2.15E-05	1.076	0.00699
1.259	22.772	-217382	2.802	19619.1	1.44159E-09	3E-12	1.690	1.66E-06	0.218	318.15	1021.135	0.202	4.4E-02	-1.2E-08	0.00010179	16.512	1355282	608.463	335.313	583.6053	1.07E-05	2.14E-05	1.071	0.007244
1.067	26.411	-191529	2.738	19316.45	1.42033E-09	2.89E-12	1.690	1.69E-06	0.218	320.15	1202.970	0.233	5.1E-02	-1.3E-08	0.00010179	14.338	1220015	622.016	348.866	573.8744	1.06E-05	2.13E-05	1.063	0.007487
0.901	30.783	-169320	2.678	19090.62	1.39126E-09	2.76E-12	1.690	1.72E-06	0.219	322.15	1385.867	0.263	5.7E-02	-1.5E-08	0.00010179	12.423	1094087	634.216	361.066	565.1147	1.05E-05	2.1E-05	1.052	0.007722
0.757	36.091	-150088	2.622	18940.01	1.35448E-09	2.61E-12	1.690	1.74E-06	0.220	324.15	1566.270	0.292	6.4E-02	-1.6E-08	0.00010179	10.730	977064.9	645.157	372.007	557.2592	1.04E-05	2.08E-05	1.038	0.007949
0.632	42.613	-133299	2.568	18864.32	1.31021E-09	2.45E-12	1.690	1.76E-06	0.222	326.15	1741.111	0.320	7.1E-02	-1.7E-08	0.00010179	9.229	868513.5	654.927	381.777	550.2438	1.02E-05	2.04E-05	1.021	0.008169
0.524	50.736	-118521	2.517	18864.64	1.25882E-09	2.28E-12	1.690	1.78E-06	0.224	328.15	1907.849	0.346	7.8E-02	-1.8E-08	0.00010179	7.896	767992.1	663.613	390.463	544.0079	1E-05	2E-05	1.001	0.008383
0.431	61.007	-105401	2.469	18943.78	1.20078E-09	2.11E-12	1.690	1.8E-06	0.228	330.15	2064.469	0.370	8.4E-02	-1.8E-08	0.00010179	6.711	675062.4	671.292	398.142	538.4937	9.78E-06	1.96E-05	0.978	0.008592
0.350	74.222	-93650.9	2.423	19106.65	1.13664E-09	1.92E-12	1.690	1.82E-06	0.232	332.15	2209.458	0.392	9.1E-02	-1.9E-08	0.00010179	5.657	589295.5	678.043	404.893	533.6468	9.51E-06	1.9E-05	0.951	0.008796
0.281	91.570	-83034.2	2.379	19360.83	1.06701E-09	1.74E-12	1.690	1.83E-06	0.237	334.15	2341.759	0.412	9.7E-02	-1.9E-08	0.00010179	4.720	510277.7	683.936	410.786	529.4156	9.21E-06	1.84E-05	0.921	0.008997
0.222	114.884	-73354.3	2.336	19717.53	9.92531E-10	1.55E-12	1.690	1.85E-06	0.243	336.15	2460.725	0.430	1.0E-01	-1.9E-08	0.00010179	3.890	437616	689.039	415.889	525.7518	8.89E-06	1.78E-05	0.889	0.009193
0.172	147.097	-64447.5	2.296	20192.95	9.13853E-10	1.36E-12	1.690	1.86E-06	0.250	338.15	2566.062	0.445	1.1E-01	-1.9E-08	0.00010179	3.156	370942.7	693.415	420.265	522.6098	8.53E-06	1.71E-05	0.853	0.009387

0.130	193.126	-56176.4	2.257	20810.57	8.31616E-10	1.17E-12	1.690	1.87E-06	0.259	340.15	2657.779	0.459	1.2E-01	-1.8E-08	0.00010179	2.512	309919.2	697.124	423.974	519.9464	8.13E-06	1.63E-05	0.813	0.009578
0.095	261.672	-48425.4	2.220	21605.02	7.46428E-10	9.93E-13	1.690	1.87E-06	0.270	342.15	2736.135	0.470	1.3E-01	-1.7E-08	0.00010179	1.950	254239.3	700.224	427.074	517.7212	7.71E-06	1.54E-05	0.771	0.009765
0.067	369.233	-41095.9	2.185	22628.74	6.58852E-10	8.2E-13	1.690	1.88E-06	0.284	344.15	2801.600	0.479	1.4E-01	-1.6E-08	0.00010179	1.466	203633.4	702.766	429.616	515.8957	7.24E-06	1.45E-05	0.724	0.009951
0.045	549.974	-34103.6	2.151	23964.84	5.69378E-10	6.57E-13	1.690	1.89E-06	0.301	346.15	2854.810	0.487	1.5E-01	-1.5E-08	0.00010179	1.055	157874.1	704.802	431.652	514.4337	6.73E-06	1.35E-05	0.673	0.010134
0.028	883.553	-27374.9	2.119	25753.52	4.78396E-10	5.05E-13	1.690	1.89E-06	0.325	348.15	2896.542	0.493	1.6E-01	-1.4E-08	0.00010179	0.714	116784.4	706.381	433.231	513.3001	6.17E-06	1.23E-05	0.617	0.010315
0.015	1589.786	-20843.6	2.088	28253.78	3.86142E-10	3.66E-13	1.690	1.89E-06	0.357	350.15	2927.682	0.498	1.8E-01	-1.2E-08	0.00010179	0.440	80254.13	707.549	434.399	512.4616	5.54E-06	1.11E-05	0.554	0.010494

Appendix C (Detonation Analysis)

C.1 Detonation velocity calculation using ZND model (Spreadsheet)

Fuel:	C12H24		C12H24+18(O2+3.76N2) -> 12CO2+12H2O+67.68N2														
T1=	1900		T2(guess)=	5065													
P1=	101325		cpCO2=	63.919		cpH2O=	59.412		cpN2=	37.873		assume:	gamma2'=gamma1				
rho1=	0.195383		hfCO2=	-9361.52		hfH2O=	-14252.6		hfN2=	0			P2>>P1				
cpC12H24=	338.3272		cpO2=	37.296		cpN2=	35.595										
hfC12H24=	9577.522		hfO2=	0		hfN2=	0										
Reactant (State 1)		MW	N	lamda	lamda*MW	Yi	cp1	q1	cv1	M1	gamma1	P2'	T2'	rho2'	rho2'/rho1	V2'	M2'
C12H24		168.322	1	0.011504	1.93629357	0.06356	3.89195	608.7506	1021.525	3.105108829	1.267195	1080140	4240.145	0.933301	4.77679	526.9603	0.435138
O2		31.999	18.25	0.209939	6.71783907	0.220518	7.829886	0									
N2		28.013	67.68	0.778557	21.8097301	0.715921	27.71275	0									
SUM			86.93		30.4638628		1.294471	608.7506									
Product (State 2)		MW	N	lamda	lamda*MW	Yi	cp2	q2	R2	gamma2	q	Vd	T2	rho2	P2	V2	M2
CO2		44.011	12	0.13089	5.76060209	0.200032	8.366361	-1872.6	0.288731	1.232350817	3648.397	2517.178	5426.81	0.353927	554563.5	1389.588	1
H2O		18.016	12	0.13089	2.35811518	0.081883	7.77644	-1167.05									
N2		28.013	67.68	0.73822	20.6797539	0.718085	27.9586	0									
SUM			91.68		28.7984712		1.53138	-3039.65									
Calculating state 2 for detonation																	
mass flux=	3000		molecular weight=		168.322												
T1=	2000		gamma1=		1.2672												
P1=	101325		q=		3648397.09												
R1=	49.39937		T2/T3=		0.36												

C.2 Variation of initial mass flux for KE fuel.

P1	T1	v1	M1	V1	c1	a	b	c	massflux	v21	v22	P21	P22	V21	V22	T21	T22	A21	A22	M21(stron	M22(weak	P21/P1	P22/P1	T21/T1	T22/T1	v21/v1	v22/v1	M21/M1	M22/M1	ηH1	ηH2
101325	1467	0.715212	7.0804	2145.636	303.038861	-3.8E+07	31007673	-6293960	3000	0.400247099	0.411841	2936010	2831663	1200.741	1235.524	23788.35	23607.5	1220.297	1215.649	0.983975	1.016349	28.97617	27.94634	16.21565	16.09237	0.55962	0.575831	0.138972	0.143544	0.759793	0.759467
		0.715212	7.198407	2181.397	303.038861	-3.9E+07	32033725	-6371328	3050	0.348679069	0.463	3510999	2447528	1063.471	1412.15	24781.93	22939.68	1245.52	1198.331	0.853837	1.17843	34.65086	24.15522	16.89293	15.63714	0.487518	0.64736	0.118615	0.163707	0.761541	0.758237
		0.715212	7.316413	2217.158	303.038861	-4.1E+07	33076735	-6449976	3100	0.325983535	0.485306	3841812	2310723	1010.549	1504.449	25351.89	22700.85	1259.762	1192.077	0.802175	1.26204	37.91573	22.80506	17.28145	15.47434	0.455786	0.678548	0.10964	0.172494	0.762509	0.757788
		0.715212	7.43442	2252.918	303.038861	-4.2E+07	34136705	-6529902	3150	0.309130882	0.501787	4130666	2219032	973.7623	1580.63	25848.84	22540.41	1272.049	1187.857	0.765507	1.330657	40.76651	21.90014	17.62021	15.36497	0.432223	0.701592	0.102968	0.178986	0.763335	0.757484
		0.715212	7.552427	2288.679	303.038861	-4.3E+07	35213635	-6611107	3200	0.295391292	0.515173	4400290	2149725	945.2521	1648.554	26312.23	22418.92	1283.4	1184.651	0.736522	1.391594	43.42749	21.21613	17.93608	15.28215	0.413012	0.720308	0.097521	0.184258	0.764089	0.757251
		0.715212	7.670433	2324.439	303.038861	-4.5E+07	36307524	-6693591	3250	0.283684955	0.526542	4659331	2094156	921.9761	1711.261	26757.07	22321.35	1294.203	1182.071	0.712389	1.44768	45.98402	20.66772	18.23931	15.21565	0.396644	0.736204	0.092875	0.188735	0.7648	0.757064
		0.715212	7.78844	2360.2	303.038861	-4.6E+07	37418372	-6777354	3300	0.273447885	0.536456	4912138	2047976	902.378	1770.306	27190.91	22240.16	1304.653	1179.919	0.691661	1.500362	48.47903	20.21195	18.53504	15.1603	0.382331	0.750066	0.088806	0.19264	0.76548	0.756907
		0.715212	7.906447	2395.961	303.038861	-4.8E+07	38546181	-6862395	3350	0.264339297	0.545257	5161245	2008650	885.5366	1826.61	27618.17	22170.93	1314.864	1178.081	0.673482	1.550496	50.93753	19.82383	18.82629	15.11311	0.369596	0.762371	0.085181	0.196105	0.766139	0.756773
		0.715212	8.024454	2431.721	303.038861	-4.9E+07	39690948	-6948716	3400	0.256133536	0.553168	5408274	1974557	870.854	1880.771	28041.66	22110.84	1324.906	1176.484	0.657295	1.598637	53.37551	19.14787	19.11497	15.07215	0.358122	0.773432	0.081911	0.199221	0.766782	0.756656
		0.715212	8.14246	2467.482	303.038861	-5E+07	40852676	-7036315	3450	0.248671451	0.560348	5654325	1944596	857.9165	1933.2	28463.31	22057.98	1334.83	1175.077	0.642716	1.64517	55.80385	19.19167	19.40239	15.03612	0.347689	0.783471	0.078934	0.202048	0.767411	0.756553
		0.715212	8.260467	2503.242	303.038861	-5.2E+07	42031362	-7125193	3500	0.241835482	0.566914	5900189	1917978	846.4242	1984.199	28884.48	22010.98	1344.669	1173.824	0.629466	1.690372	58.23034	18.92897	19.68949	15.00407	0.338131	0.792651	0.076202	0.204634	0.768029	0.756462
		0.715212	8.378474	2539.003	303.038861	-5.3E+07	43227008	-7215350	3550	0.235535674	0.572955	6146448	1894119	836.1516	2033.991	29306.2	21968.81	1354.45	1172.699	0.617337	1.734453	60.66072	18.6935	19.97696	14.97533	0.329323	0.801098	0.073681	0.207013	0.768638	0.756379
		0.715212	8.49648	2574.764	303.038861	-5.5E+07	44439614	-7306786	3600	0.229701254	0.578542	6393546	1872575	826.9245	2082.75	29729.24	21930.69	1364.191	1171.681	0.606165	1.777574	63.09939	18.48087	20.26533	14.94935	0.321165	0.808909	0.071343	0.209213	0.76924	0.756304
		0.715212	8.614487	2610.524	303.038861	-5.7E+07	45669180	-7399500	3650	0.224275279	0.58373	6641831	1852998	818.6048	2130.614	30154.2	21896.04	1373.907	1170.755	0.595823	1.819863	65.54978	18.28767	20.55501	14.92572	0.313579	0.816163	0.069165	0.211256	0.769835	0.756236
		0.715212	8.732494	2646.285	303.038861	-5.8E+07	46915704	-7493494	3700	0.21921108	0.588566	6891579	1835114	811.081	2177.693	30581.58	21864.35	1383.608	1169.908	0.586207	1.861423	68.0146	18.11116	20.84634	14.90412	0.306498	0.822925	0.067129	0.213161	0.770424	0.756174
		0.715212	8.8505	2682.045	303.038861	-6E+07	48179189	-7588766	3750	0.214469815	0.593088	7143014	1818697	804.2618	2224.08	31011.75	21835.25	1393.306	1169.129	0.577233	1.902339	70.49607	17.94915	21.13957	14.88428	0.299869	0.829248	0.06522	0.214941	0.771008	0.756116
		0.715212	8.968507	2717.806	303.038861	-6.1E+07	49459633	-7685317	3800	0.210018731	0.597328	7396318	1803566	798.0712	2269.848	31445.04	21808.4	1403.006	1168.41	0.56883	1.942681	72.99598	17.79981	21.43493	14.86599	0.293645	0.835177	0.063425	0.216611	0.771587	0.756063
		0.715212	9.086514	2753.567	303.038861	-6.3E+07	50757036	-7783147	3850	0.205829898	0.601315	7651643	1789568	792.4451	2315.062	31881.72	21783.55	1412.714	1167.744	0.560938	1.982508	75.51585	17.66166	21.7326	14.84905	0.287789	0.84075	0.061733	0.218181	0.772162	0.756014
		0.715212	9.20452	2789.327	303.038861	-6.5E+07	52071399	-7882255	3900	0.201879268	0.605071	7909118	1776575	787.3291	2359.776	32322.01	21760.47	1422.435	1167.125	0.553508	2.02187	78.05692	17.53343	22.03273	14.83332	0.282265	0.846002	0.060134	0.219661	0.772733	0.755969
		0.715212	9.322527	2825.088	303.038861	-6.6E+07	53402721	-7982643	3950	0.198145957	0.608617	8168850	1764479	782.6765	2404.036	32766.1	21738.98	1432.174	1166.549	0.546496	2.060811	80.62028	17.41406	22.33545	14.81866	0.277045	0.85096	0.058621	0.221057	0.773301	0.755926
		0.715212	9.440534	2860.849	303.038861	-6.8E+07	54751003	-8084309	4000	0.194611696	0.611971	8430932	1753189	778.4468	2447.883	33214.15	21718.9	1441.932	1166.01	0.539864	2.099367	83.20683	17.30263	22.64087	14.80498	0.272103	0.855649	0.057186	0.222378	0.773865	0.755886
		0.715212	9.55854	2896.609	303.038861	-7E+07	56116245	-8187254	4050	0.191260395	0.615148	8695443	1742623	774.6046	2491.35	33666.3	21700.11	1451.714	1165.505	0.533579	2.137571	85.81735	17.19835	22.94908	14.79216	0.267418	0.860092	0.055822	0.223629	0.774426	0.755849
		0.715212	9.676547	2932.37	303.038861	-7.1E+07	57498446	-8291478	4100	0.188077801	0.618163	8962453	1732714	771.119	2534.47	34122.67	21682.47	1461.52	1165.031	0.527614	2.175452	88.45253	17.10055	23.26017	14.78014	0.262968	0.864308	0.054525	0.224817	0.774983	0.755814
		0.715212	9.794554	2968.13	303.038861	-7.3E+07	58897606	-8396981	4150	0.18505122	0.621029	9232021	1723400	767.9626	2577.269	34583.38	21665.88	1471.353	1164.586	0.521943	2.213035	91.11297	17.00864	23.57422	14.76884	0.258736	0.868314	0.053289	0.225945	0.775538	0.755781
		0.715212	9.91256	3003.891	303.038861	-7.5E+07	60313726	-8503762	4200	0.182169291	0.623755	9504201	1714630	765.111	2619.771	35048.5	21650.26	1481.215	1164.166	0.516543	2.250341	93.79917	16.92209	23.89127	14.75819	0.254707	0.872126	0.05211	0.227019	0.776089	0.75575
		0.715212	10.03057	3039.652	303.038861	-7.7E+07	61746806	-8611823	4250	0.179421807	0.626352	9779038	1706358	762.5427	2661.997	35518.12	21635.52	1491.105	1163.769	0.511394	2.287392	96.5116	16.84044	24.2114	14.74814	0.250865	0.875757	0.050984	0.228042	0.776638	0.755721
		0.715212	10.14857	3075.412	303.038861	-7.8E+07	63196845	-8721162	4300	0.176799554	0.628829	10056574	1698541	760.2381	2703.967	35992.32	21621.58	1501.026	1163.394	0.506479	2.324205	99.25066	16.76329	24.53464	14.73864	0.247199	0.879221	0.049906	0.229018	0.777185	0.755693
		0.715212	10.26658	3111.173	303.038861	-8E+07	64663843	-8831780	4350	0.174294191	0.631195	10336845	1691143	758.1797	2745.697	36471.16	21608.39	1510.978	1163.039	0.501781	2.360795	102.0167	16.69028	24.86105	14.72964	0.243696	0.882528	0.048875	0.229949	0.777728	0.755667
		0.715212	10.38459	3146.933	303.038861	-8.2E+07	66147801	-8943677	4400	0.171898139	0.633456	10619884	1684132	756.3518	2787.205	36954.69	21595.88	1520.961	1162.703	0.497286	2.397177	104.8101	16.62109	25.19065	14.72111	0.240346	0.885689	0.047887	0.23084	0.778269	0.755642
		0.715212	10.50259	3182.694	303.038861	-8.4E+07	67648719	-9056852	4450	0.169604489	0.635619	10905720	1677478	754.74	2828.502	37442.97	21584	1530.976	1162.383	0.49298	2.433365	107.6311	16.55542	25.5235	14.71302	0.237139	0.888713	0.046939	0.231692	0.778807	0.755618
		0.715212	10.6206	3218.455	303.038861	-8.6E+07	69166596	-9171307	4500	0.167406927	0.63769	11194380	1671155	753.3312	2869.604	37936.05	21572.71	1541.024	1162.079	0.488851	2.469371	110.4799	16.49302	25.85961	14.70532	0.234066	0.891609	0.046029	0.232508	0.779343	0.755595
		0.715212	10.73861	3254.215	303.038861	-8.8E+07	70701433	-9287040	4550	0.16529967	0.639675	11485888	1665139	752.1135	2910.52	38433.96	21561.96	1551.104	1161.789	0.484889	2.505204	113.3569	16.43365	26.19902	14.698	0.23112	0.894385	0.045154	0.233289	0.779876	0.755574
		0.715212	10.85661	3289.976	303.038861	-9E+07	72253229	-9404052	4600	0.163277401	0.641579	11780264	1659409	751.076	2951.262	38936.75	21551.73	1561.216	1161.514	0.481084	2.540876	116.2622	16.3771	26.54175	14.69102	0.228292	0.897047	0.044313	0.234039	0.780407	0.755553
		0.715212	10.97462	3325.736	303.038861	-9.2E+07	73821985	-9522343	4650	0.161335229	0.643406	12077528	1653946	750.2088	2991.839	39444.45	21541.96	1571.362	1161.25	0.477426	2.576395	119.1959	16.32318	26.88783	14.68437	0.225577	0.899602	0.043503	0.234759	0.780935	0.755534
		0.715212	11.09263	3361.497	303.038861	-9.4E+07	75407700	-9641913	4700	0.159468639	0.645162	12377699	1648731	749.5026	3032.262	39957.09	21532.64	1581.54	1160.999	0.473907	2.611769	122.1584	16.27171	27.23728	14.67801	0.222967	0.902057	0.042723	0.235451	0.781461	0.755515
		0.715212	11.21063	3397.258	303.038861	-9.6E+07	77010375	-9762761	4750	0.157673457	0.64685	12680791	1643749	748.9489	3072.537	40474.69	21523.73	1591.751	1160.759	0.470519	2.647007	125.1497	16.22254	27.59011	14.67194	0.220457	0.904417	0.041971	0.236116	0.781984	0.755497
		0.715212	11.32864	3433.018	303.038861	-9.8E+07	78630009	-9884889	4800	0.155945817	0.648473	12986821	1638984	748.5399	3112.673	40997.3	21515.21	1601.994	1160.529	0.467255	2.682115	128.17	16.17552	27.94635	14.66613	0.218041	0.906687	0.041245	0.236755	0.782505	0.75548
		0.715212	11.44665	3468.779	303.038861	-1E+08	80266603	-1E+07	4850	0.154282132	0.650036	13295801	1634423	748.2683	3152.676	41524.92	21507.05	1612.27	1160.309	0.464109	2.7171	131.2194	16.13051	28.30601	14.66057	0.215715	0.908872	0.040545	0.237371	0.783024	0.755464
		0.715212	11.56465	3504.539	303.038861	-1E+08	81920156	-1E+07	4900	0.152679068	0.651542	13607744	1630055	748.1274	3192.554	42057.58	21499.23	1622.577	1160.098	0.461074	2.751969	134.298	16.08739	28.66911	14.65524	0.213474	0.910977	0.039869	0.237964	0.78354	0.755448
		0.715212	11.68266	3540.3	303.038861	-1E+08	83590669	-1E+07	4950	0.151133523	0.652992	13922661	1625866	748.1109	3232.312	42595.3	21491.73	1632.917	1159.896	0.458144	2.786726	137.406	16.04605	29.03565	14.65012	0.211313	0.913005	0.039216	0.238535	0.784053	0.755433
		0.715212	11.80067	3576.061	303.038861	-1.1E+08	85278141	-1E+07	5000	0.149642601	0.654391	14240563	1621847	748.213	3271.956	43138.1	21484.54	1643.288	1159.702	0.455314	2.821378	140.5434	16.00639	29.40566	14.64522	0.209228	0.914961	0.038584	0.239086	0.784564	0.755419
		0.715212	11.91867	3611.821	303.038861	-1.1E+08	86982573	-1.1E+07	5050	0.148203603	0.655741	14561460	1617988	748.4282	3311.492	43686	21477.63	1653.691	1159.515	0.45258	2.855928	143.7104	15.9683	29.77914	14.64051	0.207216	0.916848	0.037972	0.239618	0.785073	0.755405
		0.715212	12.03668	3647.582	303.038861	-1.1E+08	88703965	-1.1E+07	5100	0.146814003	0.657044	14885360	1614280	748.7514	3350.924	44239.02	21470.98	1664.125	1159.336	0.449937	2.890383	146.9071	15.93171	30.15611	14.63598	0.205273	0.91867	0.03738	0.240131	0.785579	0.755392
		0.715212	12.15469	3683.342	303.038861	-1.1E+08	90442316	-1.1E+07	5150	0.145471436	0.658302	15212273	1610715	749.1779	3390.257	44797.16	21464.6	1674.59	1159.163	0.44738	2.924745	150.1335	15.89652	30.53658	14.63163	0.203396	0.920429	0.036807	0.240627	0.786083	0.755379
		0.715212	12.27269	3719.103	303.038861	-1.1E+08	92197626	-1.1E+07	5200	0.144173689	0.659518	15542204	1607285	749.7032	3429.495	45360.44	21458.45	1685.085	1158.997	0.444905	2.959019	153.3896	15.86267	30.92055	14.62744	0.201582	0.92213	0.036252	0.241106	0.786585	0.755366
		0.715212	12.3907	3754.864	303.038861	-1.2E+08	93969896	-1.1E+07	5250	0.14291868	0.660694	15875163	1603982	750.3231	3468.643	45928.88	21452.53	1695.611	1158.837	0.442509	2.993209	156.6757	15.83007	31.30803	14.6234	0.199827	0.923773	0.035713	0.241569	0.787084	0.755354
		0.715212	12.50871	3790.624	303.038861	-1.2E+08	95759125	-1.1E+07	5300	0.141704459	0.661831	16211156	1600801	751.0336	3507.704	46502.48	21446.83	1706.166	1158.683	0.440188	3.027319	159.9917	15.79868	31.69903	14.61951	0.198129	0.925363	0.035191	0.242017	0.78758	0.755343
		0.715212	12.62671	3826.385	303.038861	-1.2E+08	97565314	-1.1E+07	5350	0.140529189	0.662931	16550188	1597734	751.8312	3546.682	47081.26	21441.33	1716.751	1158.535	0.437938	3.061351	163.3377	15.76841	32.09357	14.61577	0.196486	0.926902	0.034683	0.24245	0.788075	0.755332
		0.715212	12.74472	3862.146	303.038861	-1.2E+08	99388463	-1.1E+07	5400	0.13939114	0.663996	16892265	1594777	752.7122	3585.58	47665.23	21436.02	1727.365	1158.392	0.435757	3.095309	166.7137	15.73922	32.49164	14.61215	0.194895	0.928391	0.034191	0.24287	0.788566	0.755321
		0.715212	12.86273	3897.906	303.038861	-1.3E+08	1.01E+08	-1.2E+07	5450	0.138288686	0.665028	17237394	1591923	753.6733	3624.402	48254.4	21430.91	1738.008	1158.253	0.433642	3.129196	170.1198	15.71106	32.89325	14.60866	0.193353	0.929833	0.033713	0.243276	0.789056	0.755311
		0.715212	12.98073	3933.667	303.038861	-1.3E+08	1.03E+08	-1.2E+07	5500	0.137220288	0.666027	17585578	1589168	754.7116	3663.15	48848.77	21425.96	1748.679	1158.12	0.43159	3.163015	173.5562	15.68387	33.29841	14.60529	0.19186	0.93123	0.033248	0.24367	0.789543	0.755301
		0.715212	13.09874	3969.427	303.038861	-1.3E+08	1.05E+08	-1.2E+07	5550	0.136184498	0.666996	17936824	1586506	755.824	3701.827	49448.35	21421.19	1759.378	1157.991	0.429597	3.196768	177.0227	15.6576	33.70713	14.60204	0.190411	0.932585	0.032797	0.244052	0.790027	0.755291
		0.715212	13.21675	4005.188	303.038861	-1.3E+08	1.07E+08	-1.2E+07	5600	0.135179946	0.667935	18291134	1583934	757.0077	3740.436	50053.16	21416.57	1770.105	1157.866	0.427663	3.230457	180.5195	15.63221	34.1194	14.59889	0.189007	0.933898	0.032358	0.244422	0.790509	0.755282
		0.715212	13.33475	4040.949	303.038861	-1.4E+08	1.09E+08	-1.2E+07	5650	0.134205335	0.668846	18648514	1581447	758.2601	3778.98	50663.2	21412.11	1780.859	1157.745	0.425783	3.264086	184.0465	15.60767	34.53524	14.59585	0.187644	0.935172	0.03193	0.24478	0.790989	0.755273
		0.715212	13.45276	4076.709	303.038861	-1.4E+08	1.11E+08	-1.2E+07	5700	0.133259441	0.66973	19008968	1579041	759.5788	3817.461	51278.48	21407.79	1791.64	1157.628	0.423957	3.297656	187.6039	15.58393	34.95466	14.5929	0.186322	0.936407	0.031515	0.245129	0.791466	0.755264
		0.715212	13.57077	4112.47	303.038861	-1.4E+08	1.13E+08	-1.2E+07	5750	0.132341101	0.670588	19372498	1576713	760.9613	3855.881	51899	21403.61	1802.448	1157.515	0.422182	3.33117	191.1917	15.56095	35.37764	14.59005	0.185038	0.937607	0.03111	0.245467	0.791941	0.755256
		0.715212	13.68877	4148.23	303.038861	-1.4E+08	1.15E+08	-1.3E+07	5800	0.131449215	0.671421	19739109	1574459	762.4054	3894.242	52524.77	21399.56	1813.282	1157.406	0.420456	3.364629	194.8099	15.5387	35.80421	14.58729	0.183791	0.938772	0.030715	0.245795	0.792414	0.755248
		0.715212	13.80678	4183.991	303.038861	-1.5E+08	1.17E+08	-1.3E+07	5850	0.13058274	0.67223	20108804	1572276	763.909	3932.546	53155.8	21395.64	1824.142	1157.3	0.418777	3.398036	198.4585	15.51715	36.23436	14.58462	0.182579	0.939903	0.030331	0.246114	0.792884	0.75524
		0.715212	13.92479	4219.752	303.038861	-1.5E+08	1.19E+08	-1.3E+07	5900	0.129740684	0.673016	20481586	1570160	765.47	3970.796	53792.09	21391.84	1835.027	1157.197	0.417144	3.431392	202.1375	15.49627	36.66809	14.58203	0.181402	0.941002	0.029957	0.246423	0.793352	0.755232
		0.715212	14.04279	4255.512	303.038861	-1.5E+08	1.21E+08	-1.3E+07	5950	0.128922107	0.67378	20857458	1568109	767.0865	4008.994	54433.64	21388.16	1845.937	1157.097	0.415554	3.464699	205.8471	15.47603	37.10541	14.57952	0.180257	0.942071	0.029592	0.246724	0.793817	0.755225
		0.715212	14.1608	4291.273	303.038861	-1.5E+08	1.23E+08	-1.3E+07	6000	0.128126113	0.674523	21236422	1566120	768.7567	4047.14	55080.47	21384.58	1856.872	1157.001	0.414006	3.497958	209.5872	15.45641	37.54633	14.57708	0.179144	0.94311	0.029236	0.247017	0.79428	0.755218

C.3 Variation of initial pressure for KE fuel.

P1	T1	v1	M1	V1	c1	a	b	c	massflux	v21	v22	P21	P22	V21	V22	T21	T22	A21	A22	M21(stron	M22(weak	P21/P1	P22/P1	T21/T1	T22/T1	v21/v1	v22/v1	M21/M1	M22/M1	ηH1	ηH2
101325	1467	0.715212	8.968507	2717.806	303.038861	-6.1E+07	49459633	-7685317	3800	0.210018731	0.597328	7396318	1803566	798.0712	2269.848	31445.04	21808.4	1403.006	1168.41	0.56883	1.942681	72.99598	17.79981	21.43493	14.86599	0.293645	0.835177	0.063425	0.216611	0.771587	0.756063
102325		0.708223	8.88086	2691.246	303.038861	-6.1E+07	48985713	-7613483		0.211213644	0.588398	7279133	1832598	802.6118	2235.911	31122.91	21828.13	1395.801	1168.938	0.575019	1.91277	71.13739	17.90958	21.21535	14.87944	0.298231	0.830809	0.064748	0.215381	0.771157	0.756102
103325		0.701368	8.794909	2665.199	303.038861	-6.1E+07	48521059	-7543725		0.212471472	0.579555	7162994	1862308	807.3916	2202.309	30808.73	21848.66	1388.738	1169.488	0.581385	1.88314	69.32488	18.02379	21.00118	14.89343	0.302939	0.826321	0.066105	0.214117	0.770734	0.756143
104325		0.694645	8.710606	2639.652	303.038861	-6.1E+07	48065403	-7475963		0.21379494	0.570794	7047804	1892742	812.4208	2169.016	30502.11	21870.02	1381.81	1170.059	0.58794	1.853766	67.55623	18.14275	20.79217	14.90799	0.307776	0.821705	0.067497	0.212817	0.770315	0.756185
105325		0.68805	8.627904	2614.59	303.038861	-6.1E+07	47618490	-7410123		0.215187134	0.562106	6933465	1923951	817.7111	2136.004	30202.67	21892.29	1375.01	1170.655	0.594695	1.824623	65.82924	18.26681	20.58805	14.92317	0.312749	0.816956	0.068927	0.211479	0.769902	0.756229
106325		0.681579	8.546757	2590	303.038861	-6.1E+07	47180072	-7346131		0.216651559	0.553486	6819875	1955993	823.2759	2103.245	29910.03	21915.54	1368.333	1171.276	0.601664	1.795687	64.14178	18.39636	20.38857	14.93902	0.317867	0.812064	0.070397	0.210102	0.769494	0.756274
107325		0.675228	8.467123	2565.867	303.038861	-6.1E+07	46749913	-7283919		0.218192203	0.544923	6706925	1988929	829.1304	2070.708	29623.84	21939.83	1361.771	1171.925	0.608862	1.766929	62.49173	18.53184	20.19348	14.95558	0.323138	0.807021	0.071909	0.208681	0.769091	0.756322
108325		0.668995	8.388959	2542.181	303.038861	-6.1E+07	46327783	-7223423		0.21981361	0.536411	6594502	2022833	835.2917	2038.363	29343.72	21965.26	1355.317	1172.604	0.616307	1.738321	60.87701	18.67374	20.00254	14.97291	0.328573	0.801817	0.073466	0.207215	0.768692	0.756372
109325		0.662876	8.312225	2518.927	303.038861	-6.1E+07	45913463	-7164579		0.221520986	0.527941	6482485	2057783	841.7797	2006.175	29069.33	21991.94	1348.965	1173.316	0.624019	1.709833	59.29554	18.82262	19.81549	14.99109	0.334182	0.79644	0.075072	0.205701	0.768297	0.756424
110325		0.656867	8.236882	2496.095	303.038861	-6.1E+07	45506740	-7107327		0.223320316	0.519502	6370741	2093873	848.6172	1974.109	28800.29	22019.96	1342.708	1174.063	0.632019	1.681433	57.74522	18.97913	19.6321	15.0102	0.339978	0.790879	0.07673	0.204135	0.767906	0.756479
111325		0.650967	8.162892	2473.674	303.038861	-6.1E+07	45107408	-7051612		0.225218516	0.511086	6259129	2131207	855.8304	1942.126	28536.23	22049.46	1336.539	1174.849	0.640333	1.653085	56.22393	19.14401	19.4521	15.03031	0.345975	0.785118	0.078444	0.202512	0.767518	0.756537
112325		0.645171	8.09022	2451.651	303.038861	-6.1E+07	44715272	-6997378		0.22722363	0.50268	6147490	2169905	863.4498	1910.183	28276.78	22080.59	1330.449	1175.679	0.648991	1.624749	54.72949	19.3181	19.27524	15.05153	0.352191	0.779141	0.080219	0.200829	0.767134	0.756597
113325		0.639478	8.01883	2430.017	303.038861	-6.1E+07	44330139	-6944574		0.22934508	0.494272	6035648	2210110	871.5113	1878.232	28021.54	22113.53	1324.431	1176.555	0.658027	1.596382	53.25963	19.5024	19.10125	15.07398	0.358644	0.772929	0.08206	0.199079	0.766751	0.756662
114325		0.633885	7.94869	2408.762	303.038861	-6.1E+07	43951827	-6893149		0.231593993	0.485847	5923403	2251985	880.0572	1846.22	27770.08	22148.48	1318.475	1177.485	0.667481	1.567935	51.81197	19.6981	18.92985	15.09781	0.365357	0.76646	0.083974	0.197257	0.766371	0.756729
115325		0.628388	7.879766	2387.875	303.038861	-6.1E+07	43580159	-6843056		0.233983639	0.477391	5810527	2295728	889.1378	1814.085	27521.98	22185.7	1312.572	1178.473	0.677401	1.539351	50.38393	19.9066	18.76072	15.12317	0.372355	0.759707	0.085967	0.195355	0.765992	0.756802
116325		0.622986	7.812026	2367.348	303.038861	-6.1E+07	43214961	-6794249		0.236530022	0.468883	5696752	2341573	898.8141	1781.756	27276.73	22225.47	1306.71	1179.529	0.687845	1.510565	48.97272	20.12958	18.59354	15.15029	0.379671	0.752638	0.088049	0.193364	0.765614	0.756879
117325		0.617676	7.745442	2347.17	303.038861	-6.1E+07	42856071	-6746685		0.239252703	0.460302	5581761	2389807	909.1603	1749.148	27033.78	22268.17	1300.878	1180.662	0.698882	1.481498	47.57521	20.36912	18.42793	15.17939	0.387343	0.745216	0.090231	0.191274	0.765235	0.756961
118325		0.612456	7.679983	2327.333	303.038861	-6.1E+07	42503326	-6700322		0.242175964	0.451621	5465170	2440785	920.2687	1716.159	26792.51	22314.25	1295.06	1181.883	0.710599	1.452056	46.18779	20.62781	18.26347	15.2108	0.395418	0.737393	0.092526	0.18907	0.764856	0.75705
119325		0.607323	7.615621	2307.829	303.038861	-6.1E+07	42156573	-6655119		0.245330528	0.442806	5346503	2494954	932.256	1682.663	26552.17	22364.28	1289.239	1183.207	0.723106	1.422121	44.80622	20.9089	18.09964	15.24491	0.403954	0.729111	0.09495	0.186737	0.764474	0.757146
120325		0.602276	7.552329	2288.649	303.038861	-6.1E+07	41815663	-6611039		0.248756151	0.433816	5225153	2552892	945.2734	1648.5	26311.85	22419.01	1283.391	1184.654	0.736544	1.391546	43.42533	21.21664	17.93582	15.28221	0.413027	0.720294	0.097525	0.184254	0.764088	0.757251
121325		0.597312	7.49008	2269.785	303.038861	-6.1E+07	41480451	-6568044		0.252505757	0.424594	5100326	2615367	959.5219	1613.459	26070.41	22479.44	1277.489	1186.249	0.7511	1.360134	42.03854	21.5567	17.77124	15.32341	0.422737	0.710842	0.100279	0.181591	0.763697	0.757367
122325		0.592429	7.428849	2251.23	303.038861	-6.1E+07	41150797	-6526100		0.256652344	0.415067	4970939	2683435	975.2789	1577.254	25826.31	22546.94	1271.494	1188.029	0.767034	1.327622	40.63715	21.93693	17.60484	15.36942	0.43322	0.700619	0.103251	0.178712	0.763298	0.757496
123325		0.587625	7.368611	2232.975	303.038861	-6.1E+07	40826566	-6485172		0.261301374	0.405125	4835440	2758625	992.9452	1539.476	25577.4	22623.53	1265.352	1190.045	0.784718	1.293628	39.20892	22.36874	17.43517	15.42163	0.444674	0.689428	0.106495	0.175559	0.762886	0.757642
124325		0.582899	7.309342	2215.015	303.038861	-6.1E+07	40507627	-6445227		0.266615123	0.394605	4691458	2843281	1013.137	1499.5	25320.44	22712.31	1258.98	1192.378	0.804729	1.257571	37.73544	22.86975	17.26002	15.48215	0.457395	0.676971	0.110096	0.17205	0.762457	0.75781
125325		0.578248	7.251019	2197.341	303.038861	-6.1E+07	40193853	-6406235		0.272867013	0.383232	4535019	2941356	1036.895	1456.28	25050.06	22818.52	1252.24	1195.163	0.828032	1.218478	36.18607	23.46983	17.07571	15.55455	0.471886	0.662747	0.114195	0.168042	0.762	0.75801
126325		0.57367	7.193619	2179.946	303.038861	-6.1E+07	39885123	-6368164		0.280588992	0.37047	4358415	3060533	1066.238	1407.786	24755.85	22952.44	1244.865	1198.665	0.856509	1.174462	34.50161	24.22746	16.87516	15.64583	0.489112	0.645789	0.119065	0.163264	0.761496	0.758261
127325		0.569164	7.137121	2162.825	303.038861	-6.1E+07	39581316	-6330988		0.291139178	0.354961	4142011	3220428	1106.329	1348.851	24411.28	23140.49	1236.171	1203.565	0.894964	1.120713	32.53101	25.29297	16.64027	15.77402	0.51152	0.623652	0.125396	0.157026	0.760898	0.758611
128325		0.564729	7.081504	2145.971	303.038861	-6.1E+07	39282318	-6294677		0.314263496	0.326956	3745049	3561773	1194.201	1242.432	23824.85	23574.03	1221.232	1214.787	0.977866	1.022757	29.1841	27.75588	16.24052	16.06955	0.556485	0.57896	0.138087	0.144426	0.759859	0.759406

C.4 Variation of initial temperature for KE fuel.

P1	T1	v1	M1	V1	c1	a	b	c	massflux	v21	v22	P21	P22	V21	V22	T21	T22	A21	A22	M21(stron	M22(weak	P21/P1	P22/P1	T21/T1	T22/T1	v21/v1	v22/v1	M21/M1	M22/M1	ηH1	ηH2
101325	2000	0.975068	16.53437	5850.406	353.832944	-1.5E+08	1.67E+08	-2.1E+07	6000	0.146906931	0.946223	29915111	1139724	881.4416	5677.34	88963.43	21830.91	2359.875	1169.013	0.373512	4.856526	295.2392	11.2482	44.48172	10.91545	0.150663	0.970418	0.02259	0.293723	0.800844	0.742621
	2010	0.979943	16.57566	5879.658	354.716423	-1.5E+08	1.68E+08	-2.1E+07		0.147327174	0.951253	30075495	1134167	883.963	5707.518	89696.25	21839.96	2369.575	1169.255	0.373047	4.881329	296.8221	11.19336	44.625	10.86565	0.150343	0.970723	0.022506	0.294488	0.800967	0.74242
	2020	0.984818	16.61684	5908.91	355.597707	-1.5E+08	1.69E+08	-2.2E+07		0.147749118	0.956281	30235817	1128672	886.4947	5737.685	90432.64	21849.02	2379.282	1169.497	0.372589	4.906112	298.4043	11.13913	44.76864	10.81635	0.150027	0.971023	0.022422	0.295249	0.80109	0.742221
	2030	0.989694	16.65792	5938.162	356.476813	-1.5E+08	1.69E+08	-2.2E+07		0.148172733	0.961307	30396079	1123238	889.0364	5767.843	91172.63	21858.1	2388.996	1169.74	0.372138	4.930874	299.986	11.08549	44.91263	10.76754	0.149716	0.971318	0.02234	0.296008	0.801213	0.742022
	2040	0.994569	16.6989	5967.414	357.353756	-1.5E+08	1.7E+08	-2.2E+07		0.148597992	0.966332	30556282	1117862	891.588	5797.991	91916.2	21867.2	2398.719	1169.984	0.371693	4.955617	301.5671	11.03244	45.05696	10.71922	0.149409	0.971609	0.022259	0.296763	0.801336	0.741824
	2050	0.999444	16.73978	5996.666	358.228552	-1.5E+08	1.71E+08	-2.2E+07		0.149024868	0.971355	30716427	1112545	894.1492	5828.13	92663.36	21876.31	2408.448	1170.227	0.371255	4.980339	303.1476	10.97996	45.20164	10.67137	0.149108	0.971895	0.022178	0.297515	0.801458	0.741627
	2060	1.00432	16.78056	6025.918	359.101218	-1.5E+08	1.72E+08	-2.2E+07		0.149453332	0.976376	30876514	1107284	896.72	5858.258	93414.11	21885.43	2418.185	1170.471	0.370824	5.005042	304.7275	10.92805	45.34666	10.624	0.148811	0.972177	0.022098	0.298264	0.801581	0.741432
	2070	1.009195	16.82124	6055.17	359.971767	-1.5E+08	1.73E+08	-2.2E+07		0.14988336	0.981396	31036545	1102081	899.3002	5888.378	94168.45	21894.57	2427.929	1170.716	0.370398	5.029725	306.3069	10.87669	45.492	10.57709	0.148518	0.972455	0.02202	0.29901	0.801703	0.741237
	2080	1.01407	16.86182	6084.422	360.840217	-1.5E+08	1.74E+08	-2.3E+07		0.150314924	0.986415	31196521	1096932	901.8895	5918.488	94926.38	21903.72	2437.68	1170.96	0.369979	5.054388	307.8857	10.82588	45.63768	10.53063	0.148229	0.972728	0.021942	0.299753	0.801825	0.741043
	2090	1.018946	16.9023	6113.674	361.706581	-1.5E+08	1.74E+08	-2.3E+07		0.150748001	0.991431	31356442	1091838	904.488	5948.589	95687.89	21912.88	2447.438	1171.205	0.369565	5.079032	309.464	10.7756	45.78368	10.48463	0.147945	0.972997	0.021865	0.300493	0.801947	0.740851
	2100	1.023821	16.94269	6142.926	362.570875	-1.5E+08	1.75E+08	-2.3E+07		0.151182564	0.996447	31516310	1086797	907.0954	5978.681	96452.99	21922.05	2457.203	1171.45	0.369158	5.103657	311.0418	10.72585	45.93	10.43907	0.147665	0.973263	0.021789	0.301231	0.802069	0.740659
	2110	1.028696	16.98298	6172.178	363.433114	-1.5E+08	1.76E+08	-2.3E+07		0.151618591	1.001461	31676126	1081809	909.7115	6008.764	97221.68	21931.24	2466.976	1171.696	0.368756	5.128263	312.6191	10.67663	46.07663	10.39395	0.147389	0.973524	0.021713	0.301965	0.80219	0.740468
	2120	1.033572	17.02318	6201.43	364.293312	-1.5E+08	1.77E+08	-2.3E+07		0.152056058	1.006473	31835889	1076873	912.3363	6038.839	97993.97	21940.44	2476.754	1171.942	0.36836	5.15285	314.1958	10.62791	46.22357	10.34926	0.147117	0.973782	0.021639	0.302696	0.802311	0.740279
	2130	1.038447	17.06328	6230.682	365.151483	-1.5E+08	1.78E+08	-2.4E+07		0.152494942	1.011484	31995601	1071988	914.9697	6068.905	98769.84	21949.65	2486.54	1172.188	0.367969	5.177418	315.772	10.5797	46.37082	10.305	0.146849	0.974035	0.021565	0.303425	0.802433	0.74009
	2140	1.043322	17.10329	6259.934	366.007643	-1.5E+08	1.79E+08	-2.4E+07		0.15293522	1.016494	32155263	1067153	917.6113	6098.963	99549.3	21958.88	2496.332	1172.434	0.367584	5.201968	317.3478	10.53198	46.51836	10.26116	0.146585	0.974285	0.021492	0.30415	0.802553	0.739902
	2150	1.048198	17.1432	6289.186	366.861804	-1.5E+08	1.79E+08	-2.4E+07		0.15337687	1.021502	32314876	1062368	920.2612	6129.013	100332.4	21968.11	2506.131	1172.68	0.367204	5.226499	318.923	10.48475	46.66621	10.21773	0.146324	0.974532	0.02142	0.304873	0.802674	0.739715
	2160	1.053073	17.18302	6318.438	367.713981	-1.5E+08	1.8E+08	-2.4E+07		0.153819871	1.026509	32474440	1057631	922.9192	6159.054	101119	21977.36	2515.936	1172.927	0.366829	5.251012	320.4978	10.438	46.81435	10.1747	0.146068	0.974775	0.021348	0.305593	0.802795	0.739529
	2170	1.057948	17.22275	6347.69	368.564188	-1.5E+08	1.81E+08	-2.4E+07		0.154264201	1.031515	32633957	1052942	925.5852	6189.088	101909.2	21986.61	2525.748	1173.174	0.36646	5.275507	322.0721	10.39173	46.96278	10.13208	0.145814	0.975014	0.021278	0.30631	0.802915	0.739344
	2180	1.062824	17.26239	6376.943	369.412438	-1.5E+08	1.82E+08	-2.4E+07		0.154709841	1.036519	32793426	1048300	928.259	6219.113	102703.1	21995.88	2535.566	1173.421	0.366095	5.299984	323.6459	10.34591	47.11149	10.08985	0.145565	0.97525	0.021208	0.307025	0.803035	0.73916
	2190	1.067699	17.30194	6406.195	370.258745	-1.5E+08	1.83E+08	-2.5E+07		0.155156769	1.041522	32952849	1043704	930.9406	6249.131	103500.5	22005.16	2545.391	1173.669	0.365736	5.324443	325.2193	10.30056	47.26049	10.04802	0.145319	0.975483	0.021138	0.307737	0.803155	0.738977
	2200	1.072574	17.3414	6435.447	371.103122	-1.5E+08	1.84E+08	-2.5E+07		0.155604966	1.046524	33112226	1039154	933.6298	6279.142	104301.5	22014.45	2555.221	1173.916	0.365381	5.348884	326.7923	10.25566	47.40976	10.00657	0.145076	0.975712	0.02107	0.308446	0.803275	0.738795
	2210	1.07745	17.38076	6464.699	371.945582	-1.5E+08	1.84E+08	-2.5E+07		0.156054413	1.051524	33271558	1034650	936.3265	6309.145	105106.1	22023.74	2565.058	1174.164	0.365031	5.373307	328.3647	10.2112	47.55931	9.965495	0.144837	0.975938	0.021002	0.309152	0.803395	0.738613
	2220	1.082325	17.42004	6493.951	372.786138	-1.5E+08	1.85E+08	-2.5E+07		0.156505091	1.056523	33430846	1030189	939.0305	6339.14	105914.3	22033.05	2574.901	1174.412	0.364686	5.397713	329.9368	10.16718	47.70913	9.924798	0.144601	0.976161	0.020935	0.309856	0.803514	0.738433
	2230	1.0872	17.45923	6523.203	373.624803	-1.5E+08	1.86E+08	-2.5E+07		0.156956981	1.061521	33590090	1025772	941.7419	6369.128	106726	22042.37	2584.75	1174.661	0.364345	5.422101	331.5084	10.12358	47.85921	9.88447	0.144368	0.976381	0.020868	0.310558	0.803633	0.738253
	2240	1.092076	17.49834	6552.455	374.46159	-1.5E+08	1.87E+08	-2.6E+07		0.157410064	1.066518	33749291	1021398	944.4604	6399.109	107541.4	22051.7	2594.604	1174.909	0.364009	5.446472	333.0796	10.08042	48.00956	9.844507	0.144138	0.976597	0.020803	0.311257	0.803752	0.738074
	2250	1.096951	17.53735	6581.707	375.296511	-1.5E+08	1.88E+08	-2.6E+07		0.157864324	1.071514	33908450	1017067	947.1859	6429.083	108360.4	22061.03	2604.465	1175.158	0.363678	5.470825	334.6504	10.03767	48.16017	9.804904	0.143912	0.976811	0.020737	0.311953	0.803871	0.737896
	2260	1.101826	17.57628	6610.959	376.129578	-1.5E+08	1.89E+08	-2.6E+07		0.158319743	1.076508	34067567	1012777	949.9185	6459.05	109182.9	22070.38	2614.332	1175.407	0.36335	5.495162	336.2207	9.99533	48.31104	9.765654	0.143688	0.977022	0.020673	0.312646	0.803989	0.737719
	2270	1.106702	17.61512	6640.211	376.960805	-1.5E+08	1.89E+08	-2.6E+07		0.158776303	1.081502	34226643	1008528	952.6578	6489.01	110009.1	22079.73	2624.204	1175.656	0.363027	5.519481	337.7907	9.953398	48.46216	9.726755	0.143468	0.97723	0.020609	0.313338	0.804107	0.737543
	2280	1.111577	17.65388	6669.463	377.790203	-1.5E+08	1.9E+08	-2.6E+07		0.159233988	1.086494	34385678	1004320	955.4039	6518.964	110838.8	22089.1	2634.082	1175.905	0.362709	5.543784	339.3603	9.911866	48.61353	9.688201	0.143251	0.977435	0.020546	0.314026	0.804225	0.737367
	2290	1.116452	17.69255	6698.715	378.617783	-1.5E+08	1.91E+08	-2.7E+07		0.159692781	1.091485	34544674	1000151	958.1567	6548.91	111672.2	22098.47	2643.965	1176.154	0.362394	5.56807	340.9294	9.870727	48.76515	9.649987	0.143036	0.977637	0.020483	0.314713	0.804343	0.737193
	2300	1.121328	17.73114	6727.967	379.443559	-1.5E+08	1.92E+08	-2.7E+07		0.160152667	1.096475	34703630	996022.4	960.916	6578.851	112509.1	22107.85	2653.855	1176.404	0.362083	5.592339	342.4982	9.829977	48.91701	9.612109	0.142824	0.977836	0.020421	0.315396	0.804461	0.737019
	2310	1.126203	17.76964	6757.219	380.267542	-1.5E+08	1.93E+08	-2.7E+07		0.160613629	1.101464	34862548	991932.1	963.6818	6608.784	113349.6	22117.24	2663.749	1176.654	0.361776	5.616592	344.0666	9.789609	49.06911	9.574563	0.142615	0.978033	0.020359	0.316078	0.804578	0.736846
	2320	1.131078	17.80807	6786.471	381.089743	-1.5E+08	1.94E+08	-2.7E+07		0.161075653	1.106452	35021427	987880.1	966.4539	6638.712	114193.8	22126.64	2673.649	1176.904	0.361474	5.640828	345.6346	9.749618	49.22145	9.537344	0.142409	0.978227	0.020298	0.316757	0.804695	0.736674
	2330	1.135954	17.8464	6815.723	381.910174	-1.5E+08	1.94E+08	-2.7E+07		0.161538722	1.111439	35180269	983865.6	969.2323	6668.633	115041.5	22136.04	2683.555	1177.154	0.361175	5.665047	347.2023	9.709999	49.37402	9.500447	0.142205	0.978419	0.020238	0.317434	0.804812	0.736503
	2340	1.140829	17.88466	6844.975	382.728846	-1.5E+08	1.95E+08	-2.8E+07		0.162002822	1.116425	35339073	979888.3	972.0169	6698.548	115892.8	22145.46	2693.466	1177.404	0.36088	5.689251	348.7695	9.670746	49.52683	9.46387	0.142004	0.978608	0.020178	0.318108	0.804928	0.736332
	2350	1.145705	17.92283	6874.227	383.545771	-1.5E+08	1.96E+08	-2.8E+07		0.162467939	1.121409	35497841	975947.6	974.8076	6728.457	116747.7	22154.88	2703.382	1177.655	0.360588	5.713438	350.3365	9.631854	49.67986	9.427607	0.141806	0.978795	0.020119	0.31878	0.805045	0.736162
	2360	1.15058	17.96093	6903.479	384.36096	-1.5E+08	1.97E+08	-2.8E+07		0.162934058	1.126393	35656573	972043	977.6043	6758.359	117606.2	22164.31	2713.303	1177.905	0.3603	5.737609	351.903	9.593318	49.83312	9.391655	0.14161	0.978979	0.02006	0.319449	0.805161	0.735993
	2370	1.155455	17.99894	6932.731	385.174423	-1.5E+08	1.98E+08	-2.8E+07		0.163401165	1.131376	35815270	968173.9	980.407	6788.256	118468.3	22173.74	2723.23	1178.156	0.360016	5.761764	353.4692	9.555133	49.98661	9.356009	0.141417	0.97916	0.020002	0.320117	0.805277	0.735825
	2380	1.160331	18.03687	6961.983	385.986172	-1.5E+08	1.99E+08	-2.8E+07		0.163869246	1.136358	35973931	964339.9	983.2155	6818.147	119333.9	22183.18	2733.161	1178.407	0.359736	5.785903	355.0351	9.517295	50.14031	9.320666	0.141226	0.97934	0.019944	0.320782	0.805393	0.735658
	2390	1.165206	18.07472	6991.235	386.796217	-1.5E+08	1.99E+08	-2.9E+07		0.164338289	1.141339	36132557	960540.5	986.0297	6848.033	120203.2	22192.64	2743.098	1178.658	0.359458	5.810026	356.6006	9.479798	50.29423	9.285621	0.141038	0.979517	0.019887	0.321445	0.805508	0.735491
	2400	1.170081	18.1125	7020.487	387.60457	-1.5E+08	2E+08	-2.9E+07		0.164808278	1.146319	36291150	956775.2	988.8497	6877.912	121076.1	22202.09	2753.04	1178.909	0.359185	5.834134	358.1658	9.442637	50.44837	9.250872	0.140852	0.979692	0.019831	0.322105	0.805623	0.735325
	2410	1.174957	18.15019	7049.739	388.41124	-1.5E+08	2.01E+08	-2.9E+07		0.165279203	1.151298	36449709	953043.6	991.6752	6907.786	121952.6	22211.56	2762.986	1179.16	0.358914	5.858226	359.7307	9.405809	50.60272	9.216414	0.140668	0.979864	0.019775	0.322764	0.805738	0.73516
	2420	1.179832	18.18781	7078.991	389.216238	-1.5E+08	2.02E+08	-2.9E+07		0.165751049	1.156276	36608235	949345.1	994.5063	6937.655	122832.6	22221.03	2772.938	1179.411	0.358647	5.882302	361.2952	9.369308	50.75728	9.182243	0.140487	0.980034	0.019719	0.32342	0.805853	0.734995
	2430	1.184707	18.22535	7108.243	390.019575	-1.5E+08	2.03E+08	-2.9E+07		0.166223804	1.161253	36766728	945679.4	997.3428	6967.518	123716.3	22230.51	2782.894	1179.663	0.358383	5.906363	362.8594	9.33313	50.91205	9.148357	0.140308	0.980202	0.019664	0.324074	0.805967	0.734832
	2440	1.189583	18.26281	7137.495	390.82126	-1.5E+08	2.04E+08	-3E+07		0.166697457	1.166229	36925188	942045.9	1000.185	6997.375	124603.5	22239.99	2792.855	1179.915	0.358123	5.930408	364.4233	9.297271	51.06702	9.114751	0.140131	0.980368	0.019609	0.324726	0.806082	0.734669
	2450	1.194458	18.3002	7166.747	391.621304	-1.5E+08	2.04E+08	-3E+07		0.167171994	1.171205	37083617	938444.4	1003.032	7027.227	125494.4	22249.48	2802.821	1180.166	0.357865	5.954438	365.9868	9.261726	51.22219	9.081422	0.139956	0.980532	0.019555	0.325376	0.806196	0.734507
	2460	1.199333	18.33751	7195.999	392.419718	-1.5E+08	2.05E+08	-3E+07		0.167647405	1.176179	37242015	934874.2	1005.884	7057.074	126388.8	22258.98	2812.792	1180.418	0.357611	5.978453	367.5501	9.226491	51.37757	9.048366	0.139784	0.980694	0.019502	0.326023	0.806309	0.734345
	2470	1.204209	18.37474	7225.251	393.21651	-1.5E+08	2.06E+08	-3E+07		0.168123677	1.181153	37400381	931335.1	1008.742	7086.916	127286.8	22268.48	2822.767	1180.67	0.357359	6.002452	369.1131	9.191563	51.53314	9.015581	0.139613	0.980854	0.019448	0.326669	0.806423	0.734184
	2480	1.209084	18.4119	7254.503	394.011691	-1.5E+08	2.07E+08	-3.1E+07		0.168600799	1.186126	37558717	927826.6	1011.605	7116.753	128188.5	22277.99	2832.747	1180.922	0.357111	6.026437	370.6757	9.156936	51.6889	8.983062	0.139445	0.981012	0.019396	0.327312	0.806536	0.734024
	2490	1.213959	18.44898	7283.755	394.80527	-1.5E+08	2.08E+08	-3.1E+07		0.16907876	1.191097	37717022	924348.2	1014.473	7146.585	129093.7	22287.51	2842.731	1181.174	0.356865	6.050406	372.2381	9.122608	51.84486	8.950807	0.139279	0.981168	0.019343	0.327953	0.806649	0.733865
	2500	1.218835	18.48599	7313.007	395.597257	-1.5E+08	2.09E+08	-3.1E+07		0.169557548	1.196069	37875298	920899.7	1017.345	7176.412	130002.5	22297.03	2852.72	1181.427	0.356623	6.07436	373.8001	9.088574	52.00101	8.918813	0.139114	0.981322	0.019292	0.328593	0.806762	0.733706

C.5 Variation of pressure, temperature, specific volume and Mach number ratios after for individual fuel at different initial mass flux

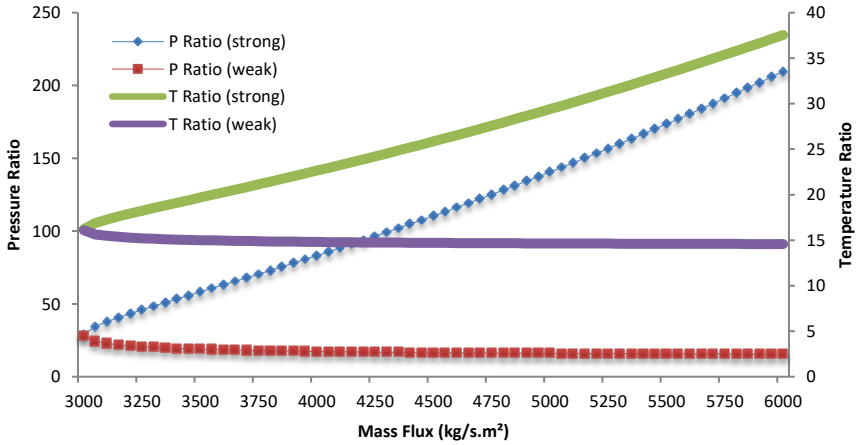

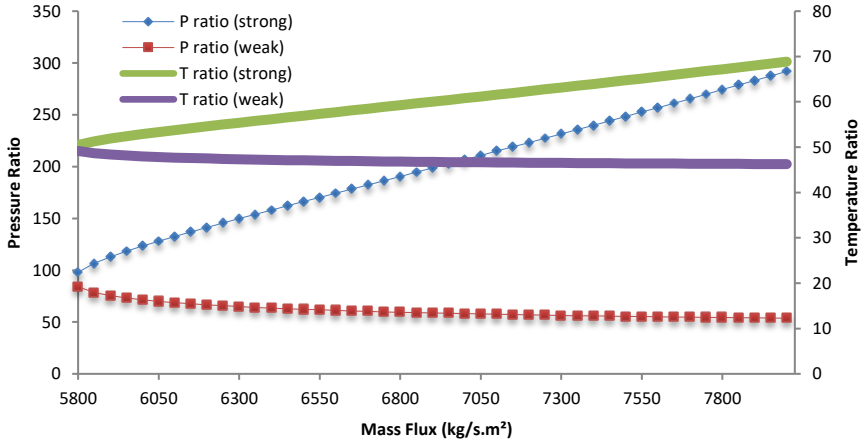

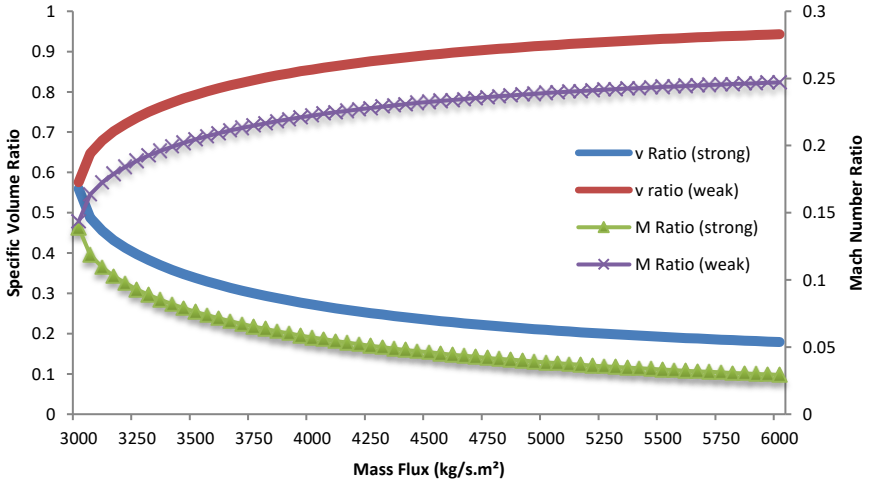

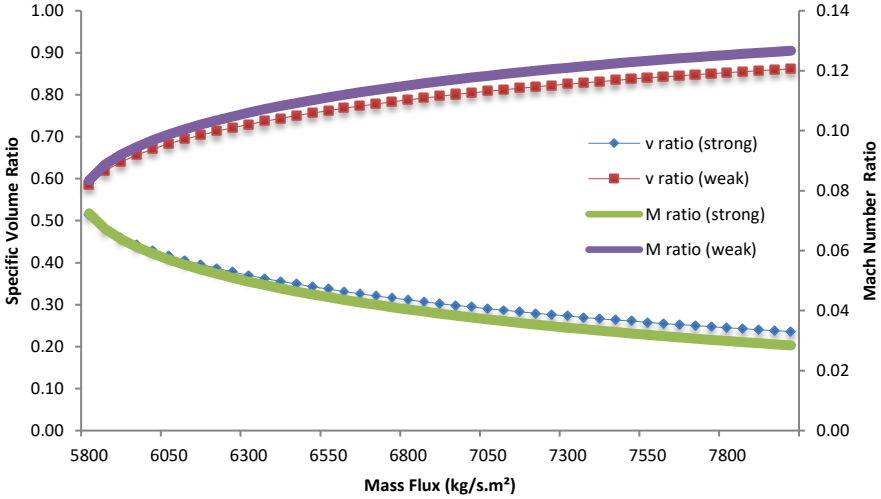

KE fuel (P=1atm T=1467K).

MA fuel (P=1atm T=2000K).

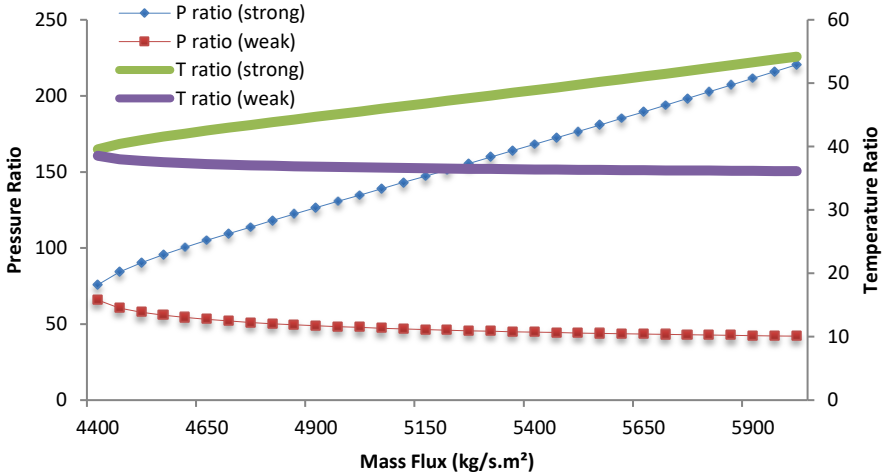

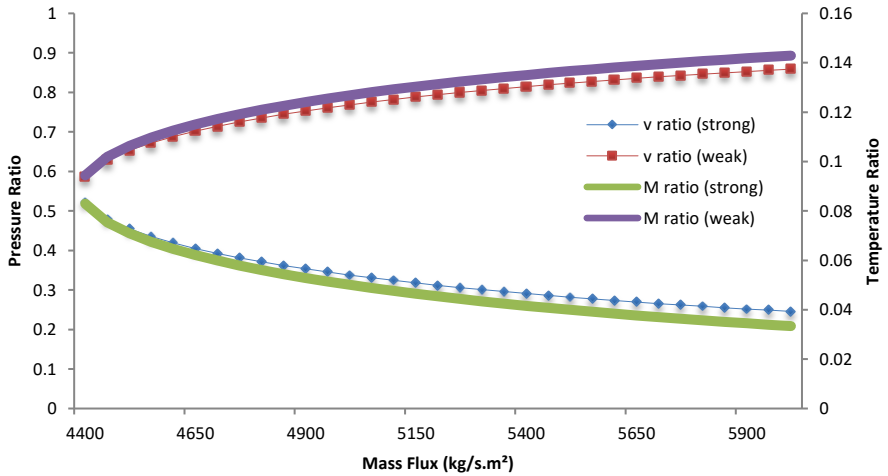

BJ fuel (P=1atm T=1700K).

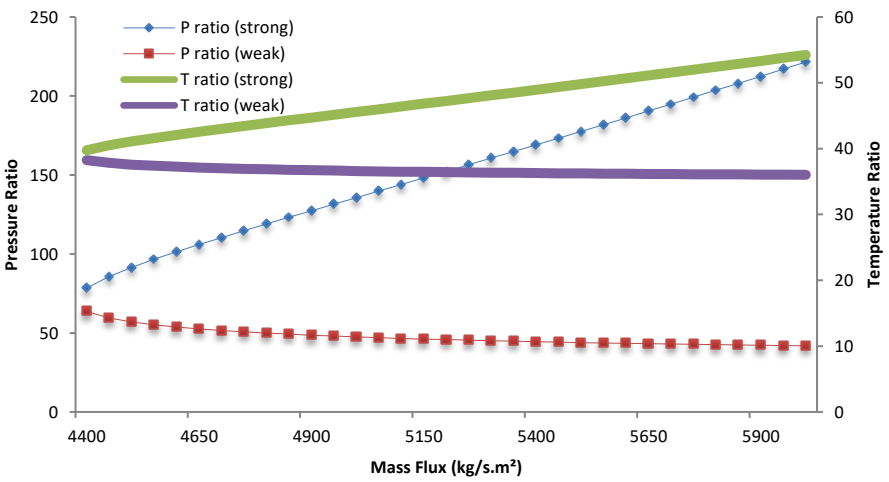

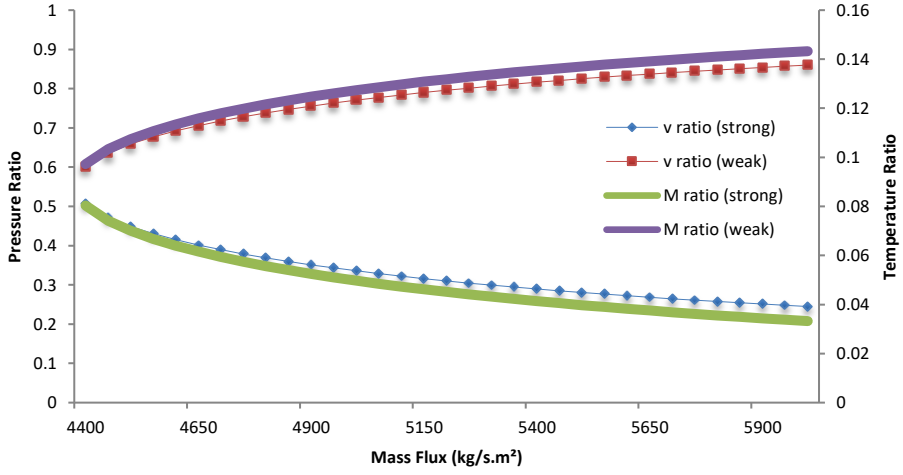

BC fuel (P=1atm T=1700K).

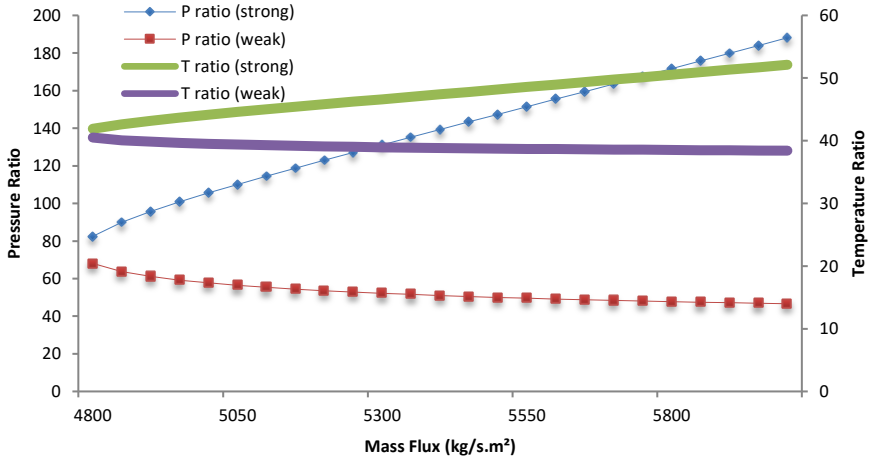

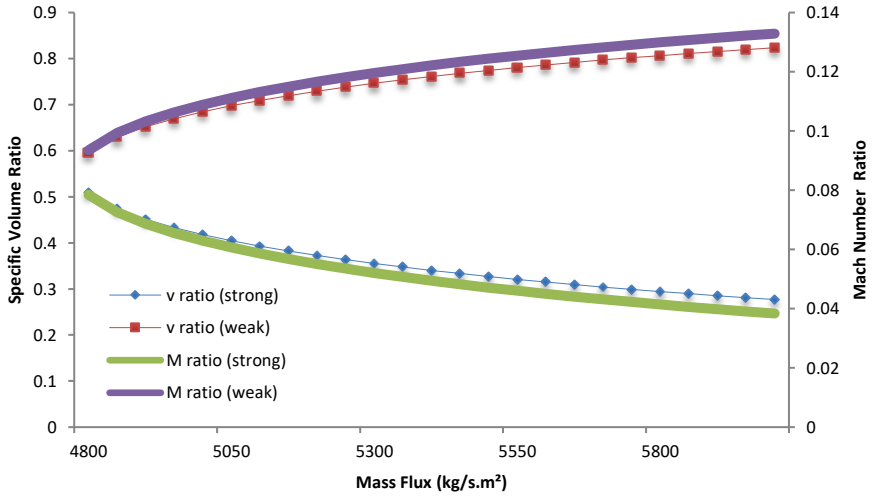

AG fuel (P=1atm T=2000K).

C.6 Variation of pressure, temperature, specific volume and Mach number ratios after for individual fuel at different initial temperatures.

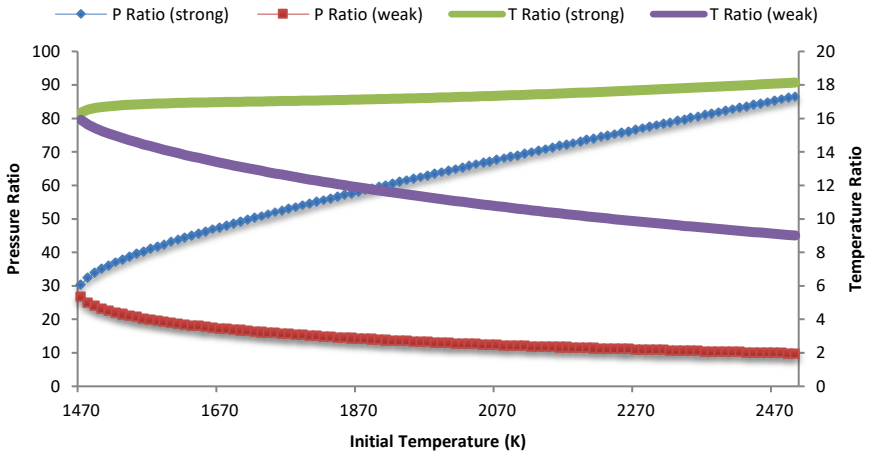

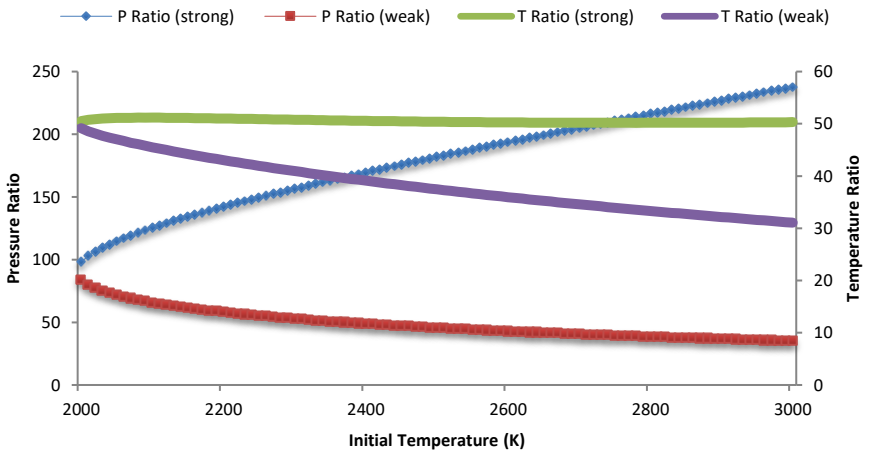

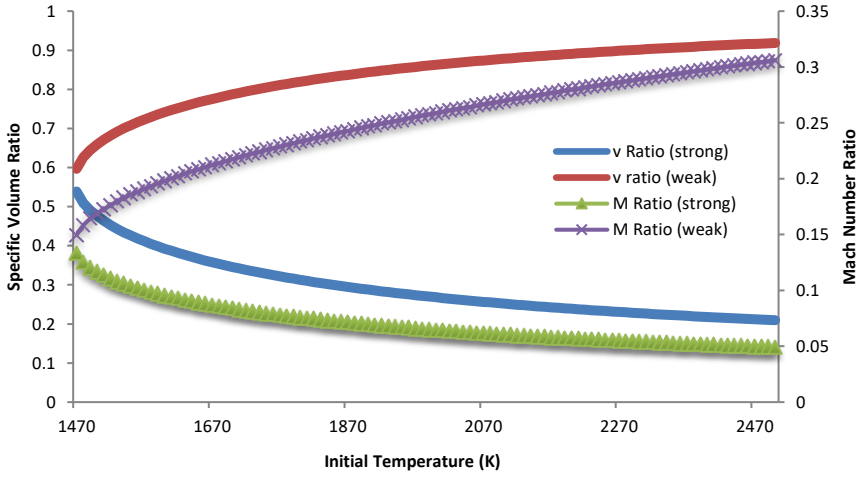

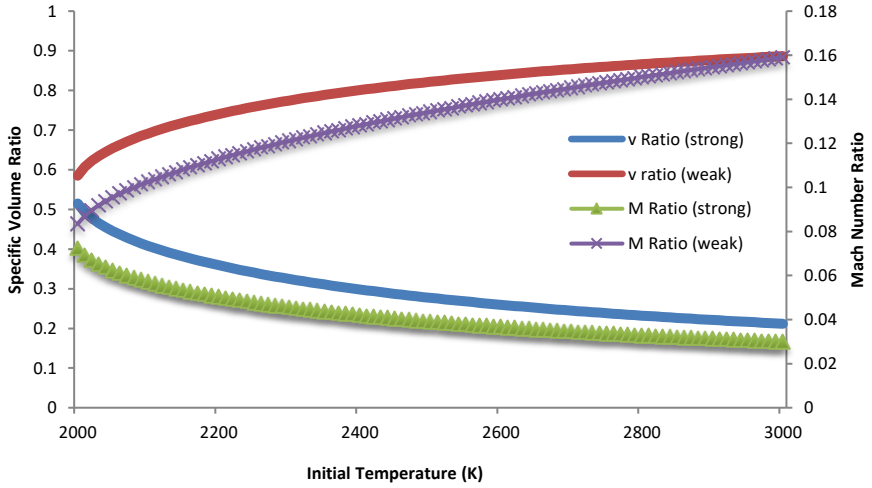

KE fuel (P=1atm G=3000 kg/s.m²)

MA fuel (P=1atm G=5800 kg/s.m²)

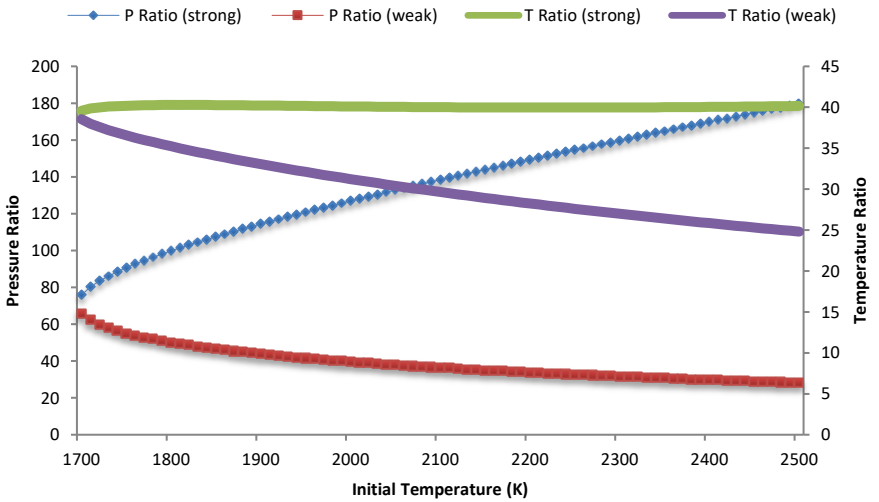

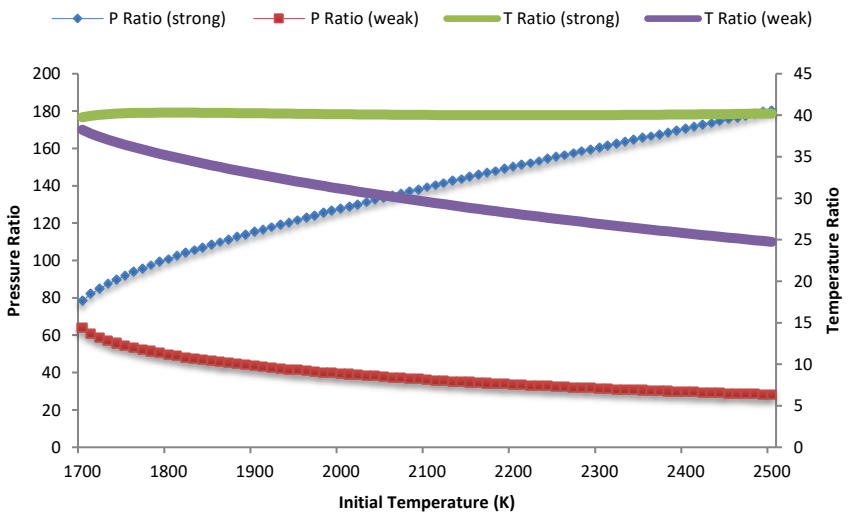

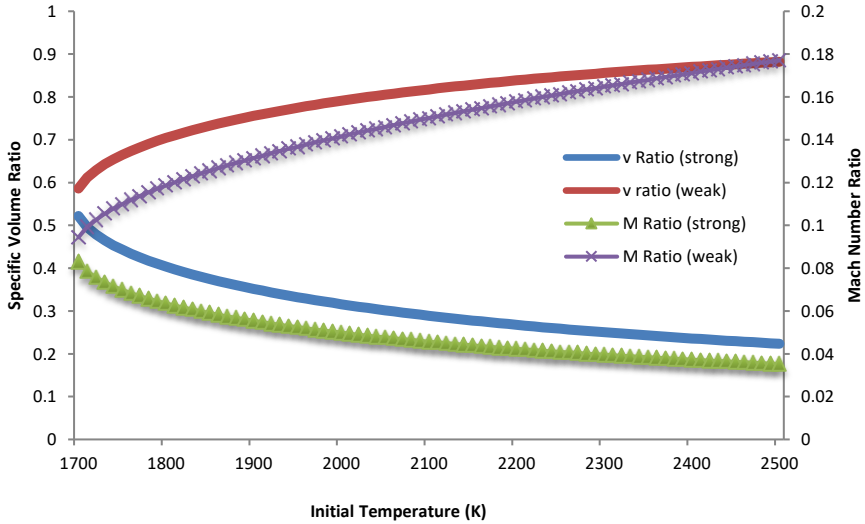

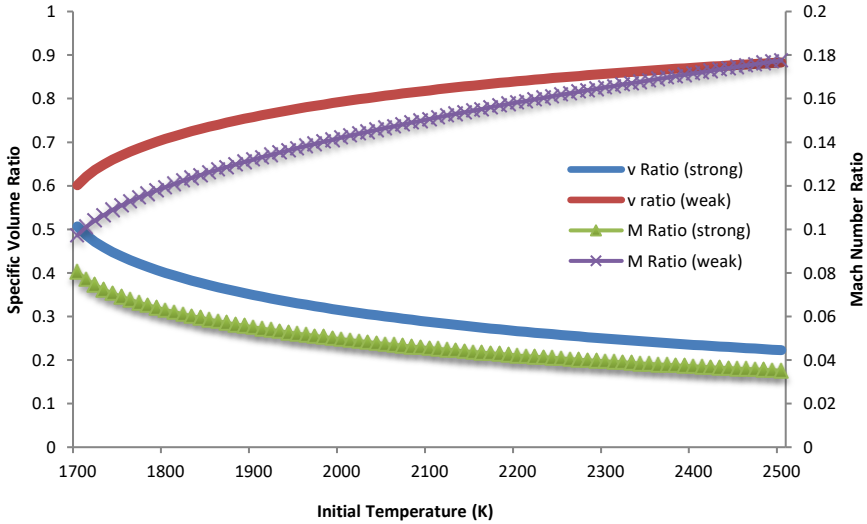

BJ fuel (P=1atm G=4400 kg/s.m²)

BC fuel (P=1atm G=4400 kg/s.m²)

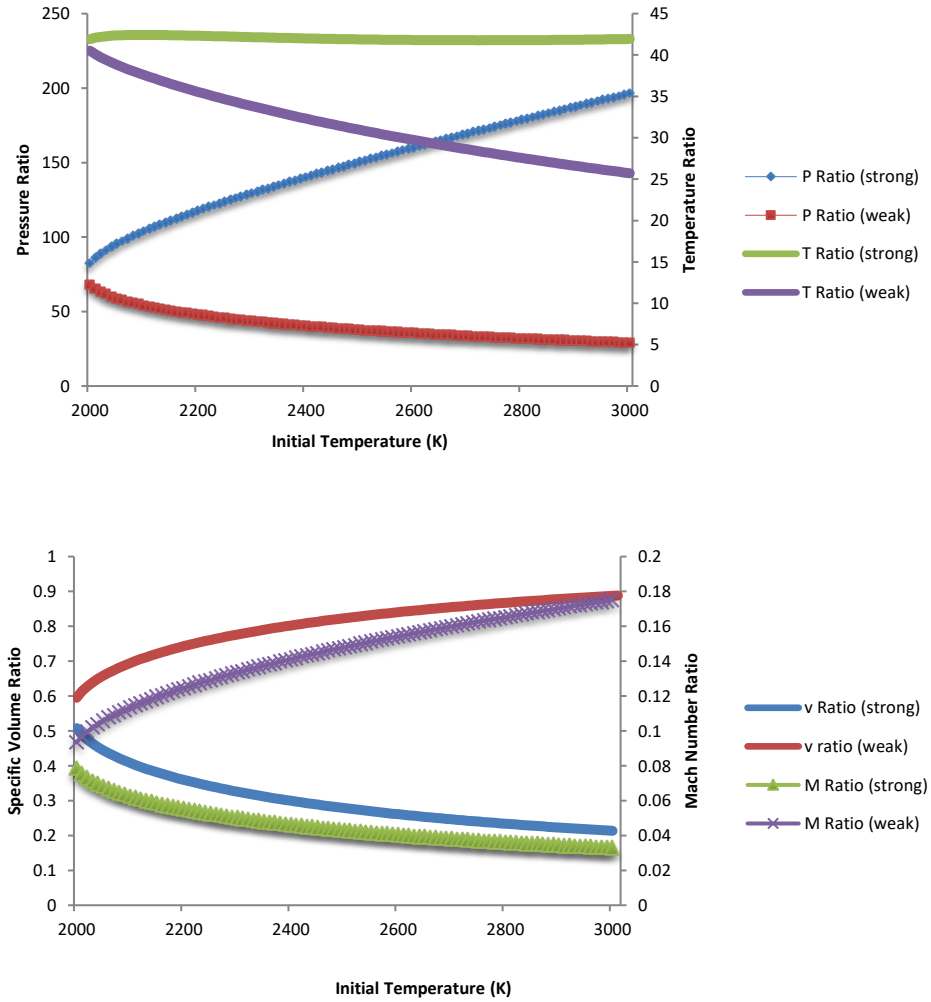

AG fuel (P=1atm G=4800 kg/s.m²)

C.7 The influence of initial pressure and mass flux to Mach number

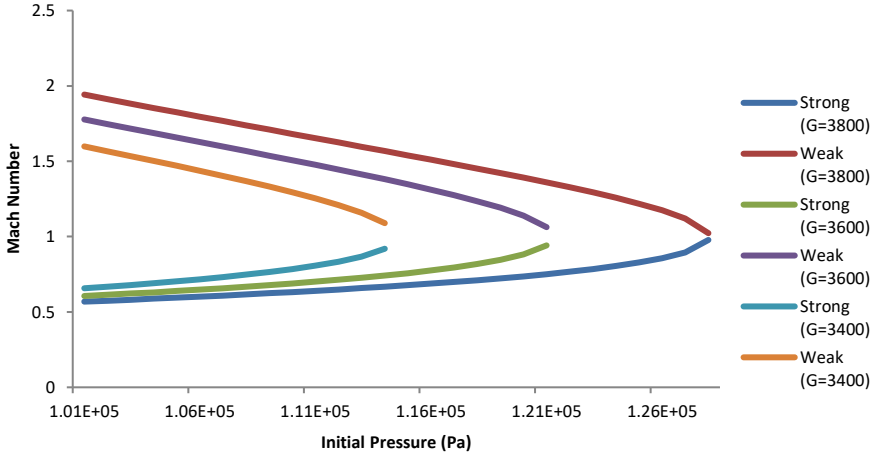

KE fuel (T=1467K)

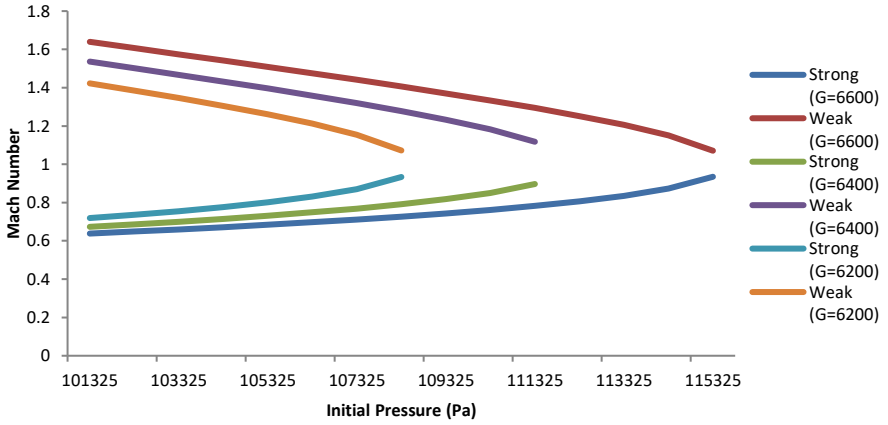

MA fuel (T=2000K)

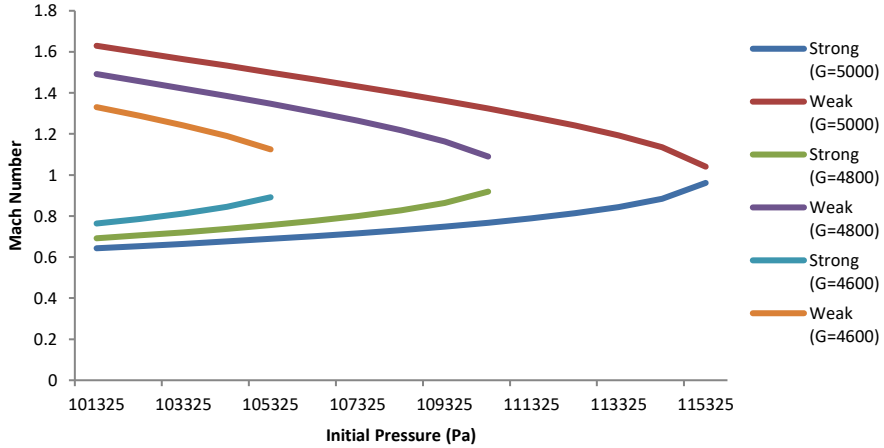

BJ fuel (T=1700K)

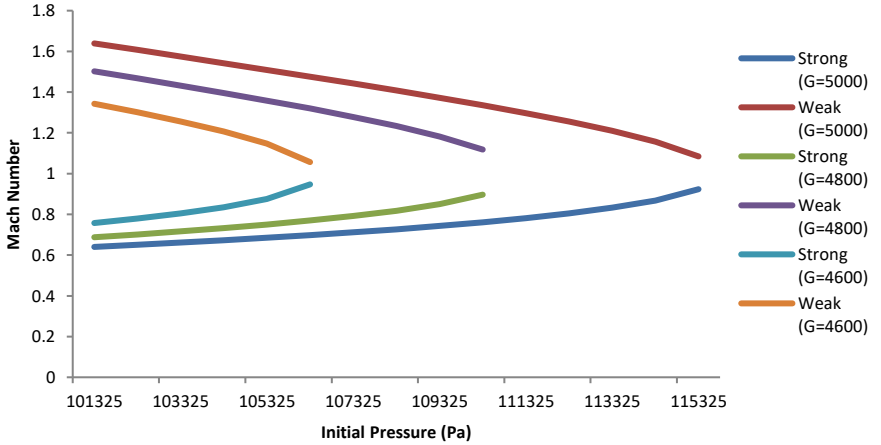

BC fuel (T=1700K)

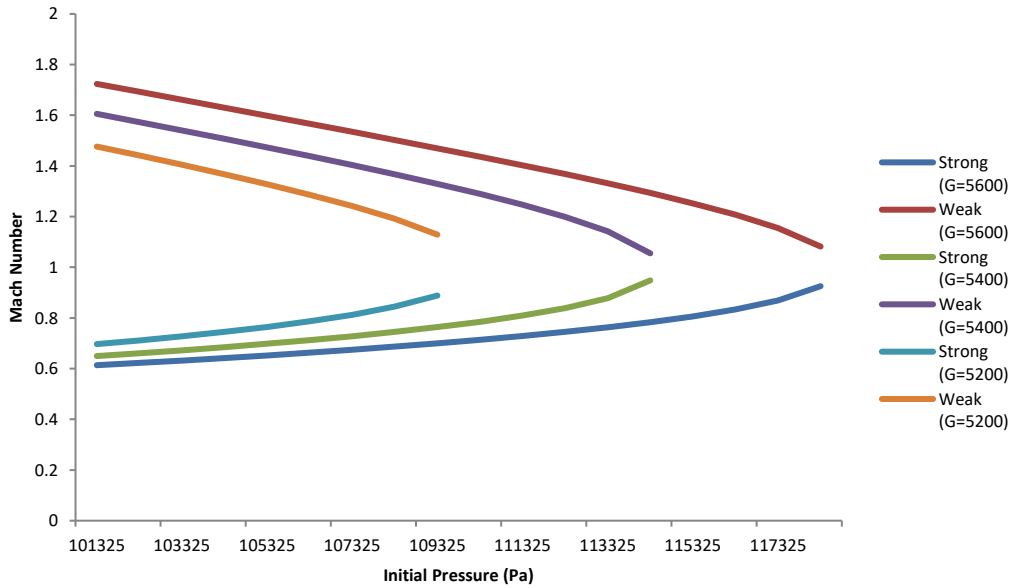

AG fuel (T=2000K)

Appendix D (Emission Analysis)

D.1 The species fractions of molar mass products for different combustion conditions.

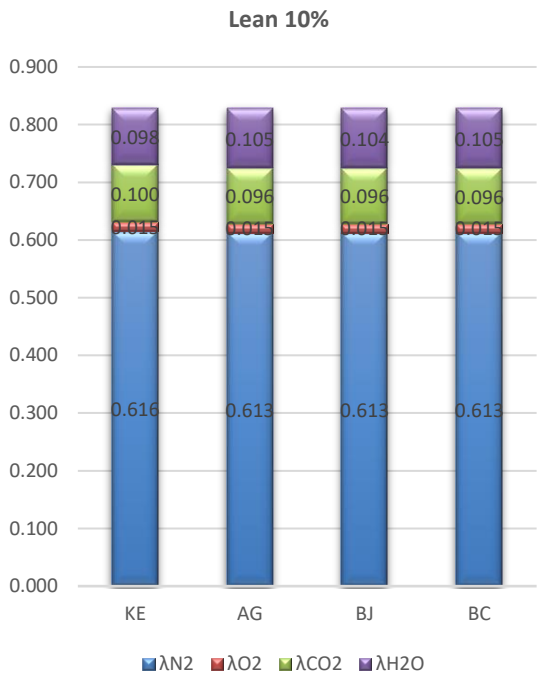

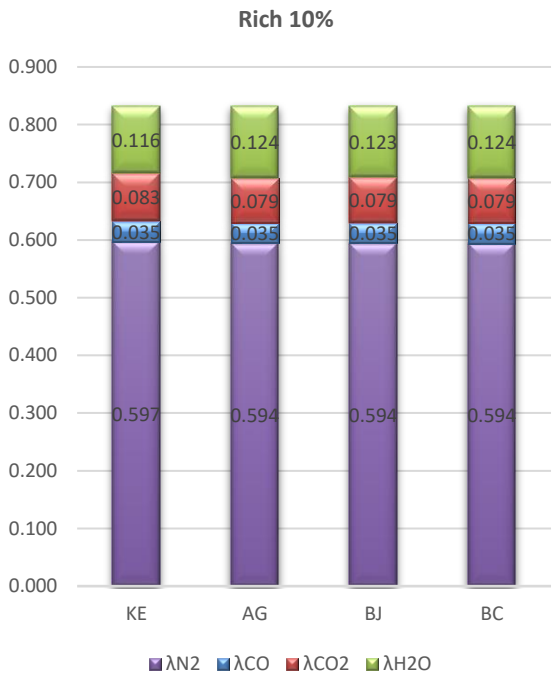

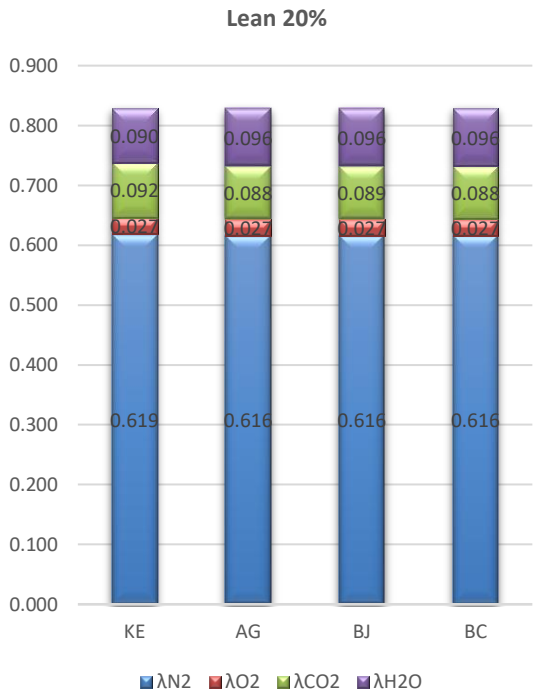

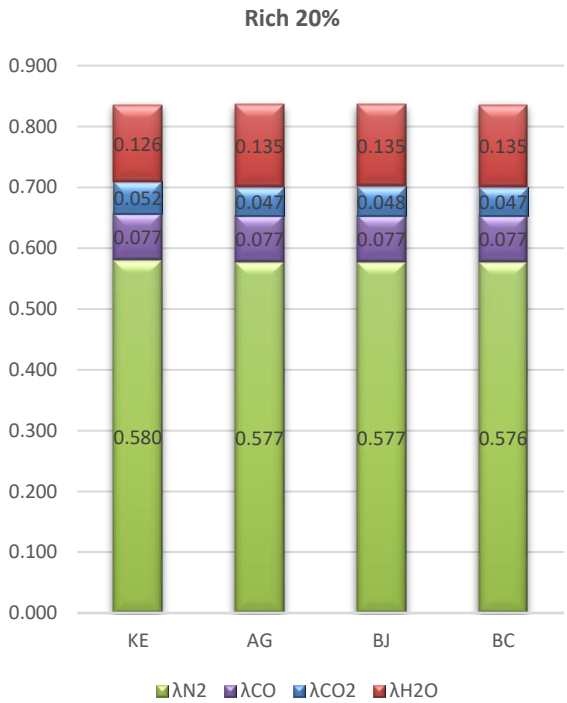

D.2 Influence of fuel flow on EINOx formation

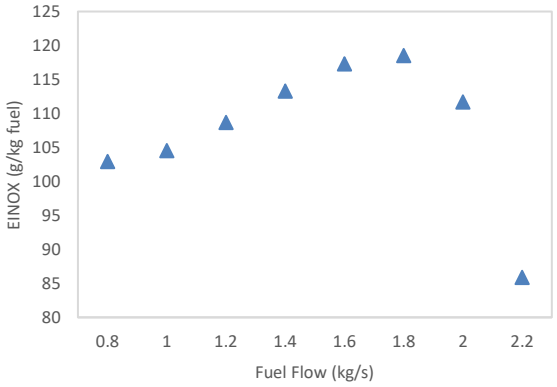

AG fuel

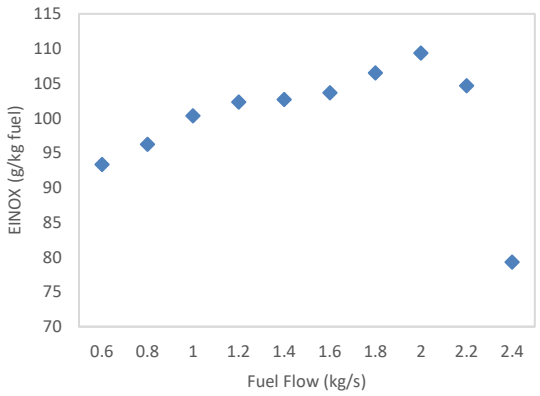

BC fuel

D.3 Flame temperature calculations for Conventional Combustor

	KE		AG		BJ		BC
STOICH							
guess T	2422.69	guess T	2426.19	guess T	2426.11	guess T	2426.33
enthalpy react	17840.61	enthalpy react	17817.21	enthalpy react	17865.74664	enthalpy react	18006.29
enthalpy prod	diff	enthalpy prod	diff	enthalpy prod	diff	enthalpy prod	diff
17857.64058	17.02659	17807.51393	-9.70035	17861.25342	-4.493222	18016.07506	9.785564
%Diff wrt KE	0		0.144468		0.141165399		0.150246
LEAN (20%)							
guess T	2119.1	guess T	2123.3	guess T	2123.07	guess T	2123.33
enthalpy react	14241.62	enthalpy react	14657.21	enthalpy react	14397.19264	enthalpy react	14660.09
enthalpy prod	diff	enthalpy prod	diff	enthalpy prod	diff	enthalpy prod	diff
14254.66581	13.04827	14669.3301	12.1161	14414.89756	17.7049248	14673.65256	13.56504
%Diff wrt KE	0		0.198197		0.187343684		0.199613
%Diff wrt Stoich	-12.5311		-12.4842		-12.49077742		-12.488
RICH (20%)							
guess T	2190.09	guess T	2194.01	guess T	2193.7	guess T	2193.65
enthalpy react	-35949.7	enthalpy react	-38003.3	enthalpy react	-37722.6847	enthalpy react	-37855.7
enthalpy prod	diff	enthalpy prod	diff	enthalpy prod	diff	enthalpy prod	diff
-35919.74702	29.92998	-38017.18321	-13.864	-37735.12918	-12.444481	-37869.97132	-14.2982
%Diff wrt KE	0		0.178988		0.164833409		0.16255
%Diff wrt Stoich	-9.6009		-9.56974		-9.579532668		-9.58979

D.4 Flame temperature calculation for pressure-rise combustor

Using Cp

STOICH	KE
P1	1.0132
T1	1700
guess T	2436.61
enthalpy react	70407.68
enthalpy prod	diff
70426.27002	18.59386
%diff wrt temp	0.459292
LEAN (20%)	
guess T	2130.88
enthalpy react	66149.72
enthalpy prod	diff
66134.60193	-15.1155
%diff wrt temp	0.424625
RICH (20%)	20%
guess T	2224.39
enthalpy react	70787.83
enthalpy prod	diff
70801.91919	14.08779
%diff wrt temp	0.630641
%T diff L vs Stoich	12.54735
%T diff R vs Stoich	8.709642

Using Cv

STOICH	KE
P1	1.0132
T1	1700
guess T	2654.63
enthalpy react	70407.68
second term	893783.8
enthalpy prod	diff
893774.8757	8.905808
%diff wrt temp	-11.2817
LEAN (20%)	
guess T	2267.66
enthalpy react	66149.72
second term	668511.1
enthalpy prod	diff
668523.198	12.0899
%diff wrt temp	-13.4177
RICH (20%)	
guess T	2419.55
enthalpy react	70787.83
second term	678013.6
enthalpy prod	diff
678026.42	12.86814
%diff wrt temp	-11.9296
%T diff L vs Stoich	14.57717
%T diff R vs Stoich	8.855471

Appendix E (Trade-Off Assessment)

E.1 Conventional Combustor

E.1.1 (Case 1 – Individual Fuel)

Main effects of TSFC and NOx for other fuels

TSFC	EINOx
BC fuel	
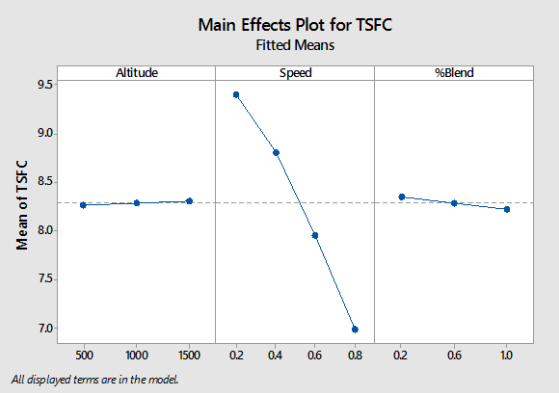	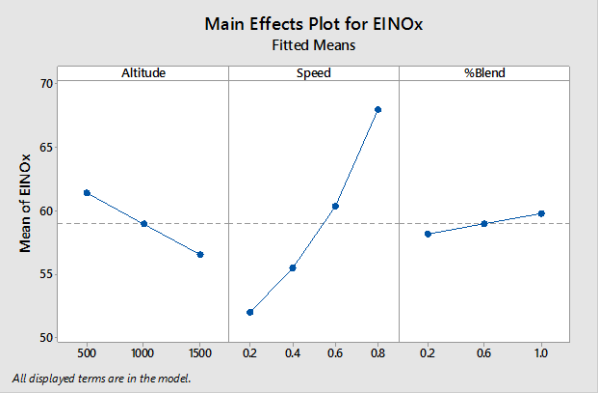
BJ fuel	
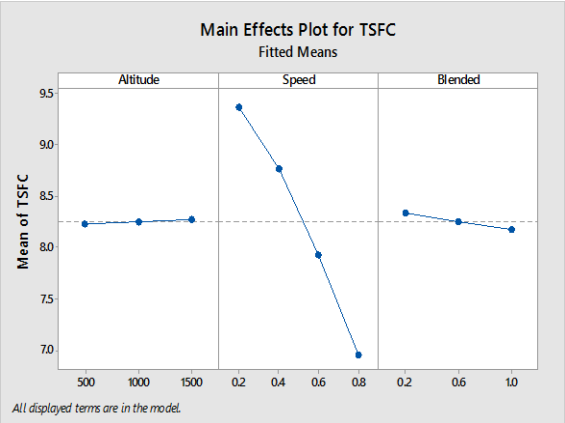	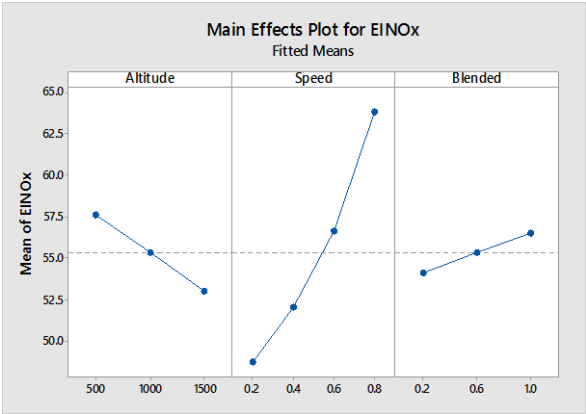

Combined effects of TSFC for individual fuel

TSFC	EINOx

BC fuel

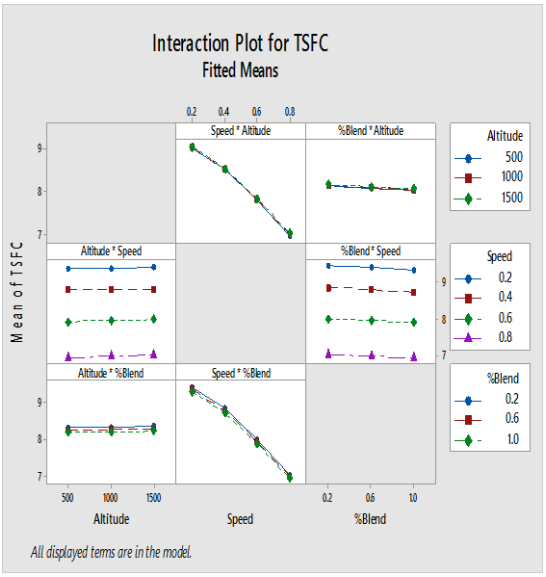

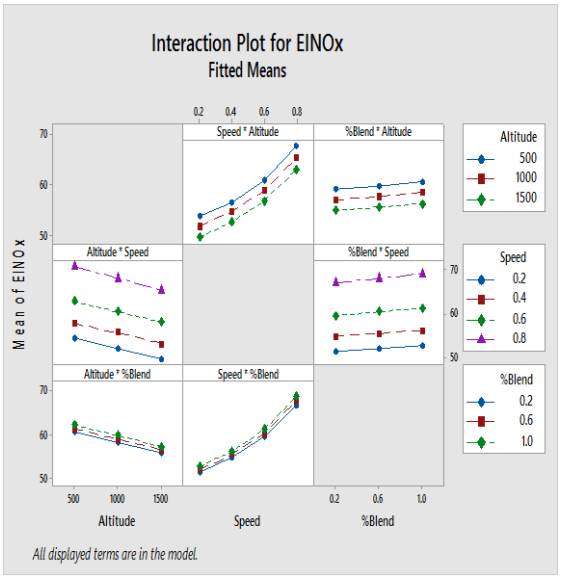

BJ fuel

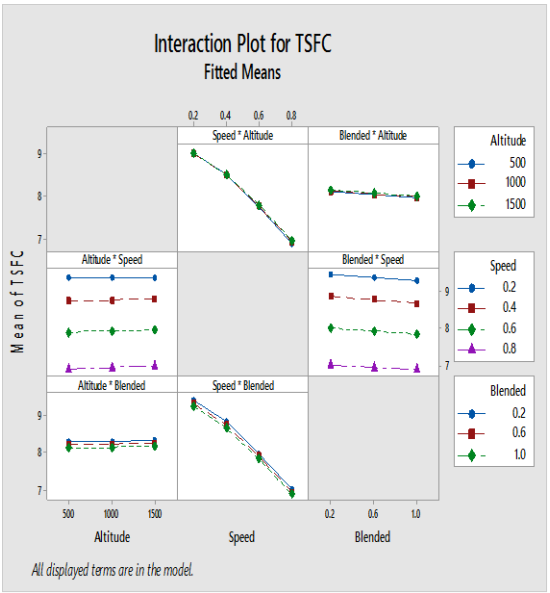

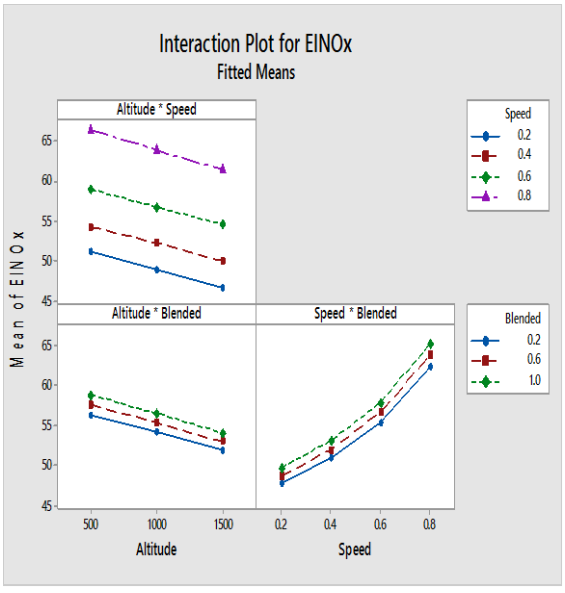

Contour plots for EINOx vs other factors

EINOx vs Speed & % Blend	EINOx vs Speed & Altitude

BC fuel

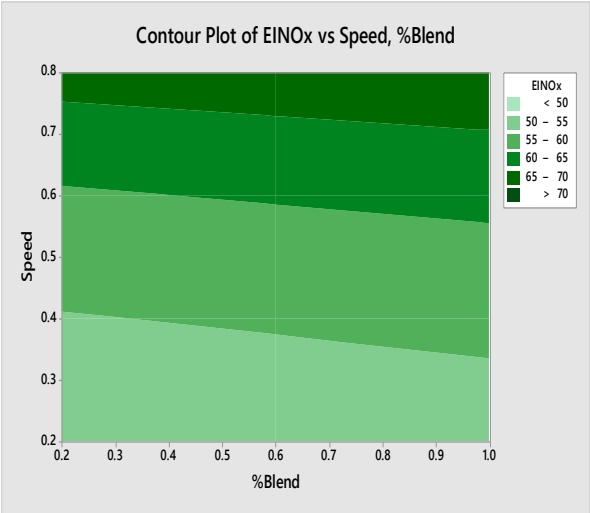

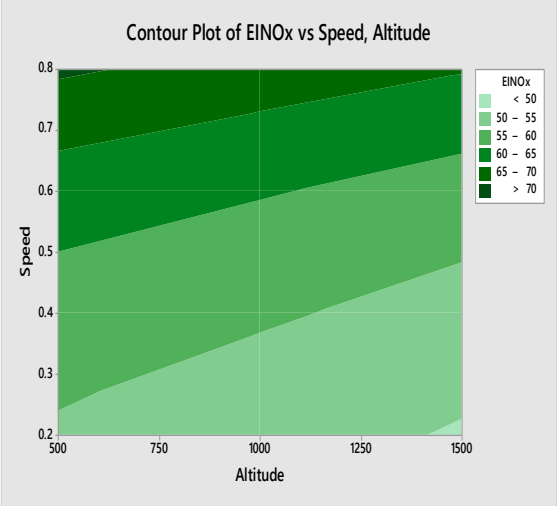

BJ fuel

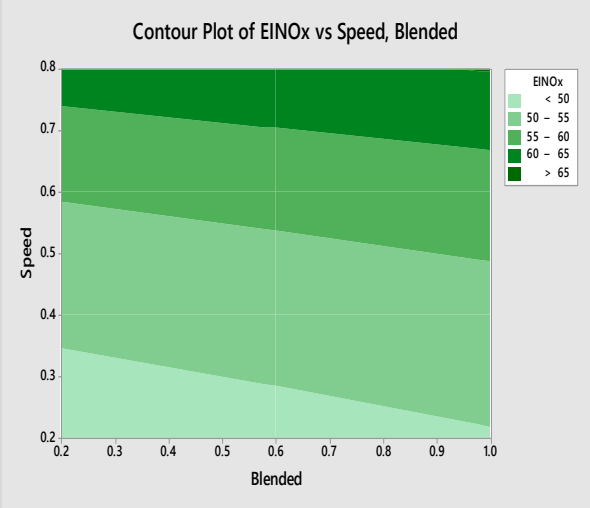

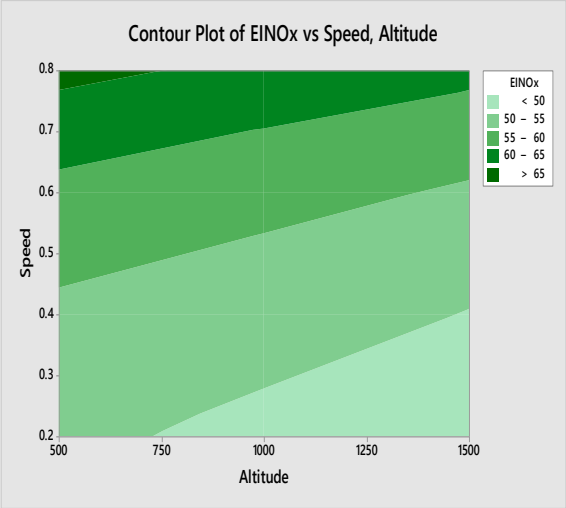

Contour plots of TSFC vs Speed and Percentage Blending Ratios

TSFC vs Speed & %Blend	TSFC vs Speed & Altitude

BC fuel

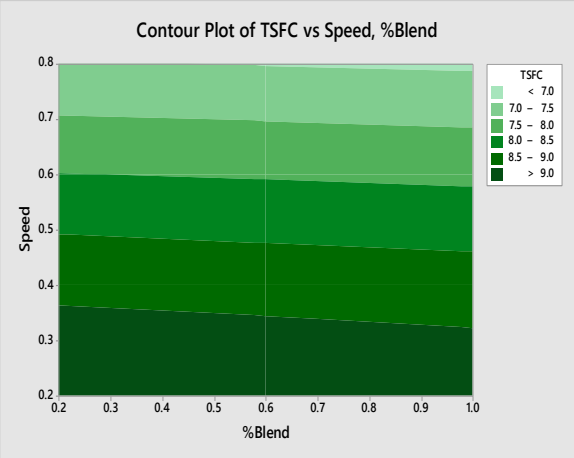

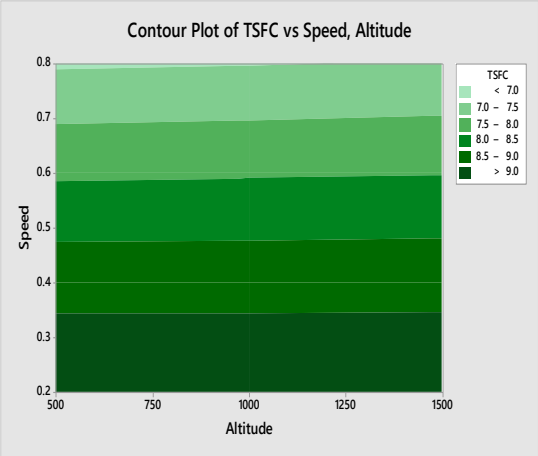

BJ fuel

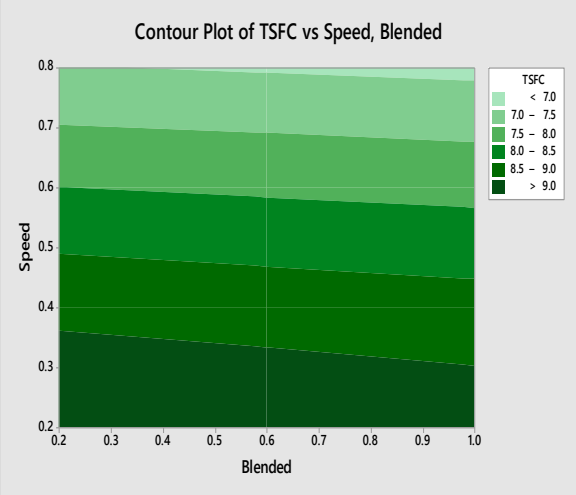

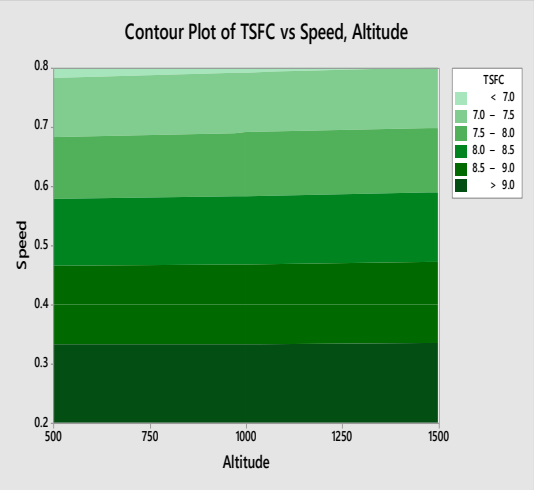

Optimal trade-off for Case 1

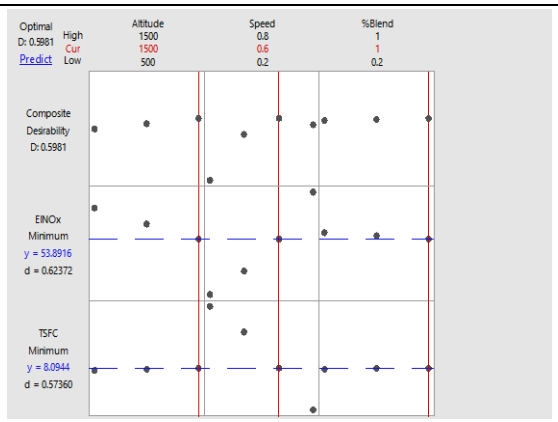

AG Fuel

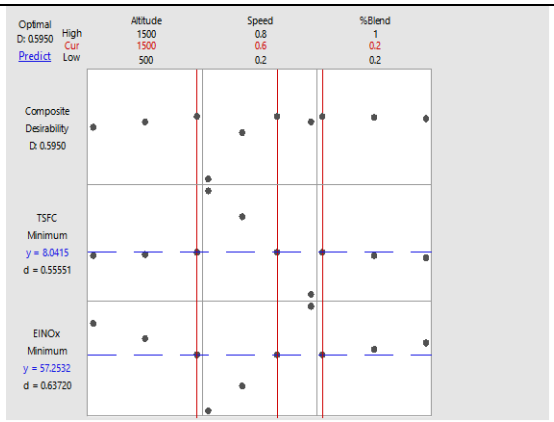

BC Fuel

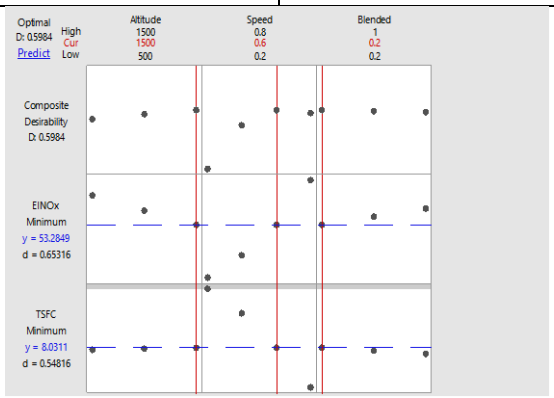

BJ Fuel

E.2 Pressure-rise Combustor

E.2.1 Relation of thermal efficiency with EINOx

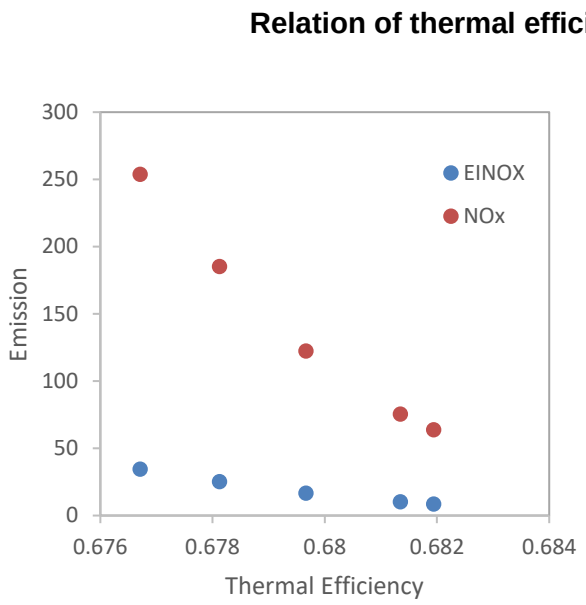

KE Fuel

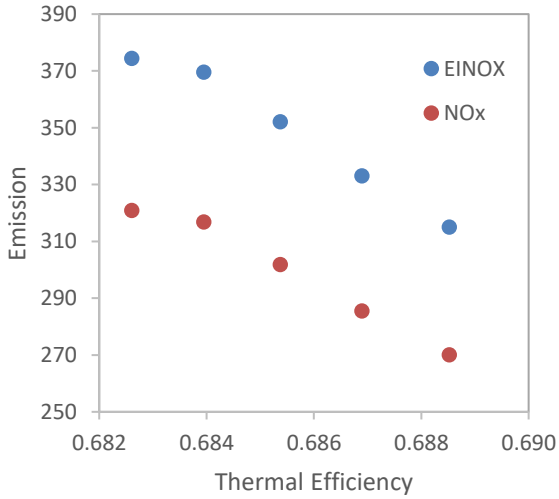

BJ Fuel

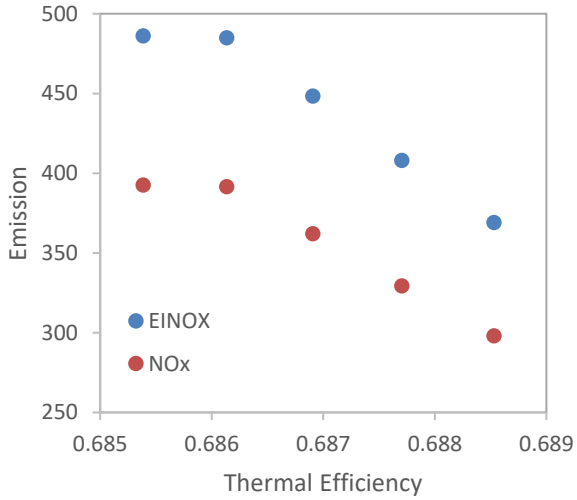

BC Fuel

	KE					BJ					BC					AG				
T1(K)	1467	1500	1600	1700	1800	1700	1750	1800	1850	1900	1700	1750	1800	1850	1900	1700	1750	1800	1850	1900
P3/P2	30.693	30.693	30.693	30.693	30.693	31.010	31.010	31.010	31.010	31.010	30.990	30.990	30.990	30.990	30.990	30.878	30.878	30.878	30.878	30.88
T2/T3	0.364	0.364	0.364	0.364	0.364	0.363	0.363	0.363	0.363	0.363	0.363	0.363	0.363	0.363	0.363	0.364	0.364	0.364	0.364	0.364
P4/P3	12.560	12.377	11.867	11.418	11.018	26.056	24.797	23.671	22.657	21.739	26.037	25.390	24.780	24.202	23.654	28.963	28.239	27.556	26.910	26.30
T4/T3	3.360	3.311	3.176	3.057	2.951	5.643	5.372	5.128	4.910	4.712	5.662	5.522	5.389	5.264	5.146	5.995	5.845	5.704	5.571	5.445
gamma	1.232	1.232	1.232	1.232	1.232	1.165	1.165	1.165	1.165	1.165	1.165	1.165	1.165	1.165	1.165	1.168	1.168	1.168	1.168	1.168
q	3648397.1	3648397.1	3648397.1	3648397.1	3648397.1	12744929	12744929	12744929	12744929	12744929	12728022	12728022	12728022	12728022	12728022	12622445	12622445	12622445	12622445	12622445
cp	1.531	1.531	1.531	1.531	1.531	1.923	1.923	1.923	1.923	1.923	1.915	1.915	1.915	1.915	1.915	2.406	2.406	2.406	2.406	2.406
R	288.731	288.731	288.731	288.731	288.731	272.680	272.680	272.680	272.680	272.680	271.332	271.332	271.332	271.332	271.332	257.985	257.985	257.985	257.985	257.985
P2	2698082.9	2658678.2	2549196	2452594	2366725.5	5597169.7	5326697.9	5084696.8	4866895.8	4669837.8	5593009	5454077.7	5322864.8	5198744.6	5081156.9	6221417.1	6066065.1	5919343.7	5780553.3	5649068
T2	1437.9883	1417.1821	1359.3741	1308.3671	1263.0275	2415.2814	2299.0201	2194.9968	2101.3758	2016.6712	2423.1989	2363.2389	2306.6101	2253.0423	2202.2938	2565.6514	2501.7986	2441.4931	2384.4474	2330.404
mdot	212.06	212.06	212.06	212.06	212.06	440	440	440	440	440	470	470	470	470	470	550	550	550	550	550
Te	892.3728	881.90406	852.66404	826.66937	803.40264	1521.211	1458.1919	1401.4228	1350.0041	1303.2022	1526.823	1494.3602	1463.5937	1434.3917	1406.6358	1579.6169	1545.927	1513.9948	1483.6841	1454.872
ue	2701.5836	2701.6083	2701.6815	2701.7529	2701.8228	5048.8163	5048.8593	5048.9	5048.9386	5048.9755	5045.464	5045.4953	5045.5259	5045.556	5045.5855	5024.487	5024.5271	5024.5663	5024.6047	5024.642
Fsp	2251.358	2251.3844	2251.4627	2251.539	2251.6137	4759.9982	4760.0442	4760.0876	4760.1289	4760.1683	4756.4153	4756.4487	4756.4815	4756.5136	4756.5452	4733.9958	4734.0387	4734.0806	4734.1217	4734.162
Isp	3337.3988	3337.4379	3337.5539	3337.6671	3337.7778	7056.191	7056.2592	7056.3236	7056.3848	7056.4433	7050.8798	7050.9294	7050.978	7051.0256	7051.0723	7017.6453	7017.7088	7017.771	7017.8319	7017.892
F	477418.48	477424.07	477440.67	477456.85	477472.69	2094399.2	2094419.4	2094438.6	2094456.7	2094474.1	2235515.2	2235530.9	2235546.3	2235561.4	2235576.2	2603697.7	2603721.3	2603744.3	2603766.9	2603789
mdotfue	14.58	14.58	14.58	14.58	14.582	7.48	7.48	7.48	7.48	7.48	7.52	7.52	7.52	7.52	7.52	7.7	7.7	7.7	7.7	7.7
nH	0.682	0.681	0.680	0.678	0.677	0.689	0.687	0.685	0.684	0.683	0.689	0.688	0.687	0.686	0.685	0.691	0.690	0.689	0.688	0.688
nB	0.578	0.578	0.578	0.578	0.578	0.476	0.476	0.476	0.476	0.476	0.475	0.475	0.475	0.475	0.475	0.481	0.481	0.481	0.481	0.481
EINOx	8.705	10.291	16.685	25.279	34.627	315.09	333.06	352.13	369.64	374.39	369.11	407.93	448.27	484.92	486.11	535.23	589.70	646.37	698.05	699.53
Nox (g/kN)	63.810	75.436	122.30	185.30	253.81	270.08	285.48	301.82	316.82	320.89	299.00	329.34	361.90	391.48	392.44	379.89	418.54	458.76	495.43	496.48

E.2.2 Main effects plot for Case 1 for all fuels

Strong Waves	Weak Waves

KE fuel

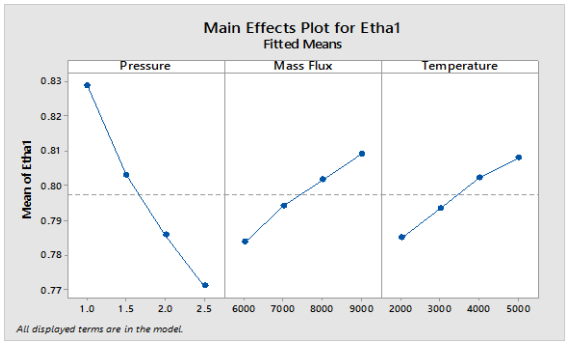

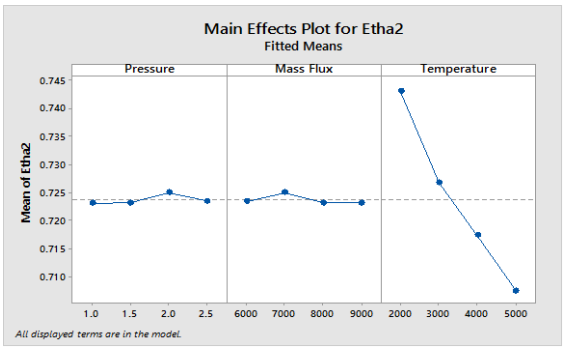

MA fuel

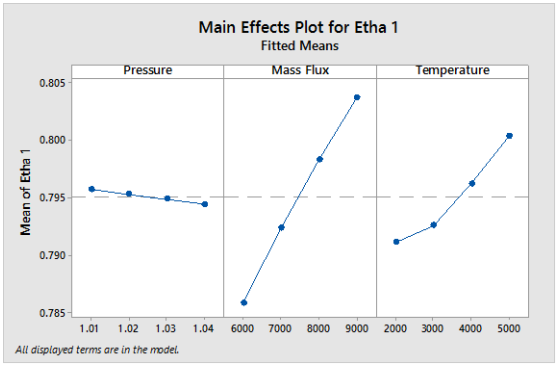

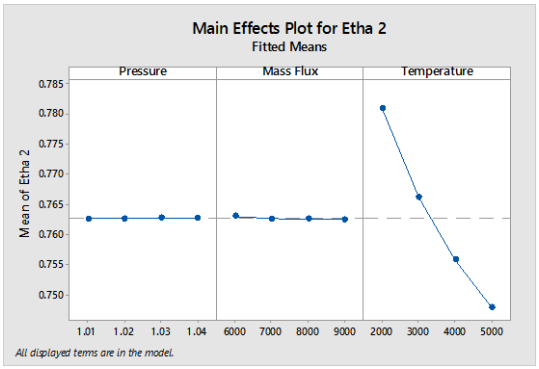

BJ fuel

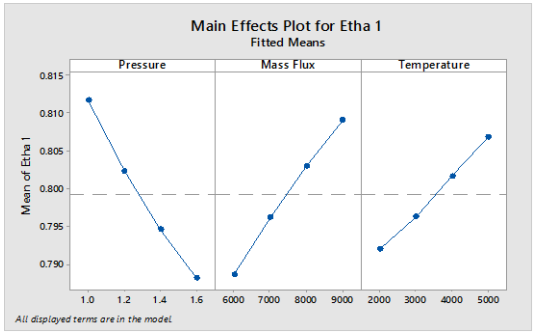

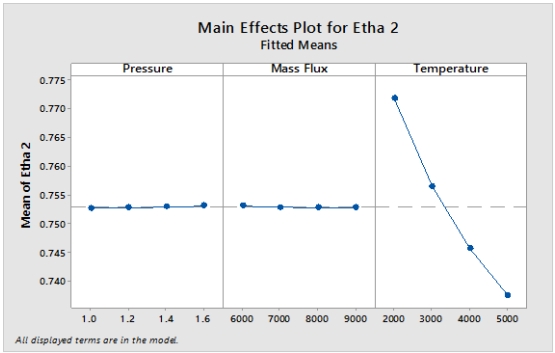

BC fuel

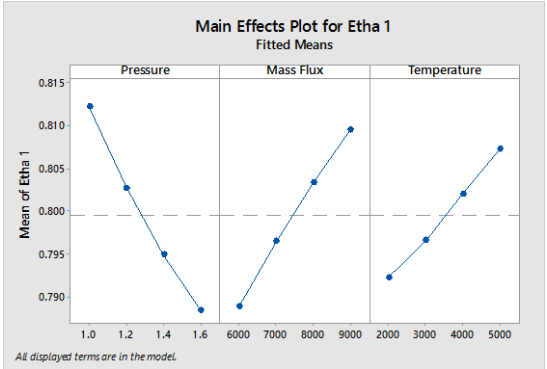

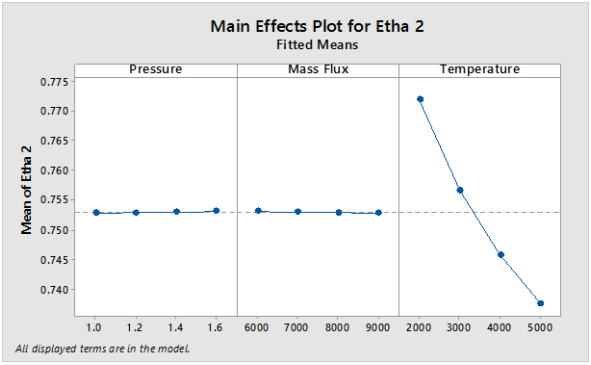

E.2.3 Interaction plots for Case 1

KE Fuel

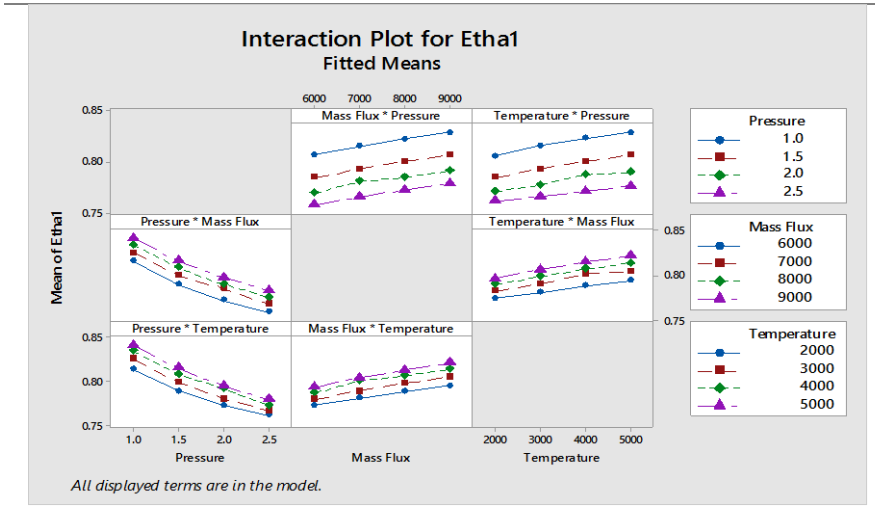

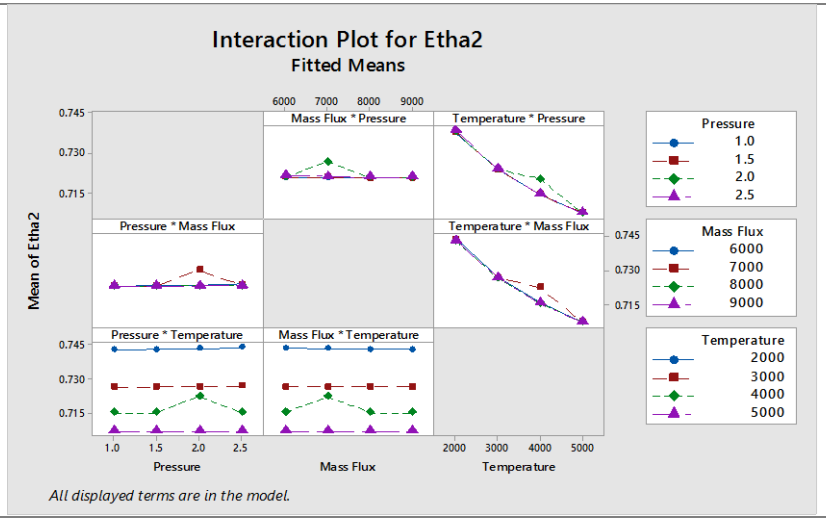

BJ Fuel

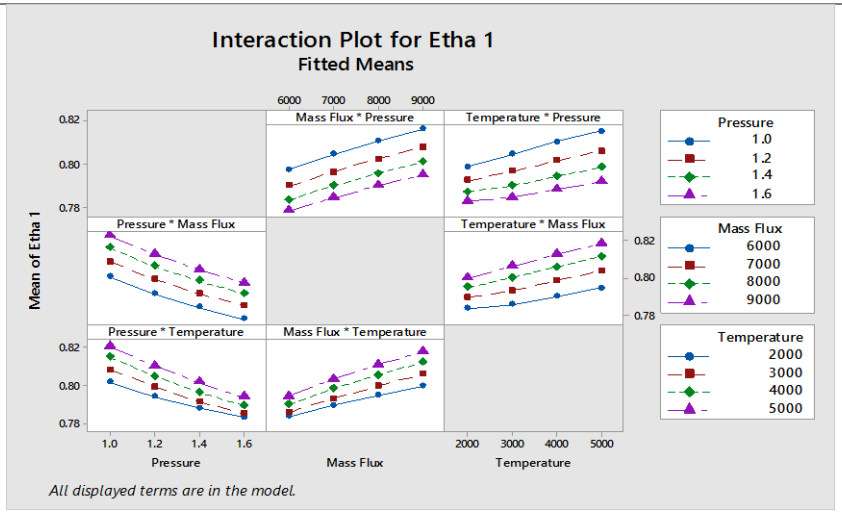

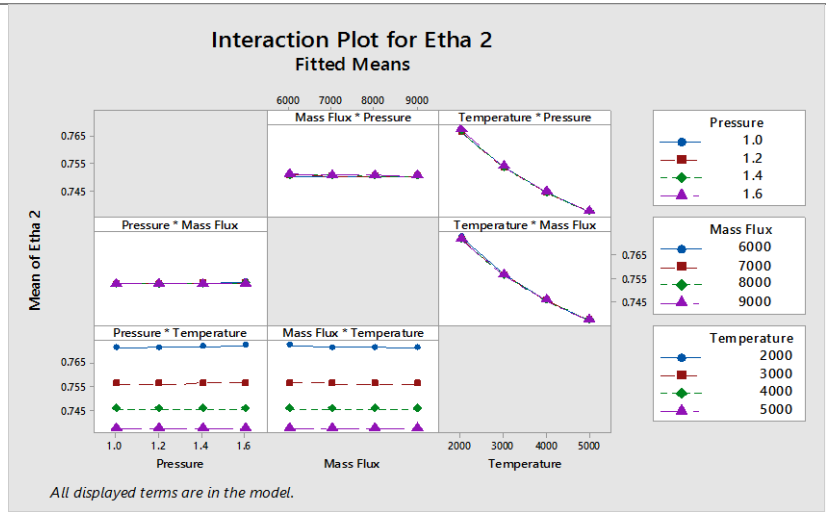

MA Fuel

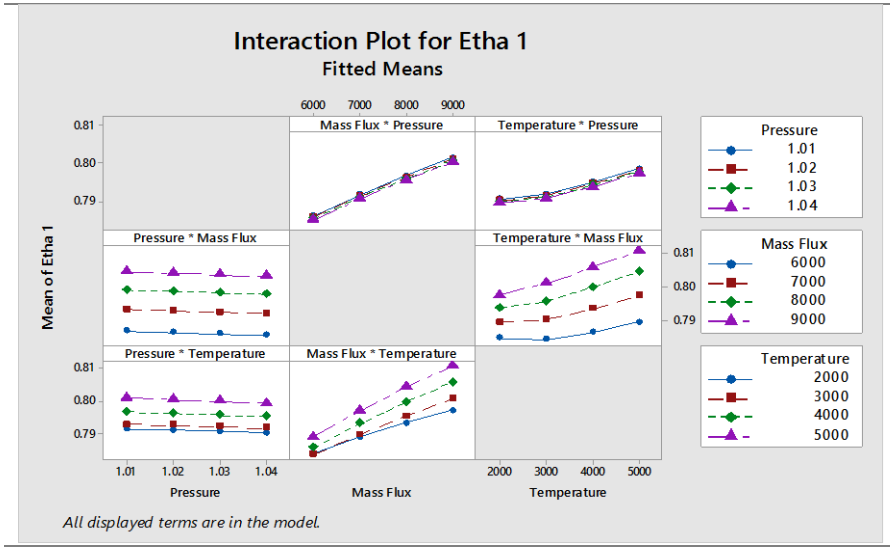

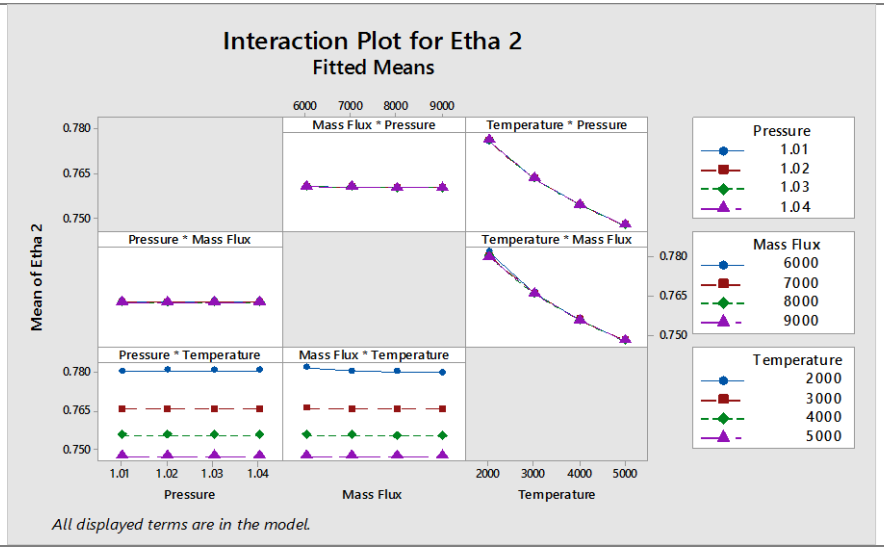

BC Fuel

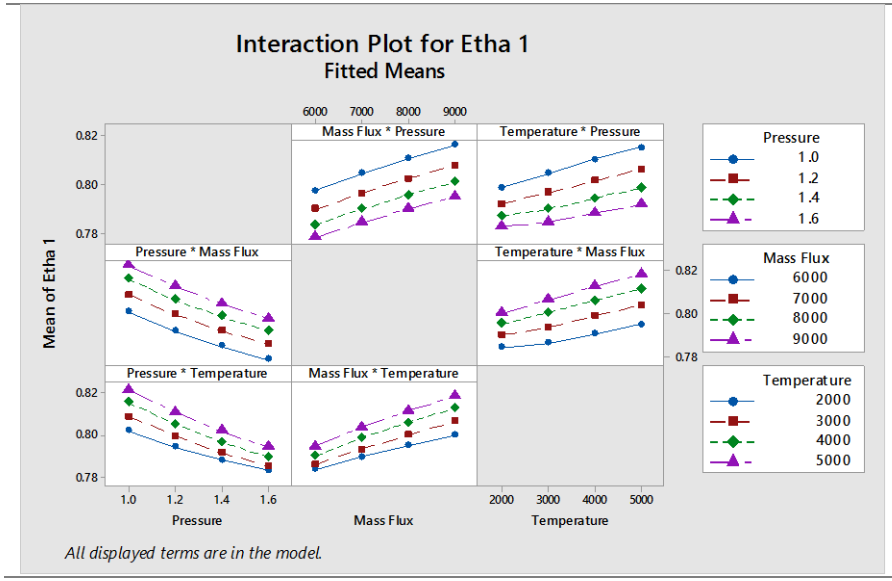

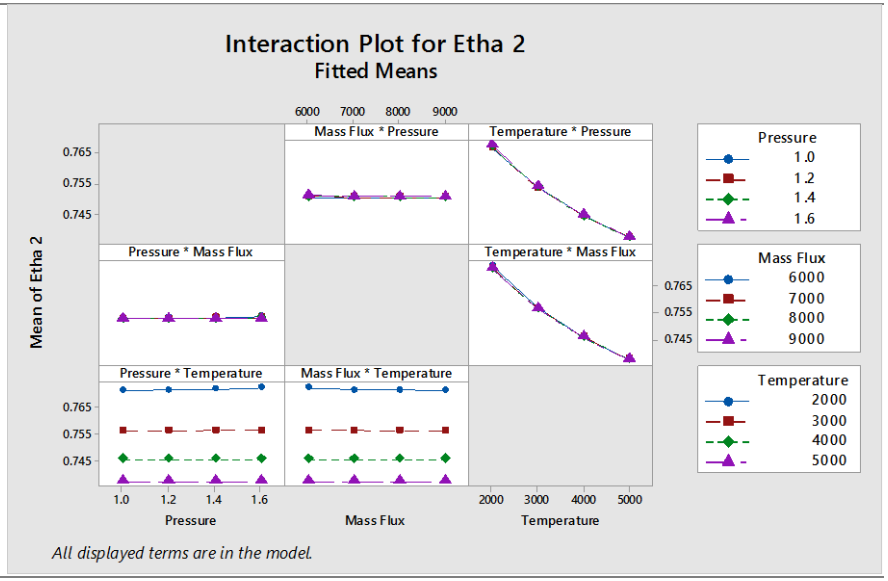

E.2.4 Effects of initial temperatures for Case 1 – Individual fuel

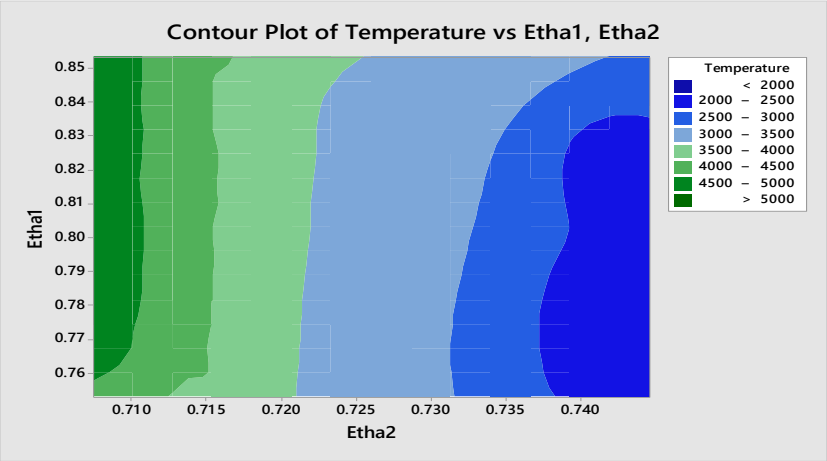

KE fuel

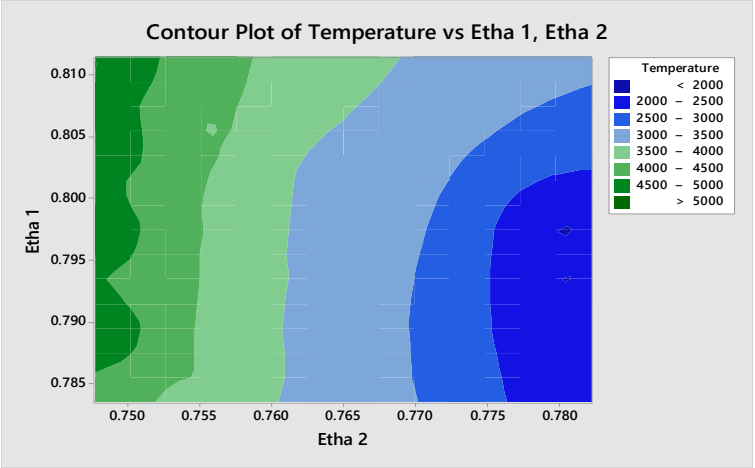

MA fuel

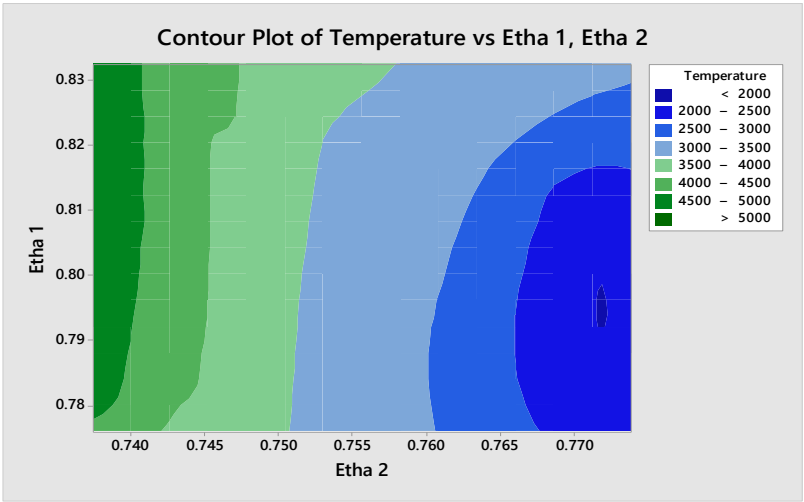

BC fuel

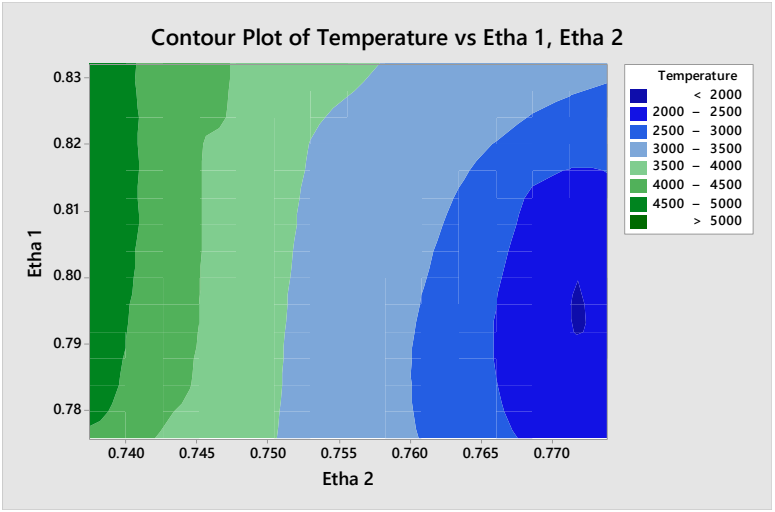

BJ fuel

Appendix F (Research Outputs and Trainings)

Journal Publications:

1. Azami, M. H. and Savill, M. (2016) 'Modelling of spray evaporation and penetration for alternative fuels', *FUEL*. Elsevier Ltd, 180, pp. 514–520. doi: 10.1016/j.fuel.2016.04.050.
2. Azami, M. H. and Savill, M. (2016) 'Comparative Study of Alternative Biofuels on Aircraft Engine Performance', PROCEEDING OF THE IMECHE, PART G: JOURNAL OF AEROSPACE ENGINEERING. SAGE Publishing.
3. Azami, M.H. and Savill, M. (2017) 'Pulse Detonation Assessment for Alternative Fuels', ENERGIES. MDPI AG.
4. Azami, M.H, Savill, M., and Li, Yi-Guang (2017) 'Comparison of Aircraft Engine Performance and Emission Analysis using Alternative Fuels', INTERNATIONAL JOURNAL OF SUSTAINABLE AVIATION. Inderscience Publishers.

Conference Proceedings:

1. Azami, M. H. and Savill, M. (2016) 'Comparison of Aircraft Engine Performance Using Alternative Fuels'. In: Proceeding of the International Symposium on Sustainable Aviation (ISSA 2016). Istanbul, Turkey; 2016.
2. Azami, M. H. and Savill, M. (2016) 'Comparative Analysis of Alternative Fuels in Detonation Combustion'. In: Proceeding of the 52nd AIAA/SAE/ASEE Joint Propulsion Conference, AIAA Propulsion and Energy Forum and Exposition 2016. Salt Lake City, Utah; 25 - 27 July 2016.

Courses Attended:

Course	Date	Time	Duration
DRCD Getting Started In Your Research	23 Oct 2014	14:00	2.5 hours
DRCD Successful Planning For Your Personal Development	11 Nov 2014	14:30	2 hours
DRCD Stages of Conducting Research	17 Nov 2014	14:00	1.5 hours
DRCD Time Management Skills	25 Nov 2014	14:00	2.5 hours
old:DRCD How To Succeed In The Global Research Community	09 Dec 2014	10:30	1.5 hours
DRCD Referencing and Avoiding Plagiarism	19 Mar 2015	09:00	1.5 hours
DRCD Technical Writing Skills for Your Progress Reviews	28 Apr 2015	09:30	2 days
old:DRCD Research Integrity and Being An Ethical Researcher	19 May 2015	09:30	2.5 hours
DRCD Papercraft - Publishing In Peer Reviewed Scientific Journals	13 Nov 2015	14:00	1.5 hours
DRCD Using Mendeley To Manage Your References	24 Nov 2015	09:30	1.5 hours
DRCD Visualising & Presenting Your Data	10 May 2016	14:00	1.5 hours
DRCD Introduction To Teaching in Higher Education	08 Dec 2016	09:30	3.5 hours
DRCD Assisting In The Supervision of MSc Students	14 Dec 2016	09:30	3.5 hours
DRCD Making An Impact With Your Publications	24 Jan 2017	10:00	2 hours
DRCD Using What You Read In What You Write	16 Feb 2017	10:00	1.5 hours
DRCD Keeping Up To Date In Your Field	17 Mar 2017	10:00	1.5 hours
DRCD Moving From Postgrad to Postdoc and into an Academic Career	03 May 2017	10:00	3 hours

Short Courses Attended:

1. Combustors Short Courses (22-26/6/2015)
2. Special Attendee for Combustors Module (Dec 2014 - June 2015)
3. Special Attendee for Simulation & Diagnostics Module (March-June 2015)
4. Special Attendee for Fortran Programming Module (March-June 2015)
5. AIAA Continuing Education Course Advanced High Speed Air Breathing Propulsion (July 2016)

IT and Library Training:

No.	Training Course	Date/Time	Venue
1.	Mendeley Training	18/11/2014 (13:05)	Blake Room, B63
2.	Word: Using the thesis template	19/11/2015 (09:30)	Blake Room, B63
3.	Word: Essentials	15/10/2015 (09:30)	Blake Room, B63
4.	Powerpoint: Creating Cranfield Presentations	18/6//2015 (09:30)	Blake Room, B63
5.	Excel: Analysing Data	10/11/2015 (11:00)	Blake Room, B63
6.	Excel: Formulas and functions	9/12/2015 (09:30)	Blake Room, B63

Cranfield University Training Course (CUTE-online):

1. Environmental Awareness (26/3/2016) – 100% score
2. ErgoWize (26/3/2016) – 100% score
3. Fire safety essentials (27/3/2016) – 100% score
4. Health and Safety Induction (4/4/2016) – 90% score
5. Slips, trips and falls (4/4/2016) – 90% score
6. Manual handling (5/4/2016) – 100% score